Exergy-based Investigation and Optimization of a Heat-driven Polygeneration System using Carbon Dioxide as Working Fluid

vorgelegt von
M. Sc.
Jing Luo
ORCID: 0000-0003-4473-0497

an der Fakultät III - Prozesswissenschaften
der Technischen Universität Berlin
zur Erlangung des akademischen Grades

Doktor der Ingenieurwissenschaften
-Dr.-Ing.-

genehmigte Dissertation

Promotionsausschuss:

Vorsitzenderin: Prof. Dr.-Ing. Rita Streblow
Gutachterin: Prof. Dr. Tetyana Morozyuk
Gutachter: Prof. Dr.-Ing. George Tsatsaronis
Gutachter: Prof. Dr. Bourhan Mohammad Tashtoush
Gutachter: Prof. Dr. habil. Wojciech Stanek

Tag der wissenschaftlichen Aussprache: 17. Dezember 2020

Berlin 2021

Dedicated to those
who have ever inspired me, encouraged me, and supported me
for going this far.

The things I learned from you
helped me become a stronger woman,
who has the courage to face the world with love, curiosity, and hope.

Acknowledgements

I dreamed of being a great scientist when I was a little girl. During the time of accomplishing this dissertation, I felt that I am closer to my dream. I wrote the entire thesis in Munich, where has my second home in Germany, in this challenging situation caused by coronavirus pandemic. So much gratitude to everyone who have ever supported me by any means; without you, the completion of this work is impossible. I miss you all, my dearest professors, colleagues, family members, and friends!

First of all, I would especially like to thank my supervisor Prof. Tetyana Morozyuk, who accepted me as her Ph.D. student and offers utmost support for her female students in her entire life. Her charm, enthusiasm, and kindness bring everyone at this institute together as a joyful family. Special thanks go to Prof. George Tsatsaronis, who is a perfect model for me in the scientific research area. As a great and well-known scientist, he is humble, empathetic, hard-working and curious. He even rigorously corrected my paper during his vacation time. Thanks to both my dearest professors, I am becoming a better person in terms of many perspectives.

I thank Prof. Bourhan Mohammad Tashtoush and Prof. Wojciech Stanek, with my deepest appreciation, of being my reviewers. I am so lucky getting to know both gentle and active professors, introduced by Prof. Tetyana Morozyuk and Prof. George Tsatsaronis during my Ph.D. study. Their support and time are priceless for me.

Heartfelt thanks also go to my family. My beloved mother and father, who are 7219 km far away, always try their best to support me. Underneath their countless "nags" and questions, it is the unconditional love. My husband, Qian, who had made unimaginable sacrifices to support me in every minute when I was writing this thesis, deserves my biggest hug. He is not only one of my most important family members, but also my best and irreplaceable friend. He is the one who taught me programming skills, commented on my codes, and helped me debugging after he was back from his office. I also thank my "best mates" family members, Wenbin, Peng, and Mo. We met 14 years ago. Now, like all the great friendships, the roots of our relationship are becoming stronger.

Last but not least, my great gratitude to all of my colleagues and friends from our department. My sincere thanks go to Sara, Sarah, Jimena, Elisa, Cristina, Gigi, Stefanie, Linda, Eko, Renzo, Bahaa, Louay, Saeed, Yuegeng, and Alex. We spent so much time creating unforgettable and delightful memories with laughs and tears. You are the greatest assets I took from the institute. Thank you for both technically and non-technically supports and discussions, in workdays and in the weekends, which offers me a shield we build and hold together.

To anyone whose name I might have inadvertently omitted, my apologies.

Abstract

To achieve global sustainable development goals, efficiency improvement of sustainable energy systems is the most cost-effective and near-term option. Polygeneration systems improve system efficiency significantly and minimize the discharge of system pollutants. In this work, a novel small-scale waste heat-driven polygeneration system using CO_2 as its working fluid was proposed for local power and thermal energy supply. Such a stand-alone system can easily be integrated with other facilities and harness different available heat sources. The novel polygeneration system's conceptual design, including system simulation, investigation, and optimization with computer-aid software, was addressed.

Exergy-based methods, including conventional and advanced exergetic and exergoeconomic analyses, were implemented to examine the system performance and identify the magnitude, location, and cause of component-wise and system-wise real inefficiencies. Moreover, Aspen HYSYS® was connected to a Python program to achieve calculation and optimization automation. The automation allows the "communication" between these two programs; thus, importing and exporting values manually can be avoided. To solve multimodal optimization problems, including single-objective, multi-objective, and superstructure-based optimization, population-based stochastic algorithms (differential evolution and particle swarm optimization) were implemented to find the global optimal results by overcoming local minima.

The system investigation results showed that temperatures and costs of the available heat sources affect system product costs notably, especially the heating cost. The pressure designed for merging two subsystems is a crucial decision parameter. Lower product costs can be obtained in cases with a lower ambient temperature. In the case study of recovering the exhaust gas from a 2 MW natural gas engine, the overall system efficiency, including the natural gas engine and the polygeneration system, is around 45% regardless of the case scenarios. However, by focusing only on the polygeneration system, the system exergetic efficiencies are 31% and 47% in the $Case_{hot\ climate}$ and the $Case_{cold\ climate}$, respectively; while the average system product cost in the $Case_{cold\ climate}$ is 41% lower than that in the $Case_{hot\ climate}$. The similarities observed in both cases are: the electric power has the lowest price, while the refrigeration capacity is more expensive than the electricity by a factor of ranging from 3-4; for the heating price, the factor decreases to approximately between 1.5-2.

For system optimization, the differential evolution and particle swarm optimization algorithms generally obtained consistent results. For better implementing these stochastic algorithms for thermal system design, many efforts were needed for designing reliable simulations in Aspen HYSYS® and tuning the optimization algorithms. A robust superstructure-based simulation ensures the smooth execution of the system structural optimization. Amongst 2304 alternative configurations, the new configuration of adding the recuperation and preheating design features to the initial system design was selected for the $Case_{hot\ climate}$; in contrast, the initially proposed system structure is the best system configuration for the $Case_{cold\ climate}$.

Zusammenfassung

Um die globale Ziele der nachhaltigen Entwicklung zu erreichen, ist die Effizienzsteigerung nachhaltiger Energiesysteme die kostengünstigste und kurzfristigste Option. Polygenerationssysteme verbessern die Systemeffizienz erheblich und minimieren den Ausstoß von Systemschadstoffen. In dieser Arbeit wurde ein neuartiges durch Abwärme betriebenes kleinausgelegtes Polygenerationssystem mit CO_2 als Arbeitsflüssigkeit vorgeschlagen, das für die lokale Strom- und Wärmeenergieversorgung verwendet wird. Ein solches eigenständiges System kann leicht mit anderen Anlagen integriert werden und die verschiedene verfügbare Wärmequellen nutzen. Der konzeptionelle Entwurf des neuartigen Polygenerationssystems, einschließlich der Systemsimulation, Systemuntersuchung und Systemoptimierung mit rechnergestützter Software, wurde konzentriert.

Exergie-basierte Methoden, einschließlich konventioneller und fortgeschrittener exergetischer und exergoökonomischer Analysen, wurden eingesetzt, um die System zu bewerten und das Ausmaß, den Ort und die Ursache komponenten- und systemweise realer Ineffizienzen zu identifizieren. Darüber hinaus wurde Aspen HYSYS$^{®}$ mit einem Python-Programm verbunden, um eine Automatisierung der Berechnung und Optimierung zu erreichen. Die Automatisierung ermöglicht die "Kommunikation" zwischen diesen beiden Programmen; so kann der manuelle Import und Export von Werten vermieden werden. Zur Lösung multimodaler Optimierungsprobleme, einschließlich der Einzelziel-, Mehrziel- und Superstruktur-basierten Optimierung, wurden populationsbasierte stochastische Algorithmen (differential evolution and particle swarm optimization) implementiert, um durch Überwindung lokaler Minima die global optimalen Ergebnisse zu finden.

Die Ergebnisse der Systemuntersuchung zeigten, dass die Temperaturen und Kosten der verfügbaren Wärmequellen die Produktkosten des Systems, insbesondere die Heizkosten, deutlich beeinflussen. Der Druck, der für die Verschmelzung zweier Subsysteme ausgelegt ist, ist ein kritischer Entscheidungsparameter. Niedrigere Produktkosten können in Fällen mit einer niedrigeren Umgebungstemperatur erzielt werden. In der Beispielstudie zur Rückgewinnung des Abgases eines 2 MW Erdgasmotors liegt der Gesamtsystemwirkungsgrad, einschließlich des Erdgasmotors und des Polygenerationssystems, unabhängig von den Beispielszenarien bei etwa 45%. Wenn man sich jedoch nur auf das Polygenerationssystem konzentriert, betragen die exergetischen Systemwirkungsgrade 31% bzw. 47% in der Fallstudie$_{\text{hot climate}}$ und in der Fallstudie$_{\text{cold climate}}$; während die durchschnittlichen Systemproduktkosten in der Fallstudie$_{\text{cold climate}}$ 41% niedriger sind als in der Fallstudie$_{\text{hot climate}}$. Die in beiden Fällen kann beobachtet werden, dass der Strom den niedrigsten Preis hat, während die Kälteleistung um einen Faktor von drei- bis vierfach teurer ist als der Strom; für den Wärmepreis sinkt der Faktor auf etwa 1,5 bis zwei.

Bei der Systemoptimierung erzielten die differential evolution and particle swarm optimization Algorithmen im Allgemeinen konsistente Ergebnisse. Für eine bessere Implementierung

dieser stochastischen Algorithmen für das thermische Systemdesign waren viele Anstrengungen erforderlich, um die zuverlässige Simulationen in Aspen HYSYS® zu entwerfen und die Optimierungsalgorithmen abzustimmen. Eine robuste Superstruktur-basierte Simulation gewährleistet die reibungslose Ausführung der strukturellen Systemoptimierung. Unter 2304 alternativen Konfigurationen wurde für die Fallstudie$_{\text{hot climate}}$ die neue Konfiguration ausgewählt, bei der die Rekuperations- und Vorwärm-Designmerkmale zum ursprünglichen Systementwurf hinzugefügt wurden; im Gegensatz dazu ist die ursprünglich vorgeschlagene Systemstruktur die beste Systemkonfiguration für die Fallstudie$_{\text{cold climate}}$.

Table of Contents

List of Figures

List of Tables

Abbreviations

CCUS	carbon capture, utilisation and storage
CDD	cooling degree days
CEPCI	chemical engineering's plant cost index
CM–P	compressor for power cycle
CM–R	compressor for refrigeration cycle
CO_2	carbon dioxide
COM	component object model
DE	differential evolution
EVAP	evaporator
EX	expander
GA	genetic algorithm
GEA	global energy assessment
GHG	greenhouse gas
GUI	graphical user interface
GWP	global warming potential
HE	heat exchanger
HPC	high-pressure compressor
HPT	high-pressure turbine
HS	heat source
HSI	heat source input
HSO	heat source output
HTR	high-temperature recuperator
IC	intercooler
ICE	internal combustion engine
IEA	international energy agency
LPC	low-pressure compressor
LPT	low-pressure turbine
LTR	low-temperature recuperator
MC	main compressor
MH	main heater
MINLP	mixed-integer nonlinear programming

Abbreviations

MIX	mixer
ODP	ozone depletion potential
ORC	organic Rankine cycle
PCHE	printed circuit heat exchanger
PH	preheater
PSO	particle swarm optimization
RC	re-compressor
RH	reheater
S-CO$_2$	supercritical carbon dioxide
SA	simulated annealing
SNL	Sandia National Laboratories
SPECO	specific exergy costing
SPLIT	splitter
SW	switch
T-CO$_2$	transcritical carbon dioxide
TV	throttling valve
VCC	vapor-compression cycle

Symbols

Sign	Description	Unit
A	heat transfer area	m^2
A	constant annuity	\$
$\dot{C}$	cost rate	\$/h
c	specific cost (per unit of exergy)	\$/GJ
CC	carry charge	\$
$CELF$	constant escalation levelization factor	-
COP	coefficient of performance	-
CRF	capital recovery factor	-
$\dot{E}$	exergy rate	kW
f	fraction/factor	-
FC	fuel cost	\$
h	specific enthalpy (per unit of mass)	kJ/kg
i_{eff}	effective interest rate	%
KE	kinetic energy	kJ
ke	specific kinetic energy (per unit of mass)	kJ/kg
LHV	lower heating value	MJ/kg
$LMTD$	logarithmic mean temperature difference	K
$\dot{m}$	mass flow rate	kg/h
n	economic lifetime of a plant	a
OMC	operating and maintenance cost	\$
P	present value	\$
p	pressure	bar
PE	potential energy	kJ
pe	specific potential energy (per unit of mass)	kJ/kg
PEC	purchased equipment cost	\$
PR	pressure ratio	-
$\dot{Q}$	heat transfer rate	kW
r	relative cost difference	-
r_i	constant average inflation rate	%
r_n	nominal escalation rate	%
r_r	real escalation rate	%
T	temperature	°C or K
TCI	total capital investment	\$

Symbols

Sign	Description	Unit
TIP	turbine inlet pressure	bar
TIT	turbine inlet temperature	°C or K
TRR	total revenue requirement	$
U	internal energy	kJ
V	volume	m³
$\dot{W}$	power	kW
XUI	exergy utilization index	%
$\dot{Z}$	cost rate associated with components/system	$/h
ε	exergetic efficiency	%
η	energetic efficiency	%
ρ	density	kg/m³
τ	annual full-load operation hours	h/a

Subscript and superscript

0	ambient condition
AV	avoidable
av.	average
CH	chemical
cv	control volume
D	destruction
e	outlet/exit stream
F	fuel
i	inlet stream
isen	isentropic
j	the serial number of stream
k	the serial number of component
KN	kinetic
L	loss/levelized
M	material/mechanical exergy
NG	natural gas
NGE	natural gas engine
P	power cycle/product/pressure
PGS	polygeneration system
PH	physical
pinch	pinch point
PT	potential
R	refrigeration cycle
T	temperature/thermal exergy
total	overall system
UN	unavoidable

1

Introduction

1.1 Background

Global energy demand grew by 2.3% in 2018 [1]. It was the fastest pace in this decade, driven by solid growth in the global economy and stronger heating and cooling requirements, which caused by the fact that more and more people are gaining access to modern energy services, and temperature anomalies have been experienced in many parts of the world caused by exceptional weather events [1, 2]. Meanwhile, in 2018, energy-related CO_2 emissions rose by 1.9%, which hit a historic high with the highest annual increment since 2013 [1] and contributed more than one third of total anthropogenic greenhouse gas (GHG) emissions [3].

In 2019, primary energy demand worldwide increased by 0.9%, which was 60% lower than the rate of growth in 2018 [4]. The dramatic slowdown can be explained by slower growth in the global economy and weather conditions (milder summer and winter in 2019) [4]. Besides, thanks to the increase in the share of renewable energies and less coal consumption, energy-related CO_2 emissions remained almost unchanged in 2019.

In 2020, the Covid-19 pandemic has caused an economic downturn worldwide, which suppressed global emissions temporarily. International energy agency (IEA) in the world energy outlook 2020 assessed that global energy demand in 2020 is set to decrease by 5% and energy-related CO_2 emissions will drop by 7% [5]. Despite these record decreases in global energy demand and emissions, weaker economic growth is not our strategy for achieving global sustainable development goals by 2050.

IEA in World Energy Outlook 2019 compared two different scenarios: a scenario based on the current stated policies and a scenario aiming for sustainable development. It revealed that in the stated policies scenario, a slowdown of annual average growth in primary energy is foreseeable [1]; however, the world is far from doing enough to achieve global sustainable development goals. With a relentless focus on improving energy efficiency and a shift from fossil fuels' combustion to renewable energies in the sustainable development scenario, the projected rise in the global economy and population can be accommodated without any increase in energy demand.

In Fig. 1.1, the projected solutions in the sustainable development scenario to transform the conventional energy systems into the sustainable energy systems are compared to that in the stated policies scenario. The solutions differ in terms of their relative proportions and the magnitudes of reducing energy-related CO_2 emissions, including a dramatic increase in energy efficiency, a larger share of renewable energies, decarbonization and modernization of energy systems powered by fossil fuels, and using the nuclear energy judiciously. Among all the solutions, increasing efficiency and boosting the share of renewable energies provide the most emission reductions of 37% and 32%, respectively [1]. Global energy assessment (GEA) [6] also mentioned that a sustainable future requires a major energy system transformation by 2050, and radical improvements in energy efficiency, shares of renewable energies, and advanced energy systems with carbon capture, utilisation and storage (CCUS) need to be addressed. Moreover, both reports [1, 6] concluded that energy efficiency improvement is the most cost-effective and near-term option, which can be achieved quickly. IEA even affirmed that energy efficiency should be considered the "first fuel" of global sustainable energy systems, and the demand for it needs to grow immediately.
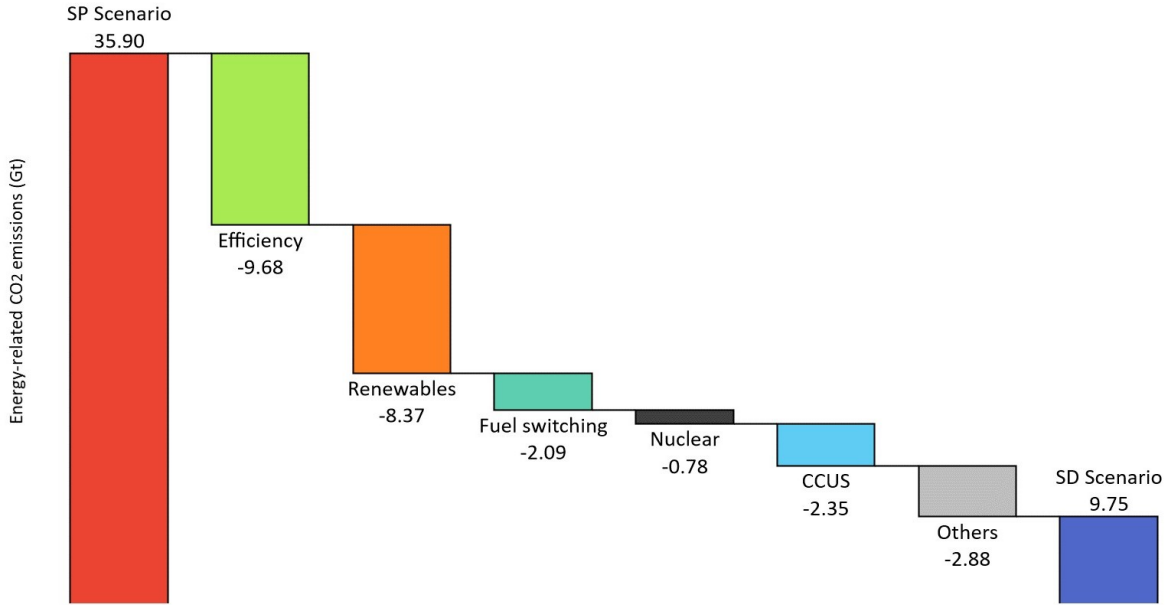
Figure 1.1: Reductions of energy-related CO_2 emissions by source from the stated policies (SP) scenario to the sustainable development (SD) scenario (adapted from [1]).

.

1.2 Motivation

For achieving the sustainable development goals, decentralized sustainable energy systems with high energy efficiency should be promoted to form the synergy between energy sectors and other sectors. Polygeneration systems, which can simultaneously produce two or more than two energy products in a single integrated process, show a significant increase in system efficiency [7, 8], in contrast to utilizing several systems to produce different products separately. Therefore, polygeneration systems are considered playing a more and more critical role in sustainable energy system development. To further mitigate the CO_2 emissions, polygeneration

systems are designed to be powered not only by fossil fuels but also by renewable energy sources [9]. There are different types of renewable energy-based polygeneration systems, including solar-based, biomass-based, fuel cell-based, and waste heat recovery-based [8].

On the demand side, of the increase in final energy demand, gas and electricity showed the strongest growth in 2018 [2]. Gas demand increase came mostly from the heating needs used in industry and buildings, while electricity demand growth was driven by its use in building sectors for heating and cooling [2]. As many countries, especially emerging and developing countries, are becoming more prosperous in the near future, more and more people will gain access to modern energy services and better quality dwellings. Consequently, the heating and cooling requirements are projected to continue to rise conspicuously. Moreover, as stated in [2], of the nearly 3 billion people currently living in the hottest regions of the world, more than 90% are without air conditioning access. Therefore, electricity demand for space cooling will triple by 2050 with the increasing air conditioning adoption worldwide.

However, the current global energy policies emphasize too much only on power generation to achieve sustainable development goals [8, 10]. The equally important thermal energies (heating and cooling) are neglected to a great extent, although around 40% of the final energy demand came from the demand of thermal energies [11]. The fact demonstrates the need to consider the global energy systems in a broader way, for example, shifting refrigeration systems from the electricity-based to non-electric (thermally activated refrigeration technologies). If the thermal energies and the power generation can be linked to use the fuels more efficiently, the polygeneration should have an excellent opportunity to play its role.

Therefore, a small-scale waste heat-driven polygeneration system using CO_2 as working fluid is proposed, evaluated, and optimized in this work. This system is designed for local power and thermal energy supply. Such a system is expected to be highly efficient, flexible, environmentally friendly, with a low investment cost and a small footprint. Besides, the product(s) cost of the system is anticipated to be appealing for the new system entering the market.

1.3   Thesis structure

The thesis focuses on the conceptual design of a small-scale waste heat-driven polygeneration system using CO_2 as working fluid. Chapter 2 reviews the recent progress in the fields of CO_2 as refrigerant applied for refrigeration systems, CO_2 as working fluid applied for closed power systems, and working fluids/working fluid pairs researched and proposed for heat-driven vapor-compression refrigeration cycle-based systems. Moreover, the novelty of the present work is also summarized in Chapter 2. Chapter 3 introduces the proposed polygeneration system using CO_2 as working fluid, inspired by the design of heat-driven vapor-compression refrigeration systems, and describes the potential benefits of applying such a system locally. Chapter 4 details and reasons the methods implemented in this study. The advantages of applying exergy-based methods over energy-based methods are discussed; the exergetic and exergoeconomic analyses applied for system investigation, as well as the stochastic algorithms used for system optimization, are explained thoroughly. Chapter 5 aims to evaluate the polygeneration system from a broad perspective without specifying waste heat sources. A

general impression of applying the polygeneration system under different operating conditions, regarding its system efficiency and product costs, is discovered by conducting several sensitivity analyses. Chapter 6 investigates a case study for engine waste-heat recovery, which utilizes the exhaust gas from a 2 MW natural gas engine to drive the polygeneration system. Conventional and advanced exergetic and exergoeconomic analyses for different cases, as well as parameter and structural optimizations, are established. Finally, Chapter 7 summarizes the conducted work, the main findings, the limitations, and the future work of the present thesis.

2

State of the art

For design engineers, working fluid selection is one of the main issues needs to be thoroughly addressed. The performance of an energy-conversion system, including refrigeration machine, heat pump, power generation system, and polygeneration system, is influenced significantly by its working fluid. Nowadays, natural working fluids are gaining more and more attention, as environmental friendliness has to be considered to design energy systems for synergizing and ultimately achieving the sustainable development goals.

In this work, CO_2 was selected as the only working fluid in this proposed polygeneration system to produce power, heating and refrigeration capacities. The design of the proposed system was inspired by the configuration of a heat-driven vapor-compression refrigeration machine. Contrary to a conventional vapor-compression refrigeration machine, heat is utilized to drive the entire polygeneration system, which couples a closed power cycle with a refrigeration cycle. In other words, CO_2 is applied as a refrigerant in the refrigeration cycle and also as a working fluid in the power cycle.

This chapter reviews the traits of applying CO_2 as the working fluid in refrigeration and power systems compared to other commonly used working fluids, and the current research regarding heat-driven vapor-compression refrigeration machines will be extensively discussed. The aim is to assert that a heat-driven vapor-compression refrigeration machine by applying CO_2 as working fluid is a promising polygeneration system in terms of its system performance, safety, and environmental benignity, which also demonstrates the main novelty of this work.

2.1   CO$_2$ as a natural working fluid

Carbon dioxide is one the the "oldest" natural refrigerants. Since CO_2 is abundant in the environment and easily available, its cost is, therefore, extremely low [12, 13]. Moreover, CO_2 is non-toxic, non-flammable, and belongs to the safety group of A1 [14]. In addition, CO_2 is very environmental benign having global warming potential (GWP) of 1 and without ozone depletion potential (ODP) [15, 16]. The comparison among CO_2 and other commonly used refrigerants regarding their environmental impacts is illustrated in Fig. 2.1.
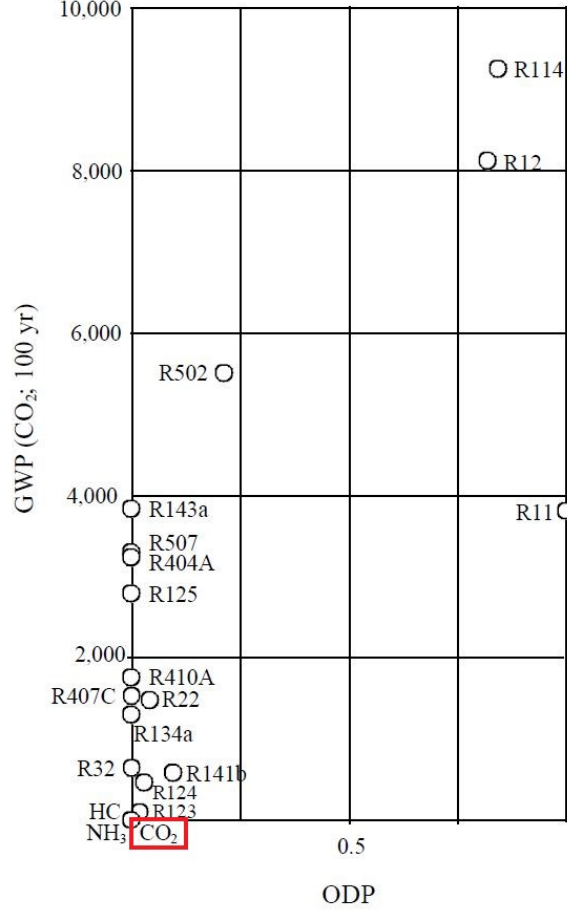
Figure 2.1: Environmental impact (including ODP and GWP) comparison of CO_2 and other working fluids [17].

One of the main reasons for reviving carbon dioxide and considering it nowadays as a nearly ideal refrigerant [12] is that it is a natural substance existing in our environment and known to be environmentally friendly. Professor Lorentzen (Norway, Norwegian Institute of Technology, and Norwegian University of Science and Technology) pointed out wisely in the 1920s [12, 18] that we should avoid the use of "foreign" substances as far as possible, which are mysterious to nature, and it turns out without exception that these "foreign" substances will eventually harm the biosphere and cause countless environmental issues.

The first closed power cycle using carbon dioxide as the working fluid was proposed and patented in 1950 [19]. However, the interests in supercritical carbon dioxide (S-CO_2) power cycles have emerged in the late 1990s and early 2000s [20, 21]. By virtue of the significant nonlinear-variations of thermophysical properties of CO_2 near its critical region, as illustrated in Fig. 2.2, the compression work of S-CO_2 power cycles is reduced dramatically due to the low compressibility (also known as the pump-like characteristic), which results in a higher system efficiency; while the unique characteristic of exhibiting an extremely high specific heat capacity in the vicinity of its critical point offers a great potential of releasing a considerable amount of heat capacity from the gas/water cooler (a heat exchanger), where the heat is rejected to the atmosphere. If the heat capacity within the gas/water cooler can be further utilized, the S-CO_2 power cycles can be considered as a cogeneration system with correspondingly a higher system efficiency.

In some applications (e.g. utilizing medium-grade heat sources), the S-CO$_2$ power cycle based technology has a great potential as a viable solution competing with conventional organic Rankine cycles (ORCs) and steam power cycles [22, 23]. Moreover, not only pure CO$_2$, but also CO$_2$-based mixtures [24, 25, 26] are profoundly investigated recently as alternative working mediums for power cycles, by blending a small quantity of properly selected inorganic compounds with carbon dioxide.
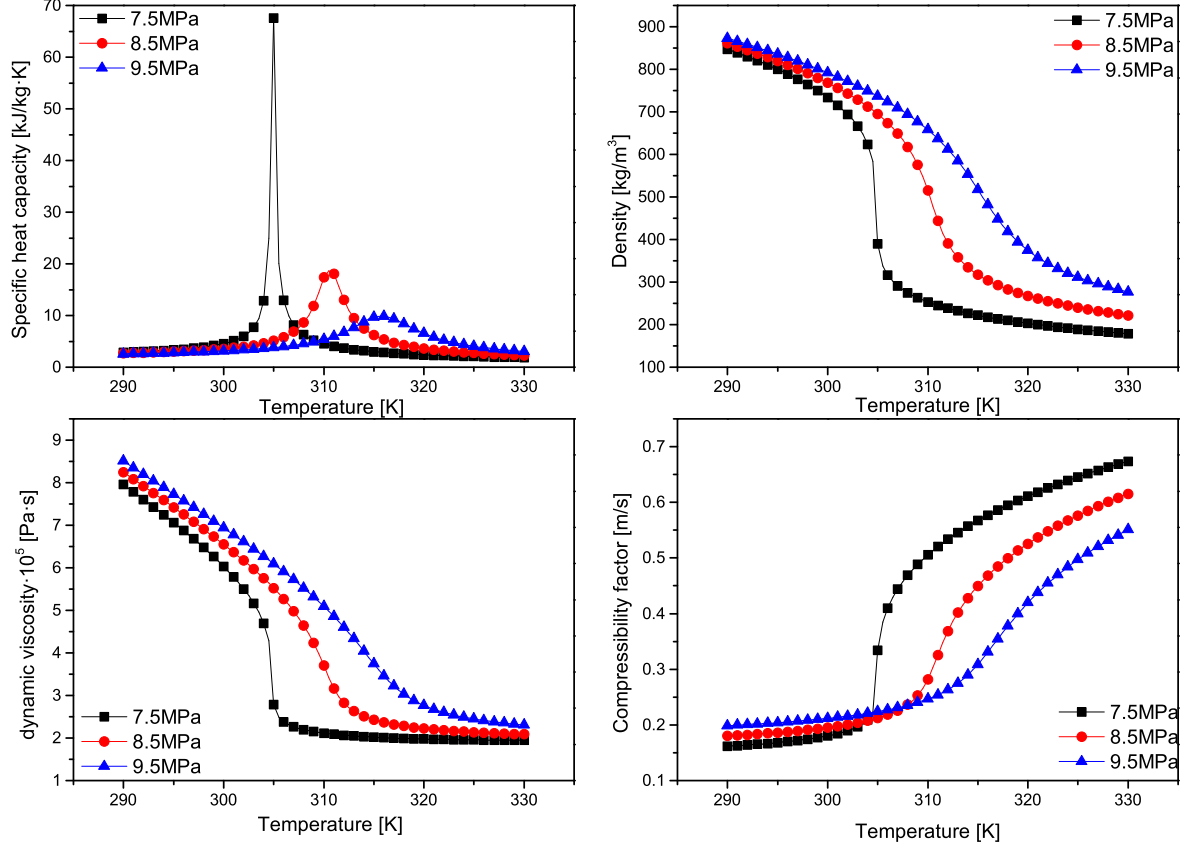
Figure 2.2: Thermophysical properties of CO$_2$ in the vicinity of its critical point [27].

2.1.1 CO₂ as a refrigerant

In human history, refrigeration technologies were discovered even earlier than the invention of electricity in the 1880s [28]. Air was applied as the working fluid in the earliest mechanical refrigeration machine [29]. In 1834, Evans and Perkins patented the vapor-compression refrigeration cycle with ether as its refrigerant [12, 30]. In 1850, Alexander Twining proposed and patented carbon dioxide using as a refrigerant [30, 31]. Later, CO$_2$ was one of the most widely used refrigerants in the infancy of refrigeration [31], along with ammonia and sulphur dioxide [12, 28]. From the 1830s to the 1930s, several refrigerants were investigated, and ether, NH$_3$, CO$_2$, SO$_2$, H$_2$O, CCl$_4$, HCOOCH$_3$, HCs, and CHCs were the mediating refrigerants. This can be considered as the first generation of the refrigerant progression (Fig. 2.3).

However, the refrigerants applied in the first generation of the refrigerant progression were mostly toxic, flammable, and accident-prone. By considering the safety and durability issues, the second generation began with the synthesis of dichlorodifluorocarbon (CCl$_2$F$_2$) molecules in 1929 [29, 33] and commercial production of chlorofluorocarbon (CFC-12) in 1932 [34]. In 1950s,
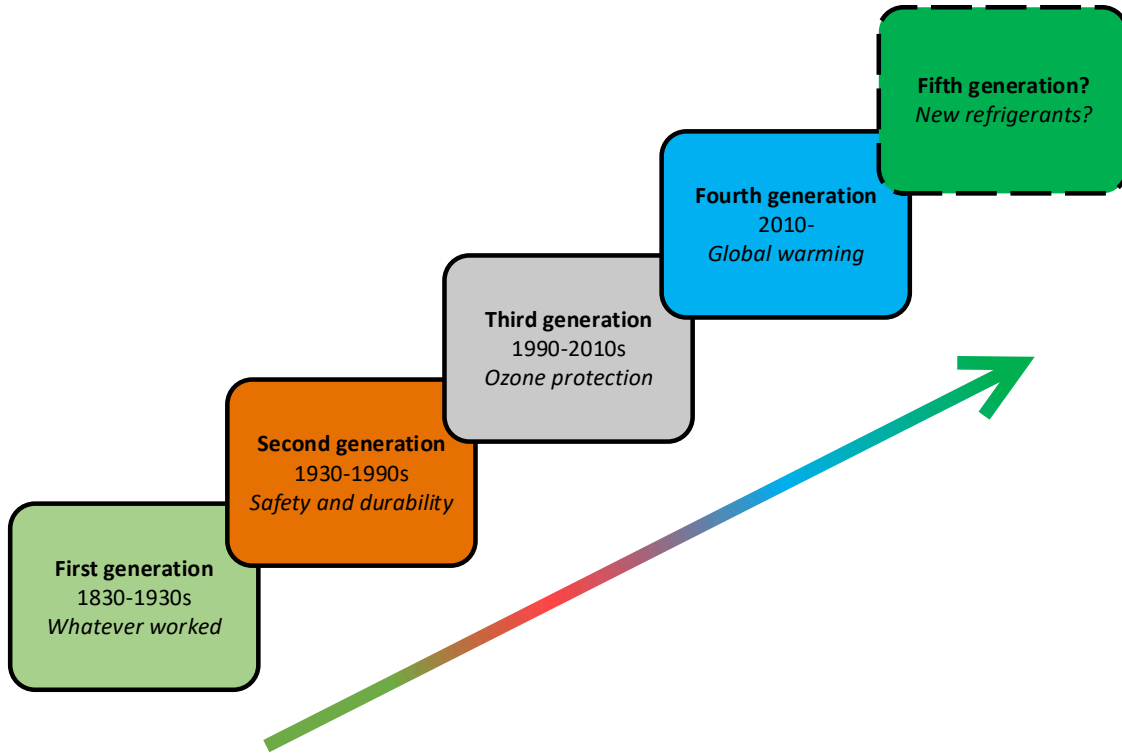
Figure 2.3: Generations of refrigerant progression [28, 32].

as illustrated in Fig. 2.4, CFCs together with hydrochlorofluorocarbons (HCFCs) became the definitive refrigerants since they were non-toxic, non-flammable, and with superior thermal performance. Meanwhile, carbon dioxide was eclipsed.

Later, CFCs and HCFC were noted to cause ozone depletion problems by releasing into the atmosphere [28, 35], therefore, were banned in 1987 under the Montreal protocol. The elimination of the chlorine containing refrigerants has been proved to counter the ozone depletion issues successfully [28, 29, 32]. As a replacement, hydrofluorocarbons (HFCs) were proposed and applied widely in almost all applications with a big success.

However, the HFCs have been revealed to bear high GWPs. They are destined to be phased out with more and more attention paid to global warming issues and aiming to achieve sustainable development goals by 2050. Several regulations for controlling emissions from fluorinated greenhouse gases (also called F-gas regulations) have been established, and more regulations will be established to address the impact of global warming. This results in a more complex choice in finding the appropriate refrigerants from environmental and thermodynamic points of view.

Compared to synthetic refrigerants, natural fluids, such as hydrocarbons (HCs), ammonia (R-717), CO_2 (R-744), water, and air, should be favored now since they are ozone-friendly and with lower GWPs. Nevertheless, no single fluid can be considered as a perfect solution, and the choice of the refrigerants for any applications has to compromise some drawbacks of a certain refrigerant. For example, most of the HCs are flammable and too dangerous to be used in large charge industrial applications [31]; ammonia is toxic and flammable, with reluctance [16]; water is inappropriate for low-temperature machines, and air can not be considered as an
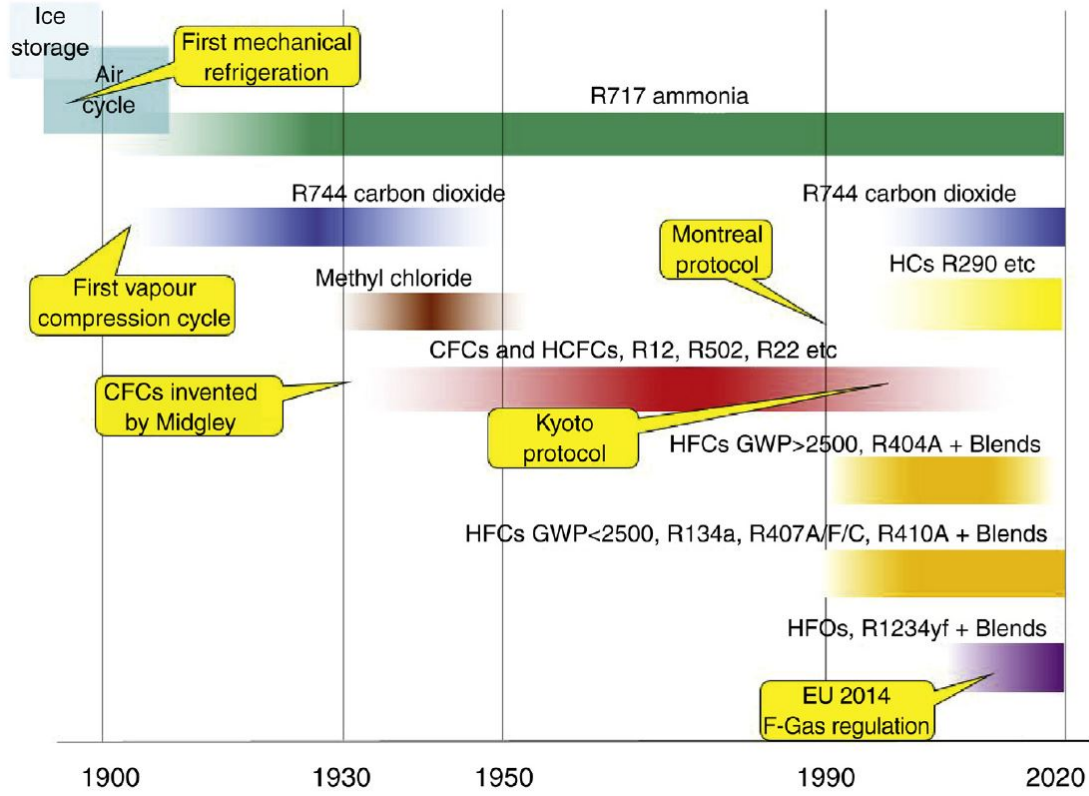
Figure 2.4: A brief histogram of refrigerants [29].

adequate refrigerant in most applications due to the low efficiency of air-based refrigeration machines; while CO$_2$-based refrigeration systems are operated at high pressure and may result in a lower coefficient of performance (*COP*).

Despite some disadvantages, CO$_2$, as a well-known natural working fluid, has strong potential to be used in refrigeration and heat pump applications. Before discovering any other new refrigerants, CO$_2$-based refrigeration systems should be addressed and immensely investigated.

2.1.2 CO$_2$ as a working fluid in power cycles

S-CO$_2$ has been proved and extensively investigated as one of the promising working fluids applied in closed-cycle gas turbine systems. The first closed-cycle gas turbine system was proposed and patented in 1935 at Escher-Wyss, in Zurich, Switzerland [36, 37]. Four years later, in 1939, Escher-Wyss built and operated its first test plant based on the design of the closed-cycle gas turbine system, driving a 2 MW generator using oil as the fuel and air as the working fluid [20, 36, 38]. In 1949, the first industrial closed-cycle gas turbine power plant was commissioned utilizing waste heat source and with air as its working fluid in Coventry, UK [39].

However, this technology was obscured and overshadowed in the late 1960s and the early 1970s by the more mature and high efficient open-cycle gas turbines [20, 37]. Because new materials and blade-cooling technologies were introduced in the late 1960s [37], a significant step improvement of open-cycle combustion turbines was achieved by allowing higher firing temperature.

Nowadays, the achievable turbine inlet temperature (TIT) in open-cycle gas turbine systems still outperforms that in closed-cycle gas turbine systems since the firing temperature of closed-cycle gas turbines is limited by the allowable maximal temperature of metallic heat exchangers [20]. Fig. 2.5 illustrates the trend of open-cycle and closed-cycle gas turbines in terms of their turbine inlet temperatures from the year 1930 until the year 2030. One can conclude that the closed-cycle gas turbines with current technology might not enable to replace the open-cycle gas turbines; however, the closed-cycle gas turbines show the potential of operating at a higher temperature and achieving better performance than steam Ranking cycles, and for some applications (such as nuclear reactors), open-cycle gas turbines are, unfortunately, not applicable, while only closed-cycle gas turbines can be deployed. Therefore, the interests in the study of the closed-cycle gas turbines are renewed and emerging, especially in the recent past, thanks to the achievement in Generation IV nuclear reactors [20, 21].
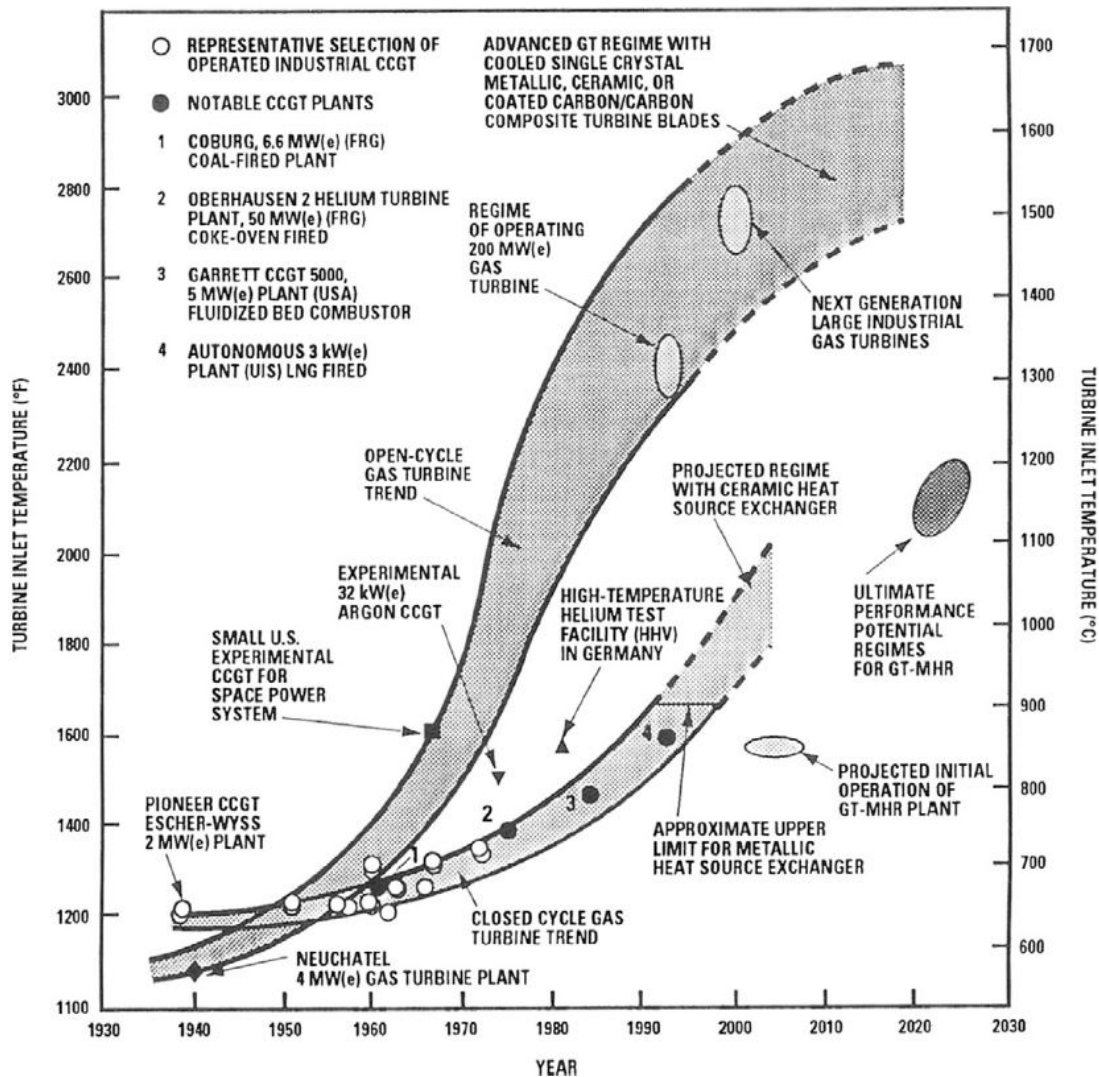
Figure 2.5: Trend of the increase in TIT of open-cycle and closed-cycle gas turbines [38].

Fig. 2.6 summarizes the commonly applied working fluids and heat sources of the closed-cycle gas turbine systems. Air, as one of the most well-known working fluids, was widely used in small closed-cycle gas turbine power plants until the 1970s; however, due to the greater power output demand, helium was considered as a more suitable working fluid [40] and it can

also be applied as a coolant for high-temperature gas reactors. The advantages of applying helium as the working fluid in closed-cycle gas turbines compared to air closed-cycle gas turbines include lower pressure loss, better heat transfer coefficient, and no Mach number restriction in turbomachinery design [20].
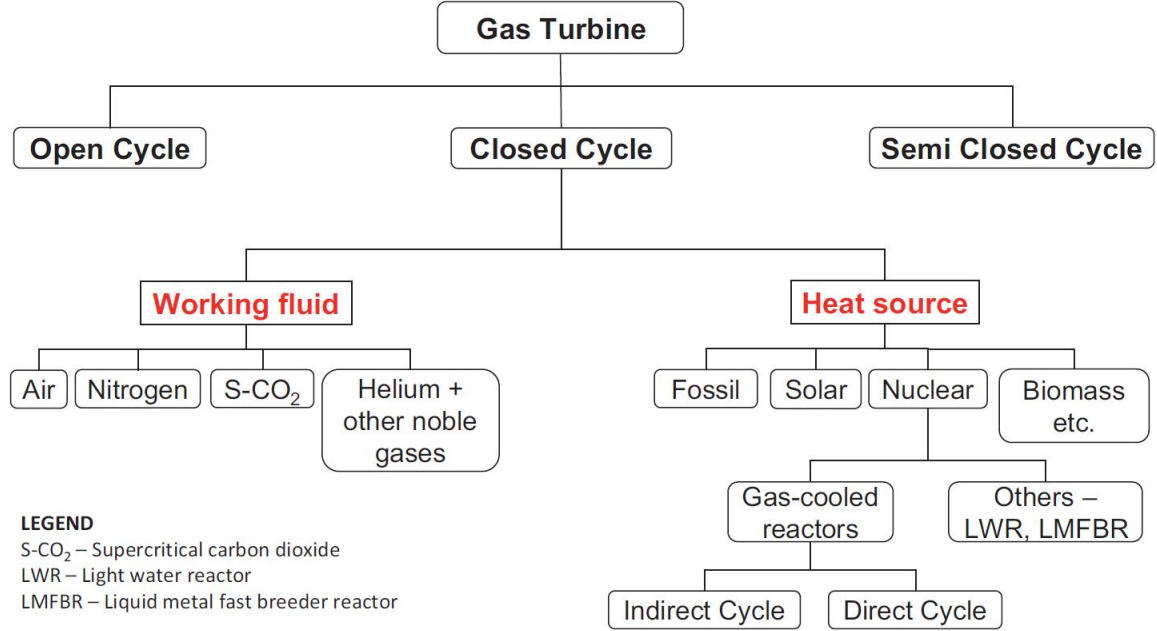
Figure 2.6: Classification of working fluids and heat sources applied in closed-cycle gas turbine systems [20].

Carbon dioxide closed-cycle gas turbine system was first proposed and patented in 1950 by Sulzer Brothers Ltd. (Gebrüder Sulzer) [19]. In the late 1960s and early 1970s, the research interests in the benefits of the unique thermophysical features of CO$_2$ as working fluid increased in the United States [41], Italy [42], Switzerland [43], and the Soviet Union [44]. The first landmark in developing the S-CO$_2$ closed-cycle power cycle was set by the pioneering works proposed by Angelino [42, 45] and Feher [41, 46]. In their pioneering works, the theoretical fundamentals of the innovatively conceptual power system design utilizing CO$_2$ as working fluid were introduced (shown in Fig. 2.7), and several possible configurations of the S-CO$_2$ closed-cycle power cycle were proposed (presented in Fig. 2.8). However, the interest in this technology after this period decayed with no deployment of the proposed system design since the technology maturity level of operating power systems at high pressure and high temperature was low.

In the late 1990s and early 2000s, since the development of Generation IV nuclear reactors got even more attention, the interest in finding alternative power conversion systems for successfully utilizing the high reactor outlet temperature (500-900 °C) increased as well [21]. When a steam cycle (with *TIT* higher than 550 °C) is applied to couple with a Generation IV nuclear power plant, the ultra-supercritical steam cycle is required for improving the system efficiency; while the plant reliability can be a significant issue [21] as the ultra-supercritical steam cycle suffers from the material degradation caused by the high operating temperature and pressure [21, 38]. Among various candidates, S-CO$_2$ closed power cycle has been considered as one of the promising solutions operating in the mild *TIT* region, which provides not only
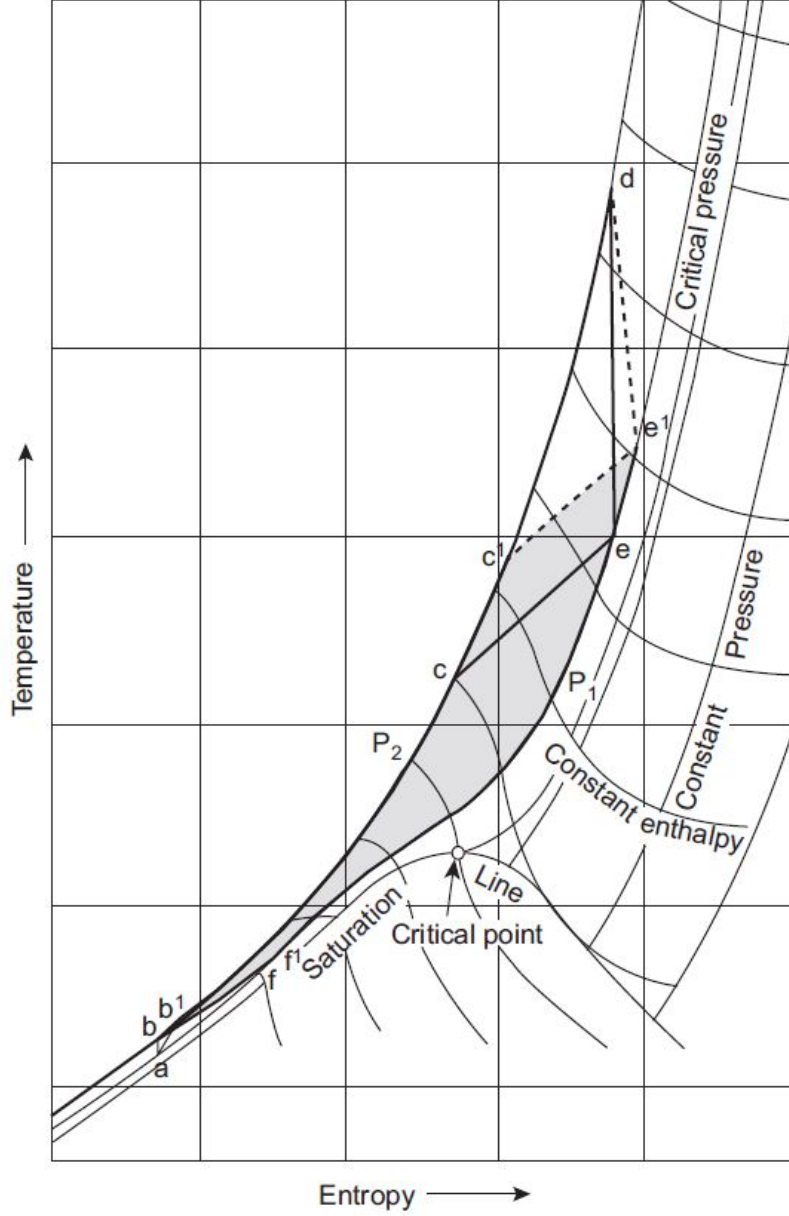
Figure 2.7: The concept of applying S-CO$_2$ as working fluid in closed-cycle gas turbine systems [42].

high system efficiency, but also better stability as well as improved safety and reliability. Since then, a renewal of interest in the closed power cycle with CO$_2$ as working fluid was kindled, and a lot of institutions and laboratories (for example, MIT in collaboration with Sandia National Laboratories (SNL) [47, 48], Czech Technical University [49], and Tokyo Institute of Technology [50]) involved intensively in the research of system design, turbomachinery investigation, prototype test, etc. Later, industry-based research also showed significant interest in commercializing this technology with commercial demonstrations in various applications [48, 51].

In Fig. 2.9, many of the applications, in which S-CO$_2$ power systems can be employed, are shown by categorizing different heat sources, including geothermal, industrial, solar, biomass/waste, nuclear, and fossil fuel combustion. In general, S-CO$_2$ power system applications offer smaller size, higher system efficiency, better utilization of the heat sources,
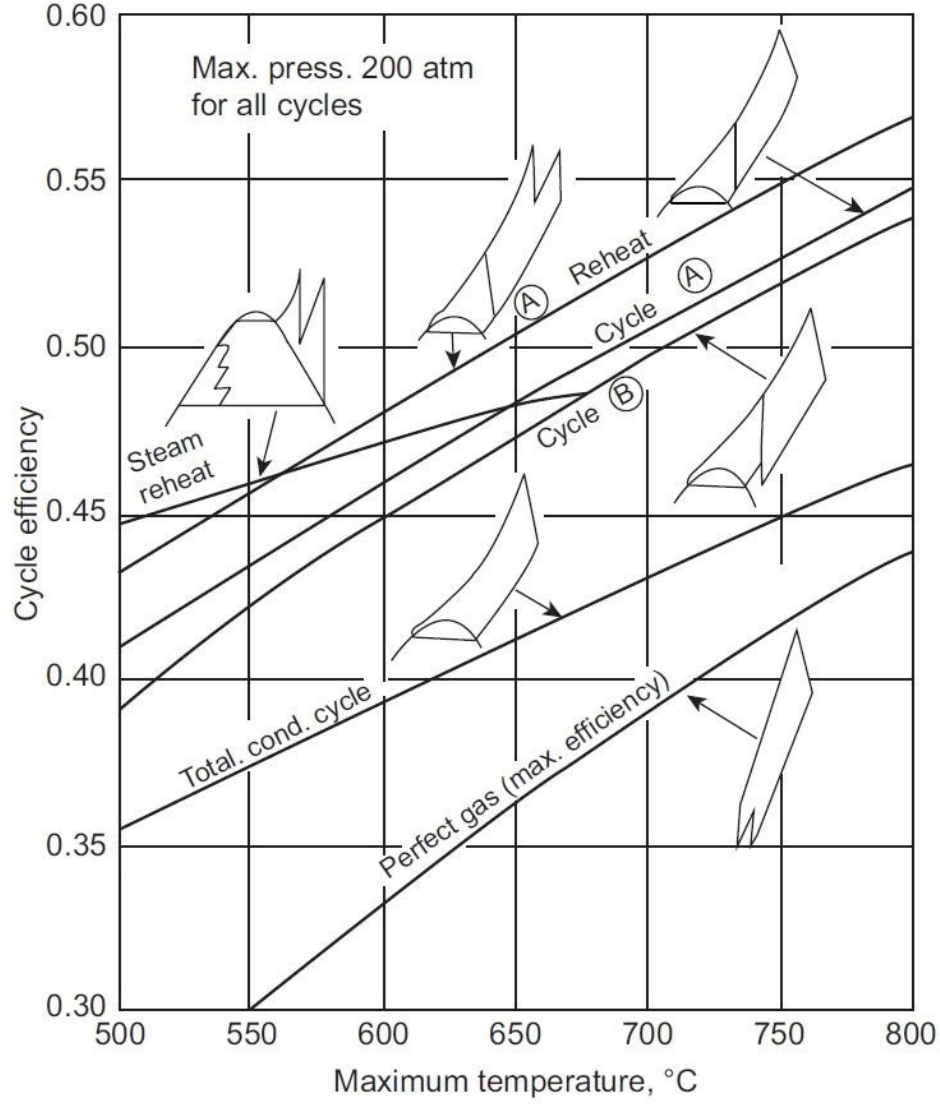
Figure 2.8: Different configurations of the S-CO$_2$ power cycles proposed by Angelino [42].

and less water usage [21, 52]. For the waste heat recovery application, the current technical solution mainly focuses on the ORCs, which use organic fluids instead of steam in a Rankine cycle. Compared to ORCs, applying S-CO$_2$ as the natural working fluid in a power cycle has the advantages of non-toxicity, non-flammability, better environmental performance, and lower capital investment cost. Moreover, the stability of S-CO$_2$ power cycles at elevated temperatures needs to be addressed, while such high temperatures may cause decomposition issues of employing ORCs. The primary disadvantage of S-CO$_2$ power cycles is the maturity and the readiness of this technology, including the technological newness and the lack of demonstration plants. Besides, thin profit margins and short expected payback time are also the additional factors that hinder the industry from adopting any waste heat recovery technologies [52].
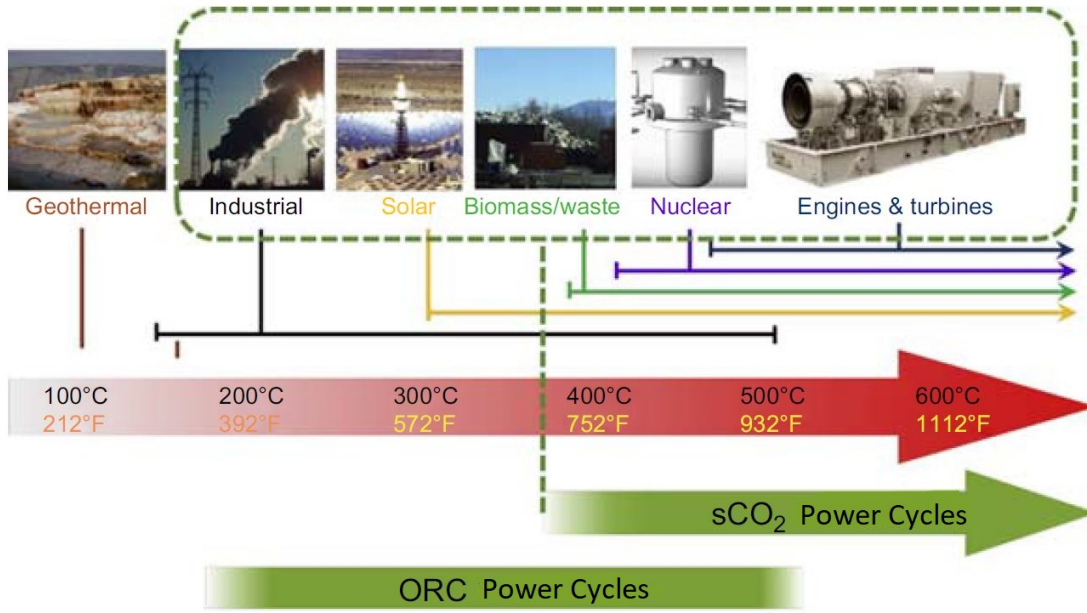
Figure 2.9: Different applications of the S-CO$_2$ power cycles by categorizing the origins and temperature ranges of various heat sources [52].

2.2 Current status and problem of space cooling

In 2016, global heating demand in buildings and industry outweighed the global cooling demand [53]. However, in recent years, as the incomes of citizens living in developing countries rise, urbanization advances [54], and global temperature increases, a dramatic increase in the use of air conditioning for space cooling [54, 55] and refrigeration for food and medical supplies [53] has been observed. Hence, the current global cooling demand is gradually growing and becoming one of the significant issues that need to be addressed worldwide, especially in developing countries [56].

Fig. 2.10 illustrates the average annual cooling degree days (CDD) for 219 countries and 1,692 cities based on the daily data obtained from more than 14,500 global weather monitoring stations from 2009–2018. By accumulating the temperature of "hot" days, having daily mean temperatures above 18.3 °C, the annual CDD are calculated, which is widely used for quantifying the cooling demand for a specific country or area [55, 57]. It can be noticed in Fig. 2.10 that vast of areas, particularly in Northern Africa, the Middle East, and Southern Asia, are exposed to more than 3,000 or even more than 4,000 average annual CDD. These areas are, in general, growing very fast; hence, no doubt that the use of air conditioning for space cooling is poised to soar.

In Ref. [57], authors modeled the worldwide energy demand for air conditioning purpose in comparison to that for heating in buildings. As shown in Fig. 2.11, the rate of the increase in electricity demand for air conditioning between 2020 and 2030 is at its peak, which is around 7% per year on average [57]; then after the year 2030, the rate of the increase stabilizes at 1% per year until the end of this century. For much of Europe, until 2030, the energy needed for cooling is likely to increase by more than 70%, while the energy demand for heating buildings will reduce by around 30% due to global warming [54]. Moreover, it is also estimated that by

14

around 2060, the amount of global energy used for air conditioning will overtake that used for heating [57]. Note that the total energy demand in heating for the buildings includes the energy used for space heating and water heating as well as cooking.
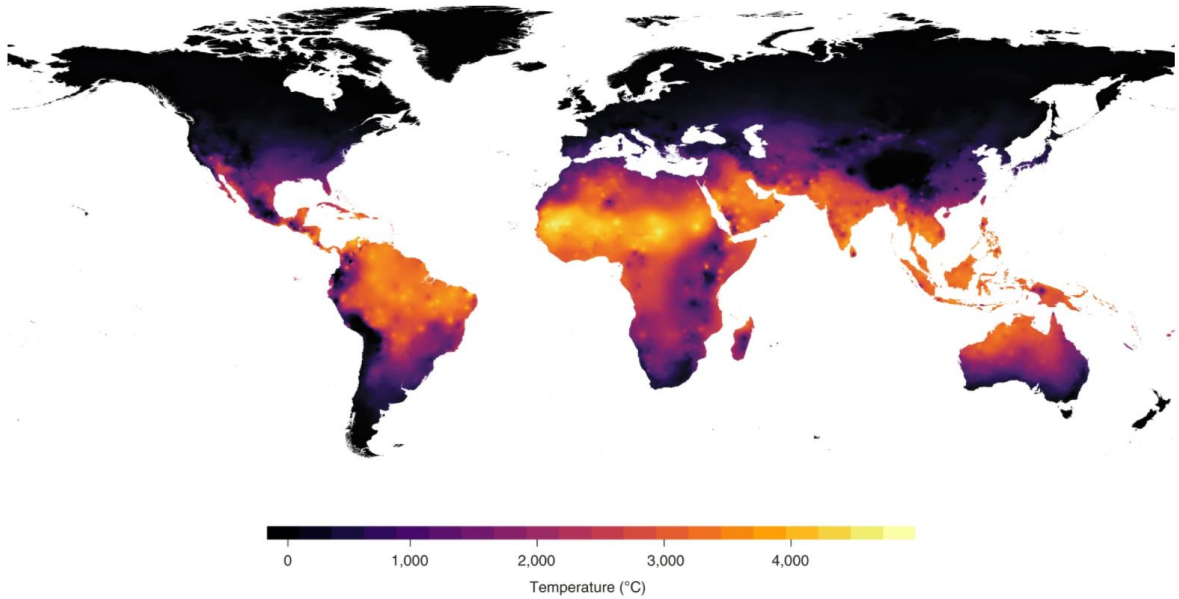
Figure 2.10: Average annual CDD for 219 countries and 1,692 cities in the period from year 2009 to 2018 [55].
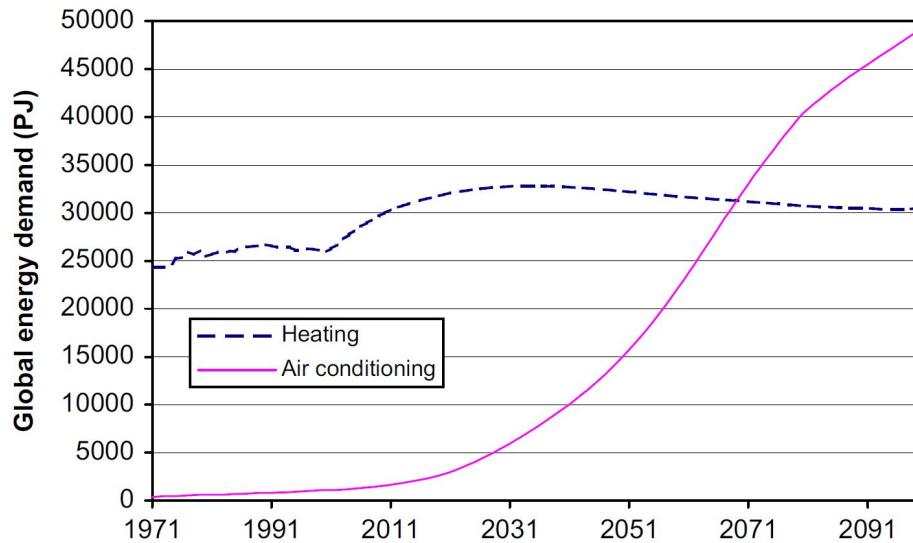
Figure 2.11: Trends of global residential electricity demand for heating and for air conditioning [57].

In terms of the global electricity demand by all end-use applications in building sectors (presented in Fig. 2.12), the amount of energy needed for each end-use application grows significantly over 2016-2050; however, no other end-use increases as fast as the space cooling. In 2016, appliances and plug loads is the largest user of electricity in buildings, but in 2050, space cooling is set to overtake the appliances and plug loads and become the largest user as the energy use for space cooling is projected to more than triple from 2,020 TWh in 2016 to

6,200 TWh in 2050 [58]. Hence, the share of space cooling energy demand in global electricity increases from around 10% in 2016 to 16% in 2050.
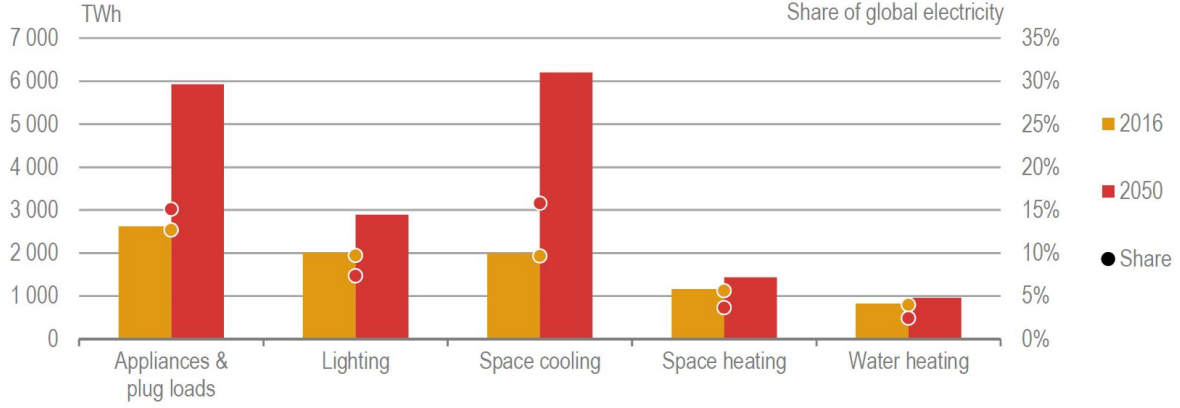
Figure 2.12: Electricity demand by end-use applications in buildings in 2050 compared to that in 2016 [58].

The conclusion is that the world is facing a looming "cold crunch", which is putting enormous strain on power systems worldwide, and its projected growth in energy use causes severe environmental issues, such as CO_2 emissions and local air pollutants [58]. Currently, the vapor-compression refrigeration system dominates the refrigeration applications for air conditioning of private residences, large public buildings, and other building services [59, 60]. The vapor-compression refrigeration machine, operating based on the most common refrigeration process–vapor-compression process, alters the working fluid's thermodynamic state in a reversed Carnot cycle with mechanical work supply [61]. Different variants of the Perkins cycle, which was the first vapor-compression cycle (VCC) patented in 1834 by Jacob Perkins [62], have been extensively investigated [60]. Fig. 2.13 demonstrates the basic concept of Perkins's closed-loop VCC. Mechanical work/electricity is required for powering such a machine.
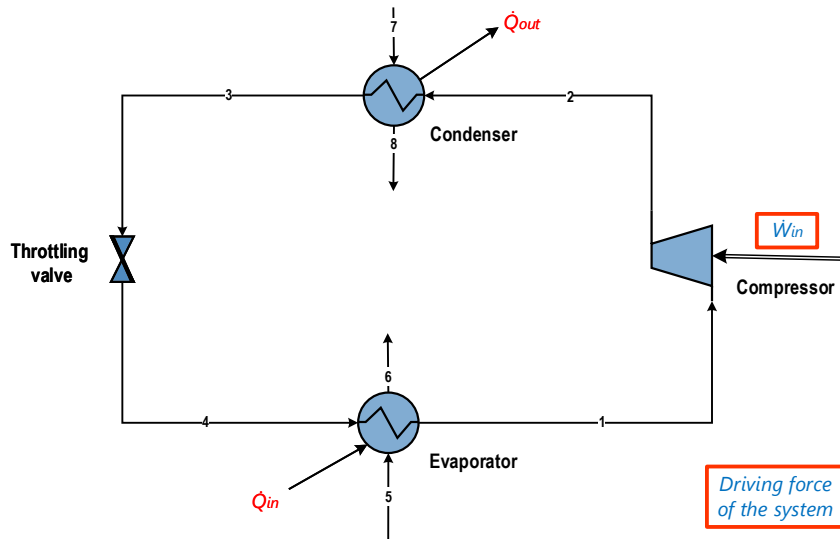
Figure 2.13: Simplified schematic of a simple one-stage vapor-compression refrigeration machine.

In the future, to reduce the energy demand in space cooling in buildings and mitigate the environmental issues caused by the projected growth in electricity use for space cooling, we need to focus on more efficient and/or renewable energy-based refrigeration systems. Refrigeration systems driven by thermal energy can be a promising alternative to tackle these problems.

2.3 Heat-driven vapor-compression refrigeration machine

There are several types of heat-driven refrigeration cycles, which can be considered alternatives to VCCs to utilize heat instead of electricity to drive a refrigeration system. The classification of the heat-driven refrigeration cycles is shown in Fig. 2.14. Among all these heat-driven refrigeration cycles, the absorption cycle is one of the most well-known technologies. Despite its well development, an absorption cycle has the following common disadvantages compared to a conventional VCC [29, 63]: 1. its initial investment is much higher due to its complexity in system design; 2. it is almost inevitable to encounter corrosion issues, which results in reducing the lifetime of the overall system; 3. since its working pressure is very low, the refrigeration system needs to be sealed very carefully; 4. its thermodynamic performance (COP) is poorer; 5. a small amount of electricity is still needed to drive the pump(s) within the system.

Clearly, VCC refrigeration systems are more commercially preferred all over the world. If a system can be designed by utilizing heat to drive the VCC refrigeration systems, which belongs to the thermo-mechanical refrigeration cycle in Fig. 2.14, the system will have a great potential of reducing emissions and harnessing different renewable energy sources.
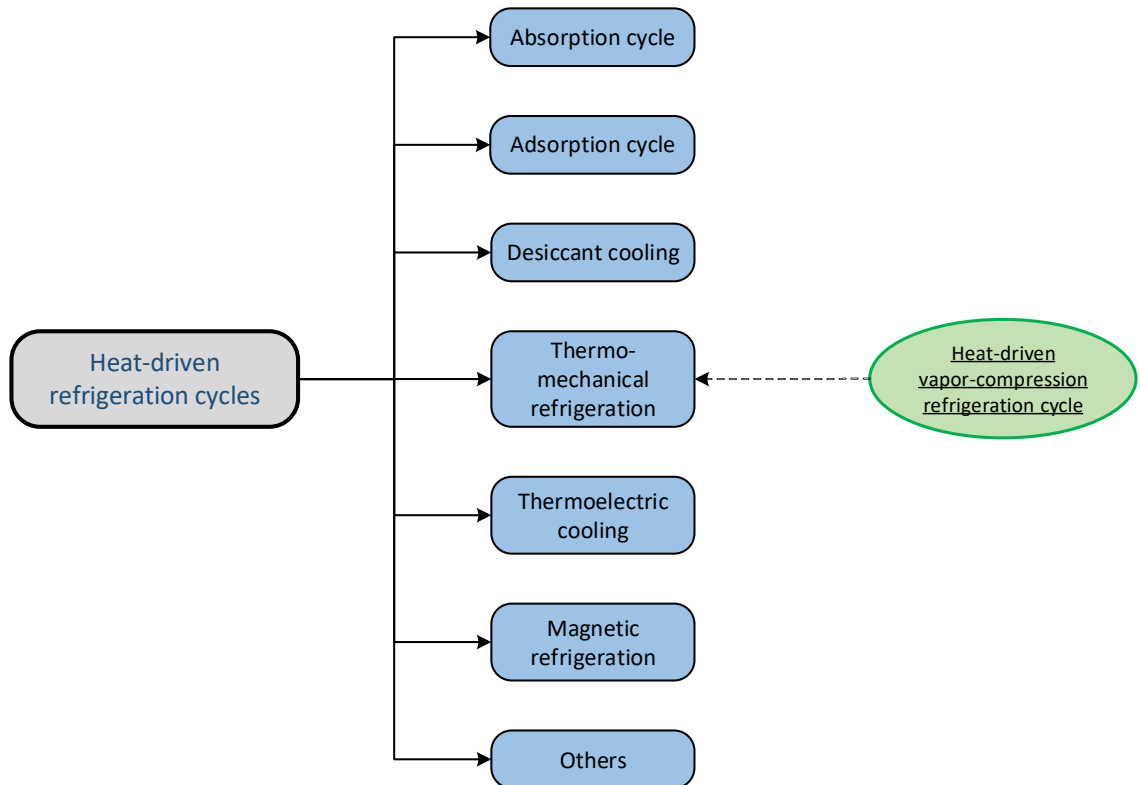
Figure 2.14: Classification of heat-driven refrigeration cycles [29, 64, 65].

The simplified schematic of a heat-driven vapor-compression refrigeration machine is shown in Fig. 2.15. The heat-driven VCC is composed of an ORC and a VCC; by harnessing heat potentially can be from different heat sources, the ORC generates enough shaft work to drive the VCC; thus, heat is the sole driving force to power the entire system and the system electricity supply is completely eliminated. Moreover, the system combines the ORC and the VCC with a mutual condenser to form a single unit. Such a stand-alone system can be integrated with other facilities easily due to its small size, or to be employed to harness available heat from different heat sources. The electricity generated from the expander and the heat capacity available within the condenser are two by-products for the system besides the refrigeration capacity obtained from the evaporator in the refrigeration cycle. Hence, the heat-driven vapor-compression refrigeration machine also has a great potential of being a polygeneration system by producing more than two products simultaneously.
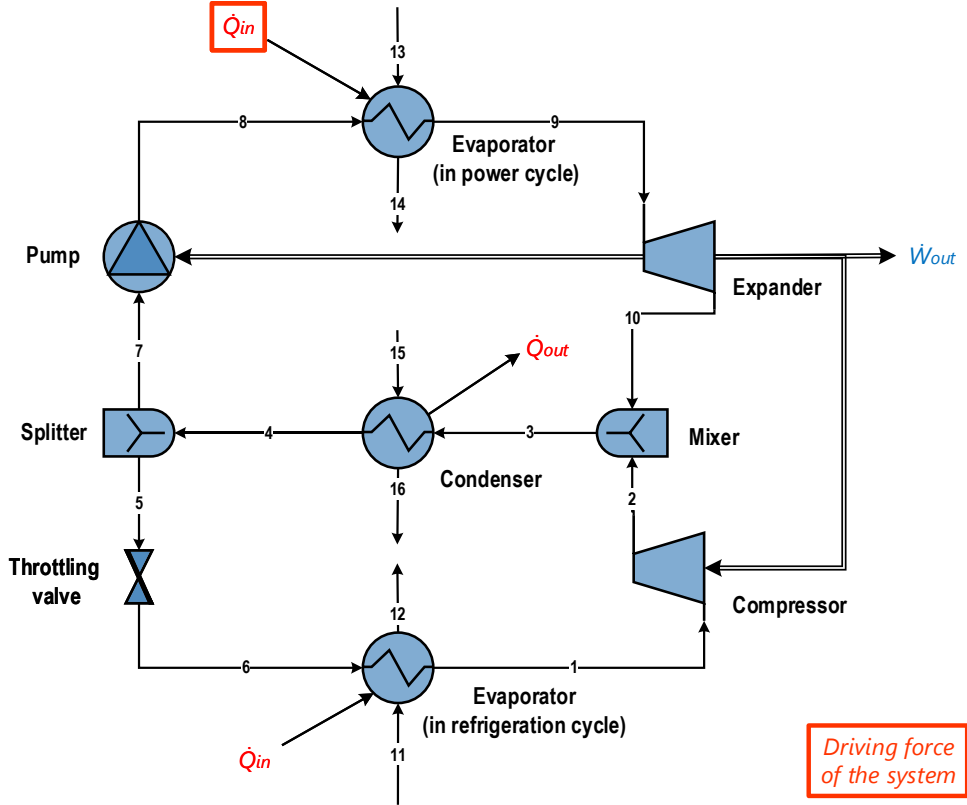
Figure 2.15: Simplified schematic of the heat-driven vapor-compression refrigeration cycle.

2.3.1 Study of heat-driven vapor-compression refrigeration cycle-based system

In spite of having several advantages, working fluid selection is still one of the major problems that need to be solved for designing a well-performed heat-driven vapor-compression refrigeration machine. Several potential working fluids, including working fluid pairs, have been proposed, investigated, and even tested for various applications. In this section, the representative studies of heat-driven vapor-compression refrigeration cycle-based systems that

have been published recently, especially regarding the working fluid selection issue, are listed and discussed chronologically.

Aphornratana and Sriveerakul [66] proposed a combined ORC–VCC system using R22 and R134a as the alternative working fluids for examining the overall system performance. The power cycle and the refrigeration cycle use the same working fluid and a mutual condenser. Low-grade thermal energy at a temperature higher than 80 °C was considered to power the entire system, and the evaporation temperature is at 5 °C. The results showed that the system applying R22 achieved a better performance than the system with R134a in terms of their *COPs*. A prototype of an ORC—VCC system was developed and tested in the laboratory by Wang et al. [67]. The system was designed to utilize low-grade waste heat from internal combustion engines (ICEs) to generate cooling for vehicles with a nominal refrigeration capacity of 5 kW. The temperature of the waste heat was simulated near 200 °C, and R245fa and R134a were selected as the working fluids for the power cycle and the refrigeration cycle, respectively. Since two different working fluids were applied in this system, two separate condensers in this experiment were used rather than a mutual condenser. The sub-cycles were only connected via the shaft work between the expander in the power cycle and the compressor in the refrigeration cycle. The same research group [68] also investigated the design configurations for a combined ORC–VCC with R245fa for military conditions operating with an extremely high ambient temperature of 48.9 °C. This study aimed to find the system's best configuration, which was designed for low- to medium-temperature applications and considered a cogeneration system by producing power and cooling. The best cycle (with subcooling and cooling recuperation) showed a 22% improvement in *COP* when compared to the base-case design. In this research, the same working fluid for both the power cycle and the refrigeration cycle was applied; thus, two sub-cycles were able to be combined through a mutual condenser.

Bu et al. [69] evaluated four working fluids (R123, R245fa, R600a, and R600) for an ORC-VCC to achieve the highest system efficiency. The authors proposed to utilize solar energy to drive an ice-making system, which is a very beneficial application in rural or remote places without sufficient electricity but with high solar radiation for food and vaccine preservation. The results revealed that the system with R123 as its working fluid achieved the highest overall system efficiency under the defined operating conditions. In Ref. [70], the authors took the system environmental performance into the system design consideration, and four natural hydrocarbons (propane R290, butane R600, isobutane R600a, and propylene R1270), therefore, were analyzed as the working fluids for an ORC–VCC system driven by low-grade thermal energy. The boiler exit temperature was set as 60-90 °C, and the evaporation temperature ranges from -15 to 15 °C. The conclusion was that R600 is the most promising working fluid with the overall *COP* of 0.47.

Similarly, in Ref. [71], the system efficiencies for an ORC–VCC using six different working fluids (R123, R134a, R245fa, R600a, R600, and R290) were evaluated and compared. Geothermal energy was harnessed for powering the ORC–VCC system for air conditioning purposes, and it concluded that R600a was the most suitable working fluid in this studied case. Kim and Perez-Blanco [72] studied an ORC–VCC cogeneration system producing power and refrigeration, which was designed to be activated by low-grade sensible energy, and eight potential working fluids were investigated. The heat source was assumed as air

at a temperature of 150 °C, and the evaporation temperature was set at 5 °C. The system performance of the refrigeration mode (a limiting case without net power production) and cogeneration mode (with power and refrigeration production) were researched in detail for all the working fluids. They concluded that the system has a great potential to utilize low-grade thermal sources, and the system performance depends on not only the working fluid selection but also the designed operating conditions. Moreover, the author pointed out that the overall system exergetic efficiency was proportional to the refrigeration capacity with a fixed heat source temperature and a given mass flow rate of the ORC. Molés et al. [73] proposed an ORC–VCC based machine to recover low-grade waste heat for generating cooling capacity. And they considered two low-GWP fluids as the working fluid for the ORC, while the other two low-GWP fluids as the working fluid for the VCC. The results revealed that the choice of the working fluid for the ORC has significant effects on the overall system performance; however, the working fluid selection for the VCC influences the overall system performance only to a limited extend. Moreover, among all the working fluid combinations, the combination of HFO-1336mzz(Z)/HFO-1234ze(E) shows the best system performance in terms of the value of *COP*; also, the system with this working fluid combination results in a promising economic performance with its payback period of 3.3 years.

Later, an ORC-VCC polygeneration system utilizing biomass fuel and solar power was proposed by Karellas and Braimakis [74]. The system was designed for producing refrigeration, heating, and power simultaneously. Besides the refrigeration and the power produced from the VCC and the ORC, respectively, the heat rejected by the mutual condenser was also considered to meet the local hot water demand. Three working fluids (namely, R134a, R152a, and R245fa) were examined. The results showed that the system with R245fa as working fluid achieved the highest thermal and exergetic efficiencies as well as *COP*. Hence, a detailed economic analysis considering a typical apartment block on an island of Greece employing the R245fa system was carried out. In this study, the system payback time is around seven years. In Ref. [75], forty-nine working fluid pairs, by combining seven potential working fluids for the ORC and the other seven working fluids for the VCC, were compared for an ORC-VCC system. The system was considered to use heat water at 100 °C as the heat source. The ambient temperature in this research was assumed between 30–40 °C, and the room with an air conditioning system should keep its temperature of 15 °C. R134a /R600a was examined as the best candidate by obtaining the system *COP* of 0.22. Saleh [76] suggested to apply ten commonly used HFCs and HCs as the candidates of the working fluid for an ORC–VCC system. The boiler exit temperature was assumed between 60-90 °C, while the evaporation temperature varies from -15 to 15 °C. The maximum system *COP* (0.72) was found by applying R600 as working fluid at the condensation temperature within the condenser at 30 °C.

Recently, the interest of researchers in CO_2 as working fluid for novel polygeneration systems is emerging. Besides the research of applying CO_2 just in power, or refrigeration, or heat pump applications, meanwhile, several new systems combining a CO_2 power cycle with (a) CO_2 refrigeration cycle(s) were also proposed and investigated. Akbari and Mahmoudi [77] investigated and optimized a cogeneration system, which coupled a CO_2 recompression closed power cycle with a modified CO_2 VCC. In the VCC, an expander was used instead of a throttling valve; and all expanders and compressors of this system were connected via

a mutual shaft. Having an expander in the VCC, no doubt, improves the system efficiency, but it may result in a considerably higher system investment cost from the economic point of view. Manjunath et al. [78] studied a CO_2 based cogeneration system producing power and refrigeration for naval ship applications. In this research, a CO_2 regenerative closed power cycle was combined with a CO_2 regenerative VCC. The shaft work generated from the expander in the power cycle was used for powering the compressor in the VCC. Two sub-cycles shared a mutual heat exchanger (a gas cooler in this case). In Ref. [79], Hou et al. reported a CO_2 trigeneration system also for shipboard applications, which recovered the waste heat from a marine gas turbine. The gas turbine waste heat was used to drive the entire system and produce refrigeration, power, and heating. In this paper, a CO_2 recompression power cycle, two CO_2 VCCs (having different evaporation temperatures but sharing a common expander), and a steam generator were included in the proposed system. All sub-cycles were connected with one shaft and a common heat exchanger. However, the design of the shared expander in both VCCs, which was supposed to have two outlet streams with various pressures, was not mentioned in detail.

2.4   Novelty of the present work

In the publications mentioned above, it is clear that for designing such a heat-driven vapor-compression refrigeration cycle-based system, the choice of a proper working fluid or a pair of working fluids is still one of the vital decision parameters. Moreover, all the system's decision parameters, particularly a novel system, need to be carefully selected in the system conceptual design phase.

CO_2, as one of the most promising working fluids in the future, has been extensively investigated in various applications. However, as reported in the literature, the CO_2 systems were mainly used for producing only one energy product. There are very few research papers where applying CO_2 as working fluid for a heat-driven vapor-compression refrigeration cycle-based system was discussed. A heat-driven vapor-compression refrigeration cycle-based system using CO_2 as its working fluid can offer excellent system efficiency by utilizing the unique thermophysical properties near its critical point of CO_2 and producing three energy products simultaneously. Moreover, such a stand-alone system is supposed to have superior environmental performance, surpassing system reliability, and considerably smaller system size.

Therefore, in this work, a novel heat-driven polygeneration system using CO_2 as working fluid, which was inspired by the system design of a heat-driven vapor-compression refrigeration machine, is proposed, analyzed, and optimized. Exergy-based methods, including conventional and advanced exergetic and exergoeconomic analyses, are implemented to evaluate the system performance. For system optimization, not only the parameter optimization but also the structural optimization are carried out. In addition, in this study, a professional simulation software (Aspen HYSYS®) is connected to a programming software (Python) to achieve optimization automation. The optimization algorithms are written in Python, while Aspen HYSYS® is used as a calculator for providing the simulation results for executing the optimization algorithms.

In short, in this thesis, a novel heat-driven polygeneration system using CO_2 as working fluid is proposed. And the conceptual design of this proposed polygeneration system is studied and investigated thoroughly from exergetic and exergoeconomic points of view. To further improve the system performance, optimization is also implemented, including optimizing the system decision parameters and the system configuration.

3

System design and description

The challenges (Fig. 3.1) for the energy supply sector are apparent [1, 2]: On the one hand, sufficient, secure, and reliable energies in different forms have to be supplied to ensure a robust global economy and to fulfill the needs of all the customers; but on the other hand, the energy-related CO_2 emissions have to be mitigated rapidly, and the energy supply sector needs to provide synergies for achieving global sustainable development goals [9], which include achieving universal energy access, decreasing the emissions causing air pollution problems, and tackling climate change and GHG emission issues. Almost all the goals for sustainable development accomplishment are closely related to energy. Thus, a realistic and cost-effective pathway for energy sector transformation towards sustainable development goals needs to be figured out. The destination of this pathway is named as sustainable energy system(s). The biggest hurdle of transforming the conventional energy system into the sustainable energy system is all the attributes of energy services [2], namely, availability, access, affordability, security, health, and environmental friendliness, must be met simultaneously.
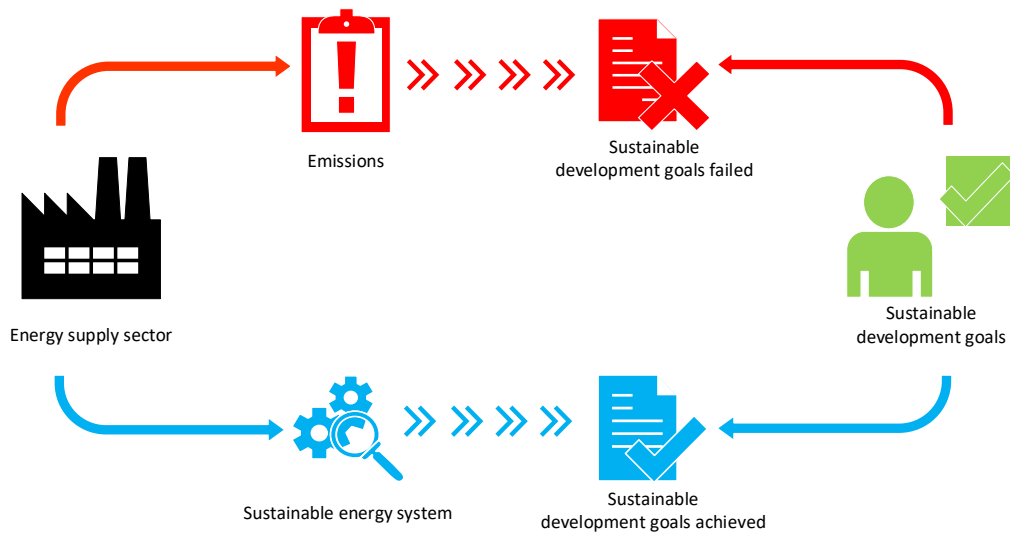
Figure 3.1: The challenges for the energy supply sector.

.

23

3.1 System design

Several design criteria need to be taken into consideration to design polygeneration systems helping to achieve sustainable development goals:

1. With the share of renewable energies in global primary energy increases and aiming at exceeding 90% in some regions by 2050 [6], the feasibility, the reliability, and the flexibility of the energy system are the crucial problems. The generation of most renewable energy sources is intermittent and variable, which is not designed to accommodate and handle the final users' requirements.

2. Consumption close to the site of generation and distributed energy systems are advocated by sustainable energy development [8]. In other words, the distributed generation concept, in contrast to the conventional centralized design, is promoted to eliminate the losses by long-distance transmission networks. Thus, the energy is produced locally, and the efficiency and the reliability of the energy systems will be improved [10, 80].

3. Waste heat potential is huge worldwide [81, 82, 83] (i.e., the waste heat potential in EU alone in industry amounts to around 300 TWh/year[81]); the technologies converting waste heat to other energy products provide avenues for sustainable energy [83]. Therefore, waste heat recovery technologies should gain more and more attention. The research should especially focus on reusing the waste heat in different sectors from the fossil fuel-based systems since it is probably inevitable that the energy system needs to still rely on fossil fuels in the short term.

4. Although innovation and efficiency are the key motivation for designers to transform an idea into a competitive industrial process. Environmental consideration is becoming a more critical factor in energy system design.

By considering all the design criteria, the design of a small-scale waste heat-driven polygeneration system is targeted in this work, as shown in Fig. 3.2. The system is designed to produce not only power but also heating and refrigeration capacities for local use. The system can be operated as a cogeneration or trigeneration system depending on the local requirement and the ambient conditions. Waste heat, as one of the renewable energy sources, is employed to drive the system. The heating and refrigeration capacities can be considered integrating into mini-district heating and district cooling networks for supplying on-site thermal energies efficiently to the end-users. Moreover, carbon dioxide is employed as the only working fluid for the entire system since it is gaining more and more attention and has been extensively researched as one of the potential working fluids in the future for both power and refrigeration cycles [52, 18, 84]. CO_2 is natural, non-toxic, non-flammable, inexpensive, and environmentally benign. The low critical temperature (31.1 °C) and the moderate critical pressure (73.8 bar) of CO_2 in conjunction with its unique thermodynamic properties (slightly above critical point and near saturation lines) create a high potential for operating the system in its supercritical region, which results in improving the thermodynamic and economic effectiveness of the power and refrigeration systems.
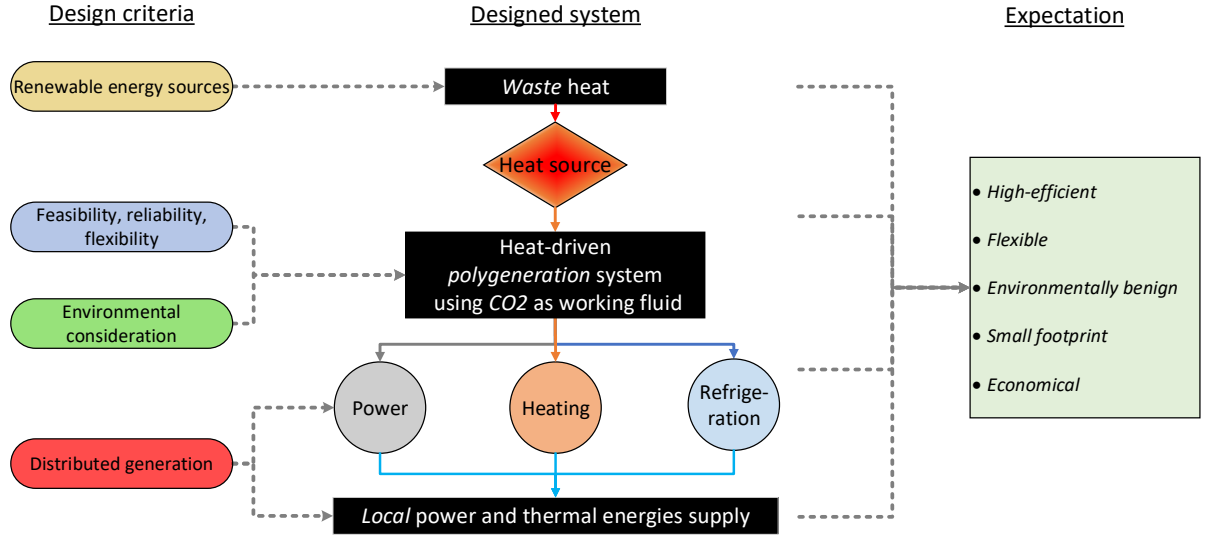
Figure 3.2: A targeted small-scale waste heat-driven polygeneration system using CO_2 as the working fluid for local power and thermal energies supply in this study.

.

3.2   System description

Fig. 3.3 presents a simplified process flow diagram of the proposed polygeneration system derived from the concept of the heat-driven vapor-compression refrigeration machine. Two sub-cycles can be observed: a power cycle and a refrigeration cycle. These two sub-cycles are combined with a mutual heat exchanger, and both of the cycles apply carbon dioxide as working fluid. The whole system consists of nine components: a heat exchanger (HE), an expander (EX), a mixer (MIX), a water/gas cooler (Cooler), a compressor for power cycle (CM–P), a splitter (SPLIT), a throttling valve (TV), an evaporator (EVAP) as well as a compressor for refrigeration cycle (CM–R). The heat source with low-medium temperature is considered as the "fuel" to drive the overall system. Any kinds of heat sources, in general, can be considered to use for driving the system, for example, solar thermal energy, heat from biomass, and waste heat from chemical plants and ICEs. The refrigeration capacity is generated from the EVAP. The heat capacity is available within the Cooler. The system can also yield power when the excess shaft work exists by deducting the work needed for powering CM–P and CM–R from the shaft work produced from the EX.
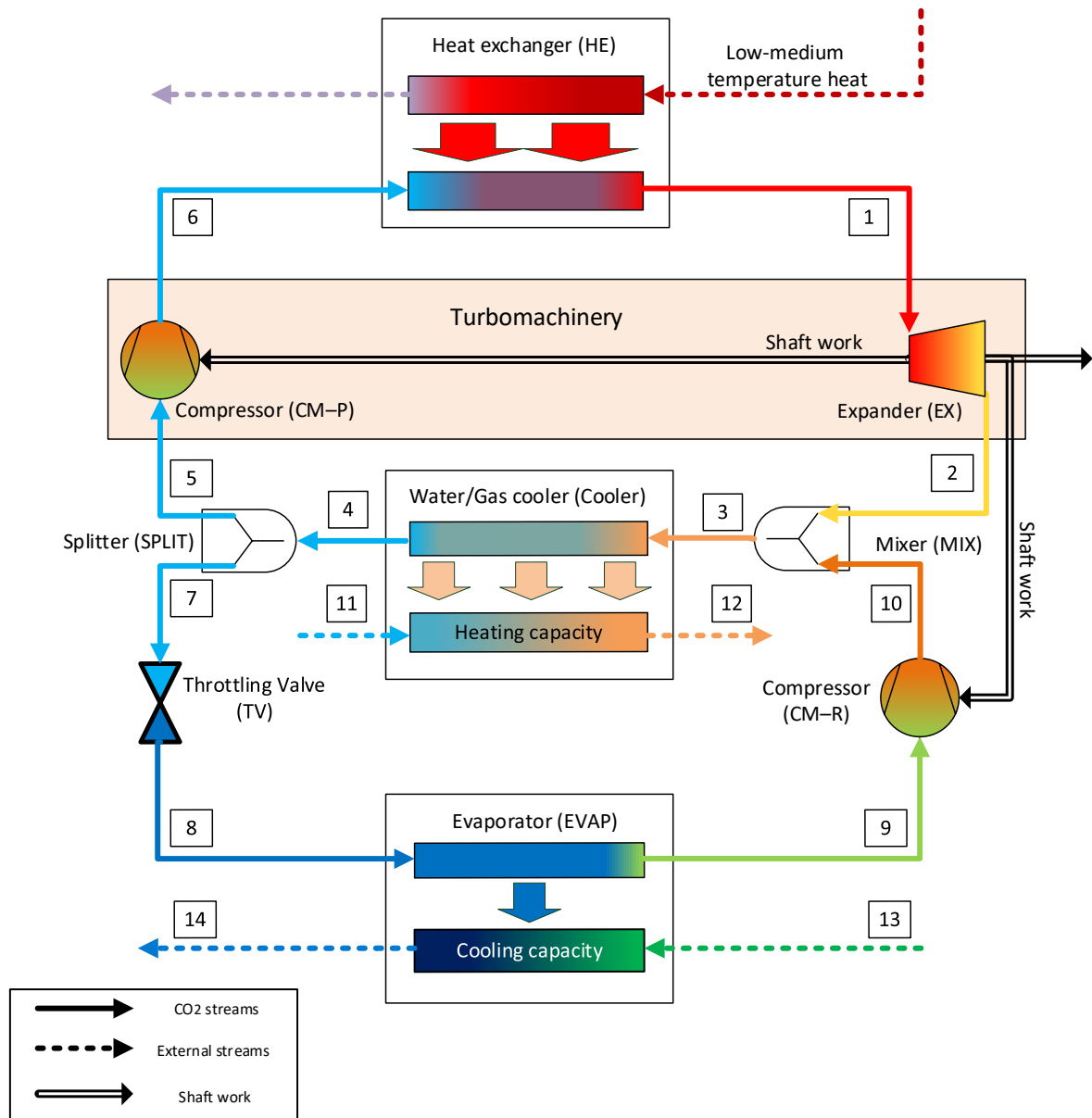
Figure 3.3: Simplified schematic of the proposed polygeneration system.

To demonstrate the novelty of a heat-driven vapor-compression refrigeration machine applying CO_2 as the working fluid compared to that with other commonly used working fluids (discussed in other studies in section 2.3.1), their pressure and enthalpy diagrams are shown in Fig. 3.4. Fig. 3.4 (a) represents the proposed polygeneration system with CO_2 as the working fluid, while the heat-driven vapor-compression refrigeration machine applying the other working fluids is shown in Fig. 3.4 (b).
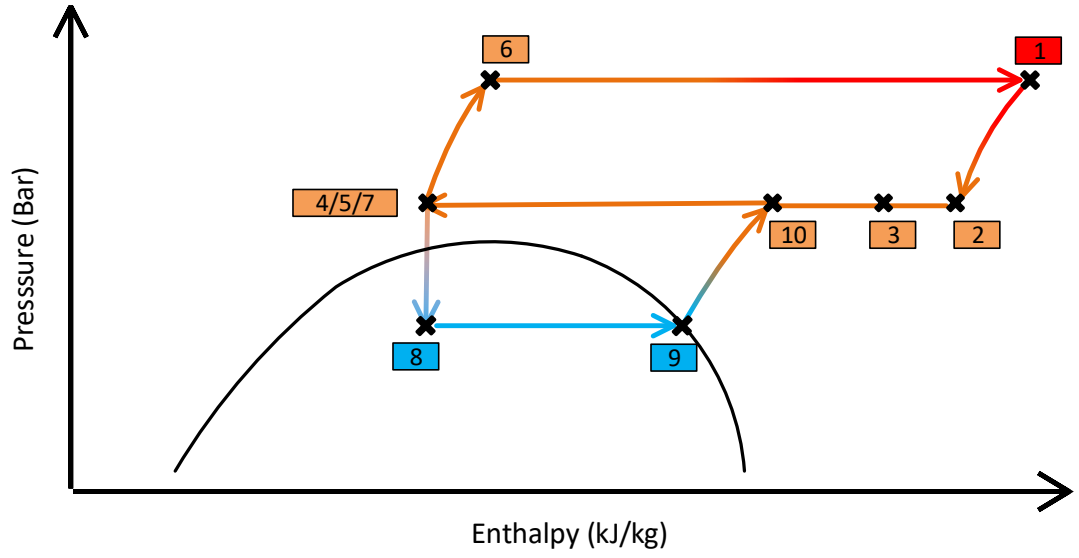
(a)
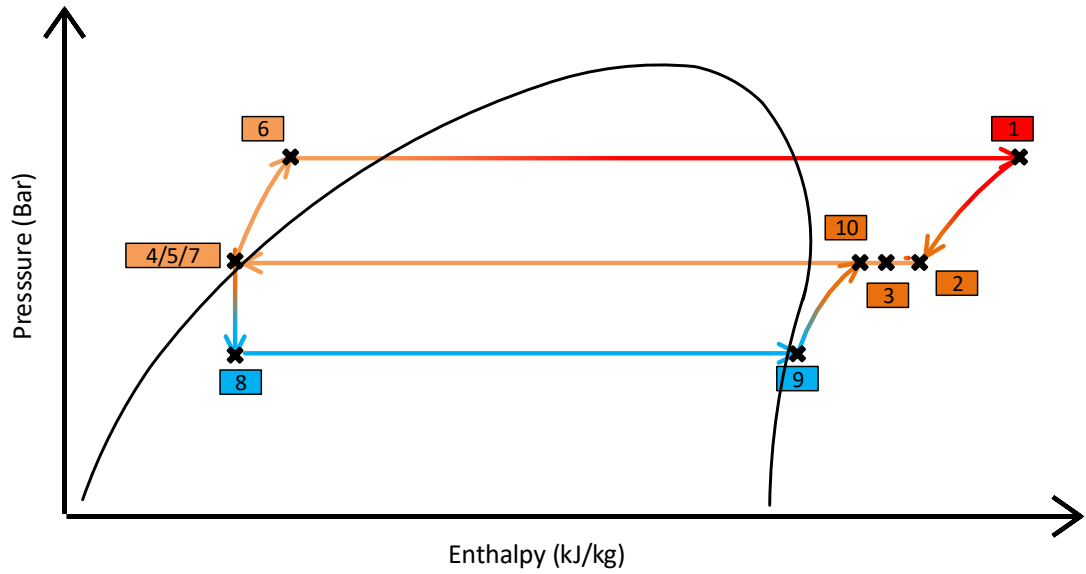
(b)

Figure 3.4: The pressure-enthalpy diagrams for heat-driven vapor-compression refrigeration machines: (a) with carbon dioxide as the working fluid, (b) with other commonly used working fluids.

It can be noticed that the whole cycle is below its critical point by applying the other working fluids. When CO_2 is selected as the working fluid for such a heat-driven vapor-compression refrigeration machine, the system operates partially above its critical point, namely, in the supercritical region, and partially in its subcritical zone. The S-CO_2 with the mass flow rate $\dot{m}_P$ is first heated by absorbing the heat from the moderate heat source within the HE. Then the supercritical working fluid with high temperature and high pressure enters the EX to generate shaft work. Subsequently, the S-CO_2 streams from the power cycle and the refrigeration cycle, which have the identical pressure p_m (merging pressure) but different

27

temperatures, are merged via the MIX. For cooling the supercritical working fluid, excess heat is rejected within the Cooler. Further, the S-CO$_2$ is split into two parts again via the SPLIT. One part enters the CM–P with $\dot{m}_P$, and the other part goes through the TV of the transcritical carbon dioxide (T-CO$_2$) refrigeration cycle with the mass flow rate $\dot{m}_R$. Finally, the outlet stream of the CM–P enters the HE again to complete the power cycle. For the refrigeration cycle, after the isentropic expansion process occurring within the TV, the CO$_2$ locates in the two-phase zone in the subcritical region, then it enters the EVAP for cooling the second refrigerant and being heated to saturated gas. Subsequently, the saturated gas is compressed by the CM–R and becomes S-CO$_2$ again before entering the MIX.

In short, with employing CO$_2$ as the working fluid for the heat-driven vapor-compression refrigeration system, the power sub-cycle operates entirely in the supercritical region, while the subcritical CO$_2$ passes its critical point and ends up with the S-CO$_2$ during the compression process of the refrigeration sub-cycle. Therefore, the design of the proposed polygeneration system, in other words, is the combination of the closed S-CO$_2$ power cycle and the T-CO$_2$ refrigeration cycle. By utilizing the advantageous characteristics of these two sub-cycles, the proposed trigeneration system is expected to be stand-alone, efficient, environmentally friendly, compact, and flexible. Moreover, it shows the potential to reduce not only the system cost but also the product(s) cost due to the high operating pressure and the low footprint.

The features of the proposed system, the general assumptions underlying the system, and the variables (including the design parameters and the nominal values of the decision variables) used for simulating the system are listed as follows:

- The system operates in steady-state conditions.

- The changes in kinetic and potential energies are neglected.

- Pressure drops in heat exchangers and pipes are neglected unless otherwise indicated.

- The refrigeration capacity is designed for air conditioning purposes, therefore, $T_{\text{EVAP}} = 5\ °C$ is selected. And the refrigeration capacity is set as 100 kW in energy.

- The heating capacity is designed for supplying domestic use of hot water and space heating locally. Thus, the cooling water enters and exits the Cooler with the temperature of 25 °C and 65 °C, respectively, which also meets the requirements of the return and supply temperatures for the fourth generation of the district heating development [85], $T_{11} = 25\ °C$; $T_{12} = 65\ °C$.

- The medium of the heat source (HS) is unknown, therefore, the average temperature of the heat source equals to 300 °C by default, $T_{\text{HS}} = 300\ °C$, unless otherwise indicated.

- The temperature of the secondary refrigerant entering the EVAP is always 15 K higher than the evaporation temperature, $T_{13} = T_{\text{EVAP}} + 15$ K.

- Two sub-systems are merged at the same pressure, which is designed to be near the critical pressure by default, $p_{\text{Merging}} = p_2 = p_{10} = 77$ bar, unless otherwise indicated.

- State 9 is saturated vapor since the influence of the superheating process within the EVAP on the performance of the T-CO$_2$ refrigeration cycle is relatively minor [86].

- The ambient temperature $T_0 = 25$ °C, the ambient pressure $p_0 = 1.013$ bar, unless otherwise indicated.

- The isentropic efficiency of both compressors (turbo-compressors), CM–P and CM–R, is equal to 0.85 [52, 87].

- The isentropic efficiency of the expander (turbo-expander) is assumed to be equal to 0.9 [52].

- Since the HE is assumed as a gas-gas heat exchanger, the turbine (expander) inlet temperature (TIT) is 20 K lower than the T_{HS} by default unless otherwise indicated.

- The Cooler and the EVAP are considered to operate with the pinch temperature difference of 5 K.

The ranges of the decision variables will be given and optimized in the sections of optimization studies; nominal values of the decision variables are selected throughout the thesis unless otherwise indicated.

3.3 Summary

In this chapter, the design of the proposed polygeneration system is described in detail. For helping energy sectors achieve their sustainable development goals in terms of increasing the system efficiency and mitigating the emissions, a novel waste heat-driven polygeneration system was proposed. The polygeneration system design was inspired by the system configuration of a heat-driven vapor-compression refrigeration machine, which combines two subsystems, namely, a closed power system and a vapor-compression refrigeration system, by a mutual heat exchanger. By utilizing CO_2 as the working fluid for the entire system, the power cycle is entirely operated in the supercritical region, while the refrigeration cycle is operated crossing the subcritical and the supercritical areas. Although the initial idea of the heat-driven compression refrigeration machine is to produce the refrigeration effect, in this study with CO_2 as the working fluid, the power and heat capacities that can be potentially produced from the system are also considered as system products. It can boost the system efficiency, and the system can be applied for supplying power, heat, and refrigeration capacities simultaneously for a local community.

4

Methodology

This chapter reasons and details the methods applied for system design, simulation, evaluation, and optimization. Essential steps applied for thermal system design are discussed first to clarify the current work's research focus and scope. The simulation and the automation processes, as well as the criteria/analyses used for evaluating the designed system, are illustrated. Lastly, the optimization procedures with associated algorithms are given in detail.

4.1 Thermal system design

For thermal system design, there are five essential steps that need to be followed [88]:

1. Understanding the problem;

2. Conceptual design and development;

3. Detailed design;

4. Project engineering;

5. Service.

In the first step, the problem needs to be identified, and the question "what to do" has been answered. Then the design phase shifts to the second step-conceptual design and development-regarding "how to do". This step is the most critical step of the design process as the decision made in this step will affect all the following steps, and it is responsible for most of the investment cost of an industrial project [89]. That is to say, the conceptual design plays a crucial role in the success of a project [88]. As shown in Fig. 4.1, if we overview the opportunity for cost reduction and the cost in all the phases of the life-cycle for an industrial project, the conceptual design phase can contribute more than 30% in cost reduction opportunities, while it takes only about 2% of the total project cost [90, 89]. In the current study, the problems we face and the urgency of high-efficient thermal system design for helping energy sectors achieve sustainable development goals are investigated and summarized in Chapters 1 and 2. In the rest of the thesis, only the conceptual design of the proposed polygeneration system

is extensively investigated, as it is the author's primary research interest. Thus, this paper's scope is limited to the conceptual design of a small-scale renewable energy-based heat-driven polygeneration system.
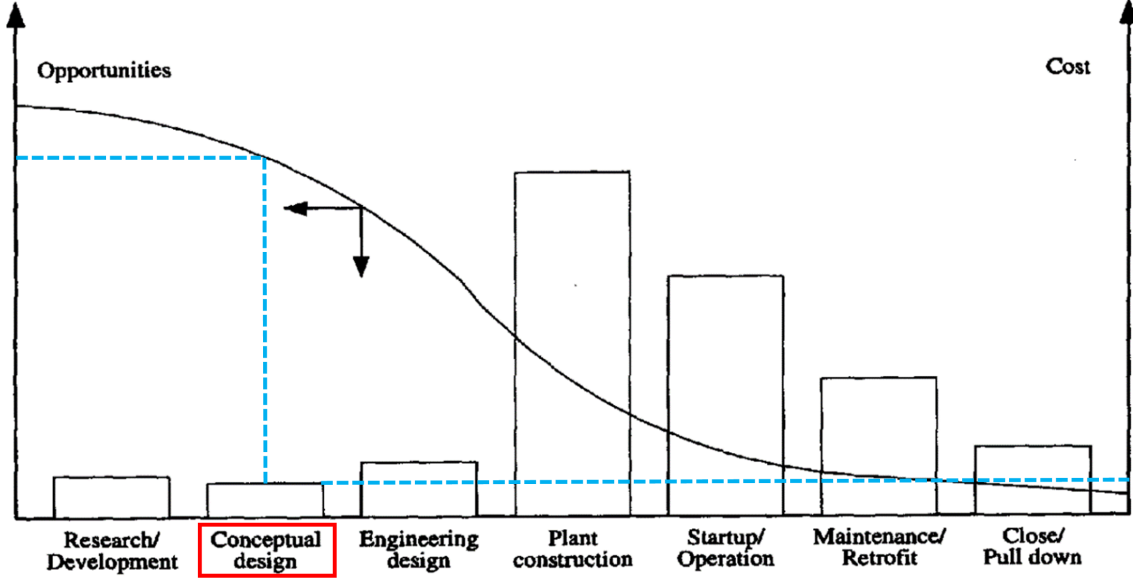
Figure 4.1: The opportunity for cost reduction and the associated cost in all phases for an industrial project [90].

.

A representative conceptual design cycle for a thermal system is illustrated in Fig. 4.2. The conceptual design cycle is, interestingly but not surprisingly, quite similar to the basic design cycle proposed by Roozenburg and Eekels [91], which is the most fundamental design model and it can be applied for almost all the design problems. A designer needs to create a new product with solid knowledge, creativity, intuition, and experience. The point of departure in the basic design cycle is identifying the new product's functions, then the design criteria in the next analysis step need to be formulated. The list of criteria is also called the "performance specification". Similarly, to design a new thermal system, its functions are identified once the problems that need to be solved are understood. Then the design requirements/criteria and the object of the newly designed system can be determined. After that, a provisional design proposal combining different new ideas needs to be generated in the synthesis step, which contains several alternative design options. The simulation process should then be carried out based on the outcome of the product synthesis step. This step is a process to form an image of the designed product by, most of the time, testing models. In the conceptual design of a thermal system, the simulations are, in general, implemented by computer-aided software. To evaluate the new design's performance, the designer needs to also check the product "quality" from different points of view. Thermodynamic performance, cost of the system product(s), environmental friendliness, safety, and reliability, etc. should be all taken into considerations in designing a thermal system. Last but not least, optimization is also an essential step in the conceptual design cycle to further improve the designed system.

In this study, the research focuses mainly on system simulation, evaluation, and optimization. For the system synthesis, the base-case design of the proposed polygeneration system, being an initial point of this conceptual design, is considered the sole provisional design. In the
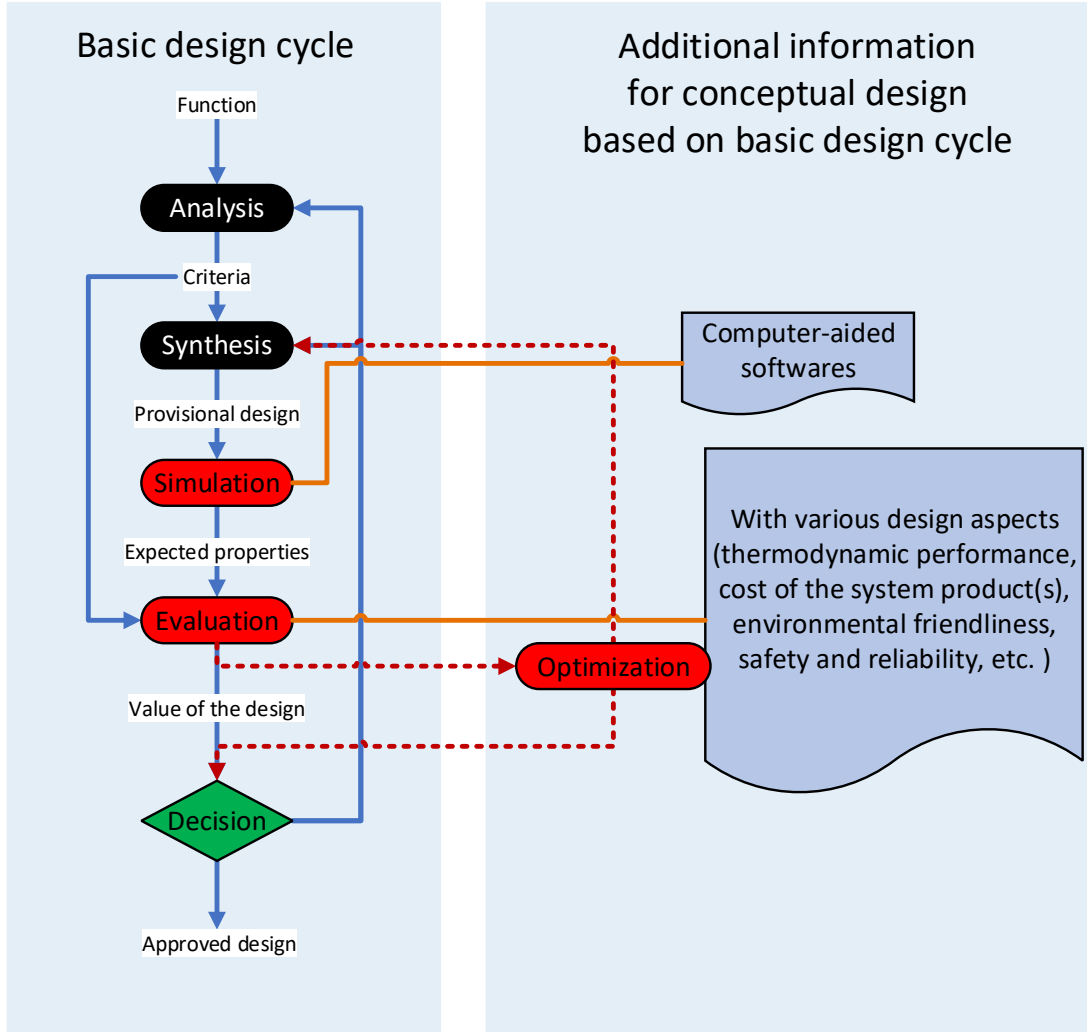
Figure 4.2: The basic design cycle adopted from [91] and the additional information for conceptual design of thermal systems.

.

optimization step, however, alternative design configurations are included and compared in the structural optimization process, which encompasses system synthesis, simulation, and evaluation. Moreover, the design criteria for the proposed polygeneration system, which should be identified in the design analysis process, are simplified and limited to the system performance in terms of having a high system efficiency and a low product cost, although there are several other criteria should also be included for designing a thermal system.

In short, this work focuses on designing the proposed polygeneration system in the conceptual design phase, and the system performance regarding the system efficiency and the product cost is examined and improved in the simulation, evaluation, and optimization processes. Other processes in the conceptual design phase are simplified, and the following steps after the conceptual design for a life-cycle design of a thermal system are out of the research scope.

4.2 Methods for system simulation and automation

Aspen HYSYS® (AspenTech, Bedford, MA, USA), a professional commercialized simulation software, is used for system simulation in this work. Thus, the fundamental thermodynamic balances (i.e., mass and energy balances) are solved in Aspen HYSYS®. The Span-Wagner equation of state is selected for calculating the thermodynamic properties of CO_2 since it is one of the most accurate models to predict CO_2 behaviors in a wide range of temperature and pressure, including at high temperature, at high pressure, and in the vicinity of its critical point [92].

Once the simulations are successfully executed in Aspen HYSYS®, the results obtained from the simulations are exported and further computed for system analysis, evaluation, and optimization. During the system analysis, evaluation, and optimization processes, however, it is inevitable that certain values need to be fed into the simulation software as well. With the aid of programming software, the values/parameters being exported from the simulation software and imported into the simulation software can be automated. In other words, there is no need to import and export the values manually all the time, and manual failures can be minimized. Therefore, in this work, the programming language, Python, is connected with Aspen HYSYS® to automate the entire calculation process.

The connection is managed through a binary-interface, component object model (COM), which allows the communication between these two programs. The "communication" process between Aspen HYSYS® and Python is illustrated in Fig. 4.3. Automation is advantageous, especially for system optimization. Since the simulation results and the combination of new values of each decision parameter need to be exported and imported between Aspen HYSYS® and Python constantly. More discussions regarding optimization methods applied in this study will be given in section 4.4.
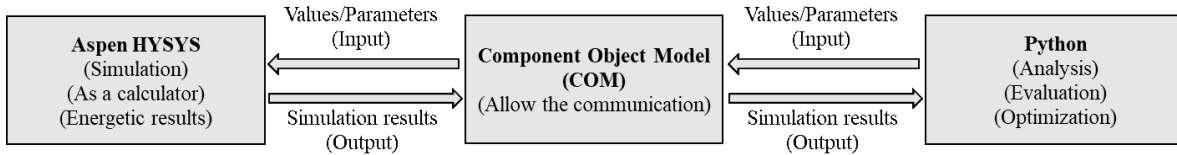
Figure 4.3: The principle of the automation process between Aspen HYSYS® and Python.
.

4.3 Methods for system evaluation

Since the provisional design needs to be evaluated and the evaluation results would determine if this design is approved or not, several thermodynamic analyses are conducted after the simulation process to examine the system performance (as design criteria in this work), including the conventional energetic analysis and the exergy-based analyses. The energetic analysis is first carried out as it is the most commonly applied thermodynamic method, while the research in this study focuses more on the exergy-based methods, which consist of exergetic, economic, and exergoeconomic analyses. The economic analysis can be conducted separately to evaluate a system from an economic point of view. However, it functions in this work as an

intermediate step for implementing the exergoeconomic analysis. Therefore, it is grouped into exergy-based methods.

Exergy-based methods are selected as the main focus in this study over energetic methods to evaluate the proposed polygeneration system because:

1. Compared to energy, exergy is a beneficial concept that considers the interactions between a given state of the entity and its environment [88], to compare different streams/systems on a common basis.

2. By applying exergy-based methods, the magnitude, location, and cause of component-wise and system-wise real inefficiencies (i.e., exergy destruction and exergy loss) can be determined.

3. It helps allocate the engineering resources and efforts to design energy systems and improve system performance.

Therefore, exergy-based methods have become the premier methods in the 1990s [93] applied for thermodynamic-wise analyses. They are especially well suited for computer-aided design and optimization of energy systems.

4.3.1 Energetic analysis

According to the first law of thermodynamics, namely, the energy conservation principle, the energy balance of a system is expressed as:

$$\frac{d(U + KE + PE)}{dt} = \sum_j \dot{Q}_j + \sum_j \dot{W}_j + \sum_i \left(\dot{m}_i \left(h_i + ke_i + pe_i \right) \right) \\ - \sum_e \left(\dot{m}_e \left(h_e + ke_e + pe_e \right) \right) \tag{4.1}$$

where U, KE and PE stand, respectively, for the internal energy, the kinetic energy and the potential energy; $\dot{Q}_j$ and $\dot{W}_j$ indicate the transfer rates of heat and work, respectively, associated with the j-th stream; while $\dot{m}_i$ and $\dot{m}_e$ denote the mass flow rates of material streams that enter the system, and exit from the system; h, ke and pe are the specific enthalpy (per unit of mass), the specific kinetic energy (per unit of mass) and the specific potential energy (per unit of mass) associated with the material streams interacting with the system, respectively.

By neglecting the changes in kinetic and potential energies and assuming the system is in a steady state, the energy balance of the studied system can be simplified as follows:

$$\sum_i \dot{m}_i \cdot h_i + \sum_j \dot{Q}_j + \sum_j \dot{W}_j = \sum_e \dot{m}_e \cdot h_e \tag{4.2}$$

Therefore, the energetic efficiency of the proposed polygeneration system is defined as follows with the considerations of operating the system as a trigeneration system, a cogeneration system, and a sole generation (refrigeration) system:

- for trigeneration (heat, refrigeration, and power):

$$\eta_{\text{total}} = \left(\dot{Q}_{\text{Cooler}} + \dot{W}_{\text{net}} \right) / \dot{Q}_{\text{HE}} \tag{4.3}$$

- for cogeneration (refrigeration and heat):

$$\eta_{\text{total}} = \dot{Q}_{\text{Cooler}}/\dot{Q}_{\text{HE}} \tag{4.4}$$

In the first two cases, the refrigeration system is operated as a cogeneration system producing heat and refrigeration capacities. However, from the energetic point of view, only the heat (generated from the Cooler) should be considered the energetic product (of the refrigeration system) since the energy content of the heat capacity contains the energy content of the refrigeration capacity according to the first law of thermodynamics.

- for cogeneration (refrigeration and power):

$$\eta_{\text{total}} = \left(\dot{Q}_{\text{EVAP}} + \dot{W}_{\text{net}}\right)/\dot{Q}_{\text{HE}} \tag{4.5}$$

- for only refrigeration:

$$COP_{\text{total}} = \dot{Q}_{\text{EVAP}}/\dot{Q}_{\text{HE}} \tag{4.6}$$

While, for two sub-systems, the equations used for computing their energetic efficiencies are expressed as:

a) the closed power cycle, η_P

* for trigeneration (heat, refrigeration, and power) or cogeneration (refrigeration and heat):

$$\eta_{\text{P}} = \left(\dot{W}_{\text{EX}} - \dot{W}_{\text{CM–P}} + \dot{Q}_{\text{Cooler,P}}\right)/\dot{Q}_{\text{HE}} \tag{4.7}$$

* for cogeneration (refrigeration and power) or only refrigeration:

$$\eta_{\text{P}} = \left(\dot{W}_{\text{EX}} - \dot{W}_{\text{CM–P}}\right)/\dot{Q}_{\text{HE}} \tag{4.8}$$

b) the refrigeration cycle, COP_R

* for trigeneration (heat, refrigeration, and power) or cogeneration (refrigeration and heat):

$$COP_R = \dot{Q}_{\text{Cooler,R}}/\dot{W}_{\text{CM–R}} \tag{4.9}$$

* for cogeneration (refrigeration and power) or only refrigeration:

$$COP_R = \dot{Q}_{\text{EVAP}}/\dot{W}_{\text{CM–R}} \tag{4.10}$$

Here, $\dot{Q}_{\text{EVAP}}$ is the desired refrigeration capacity, $\dot{W}_{\text{net}}$ is the net power output, $\dot{Q}_{\text{Cooler}}$ is the available heating capacity, and $\dot{Q}_{\text{HE}}$ is the heat absorbed from the heat sources. $\dot{Q}_{\text{Cooler,P}}$ and $\dot{Q}_{\text{Cooler,R}}$ are the heat capacities contributed by the power cycle and the refrigeration cycle, respectively, if the system is treated as two sub-systems.

The $\dot{W}_{\text{net}}$ is expressed as:

$$\dot{W}_{\text{net}} = \dot{W}_{\text{EX}} - \dot{W}_{\text{CM–P}} - \dot{W}_{\text{CM–R}} \tag{4.11}$$

Additionally, $\dot{Q}_{\text{Cooler,P}}$ and $\dot{Q}_{\text{Cooler,R}}$ are proportional to the mass flow rate ratios of the power cycle mass flow rate ($\dot{m}_{\text{P}}$) and refrigeration cycle mass flow rate ($\dot{m}_{\text{R}}$) to the overall mass flow rate ($\dot{m}_{\text{P}} + \dot{m}_{\text{R}}$), respectively. The sum of $\dot{Q}_{\text{Cooler,P}}$ and $\dot{Q}_{\text{Cooler,R}}$ should equal to the total heat capacity within the Cooler ($\dot{Q}_{\text{Cooler}}$):

$$\dot{Q}_{\text{Cooler,P}} = \frac{\dot{m}_{\text{P}}}{(\dot{m}_{\text{P}} + \dot{m}_{\text{R}})} \times \dot{Q}_{\text{Cooler}} \tag{4.12}$$

$$\dot{Q}_{\text{Cooler,R}} = \frac{\dot{m}_{\text{R}}}{(\dot{m}_{\text{P}} + \dot{m}_{\text{R}})} \times \dot{Q}_{\text{Cooler}} \tag{4.13}$$

$$\dot{Q}_{\text{Cooler,P}} + \dot{Q}_{\text{Cooler,R}} = \dot{Q}_{\text{Cooler}} \tag{4.14}$$

As no interactions between the system and its environment are considered in the energetic analysis, the system energetic efficiency is only determined by system operation conditions. Thus, the equations above formulated for calculating the system/sub-system energetic efficiency remain unchanged throughout this paper.

4.3.2 Exergetic analysis

Contrary to energy, exergy can be destroyed. The idea that something can be destroyed is helpful when it comes to design, analysis, and optimization of thermal systems [88]. Moreover, by including the interaction between a given state of the entity and its environment, an exergetic analysis gauges and provides quality of entities. This is extremely useful in the analysis and evaluation of thermal systems as the product with a greater quality has, in general, a greater economic value.

By combing the energy and entropy balances, the general exergy balance applied for a control-volume system where material streams can enter and exit is defined as:

$$\frac{d\dot{E}_{\text{total}}}{dt} = \sum_j \left(1 - \frac{T_0}{T_j}\right)\dot{Q}_{\text{j}} + \left(\dot{W}_{\text{cv}} - p_0 \frac{dV_{\text{cv}}}{dt}\right) + \sum_{\text{i}} \dot{m}_{\text{i}} e_{\text{i}} - \sum_{\text{e}} \dot{m}_{\text{e}} e_{\text{e}} - \dot{E}_{\text{D}} \tag{4.15}$$

where $\dot{E}_{\text{total}}/dt$ denotes the time rate of change in the exergy of the overall system; T_0 denotes the reference temperature; $_{\text{cv}}$ is short for control volume; e represents the stream specific exergy (per unit of mass); and $\dot{E}_D$ is the rate of exergy destruction.

In terms of exergy components, the total exergy, in the absence of nuclear, magnetic, electrical, and surface tension effects, can be divided into four parts: physical exergy $\dot{E}^{\text{PH}}$, kinetic exergy $\dot{E}^{\text{KN}}$, potential exergy $\dot{E}^{\text{PT}}$, and chemical exergy $\dot{E}^{\text{CH}}$:

$$\dot{E} = \dot{E}^{\text{PH}} + \dot{E}^{\text{KN}} + \dot{E}^{\text{PT}} + \dot{E}^{\text{CH}} \tag{4.16}$$

The changes of the kinetic exergy and the potential exergy are neglected for the exergy analysis conducted in this work, only physical exergy and chemical exergy are considered.

Besides, since the refrigeration system is operated partially below the reference temperature, the physical exergy is further split into the thermal $\dot{E}^T$ and mechanical $\dot{E}^M$ parts [94]:

$$\dot{E}^{\mathrm{PH}} = \dot{E}^{\mathrm{T}} + \dot{E}^{\mathrm{M}} \tag{4.17}$$

- *Conventional exergetic analysis*

For evaluating each individual component or the entire system from exergetic point of view, the concepts of exergy fuel $\dot{E}_F$, product $\dot{E}_P$, destruction $\dot{E}_D$ and loss $\dot{E}_L$ are necessary to be introduced [88]. The fuel is defined as the exergy rate supplied to the component/system, which is the driving force of the transformations undergone in the studied component/system; while the product represents the exergy rate of the desired result produced by the component/system. For a component k, its exergy rate balance is expressed as:

$$\dot{E}_{\mathrm{F},k} = \dot{E}_{\mathrm{P},k} + \dot{E}_{\mathrm{D},k} \tag{4.18}$$

It reveals that the $\dot{E}_{\mathrm{D}}$ within a component can be calculated by the exergy rate difference between its definitions of $\dot{E}_{\mathrm{F}}$ and $\dot{E}_{\mathrm{P}}$. However, for the overall system, not only $\dot{E}_{\mathrm{D}}$ occurs within components, but also $\dot{E}_{\mathrm{L}}$ needs to be considered if there are some streams being rejected into the environment and not being further utilized. Hence, the exergy rate balance for a system is written as:

$$\dot{E}_{\mathrm{F},total} = \dot{E}_{\mathrm{P},total} + \dot{E}_{\mathrm{D},total} + \dot{E}_{\mathrm{L},total} \tag{4.19}$$

Intuitively, the exergetic efficiency ε for a component as well as for an entire system is defined as the ratio between product and fuel:

$$\varepsilon = \dot{E}_{\mathrm{P}}/\dot{E}_{\mathrm{F}} \tag{4.20}$$

- *Advanced exergetic analysis*

Based on the conventional exergetic analysis results, advanced exergetic analysis can be further conducted since it is always useful for designers to improve the system performance by knowing not only the exergy destruction and the investment cost but also their avoidable parts associated with components. Then improvement efforts should be wisely allocated and focus on only the information regarding avoidable parts. The equation of splitting the exergy destruction within the kth component into its avoidable part and unavoidable part is written as [95]:

$$\dot{E}_{\mathrm{D},k} = \dot{E}_{\mathrm{D},k}^{\mathrm{UN}} + \dot{E}_{\mathrm{D},k}^{\mathrm{AV}} \tag{4.21}$$

where $^{\mathrm{UN}}$ stands for unavoidable and $^{\mathrm{AV}}$ represents the avoidable part.

To calculate the value of $\dot{E}_{\mathrm{D},k}^{\mathrm{UN}}$, a "best" operation condition of each component needs to be assumed. In this work, as the proposed polygeneration is a relatively simple system, the "overall-system level" approach [95] is implemented for obtaining unavoidable parts of all components simultaneously by only simulating the overall system once. Besides, a modified exergetic efficiency $\varepsilon_k^{\mathrm{AV}}$, for the kth component, which focuses only on the avoidable part of

the exergy destruction, is used as an indicator derived from the advanced exergetic analysis [95, 96]:

$$\varepsilon_k^{\mathrm{AV}} = \frac{\dot{E}_{\mathrm{P},k}}{\dot{E}_{\mathrm{F},k} - \dot{E}_{\mathrm{D},k}^{\mathrm{UN}}} \tag{4.22}$$

For the exergy analysis, as the reference temperature varies, the definitions of fuel, product, destruction, and loss for components and the system may need to be adjusted accordingly. Therefore, these component-wise and system-wise exergy-related definitions are not given in this section; more detailed discussions will be presented in sections/chapters where the exergetic analysis is conducted.

4.3.3 Economic analysis

For analyzing the system from an economic viewpoint, the method of calculating system total revenue requirement (TRR) is applied [88]. For conducting the TRR, the total capital investment (TCI) of the system need to be first estimated based on the purchased equipment cost (PEC) of each component, then the economic, financial, operating, and market input parameters are determined for the detailed cost calculation. Finally, the geometrically increasing series of expenditures will be levelized into a financially equivalent constant quantity (annuity).

The key and the most challenging part of the economic analysis is to estimate the PEC of each component with an accurate approach; this is extremely difficult, especially for the new and uncommercialized technology. In general, the inaccuracy in cost estimations is in the range of $\pm$ 10% to $\pm$ 30% [88]. Since the proposed polygeneration system is a novel system, and the S-CO$_2$ power sub-system is still under research development, the cost estimation in this work may result in having a higher inaccuracy. However, the TRR method as a basis for the exergoeconomic analysis is still a reasonable option to estimate system cost and further support system performance evaluation.

The general equation for computing the TRR is written as:

$$TRR_L = CC_L + FC_L + OMC_L \tag{4.23}$$

where CC_L stands for levelized carrying charges; FC_L is the levelized fuel cost; and OMC_L denotes the levelized operating and maintenance costs.

The CC_L is calculated as:

$$CC_L = TCI \times CRF \tag{4.24}$$

where TCI and CRF represent, respectively, the total capital investment and the capital recovery factor.

The total capital investment of a plant is made up by two parts, namely, the fixed-capital investment (FCI) and other outlays [88]. The FCI can further be broken down to the direct cost and indirect cost; the other outlays contain the startup cost, working capital, cost of licensing, research, development, etc.. For a new thermal system, its TCI can be estimated

once the purchased equipment costs of all components are available with a simplified equation. The equation is expressed as [88]:

$$TCI = 6.32 \, PEC \tag{4.25}$$

The capital recovery factor (CRF) is the ratio of a constant annuity A to the present value P of receiving that amount of annuity for a given length of time n at an effective interest rate i_{eff}. The equation of the CRF can be given by:

$$CRF = \frac{A}{P} = \frac{i_{\text{eff}} \left(1 + i_{\text{eff}}\right)^n}{\left(1 + i_{\text{eff}}\right)^n - 1} \tag{4.26}$$

where n in this work denotes the economic lifetime of the plant. And the annual money transaction is assumed to occur at the end of each year.

To levelize the fuel cost and the operating and maintenance cost, the constant escalation levelization factor ($CELF$) is applied to express the relationship between the value of the expenditure at the beginning of the first year P_0 and the levelized value A. The factor includes the considerations of the nominal escalation rate r_n, the effective interest rate i_{eff} and the CRF:

$$CELF = \frac{A}{P_0} = \frac{k \left(1 - k^n\right)}{1 - k} \times CRF \tag{4.27}$$

where

$$k = \frac{1 + r_n}{1 + i_{eff}} \tag{4.28}$$

The nominal escalation rate r_n includes the influences of the real escalation rate r_r and the average annual inflation rate r_i:

$$(1 + r_n) = (1 + r_r)(1 + r_i) \tag{4.29}$$

For calculating the operating and maintenance cost, $r_{r,OMC} = 0$ is assumed; that is to say, the annual operating and maintenance cost depends only on the constant average inflation rate, $r_{n,OMC} = r_i$. However, for the fuel cost, a positive real escalation rate is applied, $r_{r,FC} > 0$, since the fuel cost is expected to increase on a faster average rate than the predicted inflation rate over a long period of future years [88]; with the mathematical expression, $r_{n,FC} > r_i$.

Therefore, the FC_L is calculated by the equation as follows:

$$FC_L = FC_0 \times CELF_{FC} = FC_0 \times \frac{k_{FC} \left(1 - k_{FC}^n\right)}{1 - k_{FC}} \times CRF \tag{4.30}$$

with

$$k_{FC} = \frac{1 + r_{n,FC}}{1 + i_{eff}} \tag{4.31}$$

While for OMC_L:

$$OMC_L = OMC_0 \times CELF_{OMC} = OMC_0 \times \frac{k_{OMC} \left(1 - k_{OMC}^n\right)}{1 - k_{OMC}} \times CRF \tag{4.32}$$

with

$$k_{OMC} = \frac{1 + r_{n,OMC}}{1 + i_{eff}} \tag{4.33}$$

where FC_0 and OMC_0 stand for the fuel cost and the operating and maintenance cost, respectively, at the beginning of the first year.

All the assumptions made for the economic analysis are summarized in Table 4.1. The fuel cost will be discussed in sections/chapters where the fuel/heat source of the polygeneration system is specified since the fuel cost varies as the heat source utilized for driving the system changes.

Table 4.1: Assumptions made for the economic analysis.

Variable	Nomenclature	Unit	Value
The economic lifetime of the plant	n	a	20
Effective interest rate	i_{eff}	%	10
Average annual inflation rate	r_i	%	2.5
Nominal escalation rate for O&M cost	$r_{n,OMC}$	%	2.5
Nominal escalation rate for fuel cost	$r_{n,FC}$	%	3.4
O&M cost at the beginning of the first year	OMC_0	$	0.05 TCI n^{-1}

4.3.4 Exergoeconomic analysis

Based on the results of exergetic and economic analyses, exergoeconomic analysis can be conducted by combining the exergetic analysis with economic considerations of a system [88]. It provides useful information that cannot be obtained by conducting the conventional thermodynamic analysis and economic analysis separately. By assigning a cost to a unit of exergy for each stream (including power and heat streams), the component-wise and system-wise product costs per unit of exergy can be computed. The product cost is, in general, one of the most important indicators for evaluating system performance. While other results obtained from the exergoeconomic analysis also provide crucial information for system designers to optimize the system in its design phase.

In this work, the specific exergy costing (SPECO) approach [97] is adopted for the exergoeconomic analysis, which consists of three steps, namely, exergy stream identification, fuel and product definition, and cost equation formulation. The first two steps have been discussed in the exergetic analysis section 4.3.2; hence, the step of cost equation formulation is deepened in this section.

For each component, its cost balance that demonstrates the relationship between its cost rate of fuel $\dot{C}_F$ and cost rate of product $\dot{C}_P$ is written as:

$$\dot{C}_{F,k} + \dot{Z}_k = \dot{C}_{P,k} \tag{4.34}$$

where $\dot{Z}_k$ represents the total cost rate associated with the kth component, including its annual levelized capital investment $\dot{Z}_k^{CI}$ and the annual levelized operating and maintenance expenses $\dot{Z}_k^{OM}$.

$$\dot{Z}_k = \dot{Z}_k^{\text{CI}} + \dot{Z}_k^{\text{OM}} \text{ with } \begin{cases} \dot{Z}_k^{\text{CI}} = \frac{CC_L}{\tau} \times \frac{PEC_k}{PEC_{total}} \\[3mm] \dot{Z}_k^{\text{OM}} = \frac{OMC_L}{\tau} \times \frac{PEC_k}{PEC_{total}} \end{cases} \tag{4.35}$$

where τ denotes the annual full-load operation hours of the system. In this study, τ is assumed as 8000 h/year.

However, for components with more than one outlet stream, cost balance and auxiliary equations are required since the number of cost equations should equal the number of unknown stream cost rates. Therefore, F and P rules (short for fuel and product) are applied for such components [88]. The detailed cost balances and auxiliary equations regarding F and P rules for components and the overall system will be given in the sections/chapters where the exergoeconomic analysis is implemented.

- *Conventional exergoeconomic analysis*

  The component-wise specific cost of fuel c_{F} and product c_{P} per unit of exergy are defined as:

$$c_{\text{F},k} = \frac{\dot{C}_{\text{F},k}}{\dot{E}_{\text{F},k}} \tag{4.36}$$

$$c_{\text{P},k} = \frac{\dot{C}_{\text{P},k}}{\dot{E}_{\text{P},k}} \tag{4.37}$$

The cost rate associated with the exergy destruction within a component $\dot{C}_{\text{D}}$, the relative cost difference r_k, and the exergoeconomic factor f_k are given, respectively, in the following equations [88]:

$$\dot{C}_{\text{D},k} = c_{\text{F},k} \times \dot{E}_{\text{D},k} \tag{4.38}$$

$$r_k = \frac{(c_{\text{P},k} - c_{\text{F},k})}{c_{\text{F},k}} \tag{4.39}$$

$$f_k = \frac{\dot{Z}_k}{\left(\dot{Z}_k + \dot{C}_{\text{D},k}\right)} \tag{4.40}$$

While for the overall system, its cost balance is similar to the cost balance for each component:

$$\dot{C}_{F,total} + \dot{Z}_{total} = \dot{C}_{P,total} \tag{4.41}$$

with

$$\dot{Z}_{total} = \dot{Z}_{total}^{\text{CI}} + \dot{Z}_{total}^{\text{OM}} \tag{4.42}$$

Regarding the product cost, the component-wise and system-wise product costs are expressed as:

$$c_{P,k} = \frac{\dot{C}_{P,k}}{\dot{E}_{P,k}}$$ (4.43)

$$c_{P,total}^{av} = \frac{\dot{C}_{P,total}}{\dot{E}_{P,total}}$$ (4.44)

If some products generated from the system, which are considered as the available products, and they are not sold to customers in a certain case, then the average product cost should be written as:

$$c_{P,total}^{av} = \frac{\dot{C}_{P,total}}{\dot{E}_{P,total}^{'}} = \frac{\dot{C}_{F,total} + \dot{Z}_{total}}{\dot{E}_{P,total}^{'}}$$ (4.45)

where $\dot{E}_{P,total}^{'}$ denotes the exergy rate of the product in that certain case, which is lower than that in the case all the products are sold out. In turn, the overall system's average product cost should increase since the product produced but not sold is considered the exergy loss of the system, and the cost of the exergy loss is charged to other final products of the system.

The other approach to calculate the average product cost of the overall system is:

$$c_{P,total}^{av} = \frac{\sum_{i=1}^{n} \dot{C}_{i-thP,k}}{\dot{E}_{P,total}}$$ (4.46)

where n represents the number of products of the overall system, and $\dot{C}_{i-thP,k}$ refers to the cost rate of the ith product within the associated kth component.

In the case that some of the products are not sold out but rejected into the environment, the equation 4.46 should be modified as:

$$c_{P,total}^{av} = \frac{\sum_{i=1}^{n} \dot{C}_{i-thP,k}}{\dot{E}_{P,total}^{'}}$$ (4.47)

- *Advanced exergoeconomic analysis*

Similar to what we discussed in the section for the advanced exergetic analysis, the investment cost associated with the kth component in the advanced exergoeconomic analysis, is also divided into an avoidable part and an unavoidable part [95]:

$$\dot{Z}_k = \dot{Z}_k^{\mathrm{UN}} + \dot{Z}_k^{\mathrm{AV}}$$ (4.48)

where UN stands for unavoidable and AV represents the avoidable part.

Contrary to the advanced exergetic analysis, in which a "best" operation condition is assumed, assumptions of a "worst" operation condition of each component are needed to compute the value of $\dot{Z}_k^{\mathrm{UN}}$. In addition, the exergoeconomic factor f_k given in Eq. 4.40 in the conventional exergoeconomic analysis is modified as [95, 96]:

$$f_k^{\text{AV}} = \frac{\dot{Z}_k^{\text{AV}}}{\dot{Z}_k^{\text{AV}} + \dot{C}_{\text{D},k}^{\text{AV}}} = \frac{\dot{Z}_k^{\text{AV}}}{\dot{Z}_k^{\text{AV}} + c_{\text{F},k} \times \dot{E}_{\text{D},k}^{\text{AV}}} \tag{4.49}$$

where $\dot{C}_{\text{D},k}^{\text{AV}}$ denotes the avoidable cost rate of the exergy destruction associated with the kth component.

With this indicator f_k^{AV}, the contribution of the avoidable investment cost rate on the total avoidable cost rate associated with the kth component is calculated. Compared to f_k, f_k^{AV} can better help designers with more accurate and certain information [96] to improve the system performance in the cost minimization process.

4.4 Methods for system optimization

Design optimization is one of the most important steps for designers. In this step, the provisional design can be further improved, and thus, it results in a better performance in terms of the design criteria. However, design optimization is also very challenging because a considerable amount of design variations need to be taken into design consideration, and several design criteria – more than one in most of the time – have to be met. For finding the optimal designs, there are, in general, three techniques that can be applied, namely, design experimentally, design with simulated models, and design with optimization algorithms.

Conducting experiments to confirm which design is the most optimal one is tedious, expensive, and time-consuming. Therefore, simulation software is preferred nowadays to accelerate optimization procedures. Nevertheless, human is still highly involved in this process, and it is almost impossible to simulate all the potential design variations. With "clever" algorithms, the optimization process can be automated, with minimum human involvement, and accomplished in a much shorter time. Therefore, for complex design optimization problems, applying appropriate optimization algorithms might be the best option for designers. The foreseeable drawbacks of design with optimization algorithms, however, include: the designers have to handle the complexity of the algorithms; only certain algorithms work efficiently for the problem needed to be solved; and the difficulties by designing the tangled optimization problem and implementing the algorithms,etc.. In this work, as the automation between Aspen HYSYS® and Python was carried out for the system evaluation (discussed in Fig. 4.3), it is beneficial to continue the design optimization by applying algorithms based on the established automation.

In general, optimization problems consist of three basic components: objective functions, a set of decision variables, and a set of constraints [98]. The objective functions are expressed as the decisions made either to maximize or to minimize specific performance indices. Sometimes only a single performance criterion needs to be met, which in turn leads to a single objective function. In practice, cost minimization and profit maximization are two of the most commonly applied objective functions for optimizing an industrial system. Decision variables are chosen by giving a rational range for each of them to achieve the desired objective functions. Constraints are restrictions imposed on the system by combining the decision variables to yield the objective functions' best system performance.

In this study, as shown in Fig 4.4, the main objective of the design optimization is to minimize the average product cost of the overall system. The decision variables are the operating parameters as the input values fed into the simulation, which significantly influence the system performance. In contrast, the constraints are not that straightforward but concealed within the simulation software by testing the combinations of decision variables that have to result in simulating the system successfully. Once the input values fed into the simulation software end up with a simulation outcome with errors, it is considered the case that violates the constraints. The optimization loop in this work, in short, can be described as: the decision variables are fed into Aspen HYSYS® for yielding the simulation results; then the simulation results are sent to Python for evaluating the system performance; meanwhile, the optimization algorithm is implemented in Python, which sends the combinations of decision variables back to Aspen HYSYS® for checking if the constraints are violated or not.
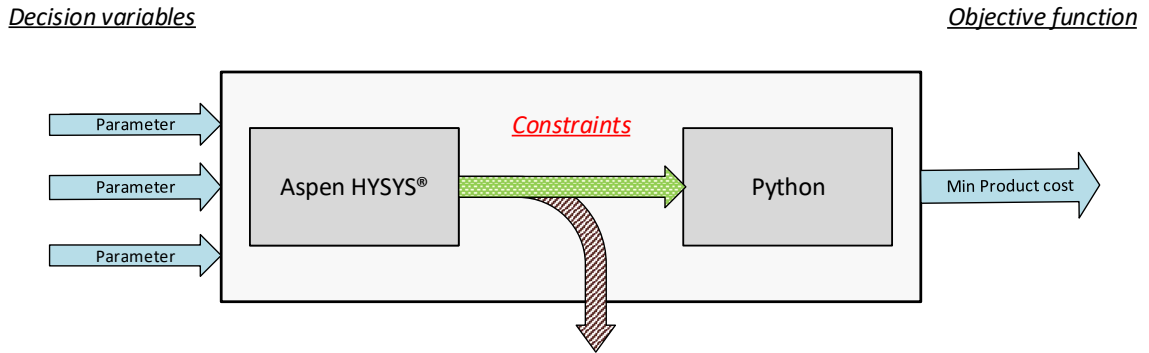
Figure 4.4: Basic components of the optimization problem (decision variables, constraints and objective function) in this study.

.

Before we move to the discussion of the optimization algorithms selected and applied in this study, the characteristics of the optimization problem and the features of the objective function need to be clarified first. There are two kinds of objective functions–unimodal and multimodal functions [98], depending on the number of peaks in the search landscape. The search landscape is the image generated when an objective function's values are plotted against its independent decision variables. If there is a single peak in the search landscape of a function (a maximum or a minimum), the function is termed as a unimodal function; by contrast, the function is multimodal if there are several peaks. The characteristics of the optimization problem determine the search landscape of the objective function. In real life, especially when dealing with complex highly non-linear optimization problems, the objective functions are, most of the time, multimodal functions. In this work, as the thermophysical properties of the working fluid and the thermodynamic behaviors within the components are highly non-linear, the search landscape of the objective function must be with several peaks, and the objective function is expected to be a multimodal function.

Since multimodal function has several local minima and/or local maxima, the biggest hurdle by solving an optimization problem with multimodal functions is to find the global minimum or global maximum among all the local minima and local maxima. It requires the algorithms to be "clever" enough to avoid local solutions and have a higher chance of finding

the global optimum. Compared to the conventional deterministic optimization algorithms, the stochastic optimization algorithms have their advantages to overcome the local optima stagnation and find the global optimum by a higher chance. Moreover, as the component models are embedded in the simulation software, which are unknown for the author, being considered "black boxes" in this work, deterministic optimization algorithms, depending highly on the mathematical models, can not even be applied. Therefore, the stochastic algorithms are selected to solve the design optimization problem in this work.

Depending on the algorithm structure, stochastic optimization algorithms can be further classified into two sub-categories, namely, individual-based and population-based algorithms (illustrated in Fig 4.5). In general, population-based algorithms will outperform the individual-based algorithms because of their high exploration and high local optima avoidance. The classic population-based algorithms widely applied in engineering fields are evolutionary algorithms, physical-based algorithms, and swarm-based algorithms. Genetic algorithms (GAs) are the earliest and most well-known evolutionary algorithms. The theory of natural selection inspires these algorithms – "survival of the fittest"; for a given optimization problem, a population of candidate solutions is created, then the "good/fit candidates" have a relatively high chance to reproduce as their "good genes" will pass to their offspring. In contrast, the "poor candidates" have a relatively low chance of reproducing. Simulated annealing (SA) is one of the representatives of physical-based algorithms. It mimics the slow cooling-annealing process of molten metal until the lowest energy state reaches. Swarm-based algorithms are based on research about foraging swarms such as ants, fish schooling, and a flock of birds. All the swarms find their food by group coordination instead of each individual. These algorithms, thus, mimic the way of swarm foraging to solve the global optimization problem by communicating the individuals within the group.
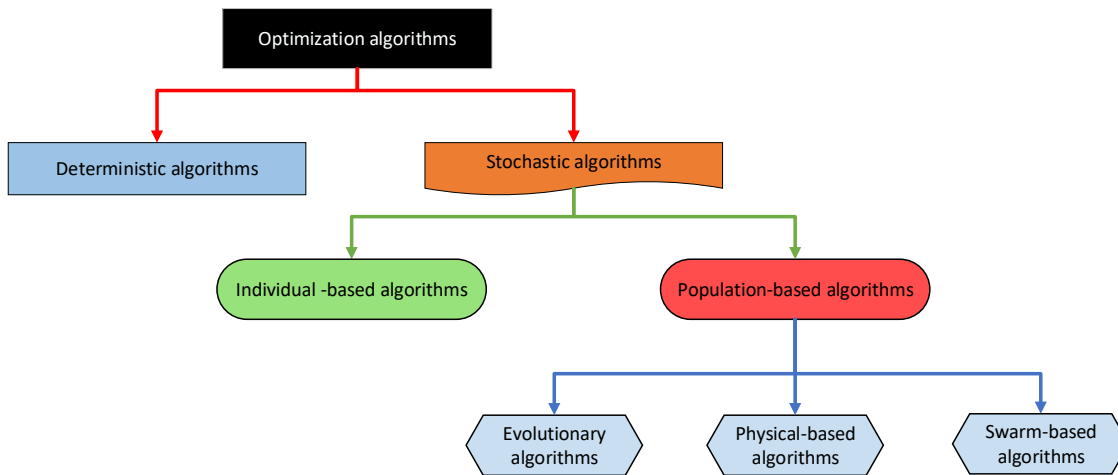
Figure 4.5: Classification of optimization algorithms.
.

In this study, two relatively new algorithms – differential evolution (DE) and particle swarm optimization (PSO) – are applied to solve the design optimization problem. DE algorithm was first introduced in 1997 by Storn and Price [99, 100], which is similar to GA but modified by exploiting more information from the current population (distance and direction information)

for simpler and more straightforward to implement. The most significant advantages of applying DE are [100]: it is simple and easy to implement; less computation time is required; and its reliability and robustness. PSO is a swarm-based algorithm, and Kennedy and Eberhart first suggested it in 1995 [101]. The potential candidates in this algorithm are called particles. A group of particles work together to continuously improve their individual performance and their collective performance on a given optimization task [102]. The PSO requires less computational effort for solving moderate-dimensional problems and is also an excellent option for solving high-dimensional optimization problems [98]. Besides, it is also robust and straightforward.

Now, let us discuss how these two algorithms are structured and operated in detail. Fig. 4.8 presents the procedures for implementing the DE algorithm. Compared to GAs, the general implementation steps of DE and GAs are the same, but the operators are designed and structured in different ways. Instead of considering two candidates as parents to reproduce their offspring for GAs, the operators in DE take the difference vector between two randomly selected individuals and add the scaled version of this difference vector to a third individual to generate a new potential candidate. A simple example of a DE operator in a two-dimensional search space is depicted in Fig. 4.6. X_{r1}, X_{r2} and X_{r3} are randomly selected candidate solutions with $r1 \neq r2 \neq r3$; F is the mutation constant that controls the amplification of the difference vector between X_{r1} and X_{r2}; the different vector is given in the figure as $X_{r2} - X_{r2}$; then a corresponding mutant vector V_i can be computed.
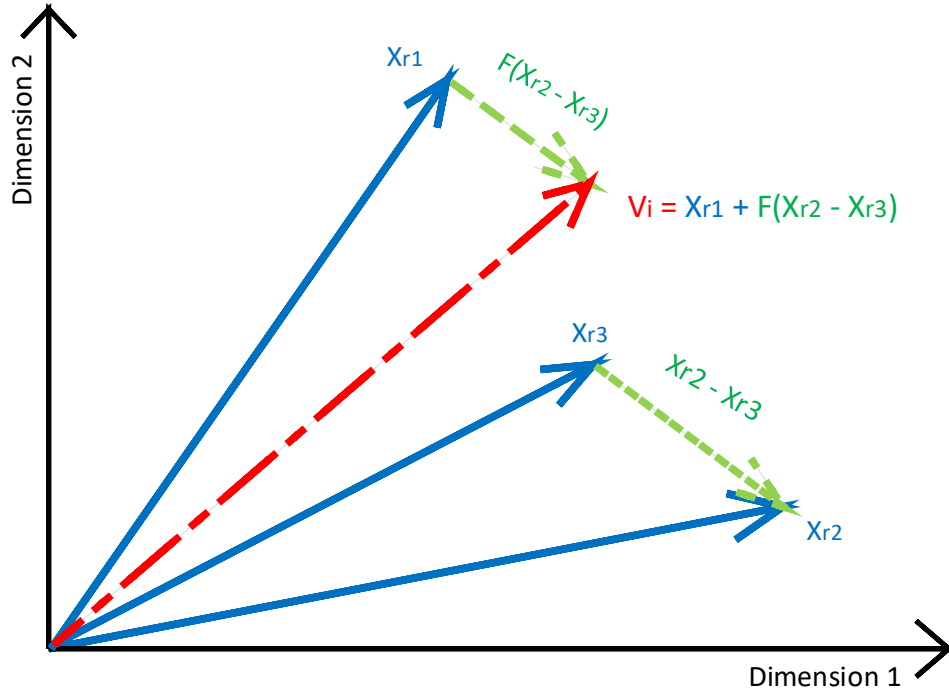
Figure 4.6: The basic idea of DE algorithm in two dimensions.

.

The basic idea for the PSO algorithm is to find the food by updating information within a swarm, then new locations based on the shared information will be targeted and explored; these processes will be iterated until the group task is achieved. As shown in Fig. 4.9, compared to DE, no operators such as mutation, crossover, and selection are implemented in PSO algorithm;

the new iteration/swarm, however, is generated by combining the information of the personal best and group best locations and results. Also, some random factors are added to update the new velocity of particles, then new positions of all particles in the next iteration can be computed. The search mechanism of PSO from the current position to the new position is illustrated in Fig. 4.7. The new position of the ith particle X'_i is determined by its current velocity V_i, the difference vector between its current position X_i and its personal best position $Pbest_i$, and the other difference vector between X_i and the group best position $Gbest$. w is the inertia weight parameter; c_1 and c_2 are the acceleration factors; r_1, r_2 are random values between 0 and 1, generated from the random operator. The first part of the equation shown in Fig. 4.7 represents the inertia of this particle at the current position, the second part is called the cognitive component, and the third part indicates the social component.
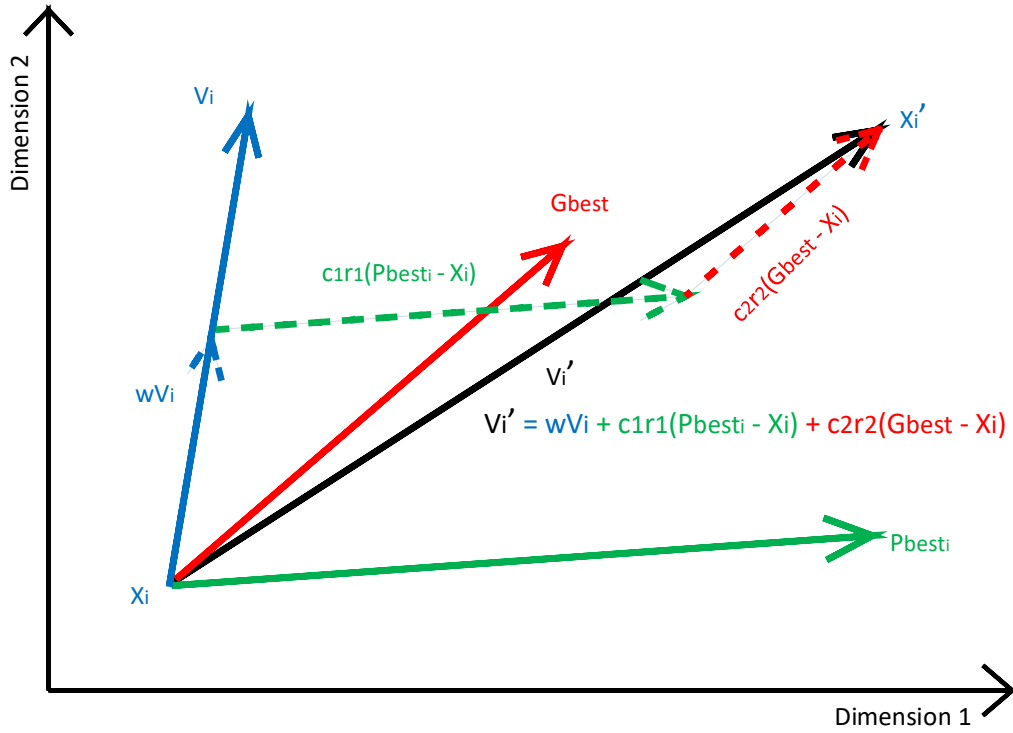
Figure 4.7: The basic search mechanism of PSO algorithm in two dimensions.

.

For all optimization procedures carried out in this study, algorithms are executed in Python, while Aspen HYSYS® functions as a calculator. With the aid of Aspen HYSYS®, the parameters needed for computing the objective function are provided, and the combinations of input parameters that violate constraints are ruled out. Only by coordinating these two programs (Aspen HYSYS® and Python) in a harmonious way, optimization procedures can be operated smoothly, and desired results will be provided. More details for implementing the optimization algorithms will be given and discussed in the optimization sections.
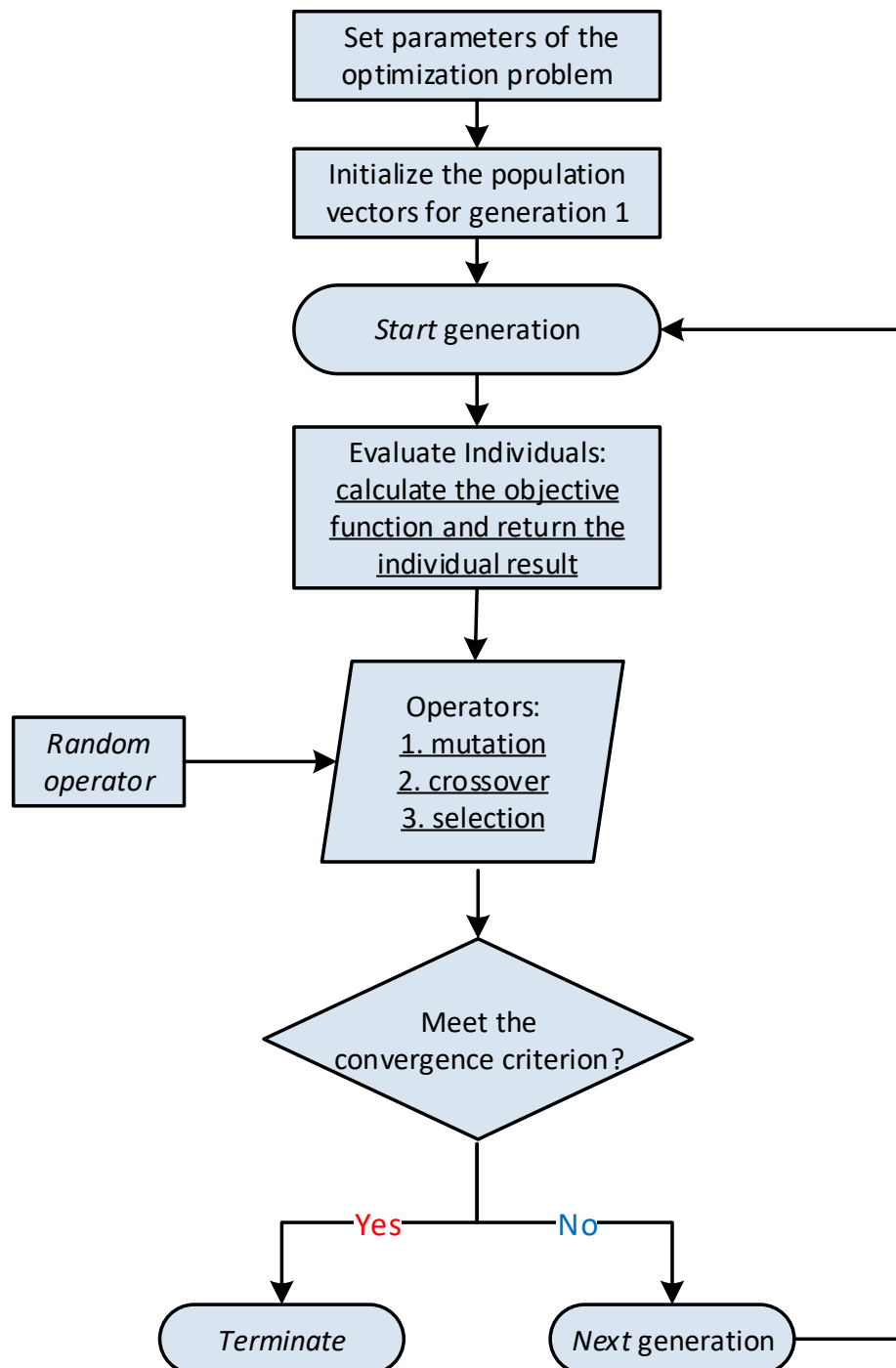
Figure 4.8: Implementation of DE algorithm.

.
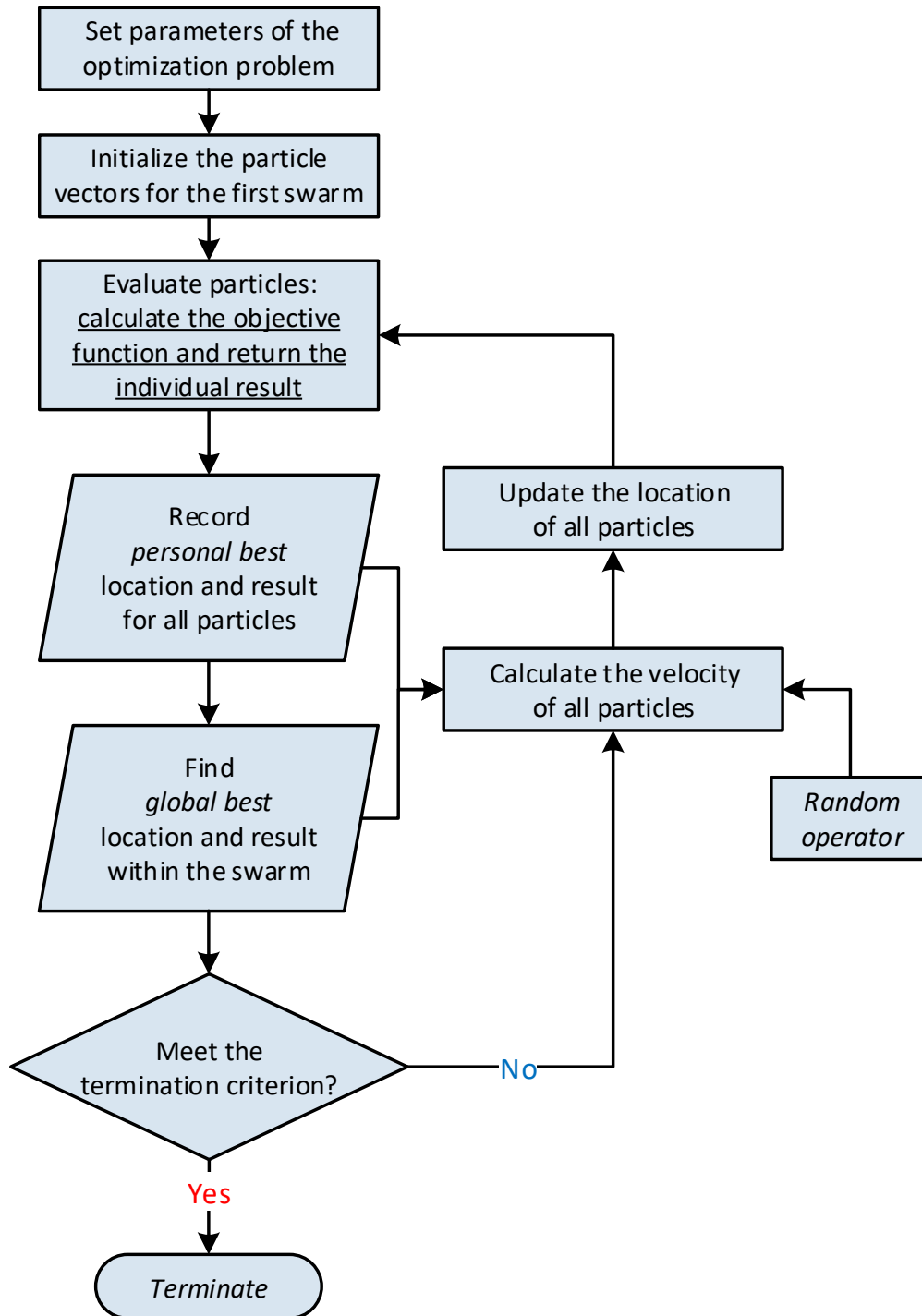
Figure 4.9: Implementation of PSO algorithm.

.

4.5 Summary

This study focuses on the conceptual design and development of the proposed polygeneration system. The step of conceptual design in terms of the life-cycle design for thermal systems

plays a crucial role in ensuring an entire project's success. System simulation, evaluation, and optimization are addressed in this work.

Regarding the system simulation, Aspen HYSYS®, being a professional commercialized simulation software, is applied. For evaluating the system performance, energetic, exergetic, economic, and exergoeconomic analyses are conducted. Exergy-based methods, including the conventional and advanced exergetic and exergoeconomic analyses, are implemented as the primary research focus in this study over energetic methods for several reasons: they consider the interaction between a given state of the entity with its ambient conditions; they identify the magnitudes, locations, and causes of real inefficiencies; they help design engineers better allocate the engineering resources and efforts for system design and optimization.

Also, for system evaluation and optimization, an automation process is carried out. In other words, the simulation software, Aspen HYSYS®, is connected with a programming language, Python, through a binary interface. The connection enables to automate the following calculation processes after the simulation by allowing the "communications" between these two programs. Thanks to the automation, the manual failure caused by exporting and importing values can be minimized, and the computation time can be reduced.

For the system optimization, stochastic algorithms (DE and PSO) are applied since the component models are embedded in Aspen HYSYS® and unknown for the users. The objective functions and decision variables of the optimization problems are specified in Python, while Aspen HYSYS® simulates the "candidate solutions" selected by the algorithms and checks if the design constraints are violated or not. Only by robustly designing the simulations and coordinating these two programs (Aspen HYSYS® and Python) wisely, optimization procedures can be executed smoothly.

<div align="right">

5

</div>

System investigation

In this chapter, the performance investigation of the proposed polygeneration system is carried out. The main focuses are the system exergetic efficiency and the costs of products under different operating conditions. The system is evaluated predominantly on the system level since the system efficiency and the final product cost(s) underlie the criteria of promoting a new technology or a new system into the market. This chapter aims to deepen the understanding of the proposed system and broadly overview its system performance by investigating the influences of predominant operating parameters on the system performance. The results from this chapter will provide important information for further evaluating and optimizing the system, which will be discussed in the following case study chapter.

5.1 Assumptions made for calculating *PEC*

First, the procedures applied for estimating the component *PEC* are explained in detail.

- *Printed circuit heat exchanger (HE and GC)*

    Since HE and GC are expected to work at high-temperature and high-pressure, printed circuit heat exchanger (PCHE) is selected to fulfill the requirements of the closed CO_2 power cycle rather than a standard shell and tube heat exchanger [103, 52]. The PCHE applies a relatively new technology used for manufacturing compact heat exchangers by photoetching micro-channels and a specific solid-state joining process to boost the mechanical integrity and efficiency, technology readiness level, and flexibility of heat exchangers [84, 104]. Meanwhile, the overall system's capital cost is expected to be reduced by replacing the shell and tube heat exchangers with the PCHEs. Based on the research of Heatric (UK) [105], a company has already started to produce PCHEs for supercritical power cycle applications, the cost of a PCHE should be estimated by its weight, namely, $Cost_{\mathrm{PCHE}} = Cost_{\mathrm{metal\ per\ unit\ of\ mass}} \times m_{\mathrm{metal\ for\ PCHE}}$, with $m_{\mathrm{metal\ for\ PCHE}} = \rho_{\mathrm{metal}} \times V_{\mathrm{metal}}$. To calculate the volume of the metal V_{metal} used for manufacturing the heat exchanger, the volume fraction f_V, which is one of the PCHE characteristics indicating the ratio of the metal volume to the entire volume of the heat exchanger, is needed. The equation is expressed as:

$V_{\mathrm{metal}} = V_{\mathrm{PCHE}} \times f_V$. The size of the heat exchanger V_{PCHE} can be estimated by the equation, $V_{\mathrm{PCHE}} = A_{\mathrm{PCHE}}/$typical area per unit of volume; where A_{PCHE} denotes the area of the heat exchanger, and the typical area per unit of volume depends mainly on the operating pressure of the PCHE. According to the information provided by Heatric (UK) [105], the typical area per unit of volume for PCHEs is around 1300 m^2/m^3 at the operating pressure of 100 bar and 650 m^2/m^3 at 500 bar. The heat transfer area of the heat exchanger A_{PCHE}, can be calculated by the equation, $\dot{Q} = U \cdot A \cdot \Delta T$ where $\dot{Q}$ stands for the heat transfer rate within the heat exchanger; U is the overall heat transfer coefficient; and ΔT denotes the log mean temperature difference ($LMTD$). The assumptions made for estimating the PCHE cost are summarized in Table 5.1.

Table 5.1: Assumptions made for the cost estimation of printed circuit heat exchangers (PCHEs).

Item	Nomenclature	Value	Unit
Overall heat transfer coefficient	U		
Gas-gas heat exchanger		250 [106, 107, 108]	$W/(m^2 \cdot K)$
Water-gas heat exchanger		400 [106, 107, 108]	$W/(m^2 \cdot K)$
The volume fraction	f_V	0.564 [109]	m^3/m^3
Construction material	SS316*[110]	-	-
The density of SS316	ρ_{SS316}	7990[110]	kg/m^3
Cost of SS316 per unit of mass	$Cost_{\mathrm{SS316}}$	50 [105]	\$/kg

*: SS stands for stainless steel

- *Turbomachinery of power cycle (CM–P and EX)*

The turbomachinery operating with CO_2 of a S-CO_2 power system is not well known for commercial application yet. Since the proposed polygeneration system is designed for producing the electric power in kW scale, the cost functions of turbomachineries discussed in Refs [109, 108] regarding MW-scaled S-CO_2 power cycle are not well suited in this case. In this work, the *PEC*s of the compressor and the turbine in the power cycle are estimated by the following equations [111]:

$$\log_{10}\left(C_{\mathrm{CM}}\right) = 2.2897 + 1.3604 \log_{10}\left(X\right) - 0.1027 \left[\log_{10}\left(X\right)\right]^2 \tag{5.1}$$

$$\log_{10}\left(C_{\mathrm{EX}}\right) = 2.2476 + 1.4965 \log_{10}\left(X\right) - 0.1618 \left[\log_{10}\left(X\right)\right]^2 \tag{5.2}$$

where X is the power capacity of compressor and turbine in kW.

- *Main components of refrigeration cycle (CM–R and EVAP)*

For the compressor (CM–R) and the evaporator (EVAP) of the transcritical refrigeration cycle, their costs are considered in this work as a function of the capacity. Furthermore, cost

correction factors regarding the design material, design pressure, and design temperature are also taken into account [112]:

$$C_E = C_B \cdot (X/X_B)^M \cdot f_M \cdot f_P \cdot f_T \tag{5.3}$$

where C_E stands for the cost of the new equipment, which has the capacity of X; C_B denotes the known base cost for an equipment with its capacity of X_B; M is an exponential factor indicating the cost correlation of the new equipment cost with the known base cost; fM, fP and fT are the correction factors in terms of design material, design pressure, and design temperature, respectively.

Regarding the component capacity X, the power consumption is used for estimating the cost of the compressor CM–R, while, for the evaporator EVAP, X refers to the heat transfer area of the heat exchanger. For calculating the heat transfer area of the evaporator, the overall heat transfer coefficient is set as 950 $W/(m^2 \cdot K)$ [113]. In Table 5.2, the values used for CM–R and EVAP cost estimation are listed.

Table 5.2: The assumptions made for computing the costs of the compressor CM–R and the evaporator EVAP [112].

		CM–R			
C_B ($)	X_B (kW)	M (-)	f_M (-)	f_P (-)	f_T (-)
98,400	250	0.95 [88]	1	1.5	1
		EVAP			
C_B ($)	X_B (m^2)	M (-)	f_M (-)	f_P (-)	f_T (-)
32,800	80	0.68	1	1.3	1

- *Other components*

  For PECs of the TV and others, the following assumptions are made:

  1. The cost of the TV equals to 100 € as mentioned by [113] for a refrigeration machine with 100 kW refrigeration capacity;

  2. The costs of the mixer and the splitter are neglected.

Finally, the costs of all the components are brought up-to-date using the chemical engineering's plant cost index (CEPCI) and applied in US$$_{2017}$:

$$Cost \text{ Reference year} = Cost \text{ Original year} \times \frac{Cost \ index \text{ Reference year}}{Cost \ index \text{ Original year}} \tag{5.4}$$

5.2 Definitions and equations applied to exergy-based methods

For computing product costs per unit of exergy for the overall system, the definitions of fuel and product are first needed for each component and the overall system (presented in Tables 5.3 and 5.4).

Table 5.3: Definitions of fuel and product for each component [88].

Comp.	$\dot{E}_F$	$\dot{E}_P$
HE	$\dot{Q}_{HE}\ (1\text{-}T_0/T_{HS})$	$\dot{E}_1 - \dot{E}_6$
EX	$\dot{E}_1 - \dot{E}_2$	$\dot{W}_{EX}$
MIX	-	-
Cooler	$\dot{E}_3 - \dot{E}_4$	$\dot{E}_{12} - \dot{E}_{11}$
SPLIT	-	-
CM–P	$\dot{W}_{CM-P}$	$\dot{E}_6 - \dot{E}_5$
TV	$\dot{E}_7^{M} - \dot{E}_8^{M} + \dot{E}_7^{T}$	$\dot{E}_8^{T}$
EVAP	$\dot{E}_8 - \dot{E}_9$	$\dot{E}_{14} - \dot{E}_{13}$
CM–R	$\dot{W}_{CM-R} + \dot{E}_9^{T}$	$\dot{E}_{10}^{T} + \dot{E}_{10}^{M} - \dot{E}_9^{M}$

Table 5.4: Definitions of fuel and product for the overall system [88].

$\dot{E}_F$	$\dot{E}_P$
$\dot{Q}_{HE}\ (1\text{-}T_0/T_{HS})$	$\dot{W}_{net} + \dot{E}_{Heating} + \dot{E}_{Cooling}$

$\dot{W}_{net}$ in Table 5.4 denotes the net power produced from the overall system, which can be expressed as:

$$\dot{W}_{net} = \dot{W}_{EX} - \dot{W}_{CM-P} - \dot{W}_{CM-R} \tag{5.5}$$

The expressions for calculating $\dot{E}_{Heating}$ and $\dot{E}_{Cooling}$ in Table 5.4 are given, respectively, in Eq. 5.6 and 5.7:

$$\dot{E}_{Heating} = \dot{E}_{12} - \dot{E}_{11} \tag{5.6}$$

$$\dot{E}_{Cooling} = \dot{E}_{14} - \dot{E}_{13} \tag{5.7}$$

These fuel and product definitions are consistent in this chapter unless otherwise indicated. Only physical exergy is considered, for now. Chemical exergy is neglected. There are no definitions of fuel and product for the MIX and the SPLIT, as the MIX is considered as a dissipative component, and the SPLIT only splits streams by their mass flow ratios.

For evaluating the costs of the products, the individual cost of each product, as well as the average product cost per unit of exergy, are taken into consideration. The individual cost of the products is calculated by solving the matrix composed of cost balances and auxiliary equations of each component, while for computing the average product cost, one single equation for the overall system can be applied. The component-wise and system-wise cost balances, as well as auxiliary equations for conducting the exergoeconomic analysis, are given in Tables 5.5 and 5.6.

Table 5.5: Cost balances and auxiliary equations of each component for exergoeconomic analysis.

Comp.	Cost balance	Auxiliary equation
HE	$\dot{Q}_{HE}\,(1\text{-}T_0/T_{HS})\,c_{HS}+\dot{Z}_{HE}=\dot{E}_1 c_1 - \dot{E}_6 c_6$	c_{HS}=5 \$/GJ(Assumption)
EX	$\dot{E}_1 c_1 - \dot{E}_2 c_2+\dot{Z}_{EX}=\dot{W}_{EX}c_W$	$c_1=c_2$ (F rule)
MIX	$\dot{E}_2 c_2 - \dot{E}_{10}c_{10}+\dot{Z}_{MIX}=\dot{E}_3 c_3$	-
Cooler	$\dot{E}_3 c_3 - \dot{E}_4 c_4+\dot{Z}_{Cooler}=\dot{E}_{12}c_{12} - \dot{E}_{11}c_{11}$	$c_3=c_4$ (F rule); $c_{11}=0$ (Assumption)
SPLIT	$\dot{E}_4 c_4+\dot{Z}_{SPLIT}=\dot{E}_5 c_5 + \dot{E}_7 c_7$	$c_4=c_5$ (P rule)
CM–P	$\dot{W}_{CM\text{–}P}c_W+\dot{Z}_{CM\text{–}P}=\dot{E}_6 c_6 - \dot{E}_5 c_5$	-
TV	$\dot{E}_7^M c_7 - \dot{E}_8^M c_8 + \dot{E}_7^T c_7+\dot{Z}_{TV}=\dot{E}_8^T c_8$	-
EVAP	$\dot{E}_8 c_8 - \dot{E}_9 c_9+\dot{Z}_{EVAP}=\dot{E}_{14}c_{14} - \dot{E}_{13}c_{13}$	$c_8=c_9$ (F rule); $c_{13}=0$ (Assumption)
CM–R	$\dot{W}_{CM\text{–}R}c_W + \dot{E}_9^T c_9+\dot{Z}_{CM\text{–}R}=\dot{E}_{10}^T c_{10} + \dot{E}_{10}^M c_{10} - \dot{E}_9^M c_9$	-

Table 5.6: Cost balance of the overall system for exergoeconomic analysis.

Cost balance for the overall system
$\dot{Q}_{HE} \cdot (1\text{−}T_0/T_{HS}) \cdot c_{HS} + \dot{Z}_{total} = (\dot{W}_{net} + \dot{E}_{Heating} + \dot{E}_{Cooling}) \cdot c_P^{av.}$

5.3 Effect of the power generation on the performance of the polygeneration system

The heat-driven compression refrigeration machine was initially designed for producing refrigeration effect. By applying CO_2 as the working fluid, the closed power cycle operates entirely in the supercritical region. The Cooler's operating condition is close to its critical point, which offers a great potential to generate power with high efficiency and produce a massive amount of hot water that should be considered to utilize instead of rejecting directly to the environment. The influences of the net power generation on system performance, including the system's exergetic efficiency and the product costs, are investigated in this section. The net power generation of the overall system varies starting from no net power generation, which means the shaft work produced from the EX is merely used for powering two compressors (CM–P and CM–R), until the net power produced equals fivefold power consumption of the refrigeration cycle, namely, the power cycle should produce six times the power which is required by CM–R.

Fig. 5.1 shows the variations of the product costs of the polygeneration system by increasing the amount of power generation. All the costs, including the cost of each product and the average cost of products, decline by producing more power. Moreover, the general trend is that the decreases in all the costs are dramatic when the system operates not only as a refrigeration machine but also producing extra power. The declines have become more and more gradual, with more net power produced. It is also worth mentioning that the power cost is the lowest among all the products. In comparison, the cost per unit of exergy regarding refrigeration is around 3-5 times more expensive than that regarding power. As the net power production increases, the cost difference between the refrigeration and the power emerges. Because the reduction in the unit cost of power (about 60%) is more significant than the decrease in the refrigeration cost per unit of exergy (about 40%).

Moreover, the products' average cost is very close to the heating cost per exergy unit when the ratio of the net power production to the power consumption of the refrigeration cycle is between 0 and 0.5. As more power is produced, the average cost of the products slowly towards the electricity cost since without net power production or with only limited power generated, the amount of heat generation is the largest compared to that of the power and the refrigeration, which in turn, it dominates the average product cost, while the dominating effect weakens with the fact that power contributes more and more to the share of the final products.

The contributions of each product to the final products in exergy are presented in Fig. 5.2. The refrigeration capacity percentage is the lowest (less than 10% except for the case without net power generation). Because the heat capacity is generated from both cycles and the temperature difference between the hot water and the ambient temperature is higher than that between the second refrigerant and the ambient temperature, the system always produces a larger amount of heating capacity than its refrigeration capacity.
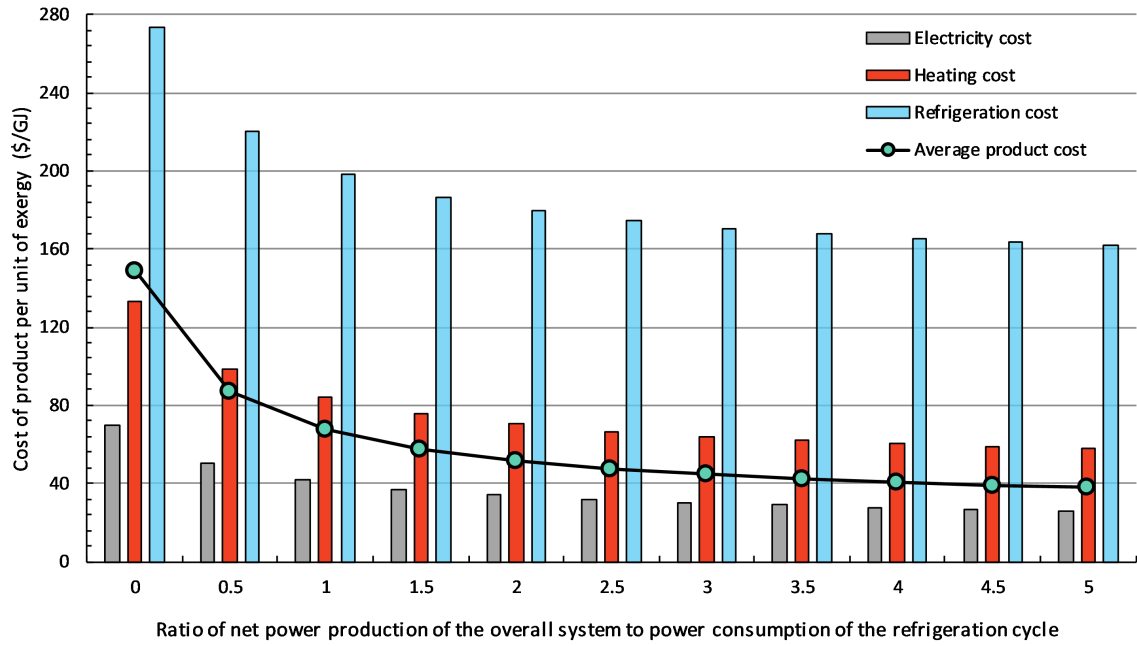
Figure 5.1: The variations of electricity, heating, refrigeration costs, and the average product cost of the overall system by increasing the ratio of the net power generation to the power consumption of the refrigeration cycle.
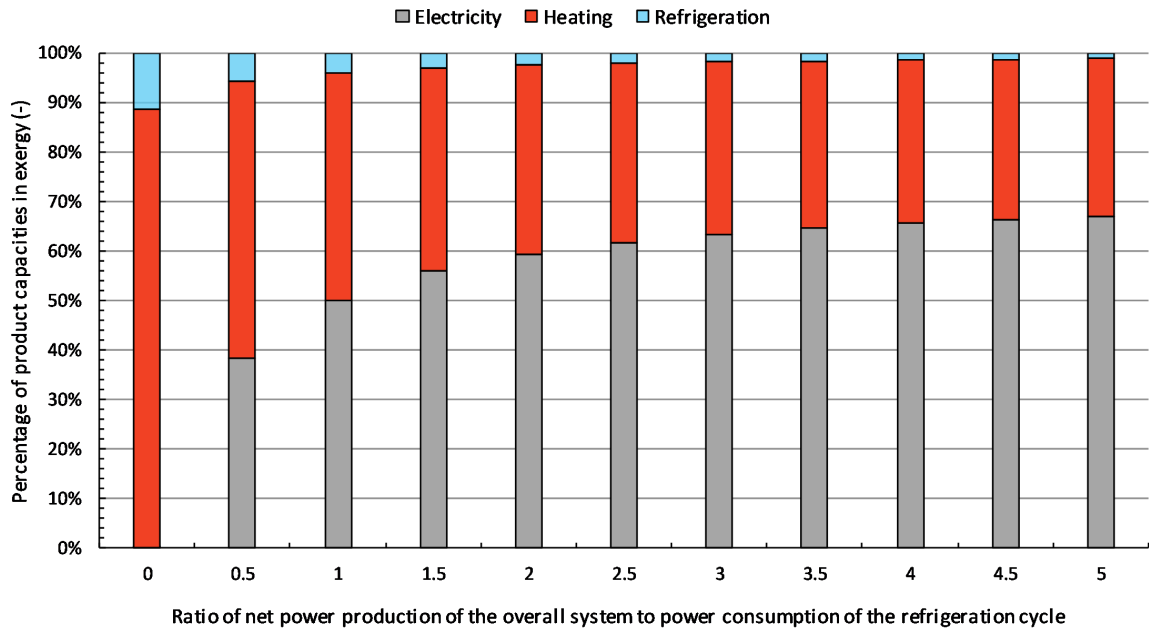
Figure 5.2: The contributions of electricity, heating and refrigeration capacities in exergy to the final products of the overall system by increasing the ratio of the net power generation to the power consumption of the refrigeration cycle.

In Fig. 5.3, the influences of increasing power generation on the mass flow rates of both sub-cycles are demonstrated on the primary Y-axis, while the system exergetic efficiency is shown on the secondary Y-axis. As expected, the mass flow rate of the power cycle increases steadily. Surprisingly, the refrigeration cycle's mass flow rate does not remain consistent but shows a gradual drop. The system exergetic efficiency doubles (from 19% to 38%) with a steep

rise when the ratio of the net power production to the power consumption of the refrigeration cycle varies from 0 to 2, then the increase becomes slower and slower.
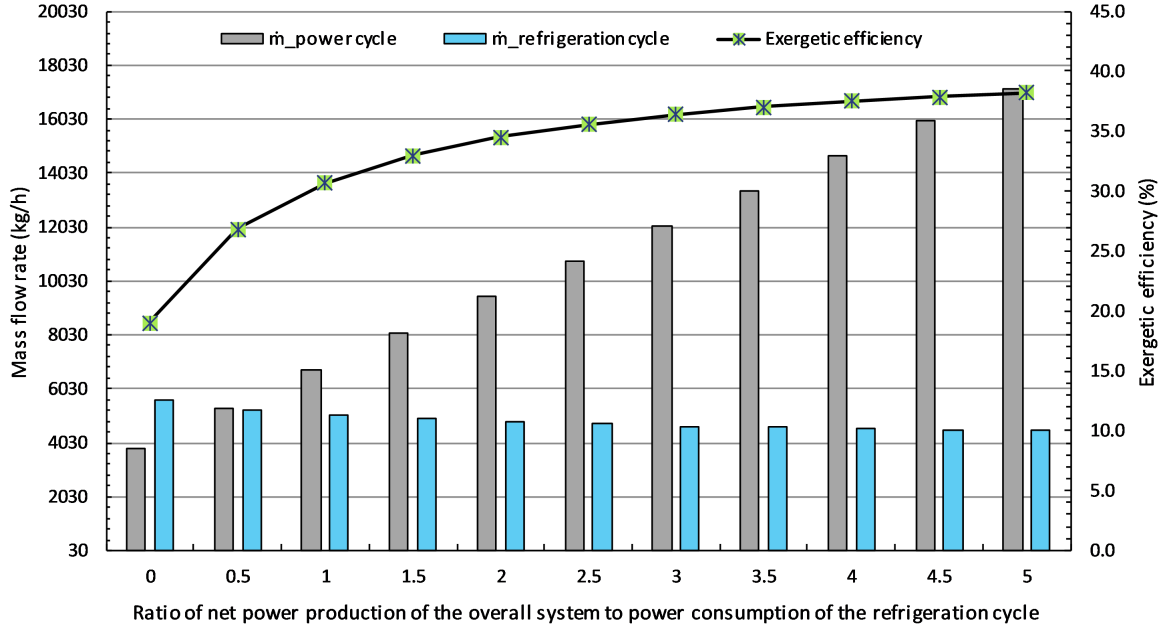
Figure 5.3: The variations of mass flow rates of power cycle and refrigeration cycle and the system exergetic efficiency by increasing the ratio of the net power generation to the power consumption of the refrigeration cycle.

To investigate why the refrigeration cycle's mass flow rate is affected by the power production, the temperature-heat flow diagrams of the mutual heat exchanger (Cooler), which connects the power cycle with the refrigeration cycle, are examined in two extreme cases. Case A without net power generation and the case B with net power produced equalling to fivefold power consumption of the refrigeration cycle are presented in Fig. 5.4 (a) and Fig. 5.4 (b), respectively. Compared to case A, the mass flow rate of the power cycle in case B is higher. Thus, a higher temperature of stream 3 can be achieved since the ratio of the mass flow rate of the power cycle to that of the refrigeration cycle increases, and the exit stream of the EX (stream 2) always has a higher temperature than the outlet stream of CM–R (stream 10). As a result, the slope of the cooling water in case A is steeper than that in case B, as more water can be heated to a specific temperature by a hotter stream per unit of mass flow rate and in turn, the curve of the cooling water in case B is flatter. By applying CO_2 as working fluid, the pinch point of the Cooler occurs in the middle of the heat exchanger rather than at the hot or the cold end. However, if the curve of the cooling water were completely flat, the pinch point will be at the cold end. This reveals that for the Cooler's pinch point, the flatter the curve of the cooling water is, the closer it moves towards the cold end. Therefore, the pinch point of the Cooler is closer to its cold end in case B than that in case A, which in turn results in a lower exit temperature of the hot stream (stream 4) leaving the Cooler.
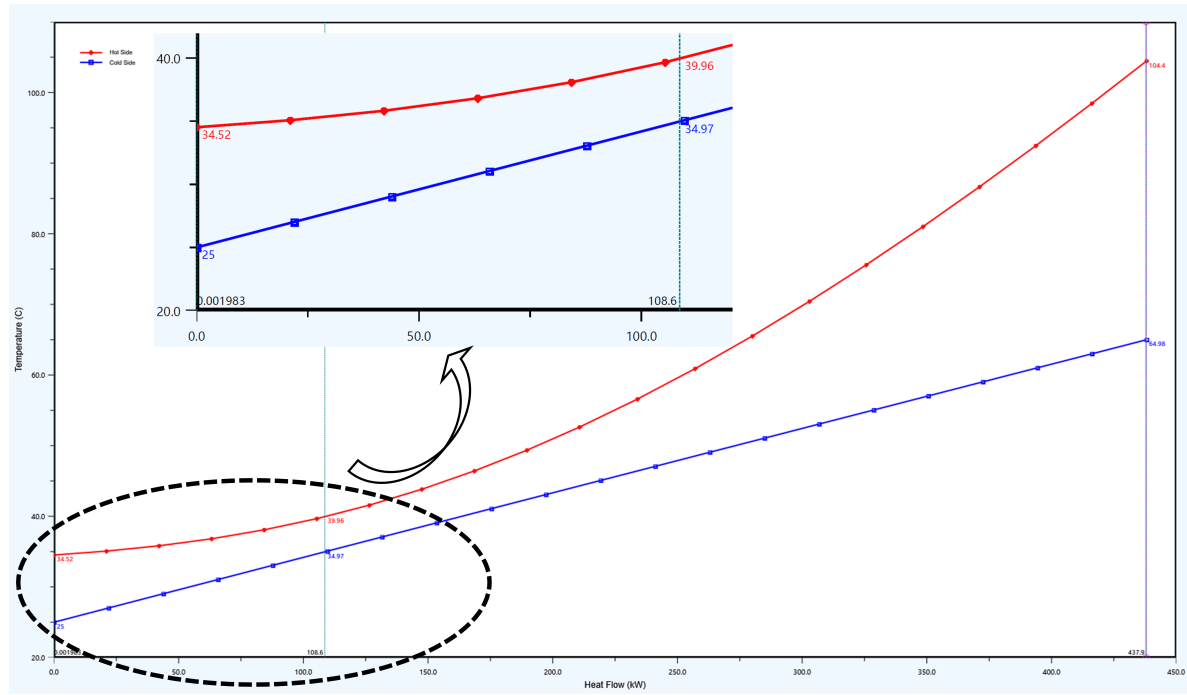
(a)
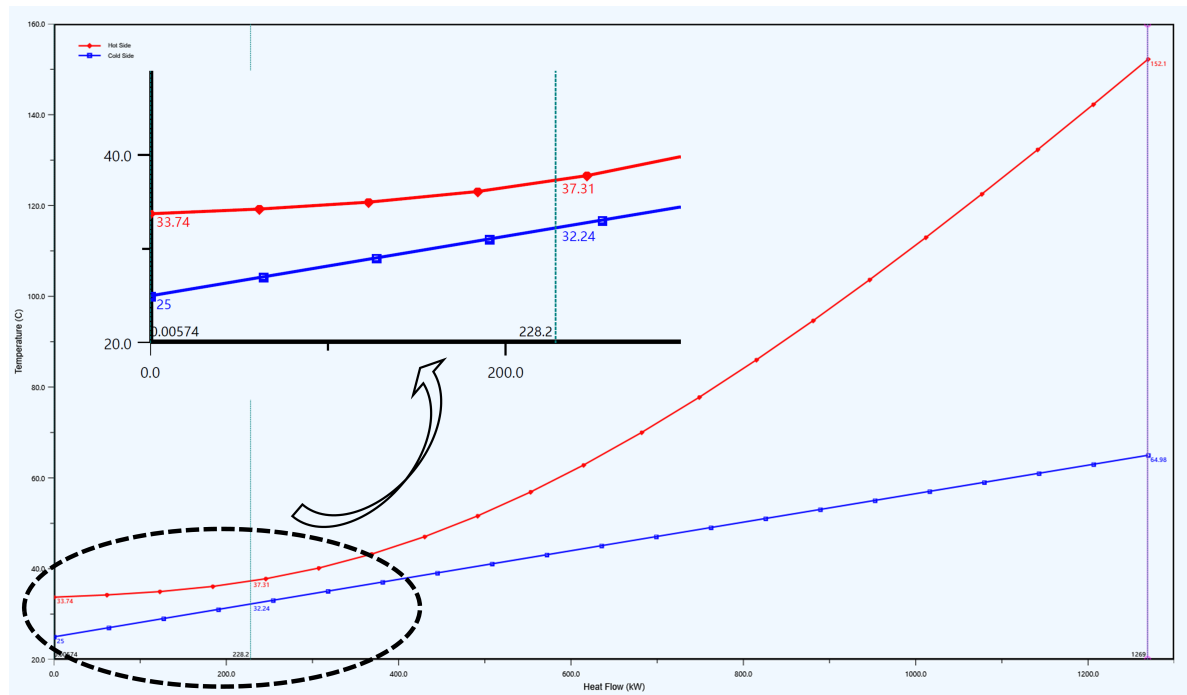
(b)

Figure 5.4: The temperature-heat flow diagrams of the gas cooler: (a) with no net power production, (b) with net power produced equalling to fivefold power consumption of the refrigeration cycle.

In Fig. 5.5, the influence of producing power on the "shape" of the cycle is demonstrated. The changes have been marked with dash lines. One can notice that the cycle becomes "fatter"; thus, less mass flow rate is required to produce 100 kW (in energy) refrigeration effect for the refrigeration cycle. For heating capacity, although the refrigeration cycle's mass flow rate decreases gradually, the mass flow rate of the power cycle rises significantly. Meanwhile, the

temperature difference between the hot inlet stream and the hot outlet stream (namely, the distance between point 3 and point 4) within the Cooler also increases. The system is expected to produce more heating and increase power production. The changes in the product capacities in exergy are listed in Table 5.7. The results reveal that the refrigeration capacity variation is trivial, while the heating capacity boosts from around 27 kW to 91 kW, which more than triples its heating production compared to the case without net power generation. However, regarding the overall system's final products, the net power production has been influenced the most, and the heating production increase is the side-effect by increasing the produced power.
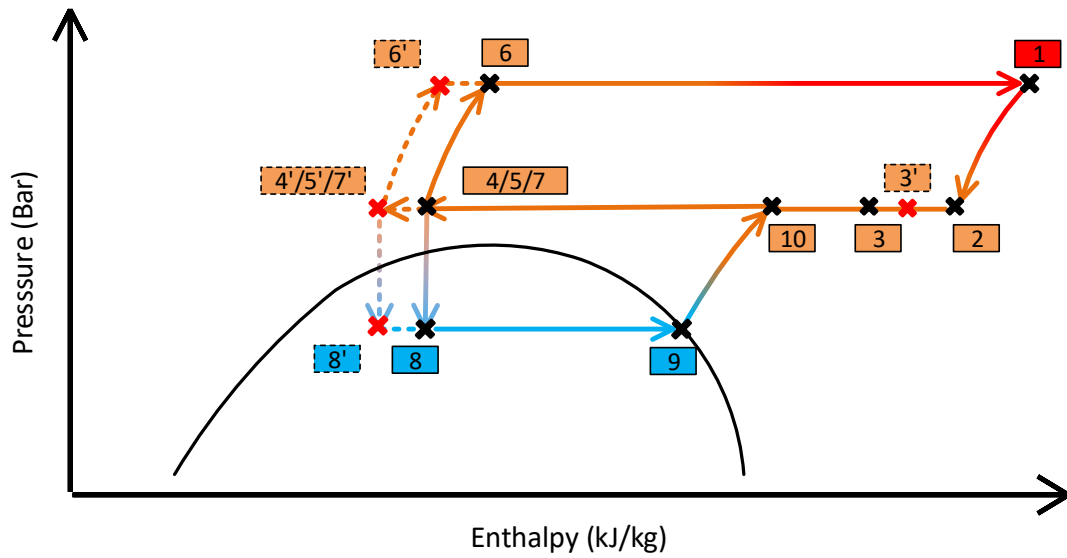
Figure 5.5: The cycle variations of the overall system shown in the pressure-enthalpy diagram (with dash lines) by increasing the ratio of the net power generation to the power consumption of the refrigeration cycle.

Table 5.7: The variations of the power, heating and refrigeration capacities in exergy by increasing the ratio of the net power generation to the power consumption of the refrigeration cycle.

$\dot{W}_{\mathrm{net}}/\dot{W}_{\mathrm{CM-R}}$	0	0.5	1.0	1.5	2.0	2.5	3.0	3.5	4.0	4.5	5.0
Power[kW]		0.00	22.98	43.71	63.17	82.53	101.37	120.08	138.54	156.85	175.00	193.21
Heating[kW]		27.03	33.60	40.06	46.33	52.86	59.26	65.69	72.10	78.46	84.78	91.16
Refrigeration[kW]	3.48	3.48	3.48	3.48	3.48	3.48	3.48	3.48	3.48	3.48	3.48

In short, by increasing the ratio of the net power generation to the power consumption of the refrigeration cycle, the cost of each product and the average cost of the final products reduce, while the exergetic efficiency of the overall system rises. The refrigeration cycle's mass flow rate decreases slowly; however, the mass flow rate of the power cycle increases dramatically. The shape of the cycle becomes "fatter", and more heating capacity is produced along with

the power production increase. In terms of the system performance, employing the proposed polygeneration system as a trigeneration system (namely, with power generation) shows the positive effects not only on the system efficiency but also on the cost of the product(s).

Thus, the assumption of producing twofold the power consumed by the CM–R as the system net power production is made in the following sections unless otherwise indicated:

- The system is considered as a trigeneration system with the ratio of the net power production to the power consumption of the refrigeration cycle equalling to 2, $\dot{W}_{\text{net}}$ / $\dot{W}_{\text{CM–R}} = 2$.

5.4 Effect of the heat source temperature on the performance of the polygeneration system

As aforementioned, any heat source can be considered the "fuel" to power the polygeneration system, but this work focuses mainly on the waste heat with low-medium temperature. In this section, the system performance is evaluated by assuming the available heat sources with different temperatures ranging from 200 to 400 °C. The calculation is based on the fixed power and refrigeration capacities; therefore, the heating capacity and the required amount of the heat source are computed. All the heat produced from the system is considered for local supply via a mini-district heating system, and the heat source is supposed to be always sufficient for powering the entire system. Two different scenarios in terms of the heat source cost are taken into consideration: 1. The heat sources with various temperatures have the same cost per unit of exergy (5 \$/GJ is assumed); 2. A cost range has been considered for different heat sources.

- *Without the consideration of the heat source cost*

For the heat source with relatively low temperature (100 °C heat source as the representative here), its pressure and enthalpy diagram is illustrated in Fig. 5.6. It can be seen that the cycle shifts entirely to the left, and the temperature of the EX outlet stream (around 35 °C with the 100 °C heat source) can be even lower than that of the outlet stream from the CM–R (around 65 °C). Therefore, in this case, the heating capacity designed for local space heating and domestic hot water supply, which needs to heat the cooling water to 65 °C, is not possible, and the Cooler should be considered as a dissipative component. By adjusting the cold outlet stream of the Cooler (stream 12) to 30 °C, it is interesting to observe in Fig. 5.7 that the pinch point within the Cooler shifts towards its cold end and as the results, the hot outlet stream exits the Cooler with the temperature lower than its critical point. Thus, a pump instead of the CM–P should be used.
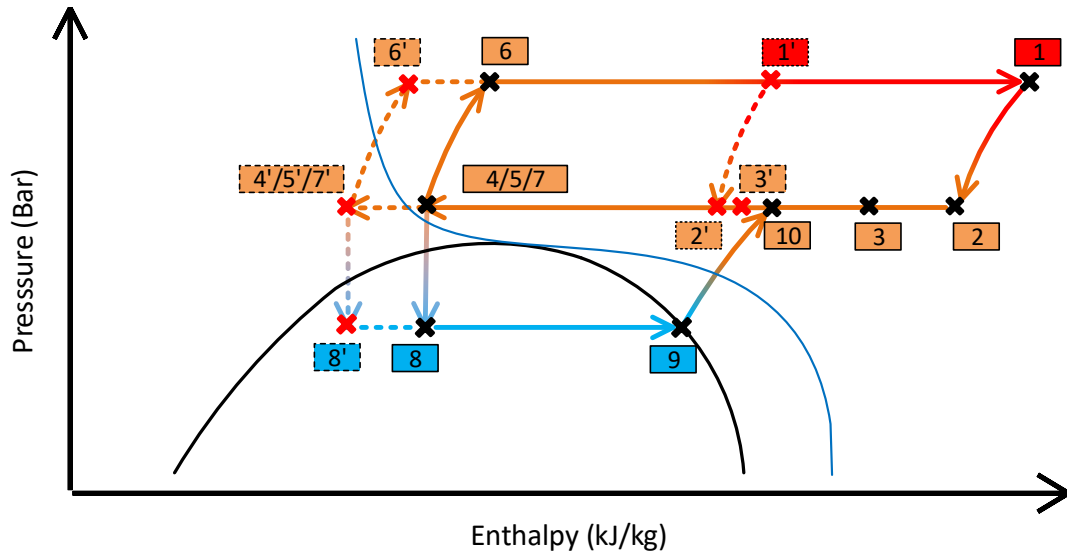
Figure 5.6: The cycle variations of the proposed polygeneration system with low temperature heat source illustrated in the pressure-enthalpy diagram (with dash lines) by using 100 °C as the representative.
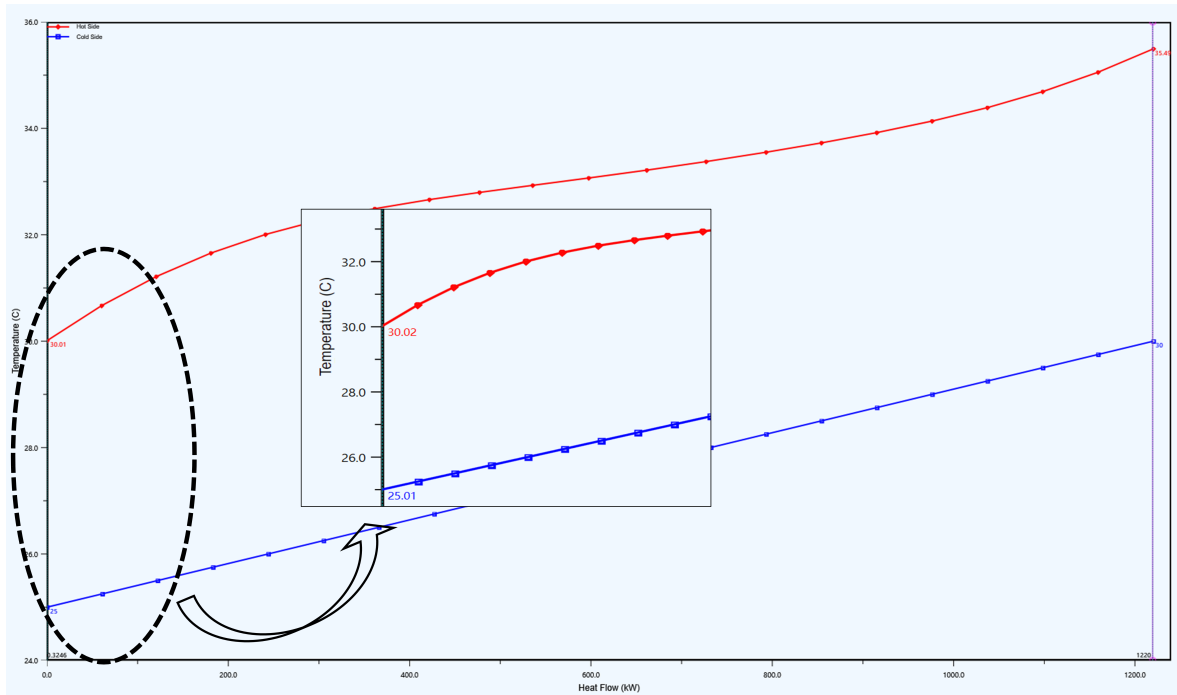
Figure 5.7: The temperature-heat flow diagram of the gas cooler in the case of driving the proposed the polygeneration system by low temperature heat source (100 °C as the representative).

Reducing the turbine inlet pressure (*TIP*) can also be considered when the heat source temperature is too low to produce heating capacity, as shown in Fig. 5.8. The power cycle becomes "shorter", the pressure ratio of the EX, as a consequence, reduces; thus, the mass flow rate of the power cycle rises. The mass flow rate of the refrigeration cycle also shows an increase. If the heat source temperature is very low, then design turbomachinery with a very low-pressure ratio would be the hurdle in this case, and also, the size of the system becomes

bigger. Therefore, in this work, the low-medium grade heat sources with temperatures higher than 200 °C are investigated, the modification of the proposed system or the specific design of the heat-driven refrigeration machine utilizing the heat source with a temperature lower than 200 °C are out of the research scope.
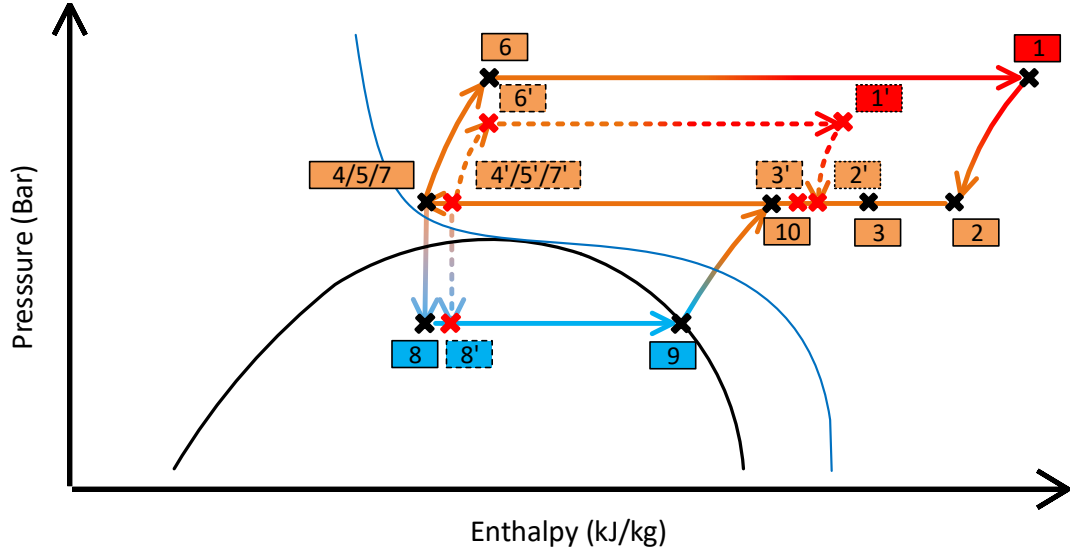
Figure 5.8: The cycle variations of the proposed polygeneration system with lower *TIP* driving by low temperature heat source illustrated in the pressure-enthalpy diagram (with dash lines) by using 100 °C as the representative.

To investigate how does the heat source temperature affect the performance of the proposed system in terms of the cost of each product and the average cost of the products per unit of exergy, heat sources with temperatures of 200, 300, and 400 °C are selected to represent the low-medium grade heat sources. The terminal temperature difference on the hot side of the HE ranges from 40 to 5 K. The results regarding the cost of the electricity, the refrigeration, and the heating per unit of exergy are presented in Figs. 5.9-5.11. The average system cost of the final products per exergy unit by varying the heat source temperature is displayed in Fig. 5.12.

It can be seen that the cost of the electricity and the refrigeration show the same tendency that the higher the heat source temperature, the lower the cost. However, for the cases with the same heat source temperature but ranging the hot side terminal temperature difference of the HE from 40 to 5 K, there is always a minimum cost, which occurs when the terminal temperature difference of the HE hot side approaches its smallest value, for the electricity cost and the refrigeration cost. It is also clear that when the heat source temperature increases, the influence of the terminal temperature difference on the electricity cost and the refrigeration cost becomes less significant. For the cases with a heat source temperature of 400 °C, the changes in the electricity cost and the refrigeration cost by varying the HE terminal temperature difference are even smaller than 0.5%.
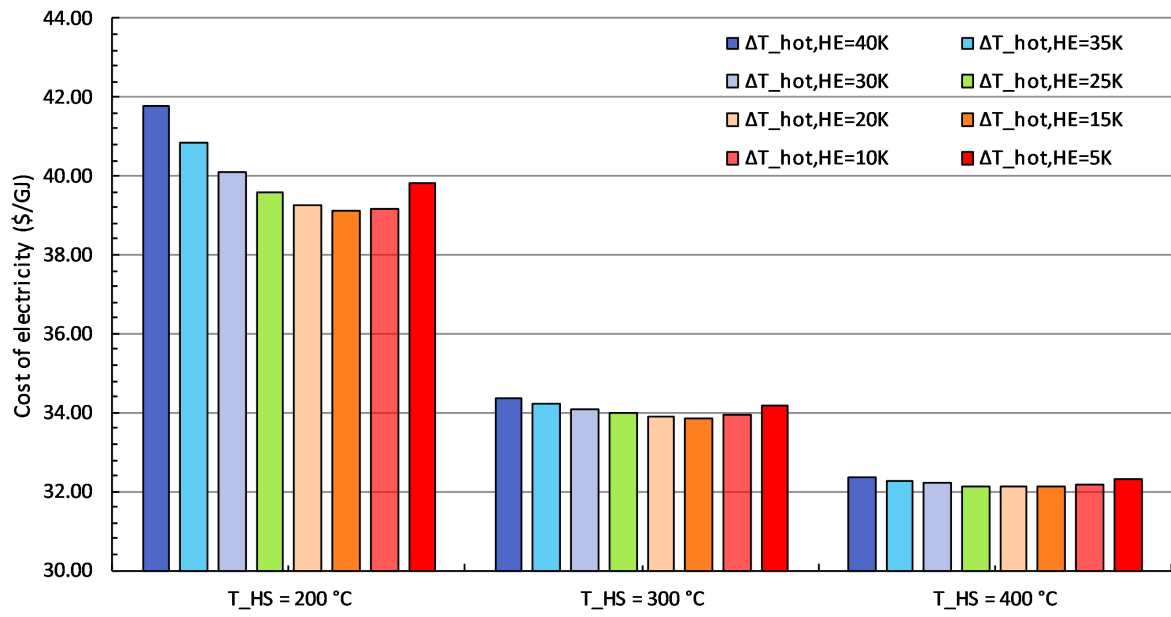
Figure 5.9: Electricity cost of the proposed trigeneration system by varying the heat source temperature from 200 to 400 °C.
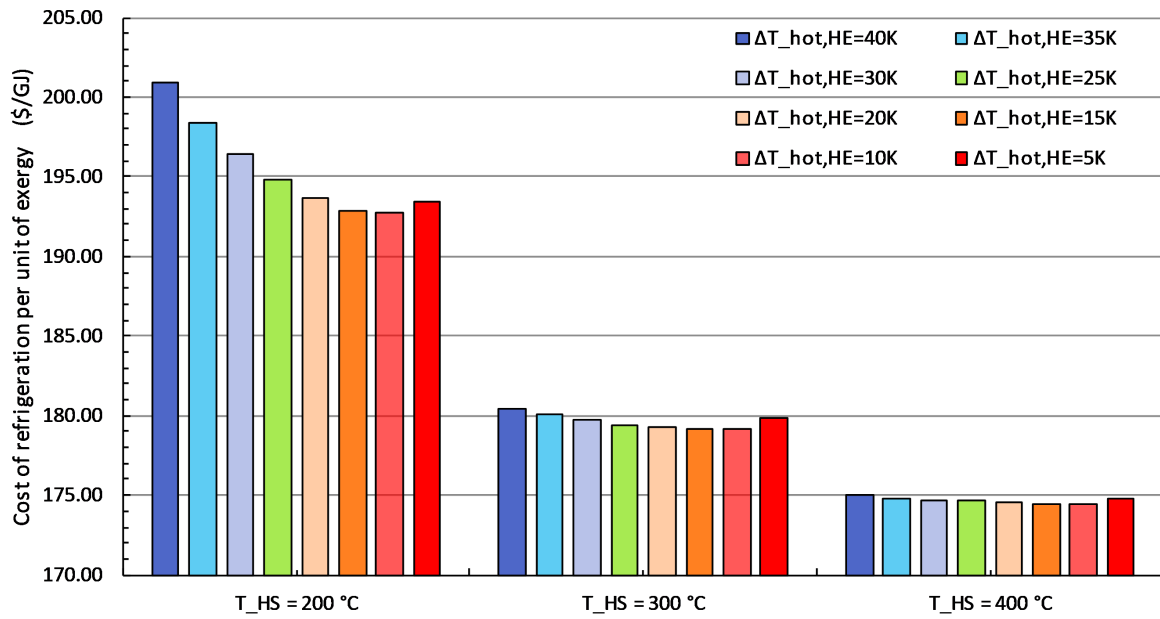
Figure 5.10: Refrigeration cost per exergy unit of the proposed trigeneration system by varying the heat source temperature from 200 to 400 °C.
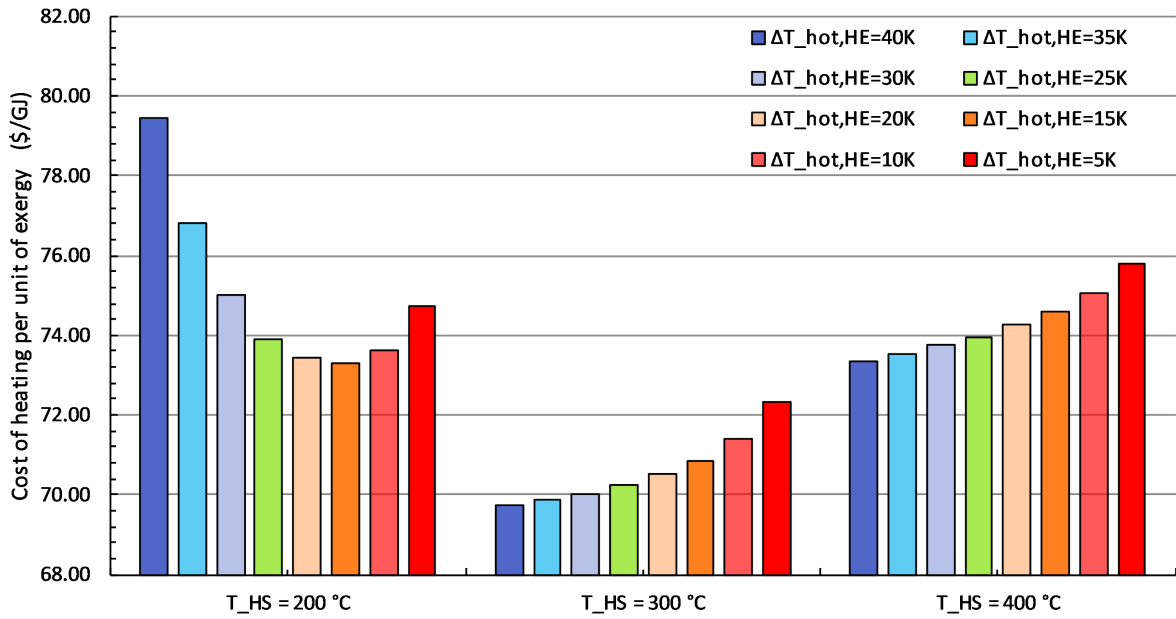
Figure 5.11: Heating cost per exergy unit of the proposed trigeneration system by varying the heat source temperature from 200 to 400 °C.
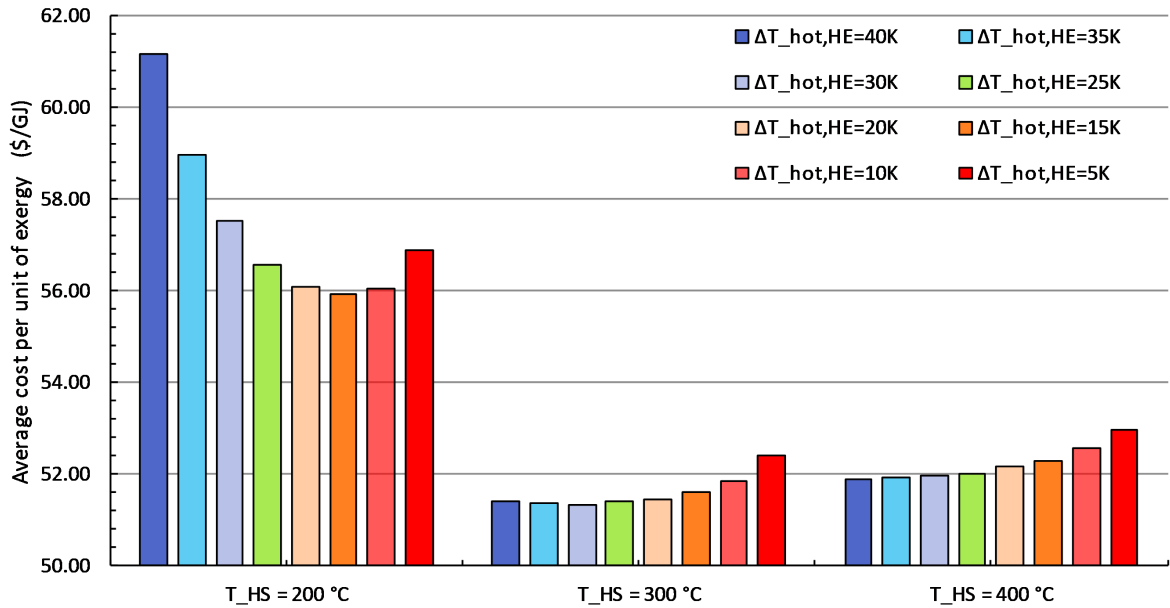
Figure 5.12: Average product cost per exergy unit of the proposed trigeneration system by varying the heat source temperature from 200 to 400 °C.

For the heating cost and the average cost of the products per unit of exergy, only the cases with a heat source temperature of 200 °C show a similar trend that the costs decrease dramatically first then increase gradually by lowering the ΔT of the HE hot side. If the heat sources with temperatures of 300 and 400 °C are available, the cost of the heating capacity and the average cost of final products rise steadily with the terminal temperature difference of the HE hot side changing from 40 to 5 K. Moreover, when the heat source temperature varies

from 300 to 400 °C, the behavior of the heating cost does not show the consistency as that of the electricity and the refrigeration cost. The heating cost increases continuously, and the growth is more noticeable with a heat source temperature of 400 °C by altering the terminal temperature difference of the HE. Since the average product cost neutralizes all the products' changes, the increase in the average cost for heat sources with temperatures of 300 and 400 °C weakens. As results, the average product cost of the proposed trigeneration system has been affected dramatically by changing the heat source temperature from 200 to 300 °C and by lowering the terminal temperature difference of the HE hot side from 40 to 5 K with the heat source temperature of 200 °C. Nevertheless, limited influences on the average cost of the final products have been seen by increasing the heat source temperature from 300 to 400 °C as well as by altering the ΔT of the HE hot side for scenarios with available heat sources with a temperature of 300 and 400 °C.

It can be concluded that the heating cost shows a different reaction compared to the electricity cost and the refrigeration cost when the heat source temperature increases, and this further influences the behaviors of the average product cost. Also, the cost variations for the cases with a heat source temperature of 200 °C differ from that with a heat source temperature of 300 and 400 °C. To discover how does the cycle change by powering the proposed system utilizing the heat sources with different temperatures, Fig. 5.13 (a) and (b) illustrate the cycle variations by lowering the ΔT of the HE hot side with a low-grade heat source (using 200 °C as the representative) and that with a medium-grade heat source (using 400 °C as the representative), respectively.

It is noticeable that for the system driven by a low-grade heat source, the "shape" of the cycle varies more remarkably compared to the cycle variation for the system driven by a medium-grade heat source by altering the terminal temperature difference of the HE hot side. This is because when it comes to the supercritical region of CO_2, the higher the pressure and the lower the temperature, the more apart the isothermal lines keeps between each other. Thus, by decreasing the ΔT of the HE hot side with a step of 5 K, the changes of the mass flow rates of the power cycle and the refrigeration cycle are more significant when the system is driven by the heat source with a temperature of 200 °C in comparison with the heat source with a temperature of 400 °C. The behaviors of the cost variations as the heat source temperature is 200 °C, therefore, differ among the others. In other words, the changes in the costs, including the cost of each product and the average product cost, are influenced dramatically by the significant variations of the mass flow rates of the power cycle and the refrigeration cycle if 200 °C heat source is assumed. For other cases with a heat source temperature of 300 and 400 °C, the "shape" of the cycle changes tenuously, which trivializes the influences of varying the HE operating condition on the system costs.
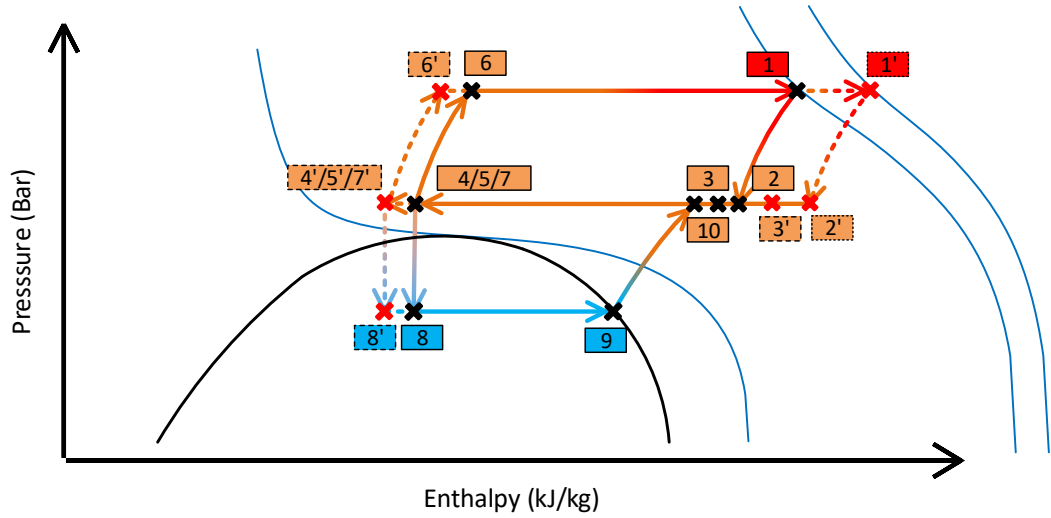
(a) System driven by a low-grade heat source
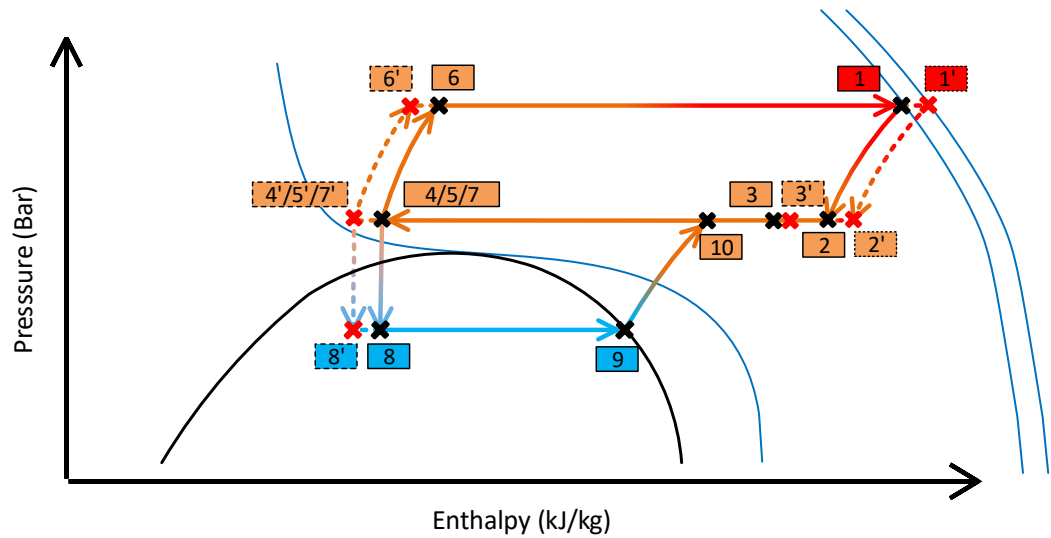
(b) System driven by a medium-grade heat source

Figure 5.13: Cycle variations of the proposed trigeneration system illustrated in the pressure-enthalpy diagram (with dash lines) by lowering the ΔT of the HE hot side with a low-grade heat source (using 200 °C as the representative) and that with a medium-grade heat source (using 400 °C as the representative).

To explain the minimal cost occurrence for the electricity cost and the refrigeration cost with a heat source temperature of 200, 300, and 400 °C, the system driven by the heat source with its temperature of 300 °C is selected as an example to be examined. Fig. 5.14 presents the produced power, heating and refrigeration capacities in exergy when the *TIT* increases from 260 to 295 °C. Since the mass flow rate of the power cycle decreases rapidly, while the mass flow rate of the refrigeration cycle also drops but steadily with *TIT* increasing (shown in Fig. 5.15), the heating capacity reduces by around 7%, which is the most considerable change among the variations of all the products, and the power decreases from 86 to 81 kW (about

6%). The influences of the *TIT* increase on the refrigeration capacity are almost negligible. However, in Fig. 5.15, one can observe that the system exergetic efficiency rises, although the capacities of all the products drop. In Fig. 5.16, the fuel and the product of the overall system (namely, the system exergetic efficiency) have been visualized. As the overall system's fuel reduces at a higher rate than the decrease rate of the sum of all the products, the system exergetic efficiency increases continuously. Nevertheless, the increase of the system exergetic efficiency, as seen in Fig. 5.15, slows after the *TIT* reaches 275 °C.
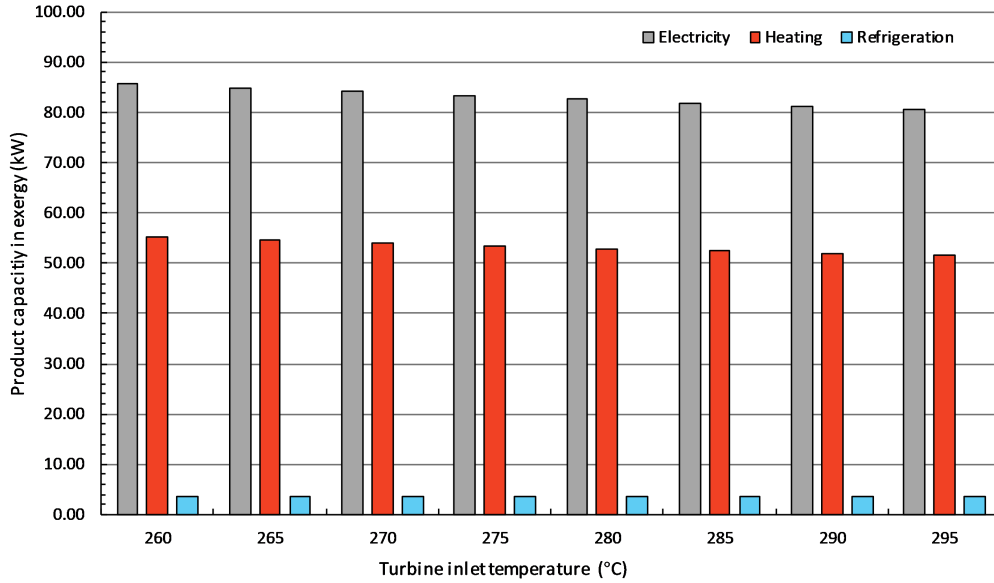
Figure 5.14: Product (Power, heating and refrigeration) capacities in exergy of the proposed trigeneration system by varying the ΔT of the HE hot side from 40 to 5 K with the heat source temperature of 300 °C.
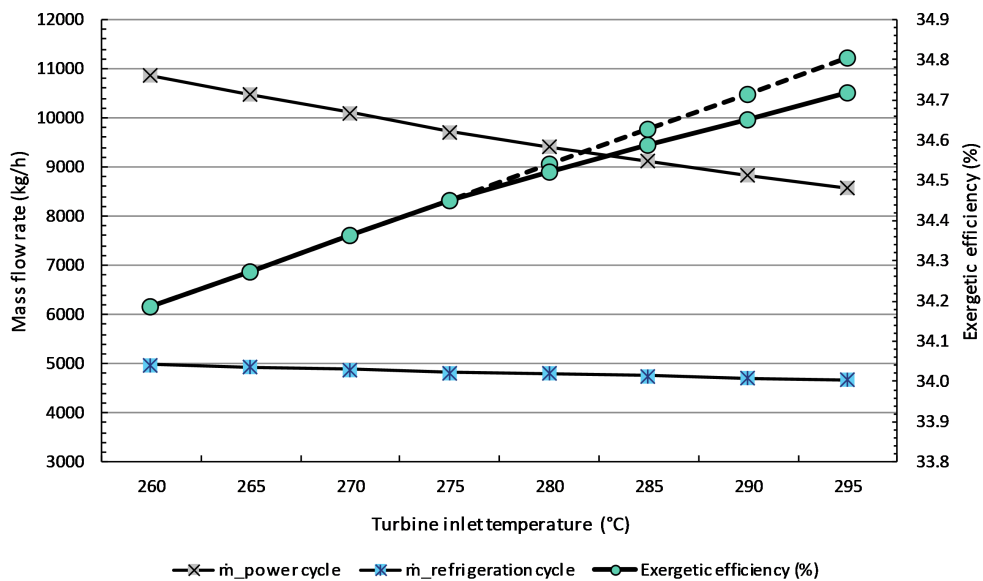
Figure 5.15: Mass flow rates of the power cycle and the refrigeration cycle as well as the system exergetic efficiency of the proposed trigeneration system by varying the ΔT of the HE hot side from 40 to 5 K with the heat source temperature of 300 °C. A hypothetical steady increase in the system exergetic efficiency is indicated with a dash line.
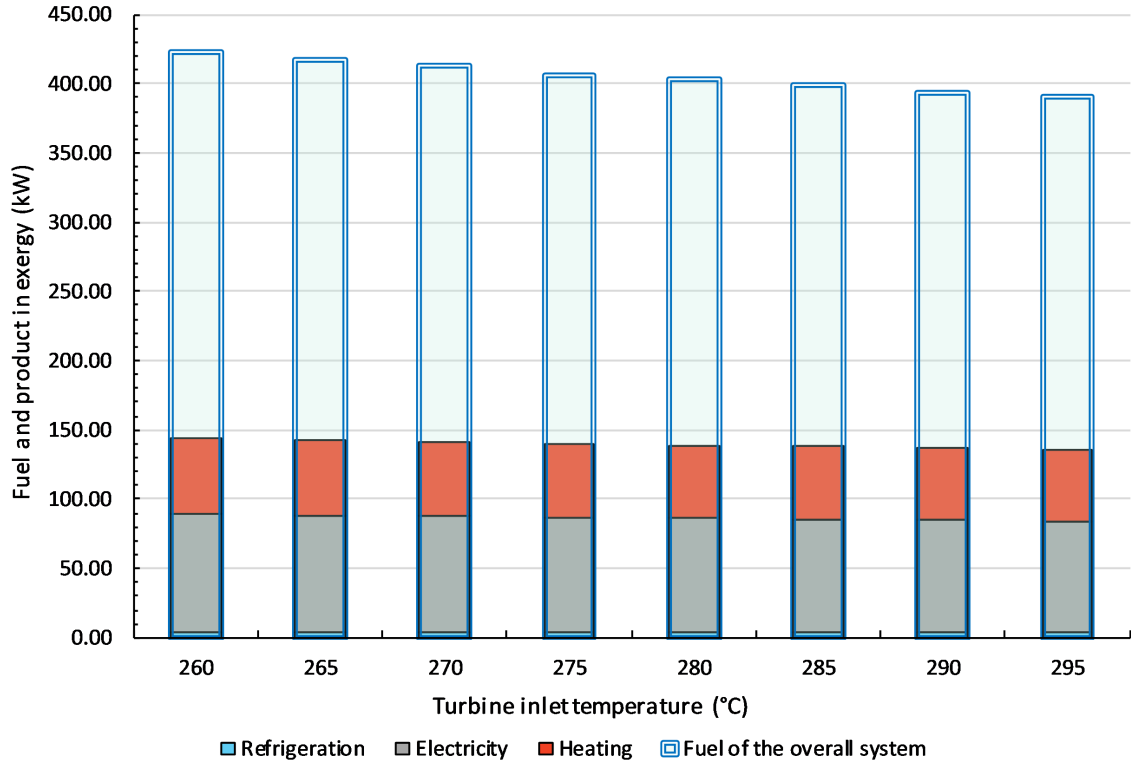
Figure 5.16: Exergetic performance (fuel and product in exergy) of the proposed trigeneration system by varying the ΔT of the HE hot side from 40 to 5 K with the heat source temperature of 300 °C.

In short, the reason behind the minimal values of the electricity cost and the refrigeration cost is complex, the general equation for explaining the behaviour can be expressed as: $c_{\mathrm{P,k}} = (\dot{E}_{\mathrm{F,k}}\, c_{\mathrm{F,k}} + \dot{Z}_{\mathrm{k}})\, /\, \dot{E}_{\mathrm{P,k}}$, where k indicates the corresponding components where the electricity and the refrigeration effect are generated, namely, the EX and the EVAP for computing the electricity cost and the refrigeration cost, respectively. With the TIT increases, the mass flow rates of the power cycle as well as the refrigeration cycle reduce. However, varying TIT has the direct influence on the power cycle, thus, the changes of the mass flow rate of the power cycle dominates the mass flow rate variation of the overall system. As illustrated in Fig. 5.13 and shown in Fig. 5.15, the change of the mass flow rate of the power cycle turns less significantly by varying the TIT with the same increment. In contrast, when the TIT increases, the reduces in power and heating capacities are stable, while the change of the refrigeration capacity can be neglected. Therefore, for the cases with relative dramatic decreases in the mass flow rate of the power cycle, the product cost also decreases, $c_{\mathrm{P,k}}(\downarrow) = (\dot{E}_{\mathrm{F,k}}(\downarrow\downarrow)\, c_{\mathrm{F,k}} + \dot{Z}_{\mathrm{k}}(\downarrow\downarrow))\, /\, \dot{E}_{\mathrm{P,k}}(\downarrow)$. While for the cases with relative trivial decreases in the mass flow rate of the power cycle, the product cost can remain the same or even increases, $c_{\mathrm{P,k}}(\rightarrow\uparrow) = (\dot{E}_{\mathrm{F,k}}(\downarrow)\, c_{\mathrm{F,k}} + \dot{Z}_{\mathrm{k}}(\downarrow))\, /\, \dot{E}_{\mathrm{P,k}}(\downarrow)$.

However, regarding the variations of the heating cost, when the TIT increases, although the $\dot{Z}_{\mathrm{Cooler}}$ reduces due to the decreases in the mass flow rates of the power cycle and the refrigeration cycle, the change of $\dot{E}_{\mathrm{F,Cooler}}$ is unclear. This can be observed in Fig. 5.13, the "shape" of the cycle becomes "fatter", and the operating conditions of the Cooler has been affected noticeably by the changes of the TIT. It is clear that the temperature of the EX outlet stream (stream 2) increases by lowering the ΔT of the HE hot side, therefore, stream 3, which

is the outlet stream after mixing the streams from both sub-cycles, is with a higher temperature. Sequentially, the Cooler pinch point approaches to its cold end, which in turn reduces the temperature of the stream exiting the Cooler (stream 4). Since $\dot{E}_{\mathrm{F,Cooler}} = e_{\mathrm{F,Cooler}}\dot{m}_{\mathrm{Cooler}}$ and the $e_{\mathrm{F,Cooler}}$ increases without doubts, the $\dot{m}_{\mathrm{Cooler}}$ decrease rate determines if there will be an increase or not in the fuel of the Cooler. For the cases with the heat source temperature of 200 °C, if the change of the mass flow rate of the power cycle is significant, the fuel of the Cooler reduces, $\dot{E}_{\mathrm{F,Cooler}}(\downarrow) = e_{\mathrm{F,Cooler}}(\uparrow)\dot{m}_{\mathrm{Cooler}}(\downarrow\downarrow)$. Thus, the heating cost decreases, $c_{\mathrm{P,Cooler}}(\downarrow) = (\dot{E}_{\mathrm{F,Cooler}}(\downarrow)\, c_{\mathrm{F,Cooler}} + \dot{Z}_{\mathrm{Cooler}}(\downarrow\downarrow))\, /\, \dot{E}_{\mathrm{P,Cooler}}(\downarrow)$. When the change of the mass flow rate of the power cycle is trivial (for the cases having lower ΔT of the HE hot side with the heat source temperature of 200 °C and all the cases with the heat source temperature of 300 and 400 °C , the fuel of the Cooler increases, $\dot{E}_{\mathrm{F,Cooler}}(\uparrow) = e_{\mathrm{F,Cooler}}(\uparrow)\dot{m}_{\mathrm{Cooler}}(\rightarrow\downarrow)$. Thus, the heating cost rises, $c_{\mathrm{P,Cooler}}(\uparrow) = (\dot{E}_{\mathrm{F,Cooler}}(\uparrow)\, c_{\mathrm{F,Cooler}} + \dot{Z}_{\mathrm{Cooler}}(\rightarrow\downarrow))\, /\, \dot{E}_{\mathrm{P,Cooler}}(\downarrow)$.

It is also worthwhile to mention that when the system is driven by the heat sources with temperatures of 300 and 400 °C, the fuel of the Cooler increases but the product of the Cooler reduces by lowering the ΔT of the HE hot side. This reveals that the destruction within the Cooler rises since the larger terminal temperature difference of the Cooler hot side leads to the higher irreversibilities. Also, the irreversibilities within the MIX can be expected to increase by mixing two streams with a larger temperature difference. In this case, a recuperator can be considered for the power cycle to reduce the temperature differences within the MIX and the Cooler, namely, reduce the exergy destructions of the MIX and the Cooler. Moreover, the lower fuel consumption of the overall system can be achieved by adding a recuperator to the power cycle. The effects of modifying the cycle configuration on the individual cost and the system performance will be discussed in detail in Chapter 5.

- *With the consideration of the heat source cost*

In this section, the heat source cost is considered to evaluate the system performance by assuming different heat sources (200, 300, and 400 °C) are available. Since the heat source is not specified yet, a cost range is considered for all the heat sources, which varies from 0 to 15 $/GJ. The ΔT of the HE hot side is 20 K for all the cases, and the cost comparison, including the average product cost, the power, the refrigeration, and the heating costs, are presented in Fig. 5.17-5.20.

In Fig. 5.17, it shows that if the heat sources have identical costs, the average product cost is the lowest with the heat source temperature of 400 °C when the heat source cost varies from 0 to 3 $/GJ. As the heat source cost increases, the system driven by the heat source with its temperature of 300 °C reveals the lowest average cost. If the heat source cost is higher than 10 $/GJ, the system with the heat source temperature of 400 °C has the most expensive product cost. These horizontal dash lines indicate that the cost of the heat source with a temperature of 200 °C has to be lower than around 3.5 $/GJ to compete with the average product cost of the system powered by the heat sources with temperatures of 300 and 400 °C with their costs of 5 $/GJ. When the heat source is with the temperature of 300 °C, and its cost is 9 $/GJ, the costs of the heat sources with temperatures of 400 and 200 °C should be lower than 8.5 and 8 $/GJ, respectively, to achieve the same average product cost. However, if the 300 °C heat source is available and with the cost of 13 $/GJ, the costs of the 200 and 400 °C heat

sources have to be, respectively, more than 4% and 8% lower than that of the 300 °C heat source to be competitive regarding the system average product cost.
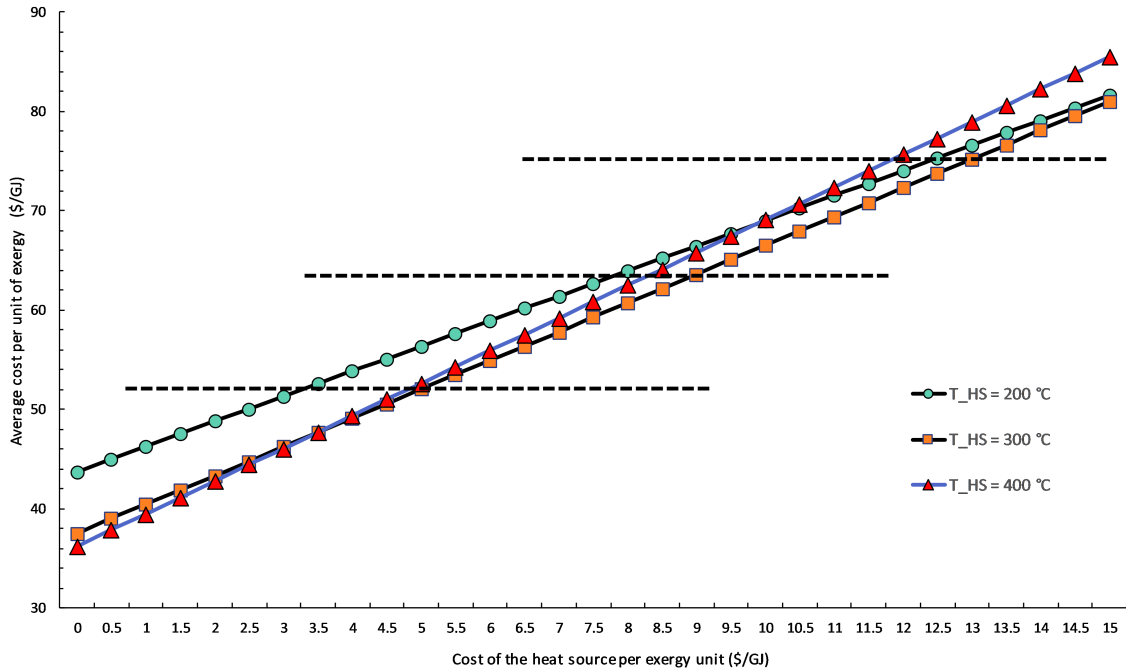
Figure 5.17: Average product cost per unit of exergy of the proposed trigeneration system by varying the heat source cost from 0 to 15 \$/GJ with the heat source temperatures of 200, 300 and 400 °C.

The results of the power cost and the refrigeration cost shown in Fig. 5.18 and 5.19 are quite similar. The 200 °C heat source has to have a dramatic lower price to compete with the heat sources with 300 and 400 °C temperatures. For example, considering the power cost, only the 200 °C heat source having the cost as low as 2.5 \$/GJ or even lower can be treated a rival compared to the 300 °C heat source costing 5 \$/GJ and the 400 °C heat source costing 6 \$/GJ. As demonstrated in Fig. 5.20, the heating cost is very sensitive not only to the temperatures of the heat sources but also their costs. With increasing the heat source cost, the heating cost variation is the steadiest when the system is driven by the heat source with a temperature of 200 °C. While for the cases with the heat source temperature of 400 °C, by raising the heat source cost, its curve appears the steepest slope. In conclusion, regarding the power and the refrigeration costs, utilizing the heat sources with higher temperatures is preferable. But for the heating cost, its changes are rapid when the heat source cost increases and different heat sources are employed. Thus, the heat source temperature preference for the heating cost is vague, which affects the behavior of the average product cost of the overall system. If various heat sources are available but with different prices, the system needs to be thoroughly designed based on the conditions of the available heat sources and the local requirements.
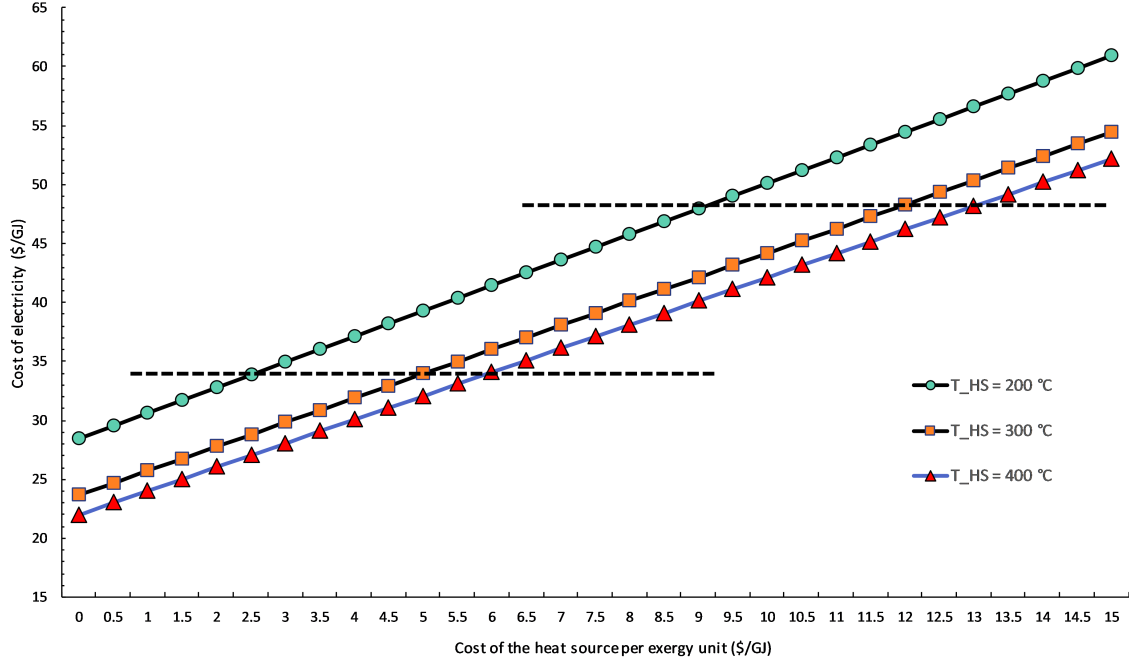
Figure 5.18: Electricity cost of the proposed trigeneration system by varying the heat source cost from 0 to 15 \$/GJ with the heat source temperatures of 200, 300 and 400 °C.
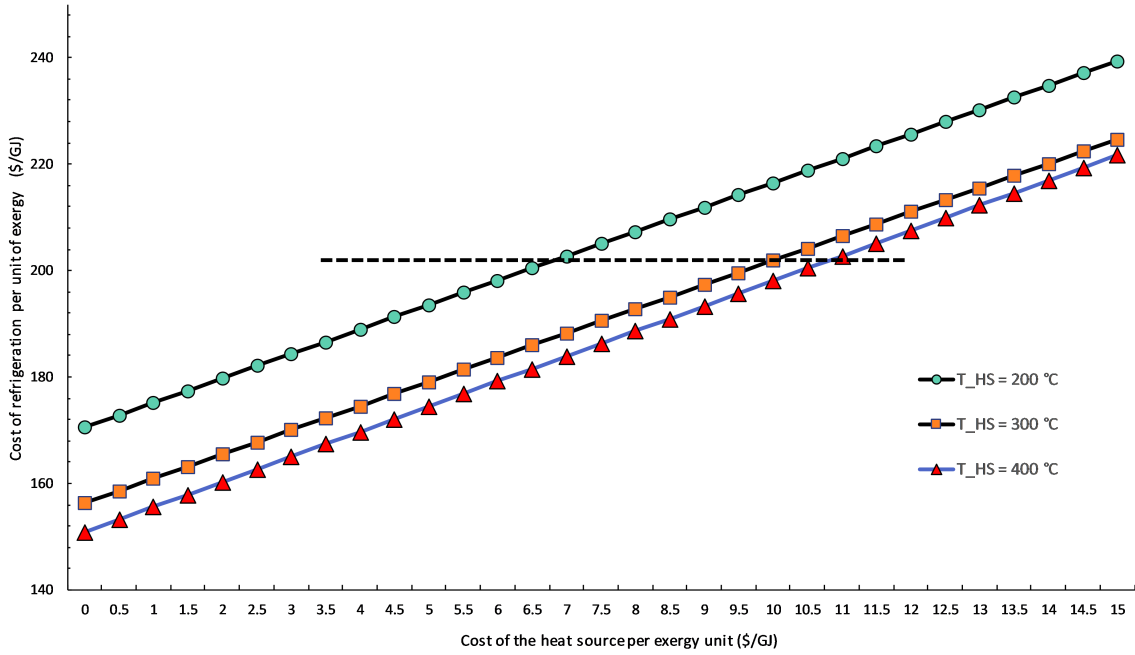
Figure 5.19: Refrigeration cost per unit of exergy of the proposed trigeneration system by varying the heat source cost from 0 to 15 \$/GJ with the heat source temperatures of 200, 300 and 400 °C.
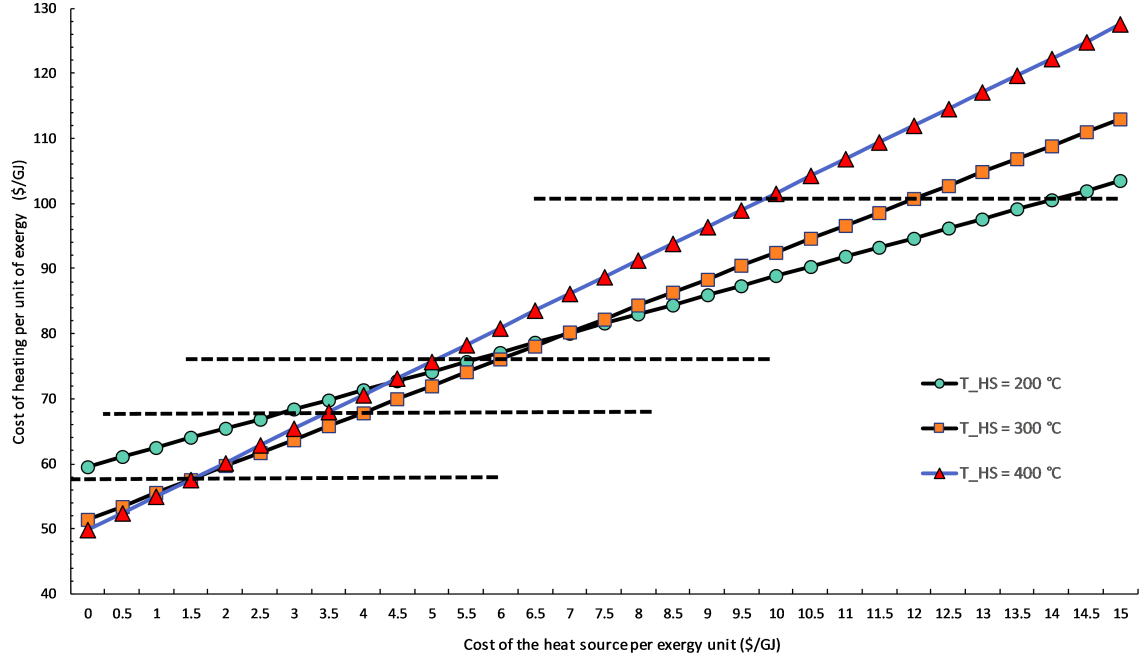
Figure 5.20: Heating cost per unit of exergy of the proposed trigeneration system by varying the heat source cost from 0 to 15 $/GJ with the heat source temperatures of 200, 300 and 400 °C.

5.5 Effect of the _TIP_ on the performance of the polygeneration system

In the previous section, the influences of the heat source temperature on the performance of the polygeneration system are discussed. As the CO_2 stream exiting the HE, where the heat from the heat source is absorbed, enters the EX, sequentially, the discussions regarding the heat source temperature and the ΔT within the HE can be also considered as the effect investigation of the _TIT_ on the overall system from a different perspective. Since both turbine inlet temperature and inlet pressure play important roles in power generation systems, in this section, we will discuss how does the _TIP_ affect the polygeneration system performance. The _TIP_ varied from 150 to 250 bar with an increased step of 10 bar is targeted, while other parameters remain unchanged.

Fig. 5.21 presents the influence of the _TIP_ on the product costs, including the cost of individual product and the average cost of all the products. By increasing the _TIP_, the cost variations of all the products (power, heating, and refrigeration) show positive correlations; but the effects of the _TIP_ on product costs are minor, e.g., the change of the refrigeration cost is the most significant among that of all the product costs, which reveals only a 7.5% rise. The average product cost is hardly affected by the variation of the _TIP_ having a value of around 52.8 $/GJ with _TIP_ of 150 bar and the value of 51.5 $/GJ with _TIP_ of 250 bar. Nevertheless, it is noticeable that with increasing the _TIP_, the average product cost reduces, although each product's cost increases. To investigate why the average product cost and the cost of each product show contrary behaviors, the contribution of each product in exergy to the final products of the overall system is demonstrated in Fig. 5.22. The results in Fig. 5.22 reveal that if the system is operated with a higher _TIP_, the power generation contributes more

75

to the overall system products. In turn, it reduces the average product cost since the power produced from the polygeneration system is much cheaper than other products (heating and refrigeration capacities).
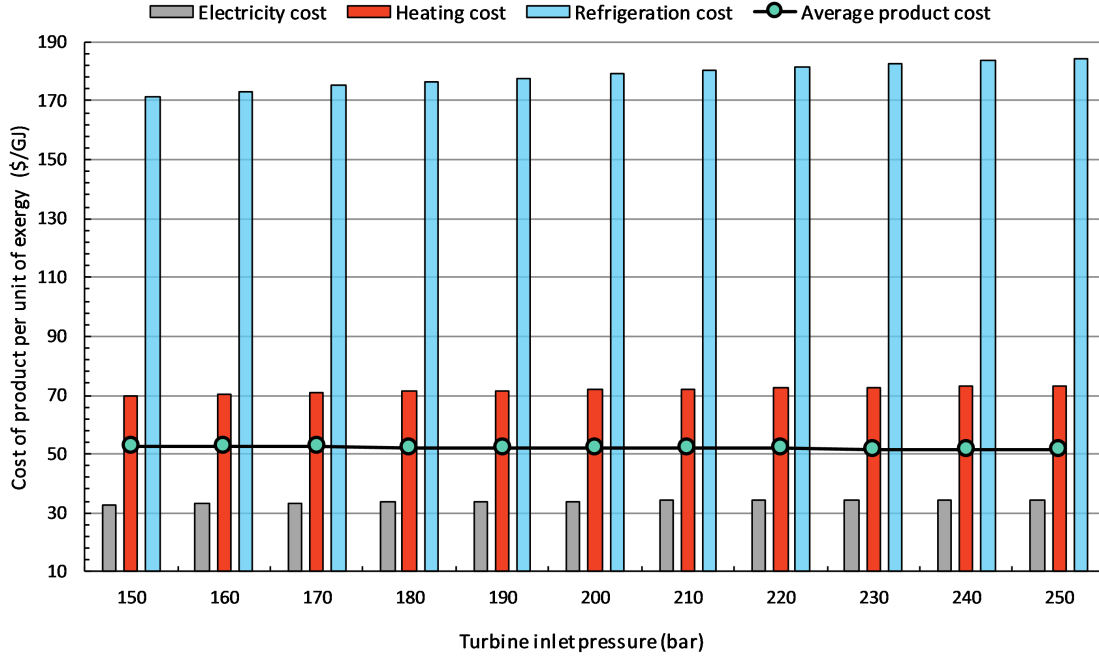
Figure 5.21: The variations of electricity, heating and refrigeration costs as well as the average product cost of the overall system by increasing the *TIP*.
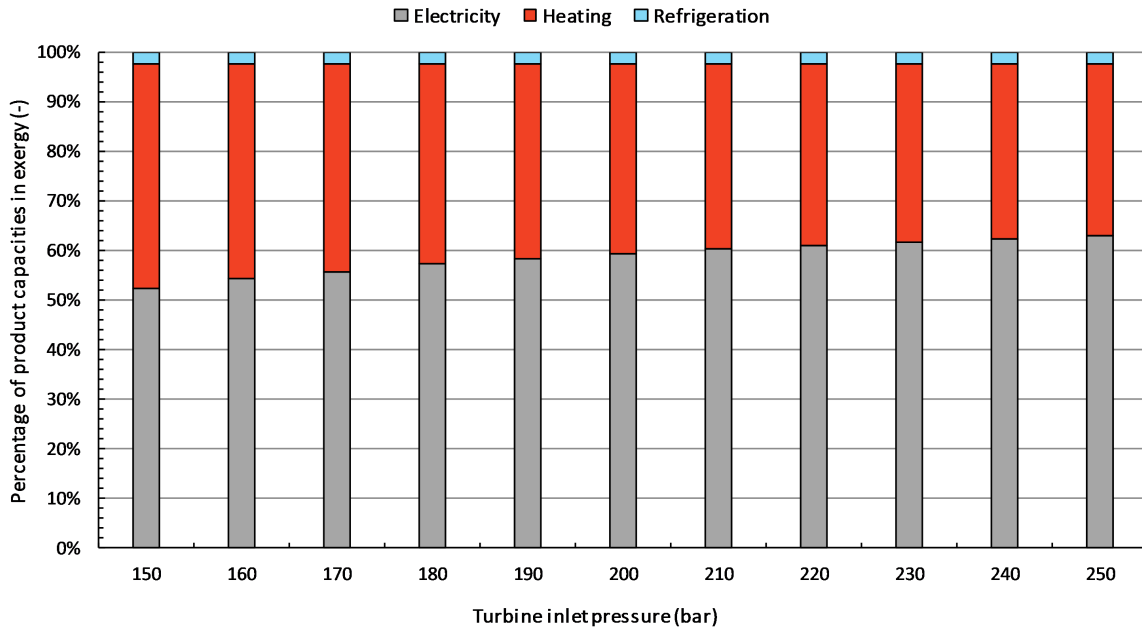
Figure 5.22: The contributions of electricity, heating and refrigeration capacities in exergy to the final products of the overall system by increasing the *TIP*.

Regarding the "shape" change of the cycle by increasing the *TIP*, the cycle becomes "taller" and "thinner" as shown in Fig. 5.23. It is very straightforward to understand that the power

cycle would be "taller" since the CO_2 stream entering the EX as well as the CO_2 stream exiting the CM–P is with a higher pressure, which results in moving the upper part of the power cycle completely to a higher pressure level (moving the pressure level of streams 6 and 1 to a higher pressure level of streams 6' and 1'). With the unchanged *TIT*, the expansion process shifts to the left, and the turbine outlet pressure decreases. As we discussed (see the discussions regarding Fig. 5.4), the lower the temperature of the CO_2 stream entering the Cooler, the higher the temperature of the CO_2 stream exiting the Cooler. Therefore, the compression process of the power cycle and the throttling process of the refrigeration cycle shift to the right.
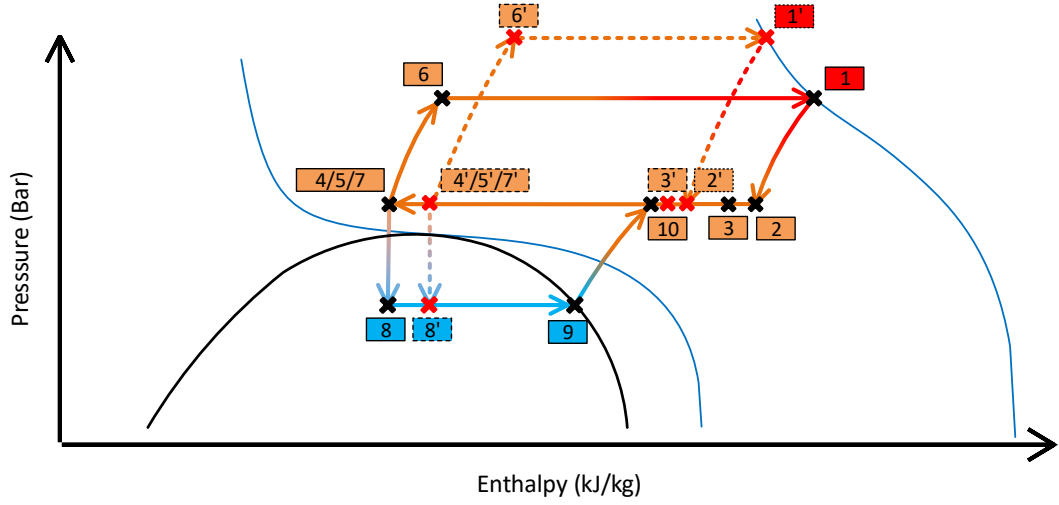
Figure 5.23: The cycle variations of the proposed polygeneration system by increasing the *TIP* illustrated in the pressure-enthalpy diagram (with dash lines).

By shifting the throttling process of the refrigeration cycle to the right, the more mass flow rate is required in the refrigeration system to produce the same amount of refrigeration capacity; the mass flow rate of the refrigeration cycle, thus, increases gradually with varying the *TIP* from 150 bar to 250 bar. For the power system, if we apply the equation for calculating energetic efficiency of a Carnot cycle ($\eta = (T_{\text{Heat source}} - T_{\text{Heat sink}})/T_{\text{Heat source}} = 1 - T_{\text{Heat sink}}/T_{\text{Heat source}}$) as an aid to understand the influence of the *TIP* on it performance, the $T_{\text{Heat source}}^{\text{av.}}$ of the power cycle increases sharply by rising the *TIP*; and the $T_{\text{Heat sink}}^{\text{av.}}$ might have a negligible change since the temperature of the CO_2 stream entering the Cooler decreases while its exit temperature increases. Hence, the efficiency of the power cycle boosts, i.e. $\eta(\uparrow\uparrow) = 1 - T_{\text{Heat sink}}(\rightarrow)/T_{\text{Heat source}}(\uparrow\uparrow))$, and the overall system efficiency shows a growth being more than 30% (from 29.1% to 37.9%). The mass flow rate in the power cycle reduces first with increasing the *TIP* up to 220 bar because of the power system efficiency increase; then, it shows a slight rise as more power is required by the refrigeration cycle. These results are summarized and illustrated in Fig. 5.24.
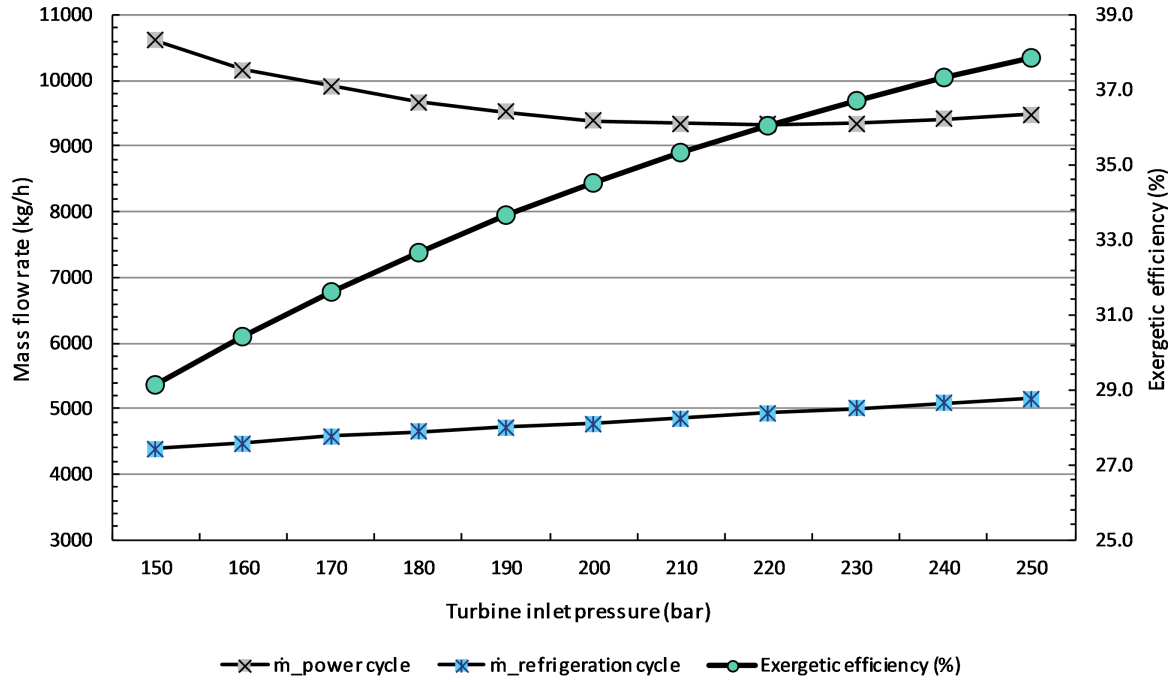
Figure 5.24: Variations in mass flow rates of the power cycle and the refrigeration cycle as well as the system exergetic efficiency of the proposed trigeneration system by increasing the *TIP*.

5.6 Effect of the merging pressure on the performance of the polygeneration system

The outlet streams of the EX and the CM–R enter the MIX with an identical pressure, where the power cycle and the refrigeration cycle are merged; i.e., the turbine (EX) outlet pressure equals the CM–R outlet pressure. And at this pressure, two sub-cycles are merged via the MIX. Thus, the pressure is also called the merging pressure of the polygeneration system. The merging pressure is expected to significantly influence the overall system's performance as the system is designed to take advantage of operating the Cooler and turbomachinery near the critical point of CO_2. However, the proposed system consists of two subsystems, and these subsystems interact strongly with each other. To confirm if the design of merging the power cycle and the refrigeration cycle close to CO_2 critical point exceeds the design that merges the subsystems at a higher pressure being relatively away from the critical point, the system performance with merging pressures of 77 bar, 83 bar and 90 bar is examined in this section from exergetic and exergoeconomic points of view.

Fig. 5.25 illustrates the cycle variations of the polygeneration system by increasing the merging pressure. In general, the overall cycle becomes slightly "fatter", while the power cycle is "shorter" and the refrigeration cycle is "taller". By shifting the throttling process to the left, the required mass flow rate in the refrigeration cycle is less, but the specific power consumption within the CM–R increases due to the rise of the CM–R pressure ratio. Combining the effects of lowering the mass flow rate and increasing the specific power consumption in the refrigeration cycle, the total power required to operate the refrigeration system decreases steadily. Because the decrease in the mass flow rate of the refrigeration cycle is a more

prominent factor, which affects the power consumption within the CM–R. The results are listed in Table 5.8. Regarding the change of the mass flow in the power cycle, its reduction is not as sharp as in the refrigeration cycle. The ratio of the mass flow rate in the power cycle to that in the refrigeration cycle, therefore, shows a gradual increase. Besides, the overall system has a lower exergetic efficiency (around 10% lower for the system with merging pressure of 90 bar compared to the system with merging pressure of 77 bar) when the merging pressure increases and is away from the CO_2 critical point. It confirms that the system design utilizing the unique thermophysical properties of CO_2 nearing its critical point shows a better performance in terms of system exergetic efficiency.
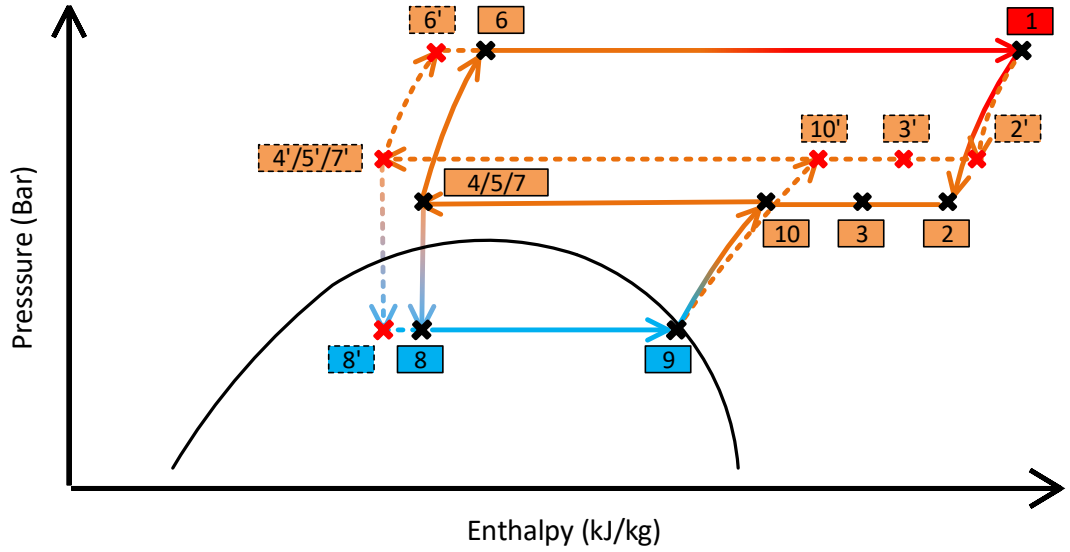
Figure 5.25: The cycle variations of the proposed polygeneration system by increasing the merging pressure illustrated in the pressure-enthalpy diagram (with dash lines).

Table 5.8: The variations of the system mass flow rate, the power consumption of the refrigeration cycle, and the system exergetic efficiency by increasing the merging pressure of the polygeneration cycle.

p_{Merging} (bar)	77	83	90
$\dot{m}_{\text{Power}}$ (kg/h)	9399	6650	5412
$\dot{m}_{\text{Refrigeration}}$ (kg/h)	4788	3155	2267
$\dot{m}_{\text{Power}}/\dot{m}_{\text{Refrigeration}}$ (-)	1.96	2.11	2.39
$\dot{W}_{\text{CM–R}}$ (kW)	41.23	30.38	24.37
$\varepsilon_{\text{total}}$ (%)	34.5	33.4	31.3

In Figure 5.26 (a)-(c), the contribution percentage of electricity, heating, and refrigeration capacities to the product of the overall system is presented for the polygeneration system at merging pressure of 77 bar, 83 bar, and 90 bar, respectively. One can notice that with increasing the merging pressure from 77 bar to 90 bar, the heating and refrigeration capacities contribute

more to the final system product; especially for the heating capacity, its contribution percentage increases by almost 17%. The higher the merging pressure, the higher the temperature of CO_2 streams exiting the EX and the CM–R; while the mass flow rate ratio, $\dot{m}_{\text{Power}}/\dot{m}_{\text{Refrigeration}}$, rises. Thus, the CO_2 stream entering the Cooler is at a higher temperature, i.e., with higher specific exergy, which in turn, more heat can be generated within the Cooler per unit of the mass flow rate. However, as the system mass flow rate, including the mass flow rates of the power cycle and the refrigeration cycle, reduces with a higher merging pressure, the absolute value of the heating generation also decreases. However, the decrease in the heating generation is less significant compared to that in the power generation. Therefore, the contribution of the heating capacity increases gradually by varying the merging pressure from 77 bar to 90 bar. In other words, if the polygeneration system is used for a local community where the heating capacity is the main demand rather than the electricity (e.g., on some winter days, the power generated from renewable energies surpluses the local power requirement but the hot water and space heating are highly required), it can be considered to increase the merging pressure to increase the heating contribution to the overall system product but with a penalty of having a lower system efficiency.

(a) $p_{\text{Merging}} = 77$ bar   (b) $p_{\text{Merging}} = 83$ bar   (c) $p_{\text{Merging}} = 90$ bar
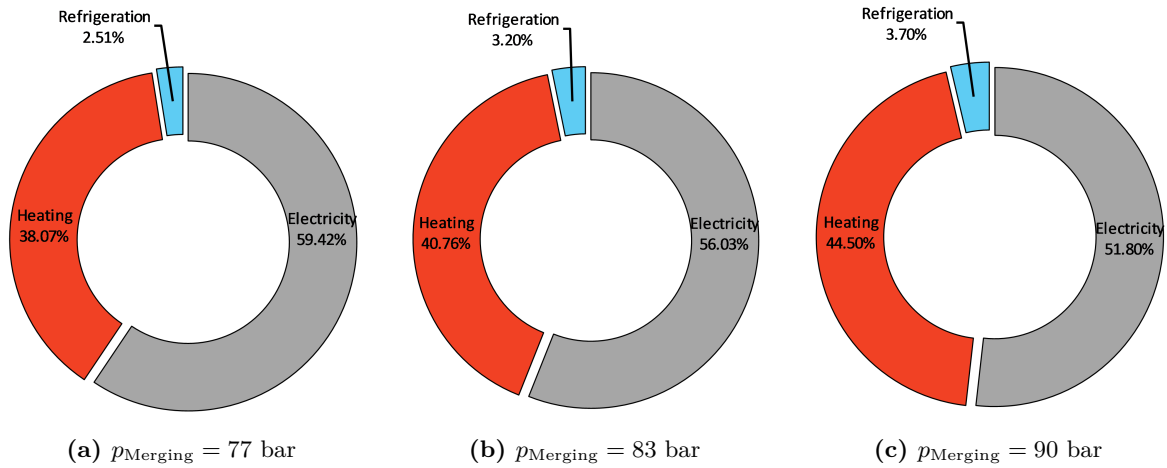
Figure 5.26: The contribution percentage of electricity, heating and refrigeration capacities in exergy to the final products of the overall system in exergy by increasing the merging pressure.

To examine the influences of the merging pressure on the system performance from the exergoeconomic point of view, the system product costs (electricity, heating and refrigeration costs and the average product cost) are compared assuming the system is operated at different merging pressures (77, 83 and 90 bar). The cost differences between the system operated at merging pressure of 77 bar and that of 83 bar are presented in Fig. 5.27 (a) with the consideration of the waste heat having its cost of 0-10 $/GJ (cost per unit of exergy). It can be observed that the electricity cost of the system operated at the merging pressure of 77 bar is more attractive in contrary to that of the system operated at the merging pressure of 83 bar. However, the refrigeration and heating capacities are cheaper when subsystems are merged at the pressure of 83 bar. And the cost differences regarding the electricity and refrigeration capacities become more evident with increasing the waste heat cost. While the disparities of the heating costs between the system with the merging pressure of 77 bar and 83 bar reduce by having a heat source with a higher cost per unit of exergy. The average

product cost difference shows similar results as the electricity cost difference. However, it is more noticeable, especially when a more expensive heat source is utilized for driving the polygeneration system. The cost differences between the system operated at merging pressure of 77 bar and that of 90 bar are shown in Fig. 5.27 (b). It is clear that the disparities in the electricity and heating costs, as well as the average product cost, are more remarkable, and they are sensitive to the waste heat cost, while the effect of the waste heat cost on the refrigeration cost difference can be negligible. Hence, from the exergoeconomic point of view, the system operated at the merging pressure nearing the CO_2 critical point shows a better system performance with a lower average product cost.
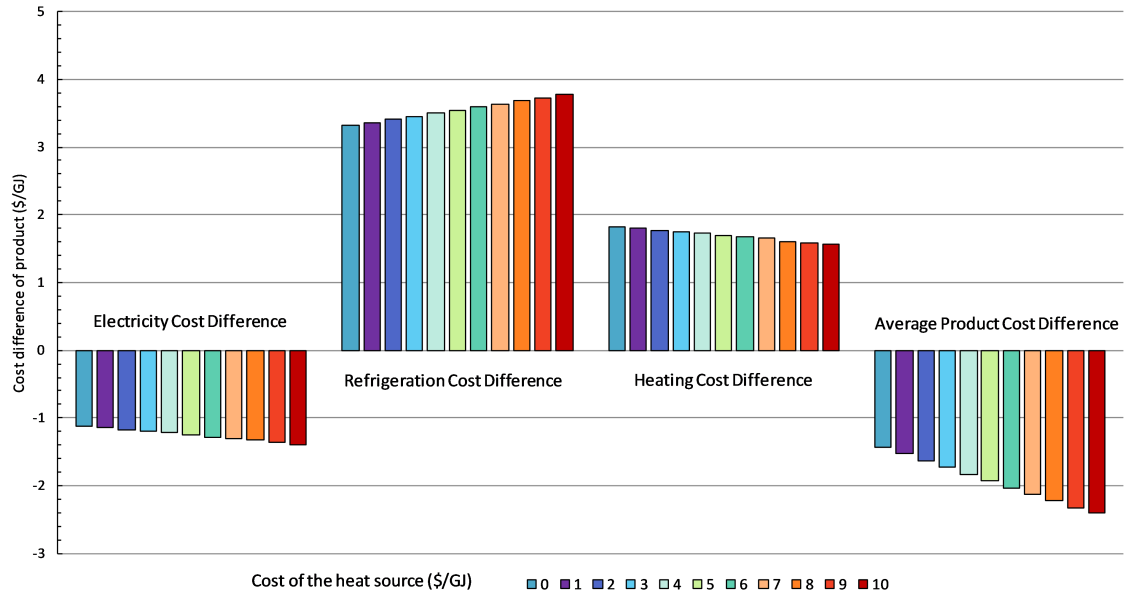
(a) $c_{(\text{Merging p = 77 bar})} - c_{(\text{Merging p = 83 bar})}$
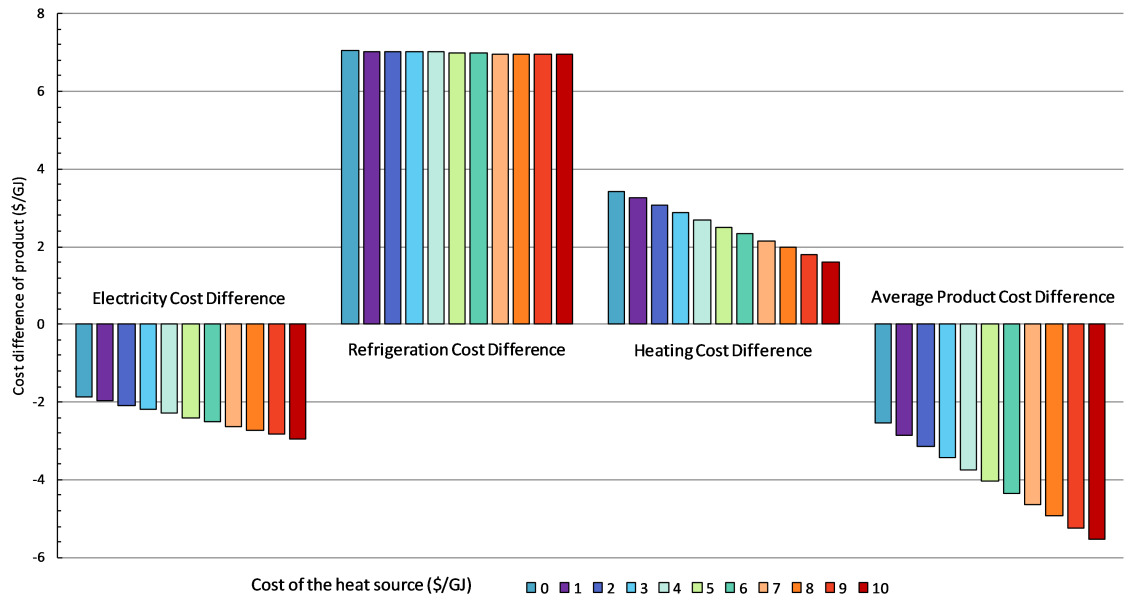
(b) $c_{(\text{Merging p = 77 bar})} - c_{(\text{Merging p = 90 bar})}$

Figure 5.27: Cost differences between the systems operated at different merging pressures (77, 83 and 90 bar) by varying the cost of the waste heating from 0 \$/GJ to 10 \$/GJ.

In conclusion, the design of merging the power cycle and the refrigeration cycle close to CO_2 critical point exceeds the design that merges the subsystems at a higher pressure being relatively away from the critical point. The proposed polygeneration system operated with the merging pressure nearing CO_2 critical point provides not only a higher system efficiency but also a lower average product cost.

5.7 Effect of the ambient temperature on the performance of the polygeneration system

Compared to an energetic analysis, an environmental condition needs to be given for implementing an exergetic analysis. The exergetic analysis takes into the interactions between a given state of the entity and its environment [88]; therefore, it is beneficial applying exergy-based methods to compare different streams/systems on a common basis. For energy systems producing heating and/or refrigeration capacities, the environmental condition determines the demand potentials of the thermal products, which can influence the definitions of fuel, product, and loss for the overall system. From the exergoeconomic point of view, the environmental condition might also affect the system product cost.

Although heating and refrigeration capacities are produced simultaneously in the proposed polygeneration system, in practice, the local communities (mainly with residential buildings) might not always need both heating and refrigeration in parallel. For example, the refrigeration capacity is, in general, highly required in summer (when the environmental temperature is high), while the heating demand drops sharply as the space heating is not needed and the hot water consumption reduces. Contrariwise, in wintertime (when the environmental temperature is low), a large amount of heating is demanded, primarily used for the space heating; the refrigeration capacity, however, is less required. Moreover, the buildings' functions in the local communities also influence the amount of local thermal energy requirements directly. If there are hospitals, hotels, universities, data centers, and some commercial buildings in the targeted community, the refrigeration effect and the heating capacity may always be needed simultaneously, regardless of the environmental temperature.

In this section, a high environmental temperature of 35 °C as the representative of summertime temperature and a low environmental temperature of 5 °C as the representative of wintertime temperature are selected to investigate influences of the reference temperature on the performance of the overall system. For the system operated in the environmental condition being at 35 °C, two scenarios are taken into consideration: 1. Heating and refrigeration capacities are demanded simultaneously. In this case, some buildings with special energy requirements, e.g., hospitals and hotels, in the local community are assumed. Thus, all the system products, including power, heat and refrigeration capacities, can be used for the local energy supply. 2. For the communities consisting of mainly residential buildings, the heat production from the polygeneration system is largely surplus than the local heat requirement, which, mainly, comes only from the hot water demand. Hence, heat production is considered the exergy loss of the overall system, i.e., the heat is given to the community for free, and the heating cost is charged to the costs of the power and the refrigeration capacities.

5.7 Effect of the ambient temperature on the performance of the polygeneration system

For the system operated in the environmental condition being at 5 °C, the refrigeration capacity produced within the EVAP discussed in other cases is no longer a system product. Because with the ambient temperature of 5 °C, the cooling process happens naturally. However, if some buildings in the community need to be cooled continuously to a specific predefined temperature, for example, data centers need to get rid of the heat generated from computers (refrigeration capacity) all year round to ensure its highly efficient function, it is impossible to be dependent on the ambient temperature achieving the desired refrigeration effect. A refrigeration system is still needed to cool the rooms in these buildings. The secondary refrigerant after the evaporation process enters the rooms at a low temperature for the refrigeration effect but returns with a higher temperature, which drives the refrigeration system to produce the heat that is required largely in winter. In other words, with a low ambient temperature, the heat absorbed from the rooms/buildings, where the refrigeration capacity is needed, can be used as the "free heat source" to drive the refrigeration system functioning as a heat pump in the proposed polygeneration system. That is to say, the polygeneration system produces, in this case, only power and heat capacities, and the refrigeration system works actually as a heat pump.

In short, the definitions of fuel, product, and loss for the overall system under different ambient conditions (named by case 1, 2, and 3) are summarized in Table 5.9. The contributions of power, heat, and refrigeration capacities to the total system product for cases 1-3 are presented, respectively, in Fig. 5.28 (a), (b), and (c). Note that case 1 and case 2 have an identical ambient temperature; thus, they have the same exergetic results; only their definitions of product and loss for the overall system differ.

Table 5.9: Definitions of product and loss for the overall system operated in different environmental conditions.

Condition	$T_0 = 35$ °C		$T_0 = 5$ °C
	Case 1	Case 2	Case 3
$\dot{E}_{\text{F,total}}$	$\dot{Q}_{\text{HE}}$ $(1\text{-}T_0/T_{\text{HS}})$	$\dot{Q}_{\text{HE}}$ $(1\text{-}T_0/T_{\text{HS}})$	$\dot{Q}_{\text{HE}}$ $(1\text{-}T_0/T_{\text{HS}})+(\dot{E}_{13}-\dot{E}_{14})$
$\dot{E}_{\text{P,total}}$	$\dot{W}_{\text{net}} + \dot{E}_{\text{Heating}} + \dot{E}_{\text{Cooling}}$	$\dot{W}_{\text{net}} + \dot{E}_{\text{Cooling}}$	$\dot{W}_{\text{net}} + \dot{E}_{\text{Heating}}$
$\dot{E}_{\text{L,total}}$	-	$\dot{E}_{\text{Heating}}$	-

To conduct the exergoeconomic analysis for these cases shown in Table 5.9, as the heat production in case 2 is defined as the exergy loss of the overall system, the heat cost needs to be distributed to the power and refrigeration costs in a reasonable way. Fig. 5.29 details the cost distribution process in case 2. The cost rate of heating $\dot{C}_{\text{Heating}}$ is charged to the cost rates of electricity $\dot{C}_{\text{Electricity}}$ and refrigeration effect $\dot{C}_{\text{Refrigeration}}$ based on their contributions to the final system product in terms of their exergy rates, $\dot{W}_{\text{net}}/(\dot{W}_{\text{net}} + \dot{E}_{\text{Cooling}})$ and $\dot{E}_{\text{Cooling}}/(\dot{W}_{\text{net}} + \dot{E}_{\text{Cooling}})$. The equations can be expressed as:

$$\dot{C}_{\text{Electricity,new}} = \dot{C}_{\text{Electricity}} + \dot{C}_{\text{Heating}} \times \frac{\dot{W}_{\text{net}}}{(\dot{W}_{\text{net}} + \dot{E}_{\text{Cooling}})} \tag{5.8}$$

5. System investigation

$$\dot{C}_{\text{Refrigeration,new}} = \dot{C}_{\text{Refrigeration}} + \dot{C}_{\text{Heating}} \times [1 - \frac{\dot{W}_{\text{net}}}{(\dot{W}_{\text{net}} + \dot{E}_{\text{Cooling}})}] \qquad (5.9)$$

(a) Case 1 with $T_0 = 35\ ^\circ\text{C}$ **(b)** Case 2 with $T_0 = 35\ ^\circ\text{C}$ **(c)** Case 3 with $T_0 = 5\ ^\circ\text{C}$
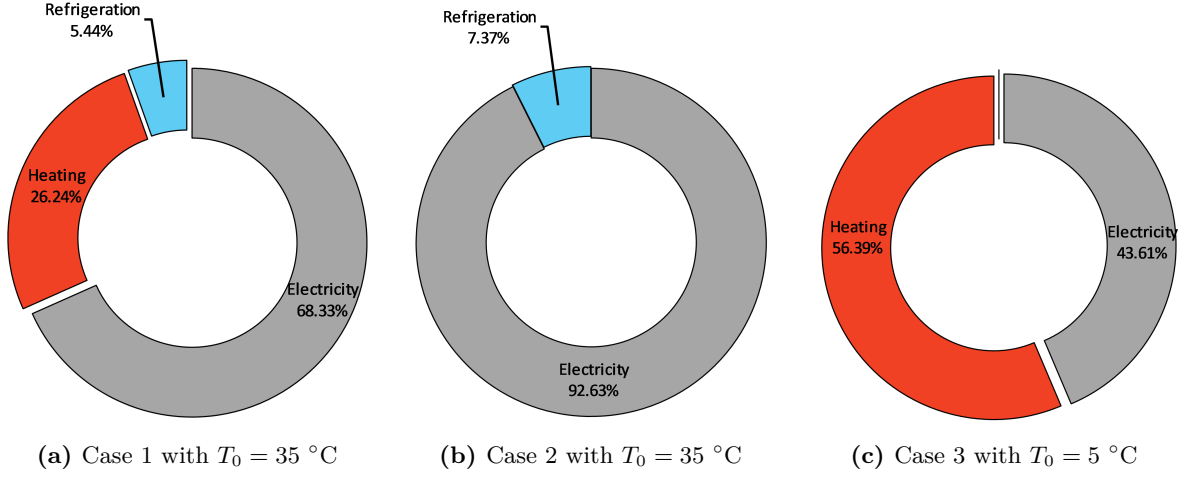
Figure 5.28: The contribution percentage of electricity, heat and refrigeration capacities in exergy to the final products of the overall system in exergy by varying the ambient temperature.
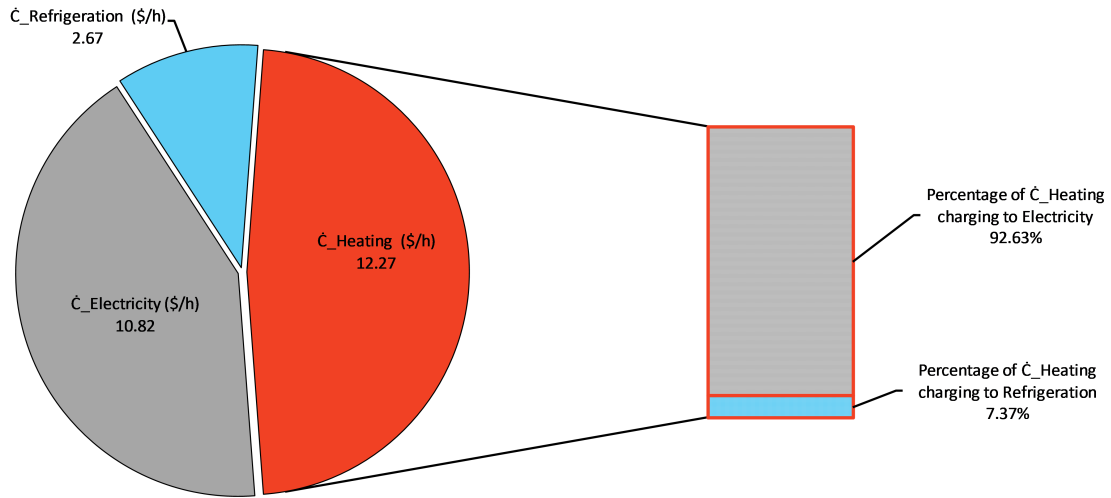
Figure 5.29: Cost distribution process (charging the heat cost to the electricity and the refrigeration costs) in case 2.

The cost of each product and the average product cost of the proposed polygeneration system are given in Table 5.10 for cases 1-3. One can notice that with the comparison of the cost results in case 1, the electricity cost in case 2 almost doubles, and the average product cost in case 2 increases by around 35% since the heat produced from the system is not used as a valuable product. For case 3 with the ambient temperature of 5 °C, the lowest electricity cost, heat cost, and the average product cost are obtained. In this case, the heat production is with a higher quality due to the higher temperature difference between the stream generating heat capacity and the assumed ambient temperature. Besides, the large amount of heat is entirely

supplied to the local community; no valuable product is rejected directly to the environment as the exergy loss of the overall system.

Table 5.10: Costs of power, refrigeration and heat as well as the average product cost for the overall system operated in different environmental conditions.

Condition	$T_0 = 35\ °\mathrm{C}$		$T_0 = 5\ °\mathrm{C}$
Case	Case 1	Case 2	Case 3
$c_{\mathrm{Electricity}}$ ($/GJex)	36.43	74.69	30.99
$c_{\mathrm{Refrigeration}}$ ($/GJex)	113.12	151.38	-
c_{Heating} ($/GJex)	107.55	-	45.10
$c_{\mathrm{P,total}}^{\mathrm{av.}}$ ($/GJex)	59.26	80.34	38.94

Hence, by comparing the product costs of these three cases, the conclusions from the exergoeconomic point of view are: lower product costs can be obtained when the proposed polygeneration system is operated at a lower ambient temperature; if the ambient temperature is high, the massive heat produced from the system might exceed the local heat requirement extensively, which results in disposing the heat production as the exergy loss to the environment and increasing the power and refrigeration costs by charging the heating cost to other products (case 2); even if the heat is fully supplied to the local community, when the ambient temperature is high (case 1), the costs of the power, heat and refrigeration capacities, as well as the average product cost, are still higher than that in case 3 with a lower ambient temperature. These are the unique features of a polygeneration system producing power, heat, and refrigeration effects simultaneously, as the system production can not always meet the requirement from the customers' side. Especially for thermal energies, the local community's requirement depends largely on the ambient temperature and the functions of buildings located in that community.

5.8 Summary

In this chapter, the effects of several operating parameters on system performance are investigated to understand the proposed polygeneration system better. Some characteristics of the waste heat source are investigated to find out how the heat source affects system performance. Besides, the effects of the power generation, the *TIP*, the merging pressure, and the ambient temperature on the performance of the polygeneration system are researched from the exergetic and exergoeconomic points of view. It aims to deepen the understanding of the novel system with a broader perspective. The results would be useful for further analyzing and optimizing the system in a case study. The investigation results are listed as follows:

- By increasing the power production, the cost of each product reduces; thus, the average product cost of the overall system shows a decrease, while the system exergetic efficiency boosts.

- The temperature and cost of the heat sources affect each product cost notably but in a rather complex way; the heating cost is, especially, very sensitive to the variations of the parameters of the heat sources; the average product cost reveals a subtle but considerable correlation with the heat source temperature and cost.

- The *TIP* influences the system exergetic efficiency dramatically: the higher the *TIP*, the higher the system efficiency; the average product cost is, however, hardly affected by varying the *TIP*.

- Merging two subsystems at a pressure nearing the CO_2 critical point provides not only a higher system efficiency but also a lower average product cost.

- Lower product costs, including each product cost and the average product cost, can be obtained with a lower ambient temperature. Because the large amount of heat produced from the system is of higher quality in terms of the exergy content, and all the heat can be utilized for hot water and space heating purposes.

<div align="right">

6

</div>

System analysis and optimization of a case study for engine waste heat recovery

In this chapter, a case study utilizing exhaust gas from a reciprocating engine to drive the proposed polygeneration system is carried out. Engine waste heat is one of the typical heat sources for bottoming cycle applications [114], and its medium-quality temperature (around 320 – 590 °C) is suitable for polygeneration systems [115]. By integrating the engine waste-heat recovery technology into the proposed polygeneration system, system performance and component performance are analyzed and evaluated; sequentially, system optimization is implemented to improve the system design.

6.1   Case study description

For a case study, the exhaust gas from a 2 MW natural gas engine is applied as the waste heat source driving the proposed polygeneration system. ICEs, as primary fossil fuel consumers, are widely applied in road cars, large vehicles, and stationary power units. For stationary power applications, they can be used for emergency backup for remote communities, grid support by incorporating renewable power generators, and base-load supply [116, 117]. Although the initial idea of applying ICEs is to generate electricity, the efficiency of the piston engines by solely producing electricity varies from 25% to close to 50% [118], which reveals that more than half of the fuel energy is lost as waste heat dumped to the atmosphere. If the waste heat in an ICE can be further utilized to produce other energy products, the engine efficiency will be improved significantly. Therefore, waste heat recovery technologies converting the otherwise wasted heats from ICEs to electricity, hot water (steam) as well as refrigeration capacity are emerging and gaining more and more attention.

Diesel engines are one of the most commonly used ICEs in power generation applications, and they are more efficient compared to spark-ignition engines [118]. However, in the nations

or areas with strict emission codes, it is almost impossible to obtain authorization to apply diesel engines without emission control systems; unless a significant penalty for purchasing extensive cleaning equipment is considered [116, 117]. The reciprocating engines burning natural gas as a transitional solution are much cleaner, and they can operate with minimum emission control having around 42% up to 49% system efficiency [116] for converting thermal energy of natural gas into electricity. Although engines burning natural gas are not renewable, the distributed power generators create the basis for a decentralized energy structure that local renewable energy sources can be utilized as fuels in the future [80].

Since Aspen HYSYS® (AspenTech, Bedford, MA, USA) has no model for ICEs, Ebsilon® Professional software (STEAG Energy Services, Zwingenberg, DE) is employed to simulate the 2 MW natural gas engine. The component called Block Heating Power Plant (in German, BHKW) is modeled in Ebsilon® Professional software based on the available data provided by the manufacturer of the machine, and it is by default used for producing power and hot water as a cogeneration system. Instead of using water to recover the heat from the exhaust gas of the natural gas engine, the proposed polygeneration system is integrated in this case study. It is expected that more waste heat can be recovered as S-CO$_2$ has no pinch point problem within the heat exchanger for absorbing the heat from the exhaust gas. Moreover, in the bottoming cycle, not only hot water but also more power, as well as refrigeration capacity, can be produced.

In Fig. 6.1, the simulation details of the 2 MW natural gas engine is presented. The system efficiency for solely producing power is around 41%, and the temperature of the exhaust gas is 409 °C. The results of the natural gas engine simulation obtained from Ebsilon® Professional software are further adopted and imported into Aspen HYSYS® for simulating the proposed polygeneration system.
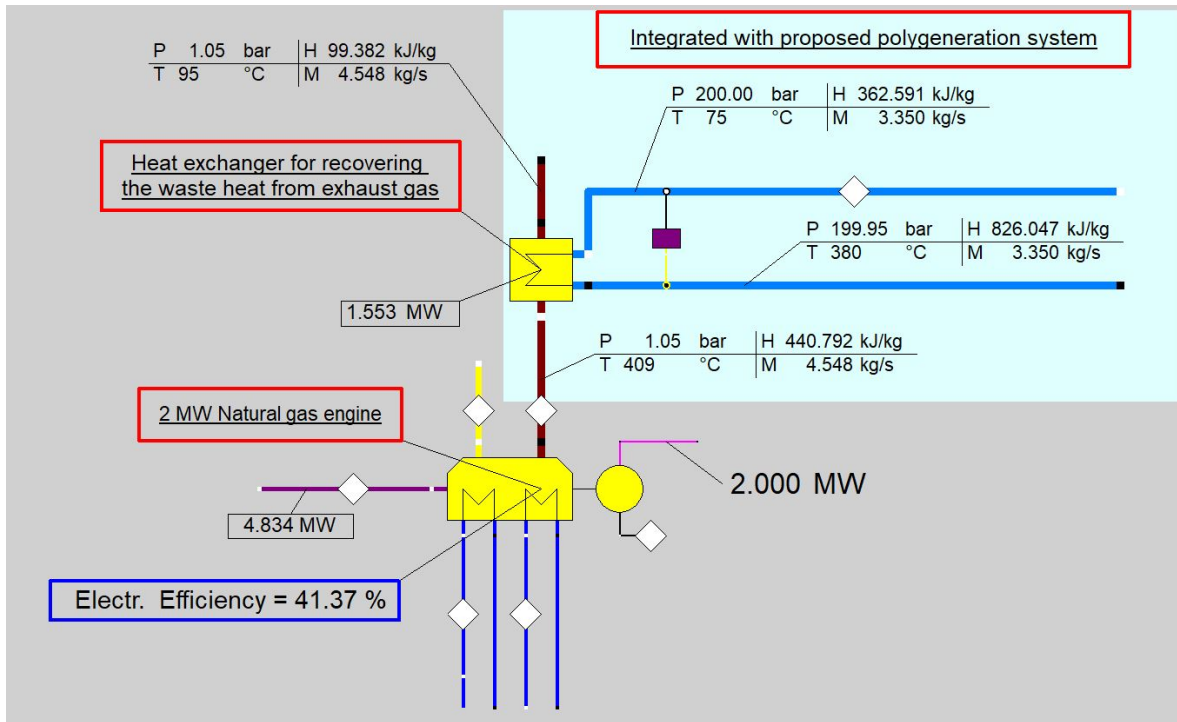
Figure 6.1: 2 MW natural gas engine simulated in Ebsilon® Professional software (STEAG Energy Services, Zwingenberg, DE) integrated with the proposed CO$_2$ polygeneration system.

6.2   System analysis

In this section, exergy-based analyses of the proposed polygeneration system regarding its overall system performance and component performance are carried out. Two system boundaries are considered, which depends on if the natural gas engine is included or not. Within the first system boundary, both the polygeneration system and the natural gas engine are included, where the system-level performance is addressed. However, since the natural gas engine is not the design focus in this work, the second system boundary considers only the proposed polygeneration system. In the second system boundary, the proposed polygeneration system is rigorously evaluated and optimized, and the detailed system-wise and component-wise analyses are also conducted.

6.2.1   System including the natural gas engine and the proposed polygeneration system

By considering the entire system, including the prime mover (natural gas engine) and the bottoming cycle (the proposed polygeneration system), then the exergy rates of fuel and product of the overall system should be modified as shown in Eq. 6.1 and 6.2, respectively. The fuel of the system is the sum of the exergy rates of natural gas and air entering the natural gas engine. The products generated from the prime mover and the bottoming system are included as the total system product; in other words, the system product comprises the power produced from the natural gas engine, and the power as well as the thermal products generated from the polygeneration as aforementioned in Chapter 5.

$$\dot{E}_{\text{F,total}} = \dot{E}_{\text{NG}} + \dot{E}_{\text{Air}} \tag{6.1}$$

$$\dot{E}_{\text{P,total}} = \dot{W}_{\text{NGE}} + \dot{E}_{\text{P,PGS}} \tag{6.2}$$

where NG, NGE, and PGS stand for natural gas, natural gas engine and polygeneration system, respectively.

Accordingly, the cost balance of the overall system including the natural gas engine and the proposed polygeneration system for the exergoeconomic analysis should be written as:

$$\dot{E}_{\text{NG}} \cdot c_{\text{NG}} + \dot{E}_{\text{Air}} \cdot c_{\text{Air}} + \dot{Z}_{\text{total}} = (\dot{W}_{\text{NGE}} + \dot{E}_{\text{P,PGS}}) \cdot c^{av.}_{\text{P,total}} \tag{6.3}$$

where c_{NG} and c_{Air} denote, respectively, the specific cost per unit of exergy of natural gas and air; $\dot{Z}_{\text{total}}$ is the sum of the hourly costs associated with all the components $\dot{Z}_{\text{k}}$ including the natural gas engine.

The assumption made for c_{Air} is: $c_{\text{Air}} = 0$ \$/GJ; while for c_{NG}, the prices of natural gas in U.S. and in Germany, used for producing electric power (electric power price), are considered as representatives of countries with low and high natural gas price, respectively. The detailed assumptions regarding c_{NG} are listed in Table 6.1.

Table 6.1: Assumptions made for natural gas price (electric power price) in U.S. and in Germany.

	Natural gas price$_{2019}$ [\$/1000 ft^3]	FC_0 [\$]	FC_L [\$/a]	c_{NG} [\$/GJex]
U.S.	2.98 [119]	423,317	552,998	3.73
Germany	4.97 [120]	706,001	922,282	6.22

For calculating the natural gas engine's cost, the purchased equipment cost estimating chart in [121] for ICEs with power capacity between 10 kW and 10 MW is adopted. Then the price is brought to the reference year using the cost indices, so that the system TCI, $\dot{Z}_{\text{total}}$, and $\dot{Z}_k$ can be computed.

With c_{Air}, c_{NG} and $\dot{Z}_{\text{total}}$, the average product cost of the overall system $c_{\text{P,total}}^{\text{av.}}$ can be easily calculated by applying the system cost balance (given in Eq. 6.3). However, for the cost of each product, as shown in Fig. 6.2, the exhaust gas of the natural gas engine, after transferring its heat to the S-CO$_2$ stream of the polygeneration system within the HE, exits the heat exchanger and is rejected to the environment, which is defined the system exergy loss; also, the cooling water used for cooling the natural gas engine is considered as the exergy loss of the overall system; thus, their costs have to be distributed to each product cost (discussed in Eq. 5.8–5.9 and Fig. 5.29). The exhaust gas streams entering and exiting the heat exchanger are, respectively, named as heat source input (HSI) and heat source output (HSO). Note that it might be beneficial to further utilize the exhaust gas HSO after the HE and the cooling water exiting the natural gas engine for other processes, where low-temperature heat sources are required; nevertheless, such processes are not considered in this study.
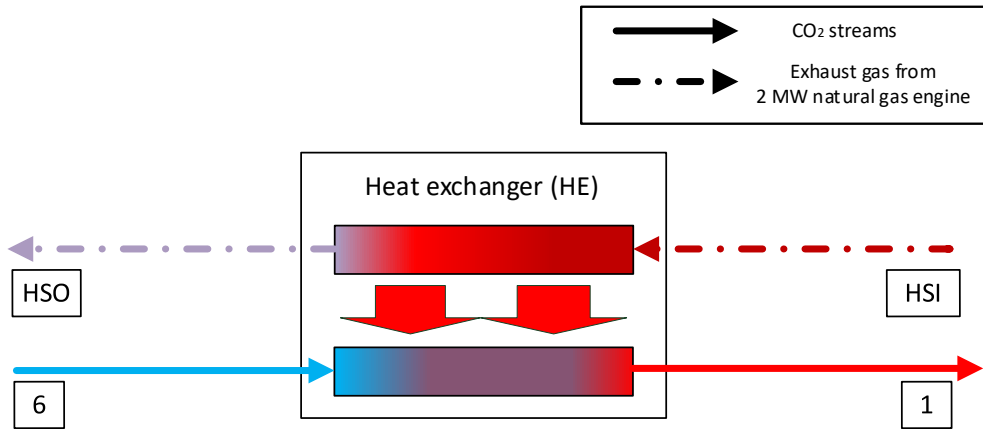
Figure 6.2: The heat exchanger transferring the heat from the exhaust gas of the natural gas engine to the CO$_2$ stream of the polygeneration system.

Once the cost rate of system exergy loss is distributed to product costs within the components, where these products are generated, the newly calculated product costs are the final system product costs. For the system product cost of electricity, since the power generation of the overall system in this case is composed of the power generated from the

natural gas engine and from the polygeneration system, an average cost is computed as the electricity cost of the overall system:

$$c_{\text{Electricity,total}}^{\text{av.}} = \frac{c_{\text{Electricity,NGE}} \cdot \dot{W}_{\text{NGE}} + c_{\text{Electricity,PGS}} \cdot \dot{W}_{\text{net,PGS}}}{(\dot{W}_{\text{NGE}} + \dot{W}_{\text{net,PGS}})} \tag{6.4}$$

In Table 6.2 and 6.3, the results of the energetic and exergetic analyses for the overall system are presented, by considering three cases with different ambient temperatures and local requirements, which is consistent with the cases listed in Table 5.9 (more details can be found in section 5.7). In terms of the system energetic efficiency, case 1 and case 3 show the highest efficiency with the value of 73.51%; while the system efficiency in case 2 is only around 46%. As shown in cases 1 and 3, the same amount of heating capacity is produced in case 2, but it is not considered the product since the assumption, in this case, is that the local community's heat requirement is very low. The system efficiencies in cases 1 and 3 are identical; however, the refrigeration system functions as a cogeneration system by producing refrigeration and heating capacities in case 1 but works as a heat pump in case 3. Only the the electricity $\dot{W}_{\text{net}}$ and heat $\dot{Q}_{\text{Heating}}$ are included for computing the system efficiency in case 1; the refrigeration capacity $\dot{Q}_{\text{Cooling}}$ is excluded otherwise it will contradict the second law of thermodynamics. From the exergetic point of view, the overall system in case 3 reveals the highest efficiency, while the lowest system efficiency is obtained in case 2. With the ambient temperature of 5 °C in case 3, the exergy rate of heating capacity $\dot{E}_{\text{Heating}}$ increases dramatically (from 72.69 kW in case 1 to 183.29 kW in case 3), which in turn, results in achieving a higher system efficiency.

Table 6.2: Energetic analysis result for the overall system (including the natural gas engine and the polygeneration system) operated in different environmental conditions.

Condition	$T_0 = 35$ °C		$T_0 = 5$ °C
Case	Case 1	Case 2	Case 3
$\dot{Q}_{\text{in,total}}$ (kW)	5000.17	5000.17	5000.17
$\dot{W}_{\text{net}}$ (kW)	2204.77	2204.77	2204.77
$\dot{Q}_{\text{Cooling}}$ (kW)	100.00	100.00	-
$\dot{Q}_{\text{Heating}}$ (kW)	1470.77	-	1470.77
η_{total} (%)	73.51	46.09	73.51

Table 6.3: Exergetic analysis result for the overall system (including the natural gas engine and the polygeneration system) operated in different environmental conditions.

Condition	$T_0 = 35$ °C		$T_0 = 5$ °C
Case	Case 1	Case 2	Case 3
$\dot{E}_{\text{F,total}}$ (kW)	5144.97	5144.97	5147.67
$\dot{W}_{\text{net}}$ (kW)	2204.77	2204.77	2204.77
$\dot{E}_{\text{Cooling}}$ (kW)	6.25	6.25	-
$\dot{E}_{\text{Heating}}$ (kW)	72.69	-	183.29
$\varepsilon_{\text{total}}$ (%)	44.39	42.97	46.39

By taking into consideration of natural gas prices in the U.S. and Germany (shown in Table 6.1), the product costs within the components as well as the final products of the overall system are listed in Table 6.4 and 6.5. One can notice that the individual product costs and the average product cost in case 3 are the lowest, followed by that in case 1, while all the costs associated with case 2 are the highest. Regarding the final product costs, in cases 1 and 2, the refrigeration capacity per unit of exergy is more expensive than the electricity by a factor of around 3.8 based on the natural gas price in the U.S., while with the natural gas price in Germany, the factor decreases to approximately 3. The cost of heat per unit of exergy is 2.8 times as high as the electricity cost in case 1, regardless of the natural gas prices. In case 3, the heat per unit of exergy is only 50-60% more expensive than the electricity with the natural gas prices in the U.S. and Germany. In all the cases, the overall system's average product cost is closed to but slightly higher than the electricity cost in that case since the electricity is the predominant product and its cost, thus, dominants the average product cost.

Table 6.4: Product costs of the overall system (including the natural gas engine and the polygeneration system) operated in different environmental conditions based on the natural gas price in the U.S..

Condition	$T_0 = 35\ °C$		$T_0 = 5\ °C$
Case	Case 1	Case 2	Case 3
Product costs within components			
$c_{\text{Electricity,NGE}}$ ($/GJex)	14.19	14.19	13.44
$c_{\text{Electricity,EX}}$ ($/GJex)	15.12	15.12	14.05
$c_{\text{Refrigeration,EVAP}}$ ($/GJex)	57.89	57.89	-
$c_{\text{Heating,Cooler}}$ ($/GJex)	44.02	44.02	22.39
Final product costs of the overall system			
$c_{\text{Electricity}}^{\text{av.}}$ ($/GJex)	15.16	16.63	14.83
$c_{\text{Refrigeration}}$ ($/GJex)	58.77	60.24	-
c_{Heating} ($/GJex)	44.90	-	23.73
$c_{\text{P,total}}^{\text{av.}}$ ($/GJex)	16.22	16.76	15.52

Table 6.5: Product costs of the overall system (including the natural gas engine and the polygeneration system) operated in different environmental conditions based on the natural gas price in Germany.

Condition	$T_0 = 35\ °C$		$T_0 = 5\ °C$
Case	Case 1	Case 2	Case 3
Product costs within components			
$c_{\text{Electricity,NGE}}$ ($/GJex)	19.41	19.41	18.30
$c_{\text{Electricity,EX}}$ ($/GJex)	18.59	18.59	17.67
$c_{\text{Refrigeration,EVAP}}$ ($/GJex)	63.82	63.82	-
$c_{\text{Heating,Cooler}}$ ($/GJex)	55.34	55.34	28.54
Final product costs of the overall system			
$c_{\text{Electricity}}^{\text{av.}}$ ($/GJex)	20.56	22.42	20.08
$c_{\text{Refrigeration}}$ ($/GJex)	65.05	66.91	-
c_{Heating} ($/GJex)	56.57	-	30.42
$c_{\text{P,total}}^{\text{av.}}$ ($/GJex)	21.83	22.55	20.88

6.2.2 System excluding the natural gas engine

Although the natural gas engine in this case study is the prime mover that drives the proposed polygeneration system, the polygeneration system's performance is still the main research interest in this current study. The natural gas engine is considered to evaluate the entire system's performance that integrates the proposed polygeneration system into the natural gas engine; however, the design evaluation and optimization of the natural gas engine is out of the author's research scope. It is worth to keep paying particular attention to the polygeneration system; thus, the system performance evaluation regarding the polygeneration system is given in detail in this section.

Before we jump to the component-wise and system-wise exergetic and exergoeconomic analyses, let us discuss the system exergetic efficiency shortly by narrowing the system boundary down to the proposed polygeneration system. There are, in general, two different expressions to evaluate the performance of the polygeneration system by considering different operating circumstances: 1. the HSO stream will be further used for some other processes; 2 the HSO stream will be rejected directly into the atmosphere. As we mentioned before, in this study, the second operating circumstance is assumed so that the HSO stream should be the system exergy loss. However, by observing both of the expressions in-depth, there is a relation between them. The exergy rate of the system product in both operating circumstances remains the same; however, the definitions of system fuel and loss diverge. With the first consideration, the fuel of the system is defined as the difference between the exergy rate of the HSI stream and that of the HSO stream, namely, the fuel of the HE is also the fuel of the system. In this way, the system performance is evaluated based on the objective amount of exergy rate transferring from the exhaust gas of the natural gas engine to the CO_2 stream of the polygeneration system. However, with the second consideration, the system fuel is defined as the exergy rate associated only with the HSI stream, while the exergy rate of the HSO stream is treated as the loss of the system as it will not be further utilized as a valuable stream. The definitions of system fuel, product, and loss under these two different operating circumstances (tagged as scenario 1 and 2) are summarized in Table. 6.6.

Table 6.6: Definitions of fuel, product and loss for the overall system excluding the natural gas engine.

	Scenario 1	Scenario 2
$\dot{E}_{\mathrm{F,total}}$	$\dot{E}_{\mathrm{HSI}} - \dot{E}_{\mathrm{HSO}}$	$\dot{E}_{\mathrm{HSI}}$
$\dot{E}_{\mathrm{P,total}}$	$\dot{W}_{\mathrm{net,PGS}} + \dot{E}_{\mathrm{Heating,PGS}} + \dot{E}_{\mathrm{Cooling,PGS}}$	$\dot{W}_{\mathrm{net,PGS}} + \dot{E}_{\mathrm{Heating,PGS}} + \dot{E}_{\mathrm{Cooling,PGS}}$
$\dot{E}_{\mathrm{L,total}}$	-	$\dot{E}_{\mathrm{HSO}}$

It is clear that the system exergetic efficiency in scenario 1 is higher than that in scenario 2. But for comparing various waste heat recovery technologies or evaluating how efficient a proposed system can utilize the thermal energy from a waste heat source, the second

consideration might be more objective and rational since the exergy rate of system fuel is a fixed value, and the system performance is evaluated not only based on how efficient the system can convert the amount of exergy rate transferring from the waste heat source into the system, but also taking the system ability for effectively recovering the waste heat into the consideration. Mathematically, the relation between these two expressions for computing system exergetic efficiency under different operating circumstances can be explained as:

$$\varepsilon''_{\text{total}} = \frac{\dot{E}''_{\text{P,total}}}{\dot{E}''_{\text{F,total}}} \tag{6.5}$$

with $\dot{E}''_{\text{P,total}} = \dot{E}'_{\text{P,total}}$, thus, the Eq. 6.5 can also be expressed as:

$$\varepsilon''_{\text{total}} = \frac{\dot{E}'_{\text{P,total}}}{\dot{E}''_{\text{F,total}}} = \underbrace{\frac{\dot{E}'_{\text{P,total}}}{\dot{E}'_{\text{F,total}}}}_{\varepsilon'_{\text{total}}} \times \underbrace{\frac{\dot{E}'_{\text{F,total}}}{\dot{E}''_{\text{F,total}}}}_{\frac{\dot{E}_{\text{HSI}} - \dot{E}_{\text{HSO}}}{\dot{E}_{\text{HSI}}}} \tag{6.6}$$

where $'$ and $''$ denote the terms associated with scenario 1 and scenario 2, respectively.

One can notice that the result of $\varepsilon''_{\text{total}}$ is composed of two parts; the first part is $\varepsilon'_{\text{total}}$, while the other part $((\dot{E}_{\text{HSI}} - \dot{E}_{\text{HSO}})/\dot{E}_{\text{HSI}})$ reveals the exergy utilization of the heat carrier (exhaust gas of natural gas engine) by the proposed polygeneration system. Recently, the second part is investigated and proposed in [122] as a novel indicator, called exergy utilization index (XUI), which is used to maximize the utilization of a heat source in a heat recovery system. The ideal case for maximizing this indicator is to reject the HSO stream with the ambient temperature and pressure, namely, $\dot{E}^{\text{PH}}_{\text{HSO}} = 0$. Therefore, in the following sections, $\varepsilon''_{\text{total}}$ is used for evaluating the system efficiency of the proposed polygeneration system, while the value of XUI is also given to indicate how efficient the system can utilize the heat source.

Moreover, as we discussed in Table 6.5, case 3 is the "best case" by obtaining the highest system exergetic efficiency and the lowest product costs, while in case 2, the system exergetic efficiency is the lowest and the products are the most expensive. Thus, cases 2 and 3 are selected for representing the performances of the proposed polygeneration system, which is operated in hot and cold climates, respectively. Furthermore, the local requirement of thermal energies varies in these regions with different ambient temperatures. In the following sections, the investigations regarding the system evaluation and optimization will focus on these two cases, and they are renamed as $\text{Case}_{\text{hot climate}}$ and $\text{Case}_{\text{cold climate}}$.

- *System-wise exergy-based analyses*

The system-wise exergetic analysis results for $\text{Case}_{\text{hot climate}}$ and $\text{Case}_{\text{cold climate}}$ are presented in Table 6.7. Compared to the exergetic efficiency of the overall system including the natural gas engine (given in Table 6.3), the disparity in system efficiencies for cases in hot and cold climates becomes larger. The system operated in cold climate shows a higher efficiency (almost 47%), which is around 50% higher than that operated in a hot climate. However, the value of XUI in the hot climate is 8% higher than that in the cold climate. In Table 6.8, the individual product cost generated within the component and the final cost of each product, as well as the average product cost of the overall system, are shown. These results are conducted based on the natural gas price in Germany, and the work in the following sections will only

stick to the German natural gas price. One can notice that the electricity price within the EX in $\text{Case}_{\text{hot climate}}$ (converted to 0.088 \$/kWh) is slightly higher than that in $\text{Case}_{\text{cold climate}}$ (0.082 \$/kWh); while the heat generated within the Cooler in $\text{Case}_{\text{hot climate}}$ is almost twice as expensive as the heat price in $\text{Case}_{\text{cold climate}}$. By charging the exergy loss cost to the product costs, in $\text{Case}_{\text{hot climate}}$, the final electricity price for the overall system increases by more than 100% contrasted with that within the EX. In contrast, for $\text{Case}_{\text{cold climate}}$, the final product costs show only slight influences by the cost of system exergy loss. Regarding the final average product cost, the system operated in a cold climate achieves a better performance from the exergoeconomic point of view by reducing the average product cost in $\text{Case}_{\text{hot climate}}$ to 59%.

Table 6.7: Exergetic analysis result for the overall system (excluding the natural gas engine) operated in hot and cold climates.

Condition	$T_0 = 35\ °\text{C}$	$T_0 = 5\ °\text{C}$
Case	$\text{Case}_{\text{hot climate}}$	$\text{Case}_{\text{cold climate}}$
$\dot{E}_{\text{F,total}}$ (kW)	674.14	829.78
$\dot{W}_{\text{net}}$ (kW)	204.77	204.77
$\dot{E}_{\text{Cooling}}$ (kW)	6.26	-
$\dot{E}_{\text{Heating}}$ (kW)	-	183.29
$\varepsilon_{\text{total}}$ (%)	31.30	46.76
XUI (%)	93.62	86.83

Table 6.8: Individual product cost and average final product cost for the overall system (excluding the natural gas engine) operated in hot and cold climates based on the natural gas price in Germany.

Condition	$T_0 = 35\ °\text{C}$	$T_0 = 5\ °\text{C}$
Case	$\text{Case}_{\text{hot climate}}$	$\text{Case}_{\text{cold climate}}$
$c_{\text{Electricity,EX}}$ (\$/GJex)	24.44	22.78
$c_{\text{Refrigeration,EVAP}}$ (\$/GJex)	96.39	-
$c_{\text{Heating,Cooler}}$ (\$/GJex)	73.48	37.50
$c_{\text{Electricity,total}}$ (\$/GJex)	51.11	24.44
$c_{\text{Refrigeration,total}}$ (\$/GJex)	123.06	-
$c_{\text{Heating,total}}$ (\$/GJex)	-	39.17
$c_{\text{P,total}}^{\text{av.}}$ (\$/GJex)	53.26	31.39

- *Component-wise exergy-based analyses*

Compared to exergy-based analyses at the system level, the component-wise exergy-based analyses offer more detailed information regarding the exergy destruction and investment cost associated with each component. With advanced exergy-based methods, the exergy destruction and investment cost of components can be further split into avoidable and unavoidable parts. These indications obtained at the component level can better help designers allocate their efforts to improve system performance.

Table 6.9 lists the assumptions made for implementing advanced exergetic and exergoeconomic analyses by considering three different operating conditions for components. The operation parameter selected for heat exchangers is the pinch point temperature difference $\Delta T_{\text{pinch},k}$, while for turbomachines, their isentropic efficiencies $\eta_{\text{isen},k}$ for different conditions are assumed.

Table 6.9: Assumptions of three operation conditions (Best case, Base case, and Worst case) for implementing advanced exergy-based analyses.

Component	Parameter (unit)	Best case	Base case	Worst case
HE	$\Delta T_{\text{pinch,HE}}$ (K)	5	20	40
EX	$\eta_{\text{isen,EX}}$ (%)	98	90	70
Cooler	$\Delta T_{\text{pinch,Cooler}}$ (K)	1	5	10
CM–P	$\eta_{\text{isen,CM–P}}$ (%)	95	85	70
EVAP	$\Delta T_{\text{pinch,EVAP}}$ (K)	1	5	10
CM–R	$\eta_{\text{isen,CM–R}}$ (%)	95	85	70

In Table 6.10 and Fig. 6.3, the results of component-wise exergetic and exergoeconomic analyses for the Case$_{\text{hot climate}}$ are summarized and illustrated. From the results of conventional exergy-based analyses, one can observe in Table 6.10 that the highest exergy destruction occurs within the Cooler, then followed by the HE, the MIX, and the EX; while the Cooler has the lowest exergetic efficiency of only 24%, and the exergetic efficiency of the TV is lower than 50%, which needs to be considered to be improved; regarding the value of r_k, the Cooler and EVAP are the highest, and the HE, the CM–R, and the TV are also noticed by showing their high values of r_k; the total cost associated with the Cooler, presented in Fig. 6.3(a), is more than 12 $/h, which is caused mainly by its high cost rate paid for the exergy destruction; while the total costs associated with the EX and the HE are also noticeable, but for them, the main contribution is the high investment cost; in general, the exergoeconomic factor f_k is relatively high (higher than 75%) for the turbomachinary, and for heat exchangers (except the EVAP), their values of f_k are relatively low, particularly, for the Cooler with it f_k of only 34%. The Cooler, having the highest values of $\dot{Z}_k + \dot{C}_{\text{D},k}$ and r_k, as well as the lowest exergetic efficiency, needs to be prioritized in the optimization process. Given its low value of f_k, reducing the pinch point temperature difference might be considered to improve its

thermodynamic performance by investing more money in this heat exchanger. Subsequently, the improvement efforts should focus on the HE and the EX.

Table 6.10: Main indications derived from component-wise exergy-based analyses of the proposed polygeneration system operated in the hot climate (Case$_{\text{hot climate}}$) based on the natural gas price in Germany.

Case$_{\text{hot climate}}$ with $T_0 = 35\,°\text{C}$					
Conventional exergetic and exergoeconomic analyses					
Component (k)	$\dot{E}_{\text{D},k}$ (kW)	ε_k (%)	r_k (-)	f_k (%)	
HE	90.05	85.73	1.49	68.52	
EX	19.68	94.22	0.58	89.51	
MIX	39.19	-	-	-	
Cooler	183.79	23.86	4.84	34.07	
CM–P	11.15	86.72	0.63	75.66	
TV	14.34	46.39	1.18	2.48	
EVAP	3.81	62.18	4.18	85.44	
CM–R	4.44	87.11	1.20	87.68	

Advanced exergetic and exergoeconomic analyses					
Component (k)	$\dot{E}_{\text{D},k}^{\text{UN}}$ (kW)	$\dot{E}_{\text{D},k}^{\text{AV}}$ (kW)	$\varepsilon_k^{\text{AV}}$ (%)	$\dot{Z}_k^{\text{UN}}$ ($/h)	$\dot{Z}_k^{\text{AV}}$ ($/h)	f_k^{AV} (%)
HE	82.18	7.87	98.57	2.08	2.31	92.91
EX	3.55	16.13	95.21	7.01	2.36	72.40
Cooler	170.62	13.17	81.39	2.55	1.75	74.61
CM–P	3.58	7.57	90.58	2.65	0.42	38.37
TV	6.28	8.05	60.64	9.58E-3	1.61E-3	0.65
EVAP	2.73	1.08	85.29	1.43	0.07	48.73
CM–R	1.34	3.10	90.64	2.67	0.08	22.80
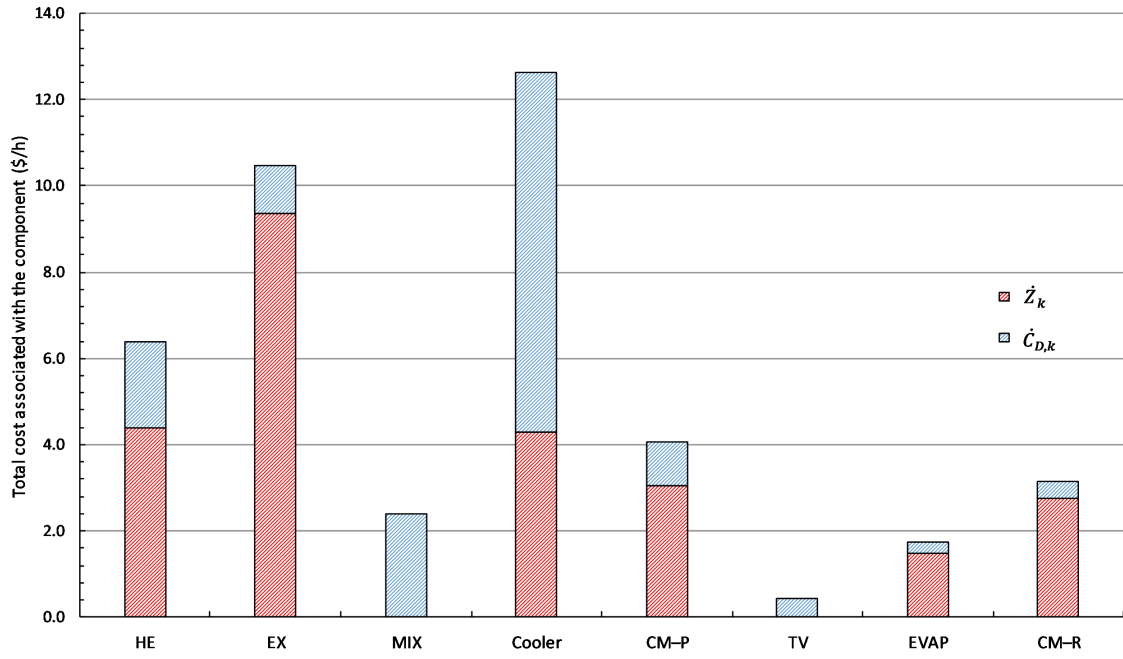
(a) $\dot{Z}_k + \dot{C}_{\mathrm{D},k}$ derived from the conventional exergoeconomic analysis
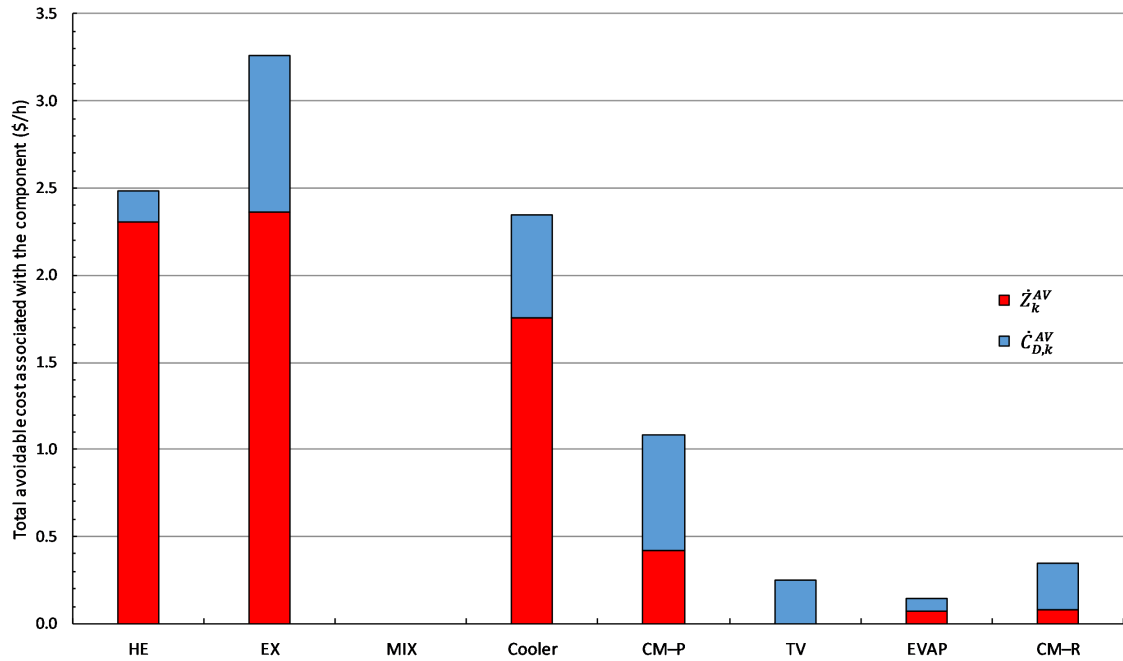
(b) $\dot{Z}_k^{\mathrm{AV}} + \dot{C}_{\mathrm{D},k}^{\mathrm{AV}}$ derived from the advanced exergoeconomic analysis

Figure 6.3: Total cost $(\dot{Z}_k + \dot{C}_{\mathrm{D},k})$ and its avoidable part $(\dot{Z}_k^{\mathrm{AV}} + \dot{C}_{\mathrm{D},k}^{\mathrm{AV}})$ associated with components of the proposed polygeneration system operated in the hot climate ($\mathrm{Case_{hot\ climate}}$) based on the natural gas price in Germany.

However, the results in advanced exergetic and exergoeconomic analyses for the $\mathrm{Case_{hot\ climate}}$ (in Table 6.10) reveal that for the Cooler, more than 170 kW exergy destruction from its total exergy destruction of 184 kW is unavoidable, and its avoidable exergy destruction is still high compared to other components but not the highest; the modified exergetic

efficiency $\varepsilon_k^{\mathrm{AV}}$ of the Cooler is higher than 80%, in contrast to the exergetic efficiency ε_k of less than 25% obtained from the conventional exergetic analysis; as shown in Fig. 6.3(b), if we focus only on the avoidable parts, the EX has the highest avoidable cost $\dot{Z}_k^{\mathrm{AV}} + \dot{C}_{\mathrm{D},k}^{\mathrm{AV}}$, while the HE and the Cooler are also considered as prominent components regarding their high improvement potentials by reducing the avoidable cost; with the f_k^{AV} of 93%, increasing its pinch point temperature difference should be implemented in the following optimization process; surprisingly, for the Cooler, the avoidable investment cost contributes around 75% on its total avoidable cost, reducing its investment cost, thus, can be suggested, which contradicts the conclusion made from the conventional exergoeconomic analysis. In addition, no results regarding the MIX are obtained from the advanced exergy-based analyses because it is considered as a dissipative component, which in turn, the exergy rate of the product is not defined for this component, and no available results associated with advanced exergy-based methods, thus, can be computed.

Similarly, Table 6.11 and Fig. 6.4 present the results of component-wise exergetic and exergoeconomic analyses for the Case$_{\mathrm{cold\ climate}}$. In this case, the Cooler still has the highest exergy destruction but its exergetic efficiency doubles compared to that in the Case$_{\mathrm{hot\ climate}}$. The exergetic efficiency of the EVAP is very low because it is operated at the ambient temperature, which results in a fairly low exergy rate of the product. Besides, for the EVAP, the f_k value is 100% since its fuel is assumed as for free, so no exergy destruction cost is charged within this component. The disparity between the total cost and avoidable cost associated with components illustrated in Fig. 6.4 (a) and (b), is analogous to the results as we discussed for the Case$_{\mathrm{hot\ climate}}$ in Fig. 6.3.

It can be realized that with advanced exergy-based analyses, more detailed and specific information is obtained by focusing on only the avoidable parts. The indications derived from conventional and advanced exergetic and exergoeconomic analyses can provide information resulting in different suggestions, even contradicted suggestions for the optimization process. However, the designers should generally follow the results from the advanced exergy-based methods if advanced exergy-based analyses are carried out.

Table 6.11: Main indications derived from component-wise exergy-based analyses of the proposed polygeneration system operated in the cold climate (Case$_{\text{cold climate}}$) based on the natural gas price in Germany.

Case$_{\text{cold climate}}$ with $T_0 = 5\ ^\circ\text{C}$					
Conventional exergetic and exergoeconomic analyses					
Component	$\dot{E}_{\text{D},k}$	ε_k	r_k	f_k	
(k)	(kW)	(%)	(-)	(%)	
HE	81.81	88.60	1.23	70.55	
EX	17.88	94.72	0.64	91.29	
MIX	35.63	-	-	-	
Cooler	166.95	52.33	1.31	30.71	
CM–P	10.15	87.92	0.64	78.66	
TV	13.04	-	-	-	
EVAP	3.46	1.89E-3	-	100.00	
CM–R	4.04	87.44	1.34	89.26	

Advanced exergetic and exergoeconomic analyses					
Component	$\dot{E}_{\text{D},k}^{\text{UN}}$	$\dot{E}_{\text{D},k}^{\text{AV}}$	$\varepsilon_k^{\text{AV}}$	$\dot{Z}_k^{\text{UN}}$	$\dot{Z}_k^{\text{AV}}$	f_k^{AV}
(k)	(kW)	(kW)	(%)	($/h)	($/h)	(%)
HE	73.57	8.24	98.72	2.10	2.28	92.52
EX	3.23	14.65	95.63	7.01	2.36	76.31
Cooler	156.70	10.25	94.70	2.54	1.76	74.69
CM–P	3.30	6.85	91.51	2.61	0.46	44.81
EVAP	3.06	0.40	1.63E-2	1.42	0.08	100.00
CM–R	1.23	2.81	90.92	2.51	0.24	51.33
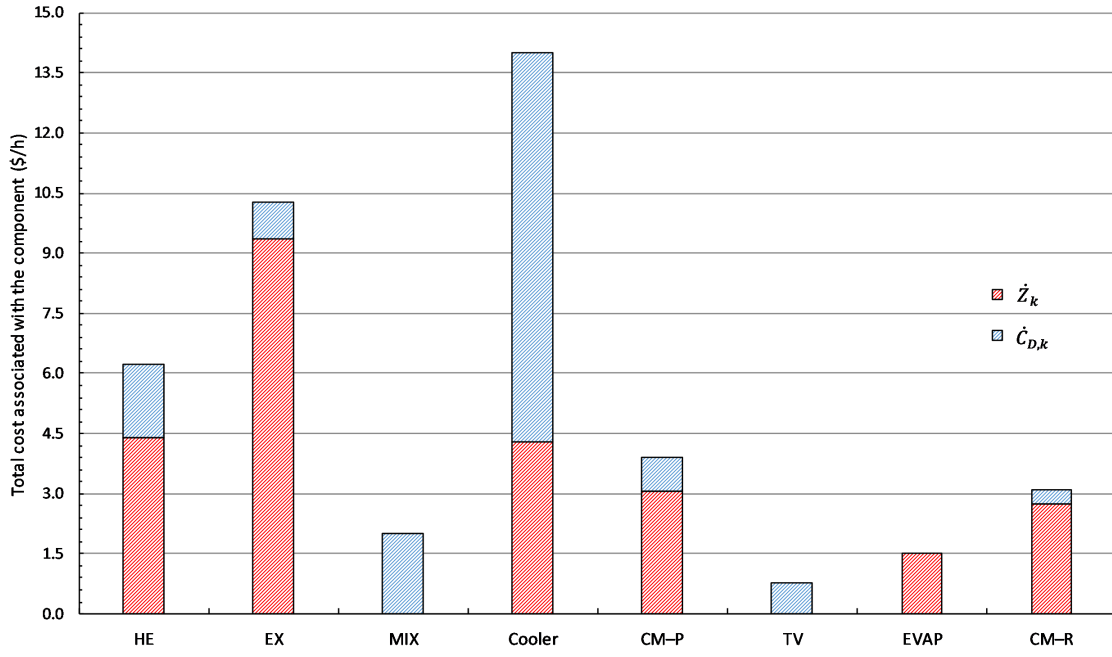
(a) $\dot{Z}_k + \dot{C}_{\mathrm{D},k}$ derived from the conventional exergoeconomic analysis
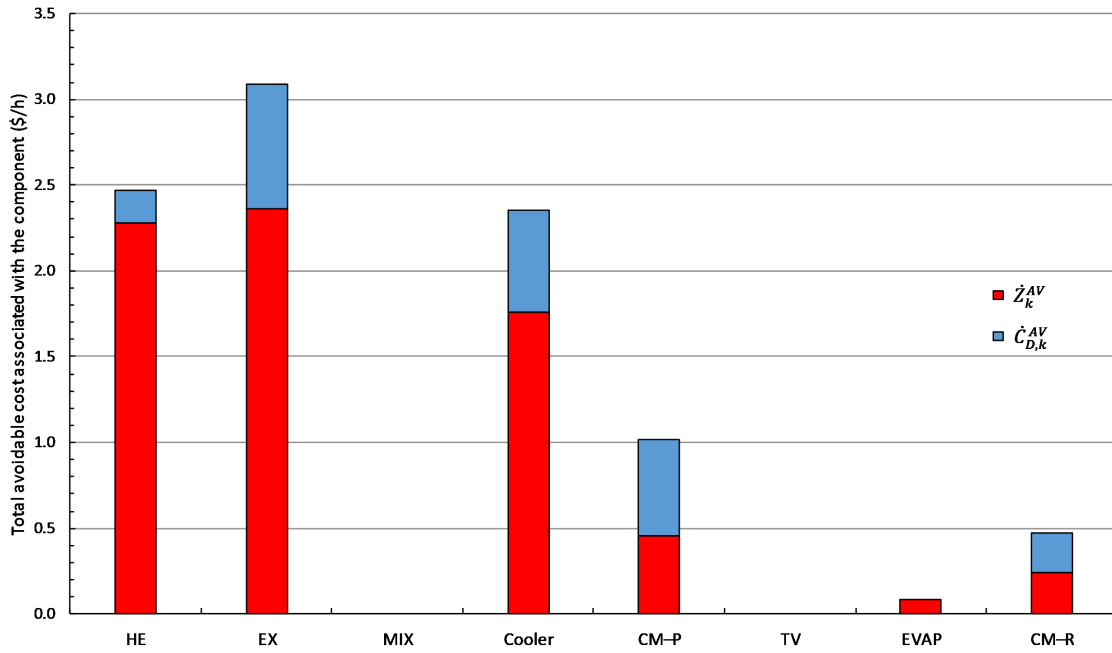
(b) $\dot{Z}_k^{\mathrm{AV}} + \dot{C}_{\mathrm{D},k}^{\mathrm{AV}}$ derived from the advanced exergoeconomic analysis

Figure 6.4: Total cost $(\dot{Z}_k + \dot{C}_{\mathrm{D},k})$ and its avoidable part $(\dot{Z}_k^{\mathrm{AV}} + \dot{C}_{\mathrm{D},k}^{\mathrm{AV}})$ associated with components of the proposed polygeneration system operated in the cold climate $(\mathrm{Case_{cold\ climate}})$ based on the natural gas price in Germany.

6.3 System optimization

For thermal system optimization, there are two general forms: parameter optimization and structural optimization [88]. In parameter optimization, decision variables applied in the

base-case design may be altered as optimal decision variables are found in this step. In structural optimization, the equipment inventory and the system topology are targeted to achieve a superior design. In other words, the equipment items and their interconnections are considered in the structural optimization, and sometimes it can also be along with parameter optimization. Note that only the proposed polygeneration system is considered for system optimization; the optimal design of the natural gas engine is out of the research scope in this work.

6.3.1 Parameter optimization

In this section, the parameter optimization is carried out for the proposed polygeneration system. First, the optimization focuses only on minimizing the average product cost of the overall system; thus, the problem is defined as a sing-objective optimization problem. Then both the system exergetic efficiency and the average product cost are targeted; the problem is upgraded to a multi-objective optimization problem.

6.3.1.1 Single-objective optimization

The decision parameters of the proposed polygeneration system are considered the input parameters into the optimization problem and need to be globally optimized. DE and PSO algorithms are investigated to obtain global optimization results. The single-objective optimization problem is formulated, as shown in Eq. 6.7. The lowest average product cost of the overall system is targeted; the component variables that influence the performance of each component (except MIX, SPLIT, and TV) and the merging pressure p_{Merging} are selected as the decision parameters. Also, the design constraints, regarding the maximum pressure at turbine inlet $TIP_{\max}$, the minimum pressure ratio of turbomachines $PR_{\min}$, and the minimum temperature at compressor inlet in the power cycle $T_{\text{in,CM–P,min}}$, are specified and listed as well.

$$min \ c_{\text{P,total}}^{\text{av.}}$$

$$
\text{subject to}
\begin{cases}
5\,^{\circ}\mathrm{C} \leq \Delta T_{\text{pinch,HE}} \leq 40\,^{\circ}\mathrm{C} \\
70\% \leq \eta_{\text{isen,EX}} \leq 98\% \\
1\,^{\circ}\mathrm{C} \leq \Delta T_{\text{pinch,Cooler}} \leq 10\,^{\circ}\mathrm{C} \\
70\% \leq \eta_{\text{isen,CM–P}} \leq 95\% \\
1\,^{\circ}\mathrm{C} \leq \Delta T_{\text{pinch,EVAP}} \leq 10\,^{\circ}\mathrm{C} \\
70\% \leq \eta_{\text{isen,CM–R}} \leq 95\% \\
75\,\mathrm{bar} \leq p_{\text{Merging}} \leq 90\,\mathrm{bar} \\
TIP_{\max} = 250\,\mathrm{bar} \\
PR_{\min} = 1.5 \\
T_{\text{in,CM–P,min}} = 32\,^{\circ}\mathrm{C}
\end{cases}
\tag{6.7}
$$

where ΔT_{pinch} denotes the pinch point temperature difference within a heat exchanger; η_{isen} denotes the isentropic efficiency of a turbomachine.

- *Implementation of DE algorithm optimization*

Table 6.12 lists the main settings for the DE algorithm implementation. The number of decision parameters determines the population size. The mutation factor varies by iteration, starting from 1 and shrinking to 0.5 to ensure that enough potential candidates are explored, and less computation time is required for solving the optimization problem. The convergence criterion is set as the optimization terminates once the standard deviation of the population σ (population) is less than or equal to 1% of the mean of the population μ (population). Either the convergence criterion is met, or the optimization reaches its 50th iteration, the optimization process ends, and the results are returned as the final optimization results.

Table 6.12: Main settings for the DE algorithm optimization.

Item	Value/Requirement
Population size	$15 \times$ number of decision parameters ($15 \times 8 = 120$)
Mutation constant	Shrinking from 1 to 0.5
Crossover constant	0.7
Convergence criterion	σ (population) $\leq 0.01 \times |\mu$ (population)$|$
Max iteration	50

The polygeneration system is optimized by considering both hot and cold climates. First, as an example, the investigations regarding the optimization algorithms and optimization results for the hot climate case ($\text{Case}_{\text{hot climate}}$) are discussed in detail. In Fig. 6.5, the optimization results for $\text{Case}_{\text{hot climate}}$ by applying DE algorithm is overviewed. The objective function results (fitness results) of all selected and tested candidates are illustrated with green dots, and they are shown on the secondary Y-axis. On the first Y-axis, average fitness results of candidates per iteration are depicted using a blue bar chart.

From the scatter plot, it can be noticed that better candidates with lower average product costs per unit of exergy are continuously discovered along with the execution time. The best candidate with its fitness result first approaches the horizontal line (indicating the fitness value of 0.15 $/kWh), then crosses it, and eventually ends in the area below the horizontal line with its fitness value of around 0.14 $/kWh. At the beginning of the optimization, the candidates are randomly distributed; afterward, it tends to go to the lower part of this plot; finally, the group of candidates in the 18th iteration converges. The optimization process terminates. The average fitness result of candidates for each iteration decreases dramatically at first; then, the decline becomes slower; in the last four iterations, the average result shows no more reduction rather than starting to increase. This behavior is very interesting, and it reveals the "smart" DE algorithm is trying to balance exploration and exploitation. Although the exploitation passes the "good genes" from the "fittest parents" to the next generation and helps the algorithm to fast convergence, it also increases the risk that the optimization result
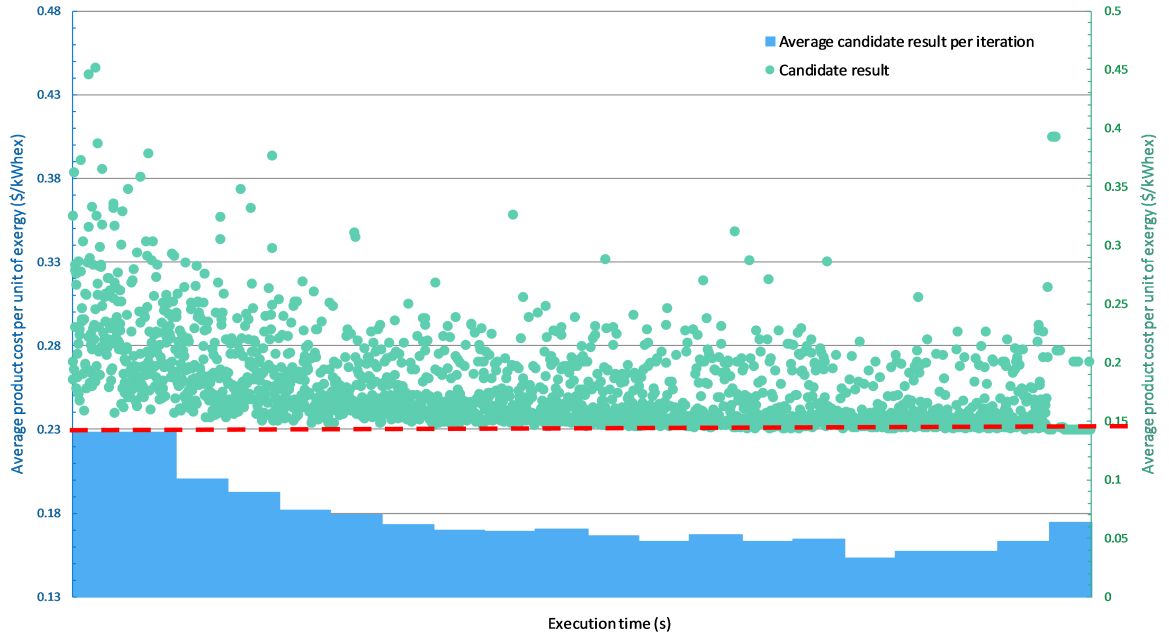
Figure 6.5: Optimization results of DE algorithm for the hot climate case (Case$_{\text{hot climate}}$): green dots denote return values of the objective function (fitness) for all candidates tested during the optimization process; the blue bar chart reveals the average results of candidates in each iteration along with the execution time.

stagnates in local optima. With the help of the mutation operator, more potential candidates can be explored and tested during the optimization process, which expands the numbers and the variations of searched candidates within the searching space. In turn, it increases the chance that optimization results are global results but not local optima. With discovering the best candidate in each new iteration, the exploration also works actively; thus, some new candidates still exist in the last several iterations. Since the newly explored candidates are relatively far from the best areas found so far, the average fitness results for the last four iterations show a slight increase.

For presenting the trade-off between the exploration and the exploitation in a clearer way, candidate fitness results in the first two and last two iterations are illustrated in Fig. 6.6. One can observe that in the first iteration, initial candidates of the first generation are generated randomly to explore various areas of the searching space. In the second iteration, by the influence of exploitation, the candidates' fitness results move significantly to the lower part of this chart. However, still, no clear tendency can be noticed. The results in the 17th iteration show that more than 75% of the candidates locate in line with their fitness results of slightly higher than 0.14 \$/kWh. In the last iteration, almost all candidates converge to the value of 0.14 \$/kWh; only a few are exempt from that. Unfortunately, these exempted candidates, generated by the effect of the exploration, do not show better results compared to the so-far best candidate, and the optimization algorithm meets its convergence criterion, thus, terminates. Although the exploration in the last iteration in this example fails and no better candidate is discovered, it shows the importance of balancing the exploration and the exploitation in the optimization process for the local optima stagnation avoidance and fast convergence.
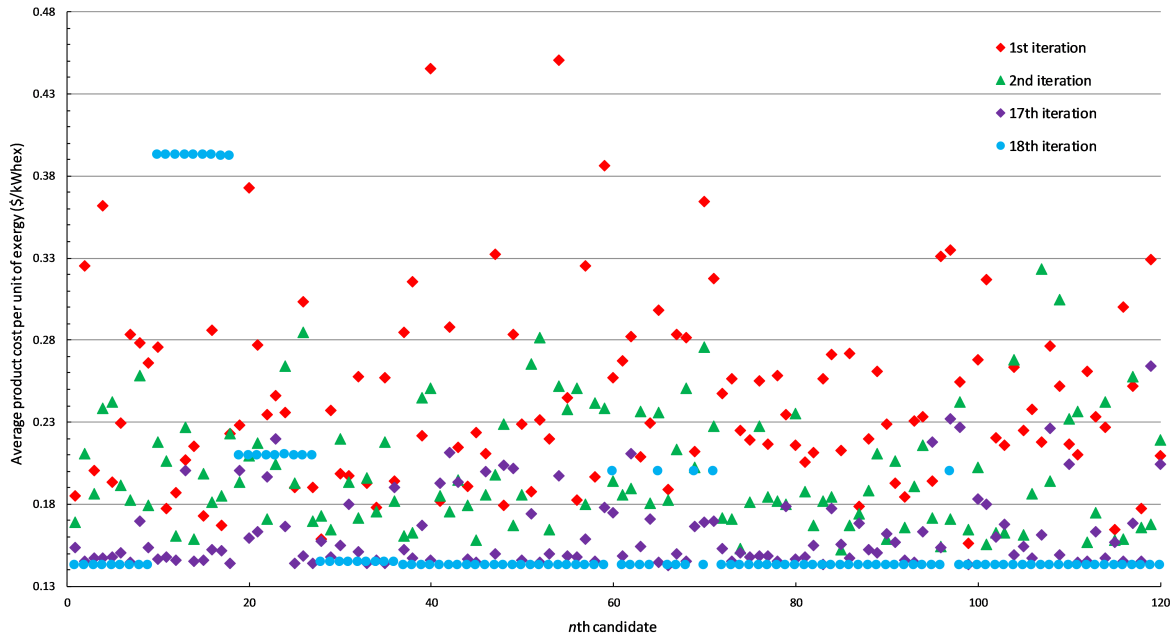
Figure 6.6: Optimization results of DE algorithm in the first two and last two iterations for the hot climate case ($\text{Case}_{\text{hot climate}}$).

- *Implementation of PSO algorithm*

PSO is also one of the commonly applied evolutionary techniques for solving optimization problems in engineering fields. It is relatively new and gaining more and more attention. For discovering the influences of selected algorithms on the optimization process and its results, the PSO algorithm is carried out to solve the same optimization problem, as shown in Eq. 6.7. In Table 6.13, the general settings for implementing the PSO algorithm are listed. As different attempts are tried for adjusting the setting parameters, detailed information for each attempt is given in Table 6.14.

For the comparison purpose, the same population size is selected as we implemented in the DE algorithm, while the maximal iteration is set as 18, which is the iteration where the DE optimization converges and terminates. Three attempts are carried out since the result of the first attempt is not as good as that obtained from the DE algorithm optimization, and it was mentioned in [98] that the drawbacks of PSO include easily suffers from the local optimization and more tuning efforts are required for achieving accurate results. Hence, the first attempt (POS-1) is used as the benchmark for comparing to other further attempts by investing more effort in tuning the setting parameters. In the second and the third attempts (PSO-2 and PSO-3), acceleration constants and the inertia weight are modified, respectively, to obtain better and more accurate optimization results. There are several options in terms of tuning the inertia weight. Among these options, the GLbestIW method [123, 124] is carried out in many energy-related applications and the results are satisfactory. Thus, in the attempt of PSO-3, the GLbestIW method is selected, and its mathematical expression for the ith particle is written as:

$$w_i = (1.1 - \frac{\text{Gbest}}{\text{Pbest}_i})$$

(6.8)

where w stands for inertia weight; Gbest and Pbest represent the global best result and the personal best result, respectively.

Table 6.13: Main settings for the PSO algorithm.

Item	Value/Requirement
Population size	$15 \times$ number of decision parameters ($15 \times 8 = 120$)
Acceleration constants	Detailed info is given in Table 6.14
Inertia weight	Detailed info is given in Table 6.14
Convergence criterion	When the result difference between the two consecutive iterations is $\leq$ 1.00E-8
Max iteration*	18

*: The max iteration is selected based on the optimization results of the DE algorithm, which converges in the 18th iteration.

Table 6.14: Settings of various attempts for implementing the PSO algorithm.

Item	Implementing attempts		
Attempt name	PSO-1	PSO-2	PSO-3
Description	Benchmark	Varying acceleration constants	Varying the inertia weight
Acceleration constants	2	0.5	2
Inertia weight	0.9	0.9	GLbestIW* [123, 124]

*: GLbestIW is short for global-local best inertia weight.

By using the proposed polygeneration system operated in the hot climate as the representative, the optimization process with implementing the PSO algorithm is illustrated in Fig. 6.7. In this figure, the results of three attempts in 18 iterations are represented in detail. One can observe that the PSO-3 obtains the best result with the lowest average product cost not only in the last iteration but also in each iteration (except the first iteration). For the initial global best results in the first iteration, which are randomly selected, PSO-2 is the "luckiest" having the best initial point, while PSO-1 and PSO-3 start from almost the same starting point. However, from the second iteration, the advantage of applying the GLbestIW method by tuning the inertia weight can be seen significantly, and this prominent advantage lasts until the 10th iteration; after the 10th iteration, the results of the global best, for the PSO-3, remain the same as the optimization process converges in the 10th iteration. For the benchmarked PSO-1 attempt, the decrease of the global best result is slower. Its most noticeable achievement occurs in the 13th iteration with a reduction of 44% in terms of the total reduction in the global best result in this attempt. In the second attempt by tuning acceleration constants, better optimization results are obtained generally compared to the

benchmarked attempt; until the 12th iteration, the merits of reducing acceleration constants, in other words, increasing the chance for exploring new candidates, are clearly perceptible; the final optimization result of the PSO-2 is, however, only less than 2% lower compared the that of the PSO-1.
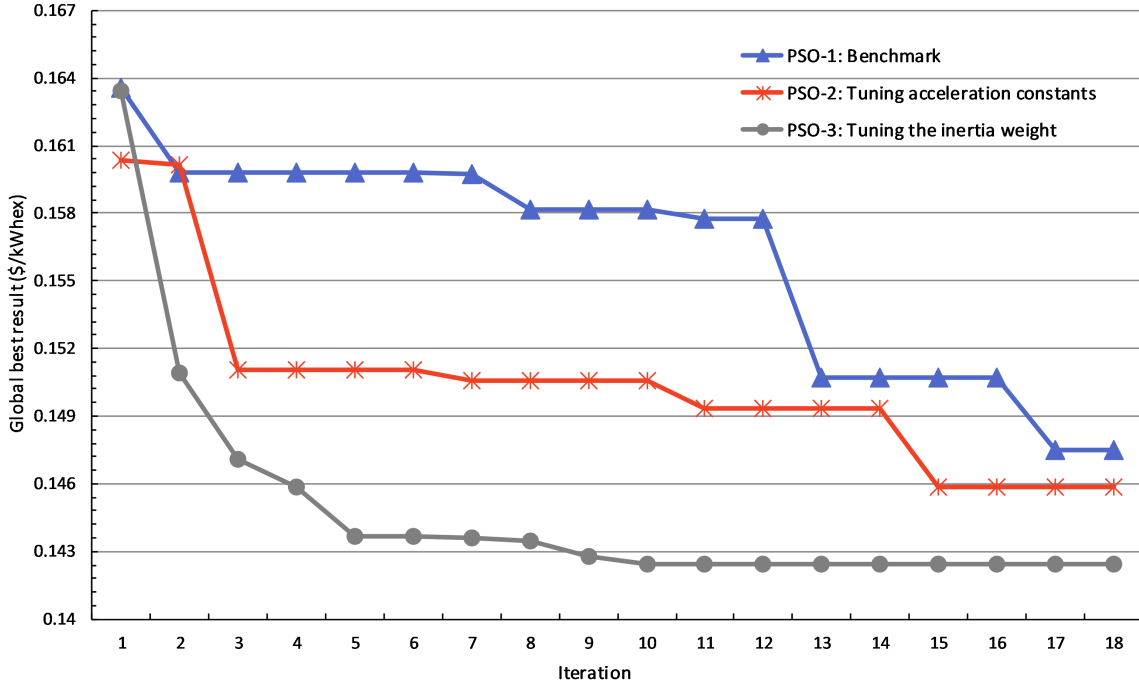
Figure 6.7: The variation of global best results in three various attempts by tuning the setting parameters of the PSO algorithm for the hot climate case ($\text{Case}_{\text{hot climate}}$).

One can conclude that tuning the inertia weight by applying the GLbestIW method in this optimization problem shows the great potential for accelerating the optimization process and obtaining better optimization results. The GLbestIW method, which varies the value of the inertia weight of each particle depending on the particle's current position and its personal and the global best positions, is an excellent example to show the importance of balancing the trade-off between exploration and exploitation in all stochastic optimization algorithms. Therefore, in the following sections, optimization results by implementing the PSO algorithm refer to the results obtained from the PSO-3, unless otherwise indicated.

- *Optimization results by implementing DE and PSO algorithms*

In this section, results of the single-objective optimization problem for the proposed polygeneration system ($\text{Case}_{\text{hot climate}}$ and $\text{Case}_{\text{cold climate}}$) are detailed, and the influences of the optimization algorithm selection on the optimization process/results are investigated. In Table 6.15, the optimization results by implementing DE and PSO algorithms are listed for the $\text{Case}_{\text{hot climate}}$, and the relative differences between the results obtained from DE and PSO algorithms are calculated. The equation for computing the relative difference is written as follows:

$$d_r(x_{\text{DE}}, y_{\text{PSO}}) = \frac{|x_{\text{DE}} - y_{\text{PSO}}|}{max(x_{\text{DE}}, y_{\text{PSO}})} \tag{6.9}$$

where $d_r(x_{\mathrm{DE}}, y_{\mathrm{PSO}})$ denotes the relative difference between the x obtained from DE algorithm and y obtained from PSO algorithm.

Table 6.15: Single-objective optimization results of the parameter optimization for the proposed polygeneration system by implementing DE and PSO algorithms for the hot climate case ($\mathrm{Case}_{\mathrm{hot\ climate}}$).

Item	Unit	Initial value	Optimal value		Relative difference
			DE	PSO	(DE,PSO)
$\Delta T_{\mathrm{pinch,HE}}$	(K)	20	33	26	21.2%
$\eta_{\mathrm{isen,EX}}$	(%)	90	98	98	0.0%
$\Delta T_{\mathrm{pinch,Cooler}}$	(K)	5	5	6	20.0%
$\eta_{\mathrm{isen,CM-P}}$	(%)	85	94	95	1.1%
$\Delta T_{\mathrm{pinch,EVAP}}$	(K)	5	8	9	12.5%
$\eta_{\mathrm{isen,CM-R}}$	(%)	85	95	95	0.0%
p_{Merging}	(bar)	77	80	82	2.5%
PR_{EX}	(-)	2.6	3.1	3.0	2.7%
Optimal result	($/GJex)	53.26	39.60	39.56	0.1%
Execution time	(s)	-	1820	1633	10.3%

Compared to initial values, the optimal operation values of each decision parameter after implementing both algorithms generally show the same tendency: the $\Delta T_{\mathrm{pinch,HE}}$ needs to be increased to a relatively large extent; the value of $\Delta T_{\mathrm{pinch}}$ within the Cooler almost remains the same; the $\Delta T_{\mathrm{pinch,EVAP}}$ should increase from its initial value of 5 K to 8 K according to the optimization results of DE algorithm, and to 9 K by considering the PSO algorithm's results; for turbomachines, all of them after the optimization process reveal that the higher the isentropic efficiency, the better the optimization results; also, a higher PR_{EX} is preferred with the value of around 3; while the optimal value of p_{Merging} increases slightly, which results in merging the power cycle and refrigeration cycle at a higher pressure being relatively far from the critical point of CO_2.

Now, if we try to reason these changes of decision parameters from their initial values to these optimal values selected by "smart" optimization algorithms, the component-wise results of advanced exergetic and exergoeconomic analyses presented in Table 6.10 and Fig. 6.3 can be considered as the reference. It is clear that the value of f_k^{AV} is quite high for the HE, while its $\varepsilon_k^{\mathrm{AV}}$ of around 99% reveals that the improvement potential regarding the exergy destruction reduction is very small. Thus, both algorithms choose to decrease its investment cost by increasing the pinch point temperature difference. For the CM–P and CM–R, the values of their f_k^{AV} are the lowest except the TV, which explains the component preference with a

higher isentropic efficiency obtained from the optimization results. Interestingly, the most expensive EX (with the highest isentropic efficiency) should also be purchased, although it has the highest avoidable cost, and the avoidable investment cost has more contribution than the cost caused by its avoidable exergy destruction. Note that in the optimization process, not only the parameters considered in the advanced exergy-based analyses but also the *TIP* and p_{Merging} are optimized simultaneously. The *TIP* and p_{Merging} determine the pressure ratio of the EX, which also affect its performance significantly. In addition, it is worth to mention that the higher value of the p_{Merging} has several influences on many component performances including the MIX, Cooler, and TV; the effects of increasing the p_{Merging} for the Cooler, which has the noticeable value of $\dot{Z}_k^{\text{AV}} + \dot{C}_{\text{D},k}^{\text{AV}}$ and thus, needs to be paid attention, are detailed in Fig. 6.8.

For the comparison purpose, the influences of increasing the p_{Merging} from 75 bar to 95 bar with the step of 10 bar on the Cooler performance are illustrated, respectively, in Fig. 6.8 (a)-(c). At the merging pressure of 75 bar, which is only approximate 2 bar higher than the critical point of CO_2, the pinch point occurs within the Cooler but close to the cold end. By increasing the merging pressure by 10 bar, a long section of the Cooler showing the curves of the CO_2/hot stream and water/cold stream are close and almost parallel. With the CO_2/hot stream within the Cooler being operated at the pressure of 95 bar, the pinch point shifts to the cold end, and the temperature difference within the Cooler becomes larger since the CO_2/hot stream after the expansion process entering the Cooler with a significantly higher temperature, which in turn, causes a more considerable temperature difference at the hot end. One can conclude that the Cooler's irreversibilities are directly affected by the value of the merging pressure; in other words, the merging pressure influences the magnitude of the exergy destruction within the Cooler. By increasing the merging pressure, the temperature difference near the hot end area increases, while the temperature difference close to the cold end becomes larger if the Cooler operates in the critical point region. There might be an optimal value of the merging pressure resulting in the lowest exergy destruction within the Cooler. Besides, since the Cooler is a dissipative component in this case (Case$_{\text{hot climate}}$), there is no need to invest more money to increase its product. Its product is defined as the exergy loss of the overall system, and the cost associated with the exergy loss has to be charged to other final system products. All factors, as mentioned above, cause the complexity of optimizing the Cooler.
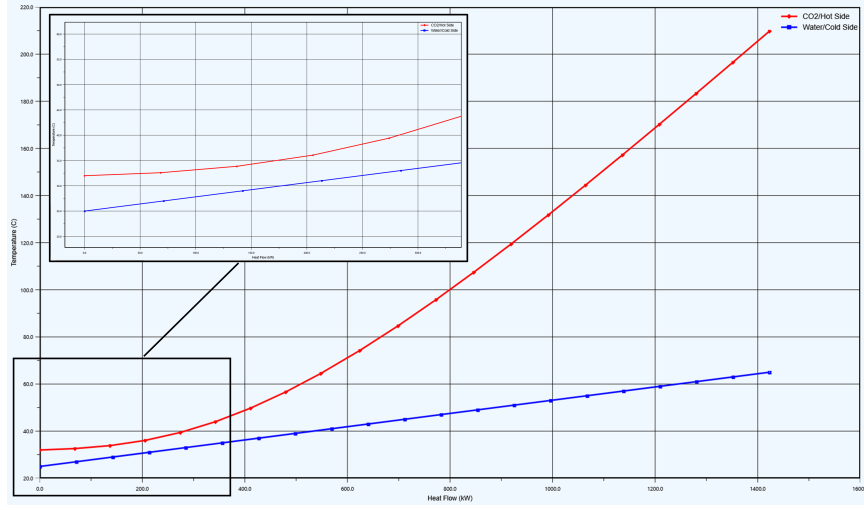
(a) $p_{\mathrm{Merging}} = 75$ bar
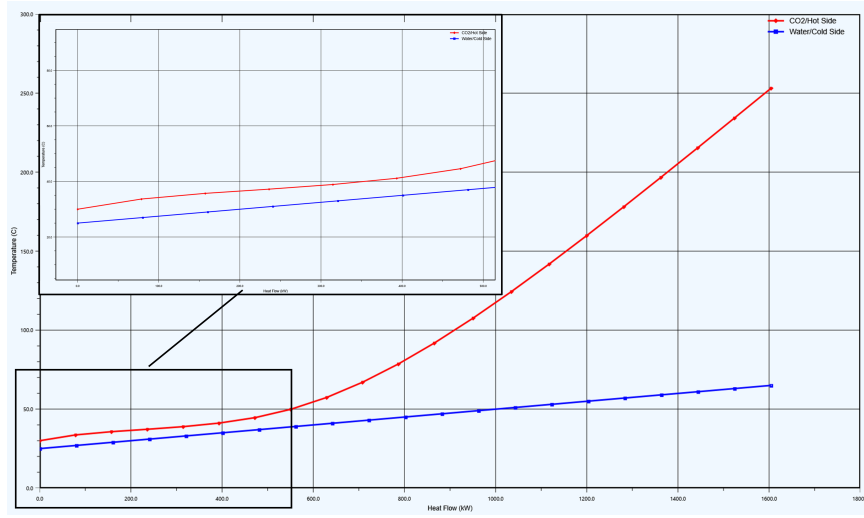
(b) $p_{\mathrm{Merging}} = 85$ bar
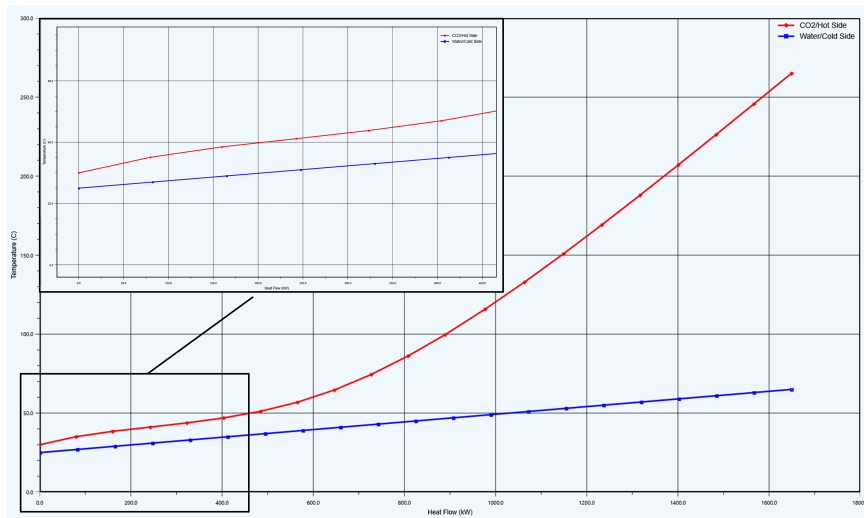
(c) $p_{\mathrm{Merging}} = 95$ bar

Figure 6.8: Influence of increasing the p_{Merging} on the performance of the Cooler.

If we pay attention, comparing the optimal results obtained from the DE and PSO algorithms, as shown in Table. 6.15, their relative differences are lower than 2.5% for decision

parameters regarding turbomachines, the *TIP*, and p_{Merging}. For heat exchangers, however, the differences between the optimal $\Delta T_{\text{pinch},k}$ values by implementing both algorithms are noticeable; and the largest disparity occurs for selecting the optimal operating condition for the HE with its relative difference of more than 20%. The initial value of the average product cost is reduced by 25% in the optimization process, and the best function value (i.e., the lowest average product cost) achieved with the PSO algorithm implementation is 0.1% lower than that obtained by carrying the DE algorithm, while the PSO algorithm takes almost 200 s less for completing the optimization process. Regarding the result of the objective function and the execution time, the PSO algorithm outperforms the DE algorithm for the hot climate case ($\text{Case}_{\text{hot climate}}$).

The optimal results for the overall system operated in the cold climate ($\text{Case}_{\text{cold climate}}$) are presented in Table 6.16. It can be observed that the EX with the highest $\eta_{\text{isen,EX}}$ is still preferred. For the CM–P and CM–R, only a slightly higher value of the isentropic efficiency is selected since they both have a moderate value of f_k^{AV} (as shown in Table 6.11 and Fig. 6.4). For the CG, both algorithms suggest increasing its pinch point temperature difference. Furthermore, the optimal value higher than 85 bar is obtained regarding the pressure for merging both sub-systems. Note that in this case, the heat capacity generated from the Cooler is one of the final products, and the higher the p_{Merging}, the more the amount of the heat capacity. However, if the p_{Merging} is too high, it results in larger exergy destruction within the MIX and Cooler since the temperature difference within these components increases dramatically.

Table 6.16: Single-objective optimization results of the parameter optimization for the proposed polygeneration system by implementing DE and PSO algorithms for the cold climate case ($\text{Case}_{\text{cold climate}}$).

Item	Unit	Initial value	Optimal value		Relative difference
			DE	PSO	(DE,PSO)
$\Delta T_{\text{pinch,HE}}$	(K)	20	29	29	0.0%
$\eta_{\text{isen,EX}}$	(%)	90	97	98	1.0%
$\Delta T_{\text{pinch,Cooler}}$	(K)	5	7	6	14.3%
$\eta_{\text{isen,CM–P}}$	(%)	85	91	91	0.0%
$\Delta T_{\text{pinch,EVAP}}$	(K)	5	10	4	60.0%
$\eta_{\text{isen,CM–R}}$	(%)	85	91	92	1.1%
p_{Merging}	(bar)	77	87	88	1.1%
PR_{EX}	(-)	2.6	2.9	2.8	1.9%
Optimal result	($/GJex)	31.39	26.76	27.03	1.0%
Execution time	(s)	-	1944	1699	12.6%

Regarding the relative difference of the optimal results between DE and PSO algorithms, the pinch point temperature difference for the EVAP has the most controversial results. According to the DE algorithm, the $\Delta T_{\text{pinch,EVAP}}$ should increase from its initial value of 5 K to 10 K, while decreasing it to 4 K is suggested by the PSO algorithm. In addition, at this time, the DE algorithm achieves a better value of the objective function. However, its computation time is still around 13% longer compared to the optimization process by applying the PSO algorithm. In Fig. 6.9, the best function values obtained from both algorithms in their optimization processes along with generating new iterations are detailed for the cold climate case (Case$_{\text{cold climate}}$). It can be seen that the PSO algorithm starts with a relatively better position in the first iteration, and lower function values are continuously found until the 5th iteration. In iterations 6-9, the algorithm struggles in overcoming a local minimum, and finally, a minor achievement can be noticed in the 10th iteration. After that, no better function value is obtained. Contrariwise, an adverse starting position is obtained for the DE algorithm, and it outperforms the PSO algorithm, eventually, in the 8th iteration; its superiority lasts until the last iteration. Note that the maximal iteration of the PSO algorithm is selected based on the DE algorithm optimization results for this cold climate case, which terminates in the 15th iteration.
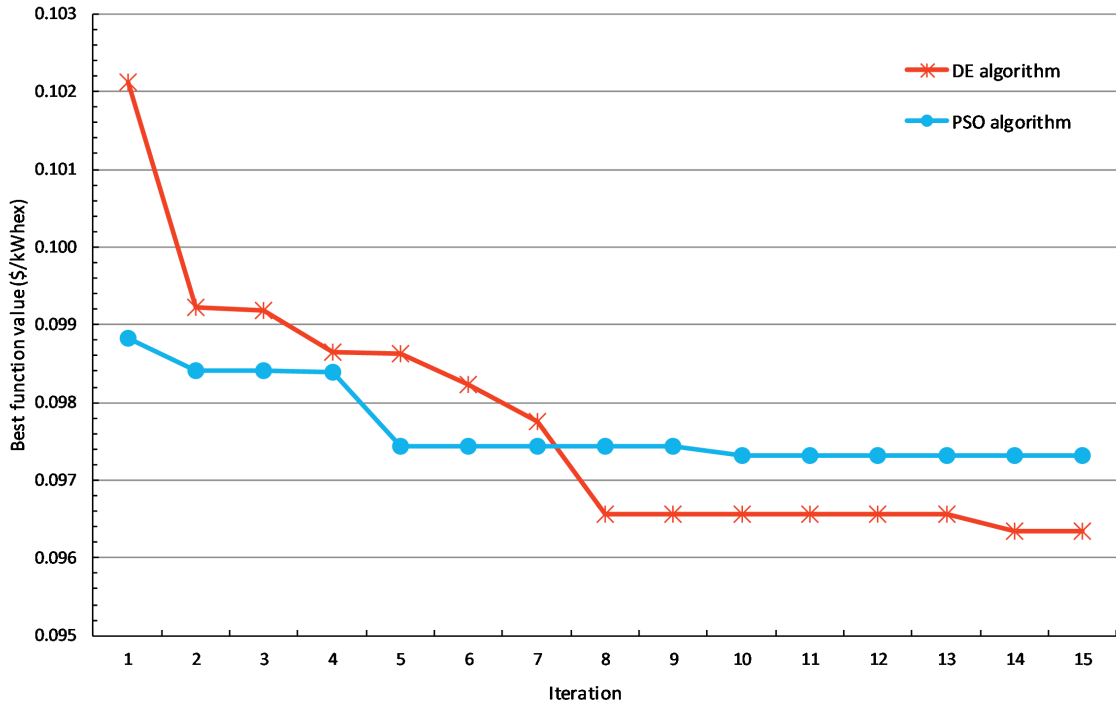
Figure 6.9: Comparing best function values obtained in the optimization process by implementing the DE and PSO algorithms for the cold climate case (Case$_{\text{cold climate}}$).

In summary, both algorithms work appropriately for the optimization problem in this study, and their optimization results are generally consistent. Compared to the DE algorithm, the PSO algorithm takes less time to execute the optimization process but more efforts into tuning parameters. Moreover, it reveals some difficulties for coping with the heat exchangers, and one can not conclude which algorithm has a better performance. The biggest hurdle for implementing these stochastic algorithms is that no global optimal results can be guaranteed.

Thus, a lot of efforts are needed for tuning the parameters to "help" algorithms overcoming local minima and achieving better and more accurate results.

6.3.1.2 Multi-objective optimization

In the single-objective optimization, only the lowest average product cost of the overall system is targeted. However, in general, decision-makers need to take into more than one consideration to make optimal decisions. In this section, the multi-objective optimization results are presented, which involves two objectives, minimizing the average product cost and maximizing the system efficiency. The multi-objective optimization problem is formulated, as shown in Eq. 6.10. The same decision variables and design constraints are selected as those in the single-objective optimization problem.

$$min\ c_{\mathrm{P,total}}^{\mathrm{av.}}\ \text{and}\ max\ \varepsilon_{\mathrm{total}}$$

$$\text{subject to} \begin{cases} 5\,^{\circ}\mathrm{C} \leq \Delta T_{\mathrm{pinch,HE}} \leq 40\,^{\circ}\mathrm{C} \\ 70\% \leq \eta_{\mathrm{isen,EX}} \leq 98\% \\ 1\,^{\circ}\mathrm{C} \leq \Delta T_{\mathrm{pinch,Cooler}} \leq 10\,^{\circ}\mathrm{C} \\ 70\% \leq \eta_{\mathrm{isen,CM\text{-}P}} \leq 95\% \\ 1\,^{\circ}\mathrm{C} \leq \Delta T_{\mathrm{pinch,EVAP}} \leq 10\,^{\circ}\mathrm{C} \\ 70\% \leq \eta_{\mathrm{isen,CM\text{-}R}} \leq 95\% \\ 75\,\mathrm{bar} \leq p_{\mathrm{Merging}} \leq 90\,\mathrm{bar} \\ TIP_{\mathrm{max}} = 250\,\mathrm{bar} \\ PR_{\mathrm{min}} = 1.5 \\ T_{\mathrm{in,CM\text{-}P,min}} = 32\,^{\circ}\mathrm{C} \end{cases} \quad (6.10)$$

The non-dominated sorting genetic algorithm-II (NSGA-II) [125] is implemented as it is one of the most popular algorithms for solving multi-objective optimization problems [102, 126]. The final solutions presented as a non-dominated set, which is also called as Pareto front, demonstrate the optimization results where no other better solution exists that outperforms it in terms of both objective functions [126].

The scattered distributions of Pareto frontiers for the hot climate and cold climate cases are illustrated in Fig. 6.10. It is clear that for each case, there is no absolute optimal solution, which yields the highest system efficiency and the lowest product cost. Once the system efficiency increases, the average product cost inevitably rises simultaneously as a penalty. The decision-makers, therefore, have to determine the system operating conditions according to their subjective preferences. Comparing the Pareto frontiers of the proposed polygeneration system in $\mathrm{Case_{hot\ climate}}$ and $\mathrm{Case_{cold\ climate}}$, one can notice that the system exergetic efficiency in the $\mathrm{Case_{cold\ climate}}$ reveals an increase of more than 25% than that in the $\mathrm{Case_{hot\ climate}}$; the lowest obtained average product cost in the $\mathrm{Case_{cold\ climate}}$ is less than 0.1 \$/kWhex, while the average product cost per unit of exergy in the $\mathrm{Case_{hot\ climate}}$ ranges from 0.14 \$/kWhex to 0.18 \$/kWhex. However, in the $\mathrm{Case_{hot\ climate}}$, there is a relatively extensive flat area, which indicates an insignificant rise in the average product cost with improving the system efficiency. In contrast, such a flat area in the $\mathrm{Case_{cold\ climate}}$ is rather limited.
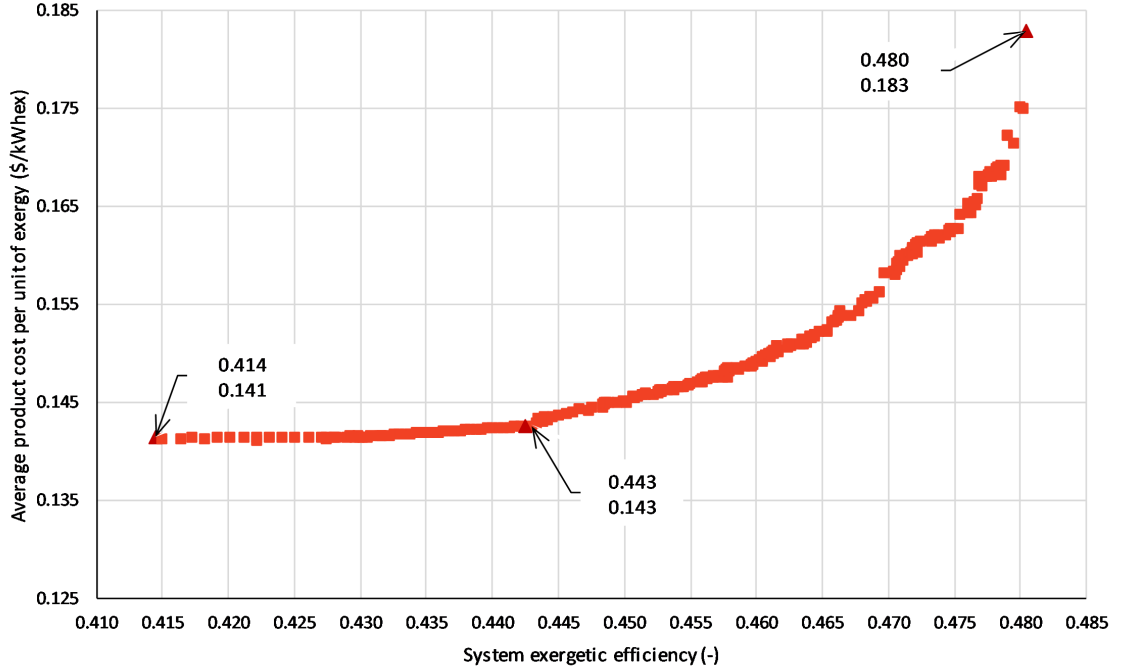
(a) Hot climate case ($\text{Case}_{\text{hot climate}}$)
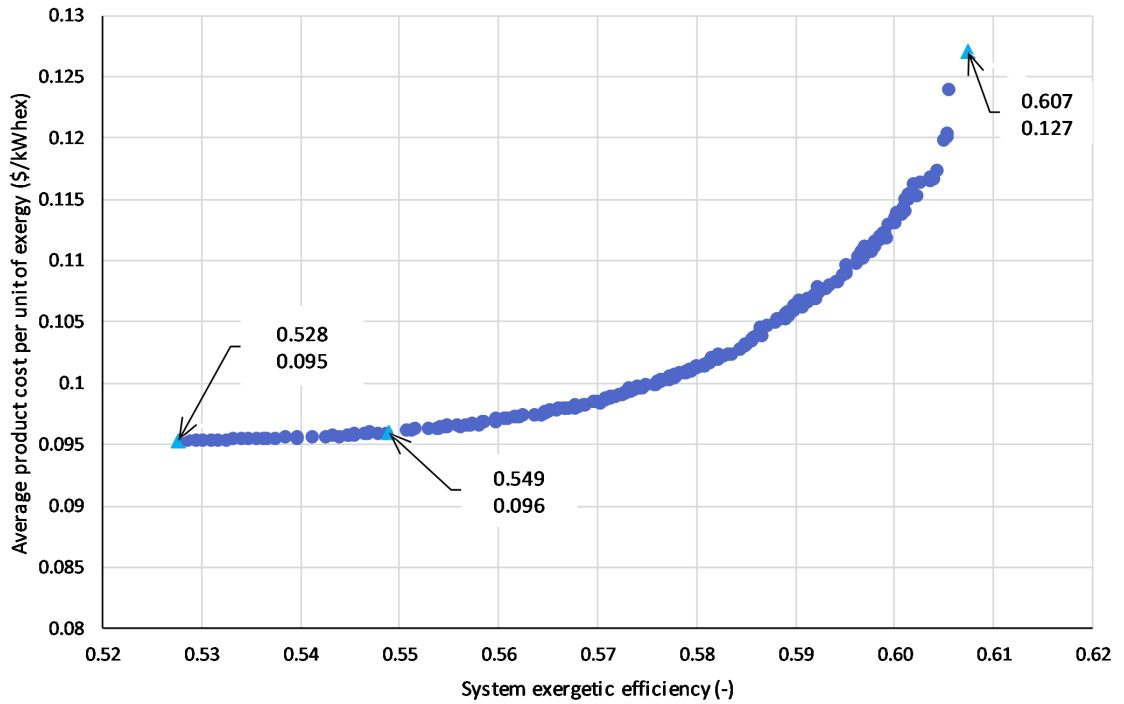
(b) Cold climate case ($\text{Case}_{\text{cold climate}}$)

Figure 6.10: The Pareto frontiers of the overall system considering system exergetic efficiency and average product cost per unit of exergy for cases in hot and cold climates.

6.3.2 Structural optimization

This section performs a structural optimization of the proposed polygeneration system. Both the system topology and decision parameters can be optimized simultaneously by applying the superstructure-based technique. Several promising structural designs regarding S-CO$_2$

power and refrigeration cycles are categorized and integrated into one comprehensive system topology design. DE algorithm is implemented to search for the optimal cycle configuration by minimizing the average product cost per unit of exergy of the overall system. The natural gas engine is still out of consideration in this optimization phase.

6.3.2.1 Superstructure modelling

Compared to the parameter optimization, Aspen HYSYS®, in a superstructure optimization process, is used for not only simulating and returning the simulation results to Python but also examining the feasibility of new cycle designs. Hence, the robustness of the design in Aspen HYSYS® determines the execution of the superstructure optimization. If the simulation is designed to be error-prone, then either no results or the results with errors will be reported; for the optimization process, obtaining inaccurate returned data "misleads" the algorithm and results in unexpected interruptions and disturbances. Therefore, it is noteworthy to detail first the approaches for designing a complex yet robust simulation representing the integrated-topology in Aspen HYSYS®.

In contrast to modeling a system in programming-based software, adding/deleting components in Aspen HYSYS®, being designed as a graphical user interface (GUI), can not be easily carried out in the automation process. Although it is possible to add/delete a specific component in Aspen HYSYS® by executing codes in Python, its associated material and energy streams need to be handled appropriately as well for ensuring the simulation completion. It is generally not practical to alter the simulation by adding/deleting several components and their associated streams in structural optimization. It dramatically increases the complexity of solving such an optimization problem and results in a considerably longer computation time.

For overcoming this hurdle, the other approach is embedding all possible system structures into one complex topology and modeling this topology in Aspen HYSYS®. By applying this method, system structure modification by automation during the superstructure optimization process is not required. However, as a penalty, designing bypasses by adding more splitters and mixers is necessary. In Fig. 6.11, an example of the bypass design is illustrated. There are two options for stream 1: passing the bypass route or going through the heat exchanger. The heat exchanger represents the alternative options, which are randomly selected by the optimization algorithm and may result in better system performance.
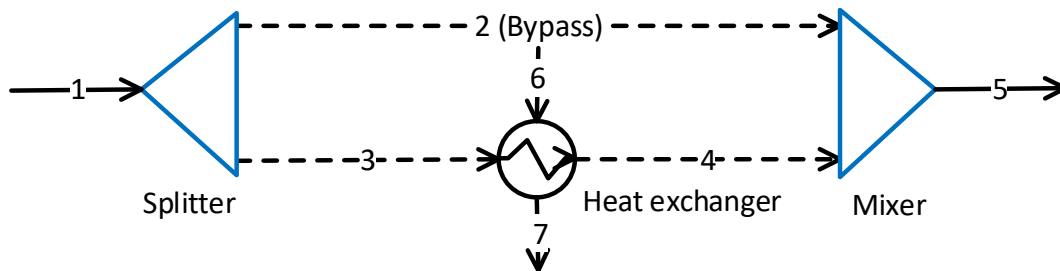
Figure 6.11: Example of bypass design in Aspen HYSYS® for modelling a superstructure topology by adding splitters and mixers.

Theoretically, the splitter should function as a switch, which controls where streams 1 should flow. For example, by setting the split ratio of mass flow rate as 1 and 0, respectively, for stream 2 and stream 3, the mass flow rate of stream 2 equals the mass flow rate of stream 1, which indicates the bypass route is selected. However, in practice, such modeling leads to an error-prone simulation if the splitter is executed as a switch in Aspen HYSYS®. Because the mass flow rate of stream 3, in this case, is zero, and for the heat exchanger, its energy balance is unsolvable. The energy balance of the heat exchanger is expressed as:

$$\dot{m}_3 \times h_3 - \dot{m}_4 \times h_4 = \dot{m}_7 \times h_7 - \dot{m}_6 \times h_6 \tag{6.11}$$

where according to mass balances, $\dot{m}_3 = \dot{m}_4 = 0$ kg/s and $\dot{m}_6 = \dot{m}_7$.

Then the energy balance can be rewritten as:

$$0 \times (h_3 - h_4) = \dot{m}_6 \times (h_7 - h_6) \tag{6.12}$$

With this equation, since h_3 is known via the splitter, h_4 is unsolvable and can be any value regardless of the heat exchanger's assumptions and the associated other streams (stream 6 and 7). Therefore, a typical error occurs in Aspen HYSYS®, reporting the heat exchanger can not be solved. By the nature of Aspen HYSYS®, being a sequential modeling solver, all calculations regarding following streams and components after the heat exchanger are brutally interrupted (shown in Fig. 6.12).
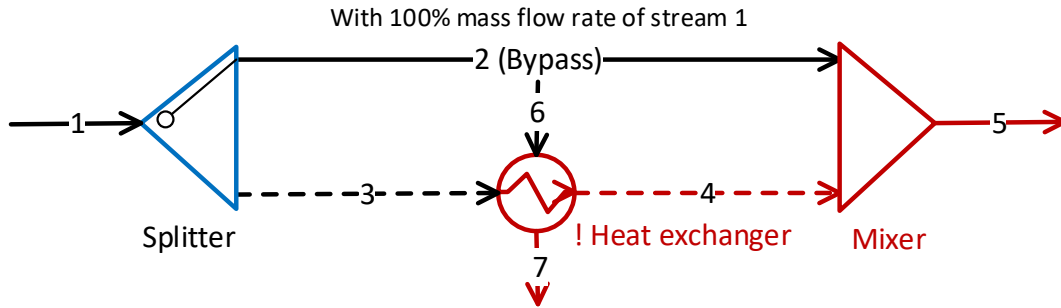
Figure 6.12: Example of a typical error in bypass design in Aspen HYSYS® for modelling a superstructure topology.

To design a robuster simulation, the following adjustments can be implemented for designing splitters to avoid zero mass flow rate:

$$\text{Split ratio in splitter } (\dot{m}_{\text{route}}/\dot{m}_{\text{total}}) = \begin{cases} 0.9999, & \text{if this route is selected.} \\ 0.0001, & \text{if this route is not selected.} \end{cases}$$

If there are splitters in the simulation, splitting a stream into more than two streams, the split ratio in these splitters should be modified as:

$$\text{Split ratio in splitter } (\dot{m}_{\text{route}}/\dot{m}_{\text{total}}) = \begin{cases} 0.9999, & \text{if this route is selected.} \\ 0.0001/n, & \text{for those } n \text{ routes are not selected.} \end{cases}$$

where $n + 1$ depicts the number of streams after the splitter.

Apparently, in contrast to functioning the splitter as a switch, this approach causes a slight inaccuracy in the calculations. A tiny portion of the working fluid passes the unwanted route(s). In this case, the results obtained from the stream(s), passing through the unwanted route(s), are inevitably merged with the desired results via the mixer, resulting in disturbances in the final result. Nevertheless, the disturbances are trivial, while the robustness of the simulation is improved significantly.

For avoiding the typical errors and disturbances in the bypass design in Aspen HYSYS® for modeling a superstructure topology, a subtle yet straightforward approach is depicted in Fig. 6.13. One can notice that there is no splitter, bypass, nor mixer in this simplified design. If the route with the heat exchanger is selected, no modification is needed. If the bypass route is selected, an additional specification, $\dot{Q}_{\text{heat exchanger}} = 0$ kW, is required. Once one more specification is added, one of the pre-defined specifications within the heat exchanger needs to be deactivated to keep its degree of freedom being zero. Stream 5, in this case, has the same parameters as those associated with stream 1, while no errors, which stop the simulation, nor disturbances, which cause inaccuracy in simulation results, will be confronted.
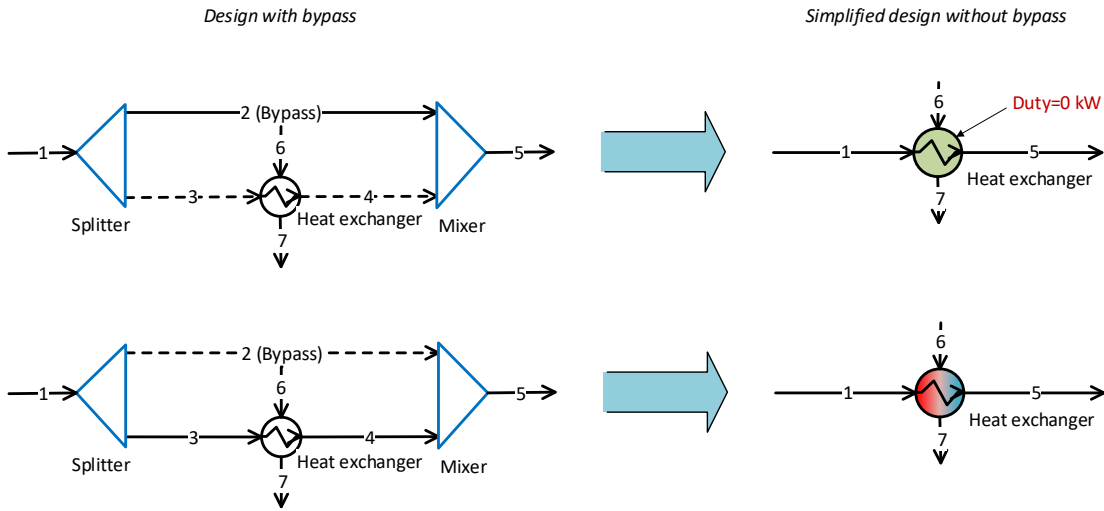
Figure 6.13: A simplified design without bypass in Aspen HYSYS® for modelling a superstructure topology.

Therefore, in this work, the simplified design without a bypass is applied to ensure the modeling robustness in Aspen HYSYS® and reduce the computation time of the structural optimization. By implementing this simplified design, one thing that needs to be noticed is that the heat exchanger's cost should not be included in the economic analysis if the bypass route is selected. Moreover, this design is not only suitable for heat exchangers (here as an example used in this section); for other components, the same strategy can be applied similarly.

6.3.2.2 Superstructure design

Since the proposed polygeneration system is composed of two sub-systems, namely, a closed S-CO$_2$ power system and a T-CO$_2$ refrigeration system, the superstructure design of the proposed polygeneration system needs to consider new structures regarding both the power and the refrigeration systems.

According to Ref. [37], which reviewed recent publications with respect to the S-CO$_2$ power system, new cycle proposals are of great interest in the scientific community; the authors categorized these new cycle proposals into more than 25 categorizations. It is nearly impossible to integrate all these proposals into one superstructure design. Moreover, for a given application scenario, only a few proposals can be considered to be appropriate.

Compared to the number of new cycles proposed in publications regarding the S-CO$_2$ power system, for the T-CO$_2$ refrigeration system, only a few new configurations were investigated. The main reason behind that is that power systems are, generally, much bigger in terms of system capacity and size than refrigeration systems; system optimization, including structure optimization, plays a vital role in power system design. For refrigeration systems, complex configurations are not preferred most of the time, and these configurations may result in economic penalties, although they can probably increase the system efficiency.

In this work, the principle applied to design the superstructure is to keep the proposed polygeneration system simple due to its small capacity. On this principle, some promising but complicated power system designs, e.g., double recompression, cascade, and quasi combined designs, are not included. For the structure design of the T-CO$_2$ refrigeration system, the idea of using an expander instead of a throttling valve is not adopted due to its low efficiency and high cost. In addition, T-CO$_2$ refrigeration cycles with ejector devices [127, 128, 129] are not taken into consideration for the superstructure design, as these new layouts, being under development [83], require high initial investments [130] and can be operated in limited conditions [131].

In Fig. 6.14, the superstructure design of the proposed polygeneration system is illustrated. The topology is designed by integrating different design features of S-CO$_2$ power systems and T-CO$_2$ refrigeration systems. Switch (SW) 1-10 are used for randomly combining these design features. Except for SW-6 and SW-9, which are ternary switches, other switches are binary with design options: 0 and 1. Some design features are controlled only by one of the switches; other features, however, can be selected only if two or even three switches happen to choose certain combinations. The following sections will detail these design features in the S-CO$_2$ power system and the T-CO$_2$ refrigeration system, respectively.
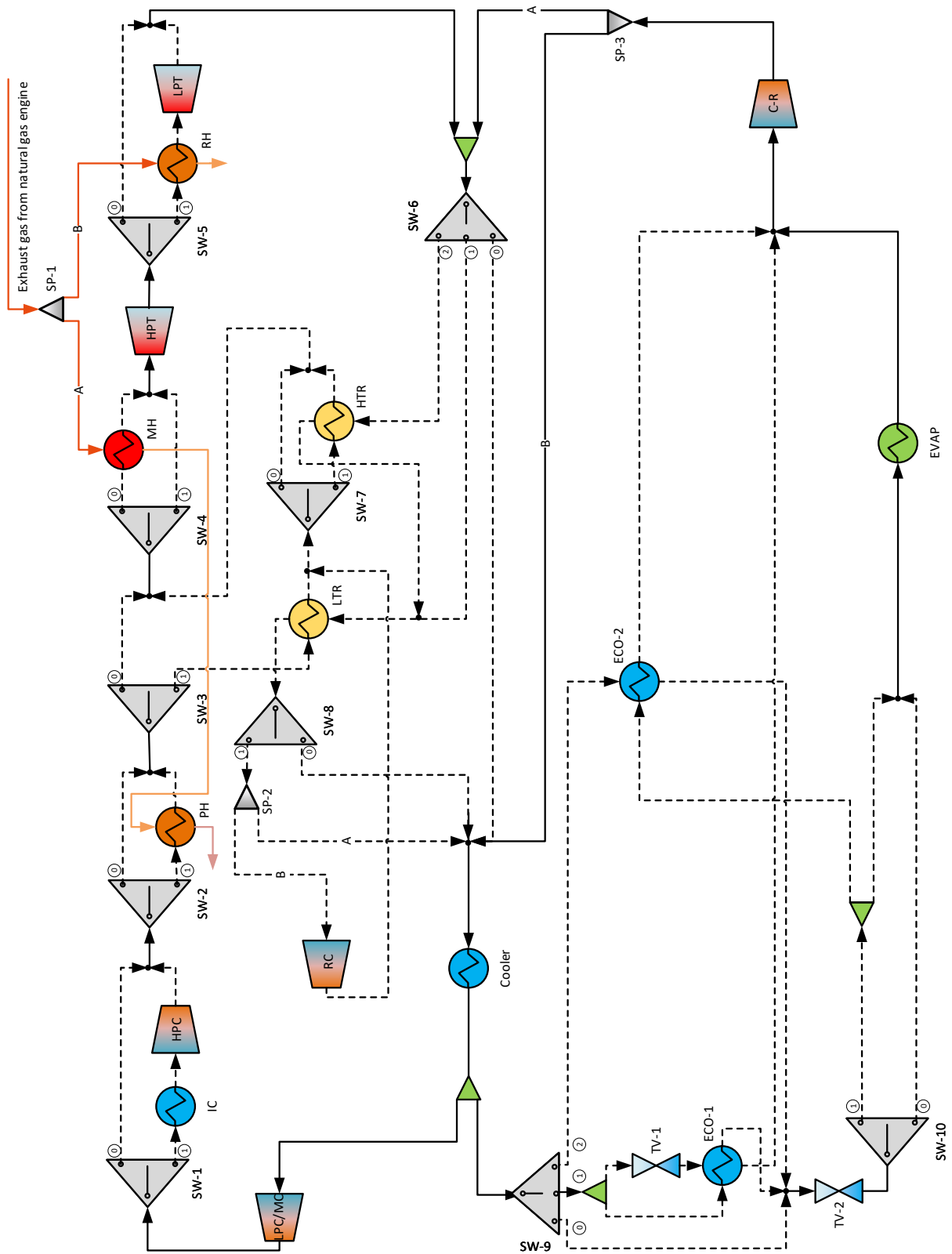
Figure 6.14: Superstructure design for the proposed polygeneration system.

a) *Design features considered in the S-CO₂ power system*

- Intercooling: intercooling is a traditional way to improve power system efficiency by reducing the compressor power consumption; an intercooler (IC) is required between compressors. SW-1 offers the option to include an IC and a high-pressure compressor (HPC) into the new system structure after a low-pressure compressor (LPC) (details given in Table 6.17).

Table 6.17: Corresponding switch states of intercooling.

Design feature	Intercooling
Corresponding component(s)	IC and HPC
Controlling switch(es)	SW-1
Switch state(s)	SW-1=1

- Preheating: further utilizing the waste heat after the main heater (MH) for preheating the working fluid shows the potential to improve system efficiency and recover more heat from a given heat source. It is especially beneficial if the power system is designed with recuperators. With recuperators, the stream entering the MH has a relatively higher temperature, and the heat source stream exiting the MH contains more energy than that in a power cycle without recuperators. A preheater (PH), hence, is designed to fully utilize the waste heat from the exhaust gas of the natural gas engine, and its controlling switch, as well as the corresponding switch state, is tabulated in Table 6.18.

Table 6.18: Corresponding switch states of preheating.

Design feature	Preheating
Corresponding component(s)	PH
Controlling switch(es)	SW-2
Switch state(s)	SW-2=1

- Recuperation: several S-CO₂ recuperated power cycles (e.g., in Refs [132, 133, 134]) were proposed in different applications. The recuperation feature improves the thermal efficiencies of CO₂-based power systems. In this work, a low-temperature recuperator (LTR) and a high-temperature recuperator (HTR) are included in the superstructure design. The states of SW-3, SW-6, and SW-7 determine whether the recuperation feature

and how many recuperators will be adopted. Table 6.19 details the corresponding switch states of the recuperation feature.

Table 6.19: Corresponding switch states of recuperation.

Design feature	Recuperation
Corresponding component(s)	LTR and HTR
Controlling switch(es)	SW-3, SW-6, and SW-7
Switch state(s)	Only LTR: SW-3=1, SW-6=1, and SW-7=0 LTR and HTR: SW-3=1, SW-6=2, and SW-7=1

- Reheating: by introducing the reheating feature, a twofold cycle performance improvement can be expected [37]: increasing the expansion work and reducing the thermal stresses at the turbine inlet. A reheater (RH) is, hence, applied between a high-pressure turbine (HPT) and a low-pressure turbine (LPT). The random number selected by the algorithm for SW-5 decides the adoption of reheating, as presented in Table 6.20.

Table 6.20: Corresponding switch states of reheating.

Design feature	Reheating
Corresponding component(s)	RH and LPT
Controlling switch(es)	SW-5
Switch state(s)	SW-5=1

- Split-expansion: the split-expansion cycle [135, 136, 21] contains design features of recuperation and reheating. The layout of the split-expansion cycle is simple, and this cycle has the strength of increasing expansion work. In this cycle, the working fluid exiting from the recuperators flows directly into the HPT, without going through the MH. The stream is then reheated by adding external heat and flows into the LPT. Therefore, SW-4 is designed to bypass the MH and allow the working fluid to be expanded right after the recuperation process(es). Table 6.21 tabulates the switch states of selecting the split-expansion cycle.

Table 6.21: Corresponding switch states of split-expansion.

Design feature	Split-expansion
Corresponding component(s)	LTR, HTR, RH and LPT
Controlling switch(es)	SW-3, SW-4, SW-5, SW-6 and SW-7
Switch state(s)	SW-3=1, SW-4=1, SW-5=1 Only LTR: SW-6=1, and SW-7=0 LTR and HTR: SW-6=2, and SW-7=1

- Recompression: as a design feature derived from the S-CO_2 recompression cycle, being an evolution of the previous work from Angelino and Feher [42, 41, 45], a re-compressor (RC) is located in parallel to the main compressor (MC). In this work, the LPC can be also named as the MC, once the RC is selected. The working fluid is split into two before the compression process, and these two split streams enter the MC and the RC, respectively. The binary selection of SW-8 and the split ratio within the second splitter (SP-2) have a joint effect on the recompression feature (detailed in Table 6.22).

Table 6.22: Corresponding switch states of recompression.

Design feature	Recompression
Corresponding component(s)	RC
Controlling switch(es)	SW-8
Switch state(s)	SW-8=1

b) *Design features considered in the T-CO_2 refrigeration system*

An internal heat exchanger, i.e., a recuperator, has been proved that it has only a very small effect on the *COP* of the T-CO_2 refrigeration system [86]. In Ref. [113], two new structures for improving the system efficiency of the T-CO_2 refrigeration machine are proposed by introducing an economizer (ECO). Since the idea of using an economizer is well-known and widely applied to multi-stage T-CO_2 refrigeration systems, in this work, two options of applying an economizer are implemented in the structure design. Table 6.23 shows that the adoption of the ECO-1 is determined only by SW-9, while the ECO-2 is selected by the switch states of SW-9 and SW-10.

Table 6.23: Corresponding switch states of economizers.

Design feature	Economizers
Corresponding component(s)	Option 1: TV-1 and ECO-1
	Option 2: ECO-2
Controlling switch(es)	Option 1: SW-9
	Option 2: SW-9 and SW-10
Switch state(s)	Option 1: SW-9=1
	Option 2: SW-9=2 and SW-10=1

6.3.2.3 Superstructure optimization implementation

In the superstructure optimization problem, the states of the discrete switches and several continuous decision variables need to be optimized simultaneously. In contrast to other optimization problems in the sections mentioned earlier, Aspen HYSYS® needs to prove the feasibility of new integrated system designs. To reduce the computation time of this structural optimization, certain switch states combinations, which integrate some of the design features and result in implausible structures, are pre-excluded in Python to prevent feeding them into Aspen HYSYS®. This approach has the advantages of shortening the optimization time and maintaining the robustness of the simulation. Because Aspen HYSYS® is a sequential-modeling software, and the results from the previous simulation are applied as the starting point to solve the current simulation problem, it is essential to rule out the error-prone simulations as many as possible.

The optimization model, including the optimization objective and decision variables, and the implemented optimization algorithm, will be discussed thoroughly in the following sections.

- *Optimization model*

The structural optimization problem is, generally, expressed as:

$$min\ c_{\text{P,total}}^{\text{av.}}$$

$$\text{subject to} \begin{cases} h(\overrightarrow{SW}, \overrightarrow{Var}) = 0 \\ g(\overrightarrow{SW}, \overrightarrow{Var}) \leq 0 \\ \overrightarrow{SW} \in Z^{\text{n}} \\ \overrightarrow{Var} \in R^{\text{n}} \end{cases} \tag{6.13}$$

where Z^{n} is the set of integers; R^{n} is the set of real numbers; $\overrightarrow{SW} = [SW\text{-}1, SW\text{-}2, SW\text{-}3, SW\text{-}4, SW\text{-}5, SW\text{-}6, SW\text{-}7, SW\text{-}8, SW\text{-}9, SW\text{-}10]$; $\overrightarrow{Var} = [PR_{\text{C}}, p_{\text{Merging}}, SR_{\text{SP-1}}, SR_{\text{SP-2}}, SR_{\text{SP-3}}]$.

The fulfilment of the optimization constraints, namely, functions of equalities and inequalities ($h(\overrightarrow{SW}, \overrightarrow{Var})$, $g(\overrightarrow{SW}, \overrightarrow{Var})$), is carried out in Aspen HYSYS®. If the input values of $\overrightarrow{SW}$ and $\overrightarrow{Var}$ can not meet the constraints, a number (e.g., 100 in this work), indicating

unmet constraints, is returned. Only the feasible and plausible system designs with constraint fulfilment are considered in the optimization process.

The items in the $\overrightarrow{Var}$ and in $g(\overrightarrow{SW}, \overrightarrow{Var})$ are specified in Table 6.24 and Table 6.25, respectively. The decision variables are the continuous parameters that need to be optimized beside the switches. $PR_{\text{C,power}}$ stands for the pressure ratio of compressors in the power cycle. In contrast, the pressure ratio of the compressor in the refrigeration cycle is not considered since its inlet and outlet pressures are determined, respectively, by the evaporation temperature and the merging pressure. $SR_{\text{SP-1}}$ determines the amount of the exhaust gas from the natural gas engine entering the MH, while $SR_{\text{SP-2}}$ decides the mass flow rate flowing into the MC. $SR_{\text{SP-3}}$ offers the choices of mixing the CO_2 from the refrigeration cycle after the compression process before and after the recuperators. The design constraints ensure the power cycle is operated in the supercritical region, and sufficient power can be supplied to the refrigeration cycle.

Table 6.24: Decision variables of the superstructure optimization.

Variable	Definition	Unit	Range
$PR_{\text{C,power}}$	$PR_{\text{C,power}} = p_{\text{out,C,power}}/p_{\text{in,C,power}}$	(-)	1.5–4
p_{Merging}	-	(bar)	75–90
$SR_{\text{SP-1}}$	$SR_{\text{SP-1}} = \dot{m}_{\text{A,SP-1}}/\dot{m}_{\text{A+B,SP-1}}$	(-)	0.5–1
$SR_{\text{SP-2}}$	$SR_{\text{SP-2}} = \dot{m}_{\text{A,SP-2}}/\dot{m}_{\text{A+B,SP-2}}$	(-)	0.5–1
$SR_{\text{SP-3}}$	$SR_{\text{SP-3}} = \dot{m}_{\text{A,SP-3}}/\dot{m}_{\text{A+B,SP-3}}$	(-)	0–1

Table 6.25: Design constraints of the superstructure optimization.

Variable	Unit	Limit
TIP_{max}	(bar)	250
$T_{\text{out,Cooler,min}}$	(°C)	32
$\dot{W}_{\text{net,min}}$	(kW)	0

- *Optimization methods*

The structural optimization problem is a mixed-integer nonlinear programming (MINLP) problem, having the discrete switches and continuous decision variables. Traditional optimization algorithms are, sometimes, not sufficient to tackle such a MINLP problem, and deterministic optimization algorithms can not be applied in this work due to the unknown mathematical modelings. Because the simulations solved by Aspen HYSYS® are considered

as black boxes. The stochastic optimization algorithms (DE and PSO), applied successfully in aforementioned single-objective and multi-objective optimization problems, are also able to solve this MINLP problem by "smartly" escaping from the local optima and efficiently finding satisfactorily good solutions. In contrast to the solutions obtained from deterministic algorithms, the solutions found by stochastic optimization algorithms can be near-optimal, but optimality can not always be guaranteed. However, no derivative information is required in these derivative-free stochastic algorithms, which is practical and easier to be implemented.

In this work, the DE-based algorithm is applied to solve the structural optimization problem. The main settings of implementing this algorithm were tuned by conducting several trial and error tests to ensure the good solutions can be satisfactory, and the optimization problem can be solved in an acceptable computation time. In Table 6.26, the main parameters selected for the DE algorithm, obtained from the trial and error tests, are listed.

Table 6.26: Main settings for the DE algorithm applied in superstructure optimization.

Item	Value/Requirement
Population size	$15 \times$ number of optimization parameters ($15 \times 14 = 210$)
Mutation constant	Shrinking from 1 to 0.3
Crossover constant	0.7
Convergence criterion	σ (population) $\leq 0.01 \times |\mu$ (population)$|$
Max iteration	100

Fig. 6.15 summarizes the key steps of implementing the DE algorithm to solve the superstructure optimization problem. The correlation between the simulation software (Aspen HYSYS®) and the programming software (Python) is addressed. Python executes the DE algorithm and pre-excludes the implausible input combinations, while Aspen HYSYS® is used for checking the system feasibility and returning the simulation results. Once the termination criterion is met, or the maximal iteration is reached, the optimization process terminates.
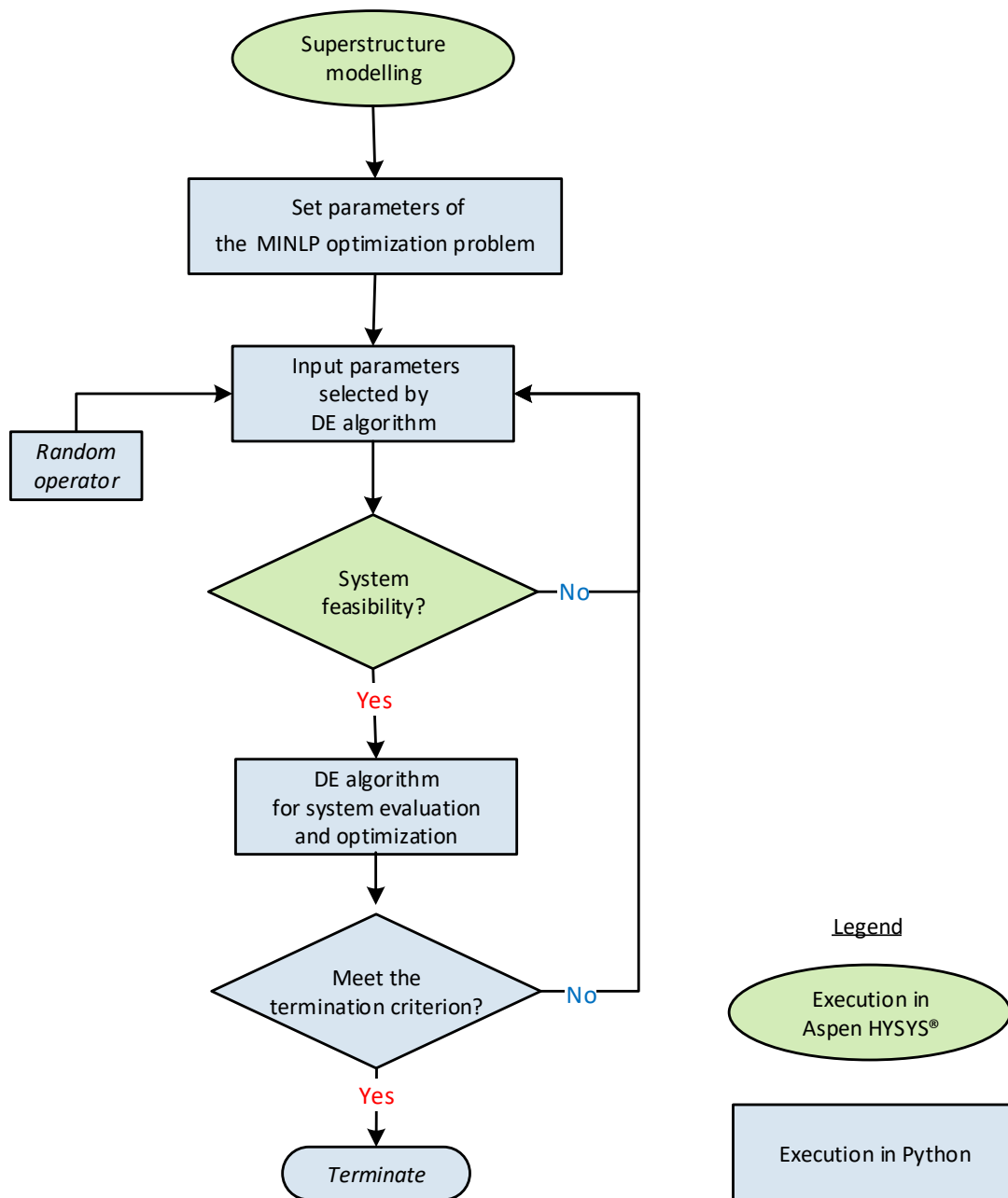
Figure 6.15: Method of implementing superstructure optimization by executing DE algorithm in Python and simulating new system design in Aspen HYSYS®.

6.3.2.4 Results and discussion

In this section, the superstructure optimization results for two representative cases (Case$_{\text{hot climate}}$ and Case$_{\text{cold climate}}$) are presented and discussed. For the Case$_{\text{hot climate}}$, its structural optimization results are listed in Table 6.27 and illustrated in Fig. 6.16. The state of the SW-2 indicates that a PH is preferred; according to the switch states of SW-3 and SW-6, one recuperator should be added in the power cycle, while the simplest configuration is selected for the refrigeration system. It is clear that by adding the LTR and the PH, the power system efficiency increases, and the waste heat, contained by the exhaust gas from the

natural gas engine, is utilized more thoroughly. Note that in the Case$_{\text{hot climate}}$, the overall system's final products are only the electric power and the refrigeration capacity. Since the heating capacity, being available in Cooler, is not included in the final system products, it is reasonable to transfer the heat from the outlet stream after the expansion process to the inlet stream of the compressor by integrating the recuperation feature in the power cycle. Thanks to the recuperation design feature, more electricity, in this case, can be generated, while the available but unused heating capacity is reduced.

Table 6.27: Superstructure optimization results for the Case$_{\text{hot climate}}$.

Optimal switch states					
Item	State	Unit	Item	State	Unit
SW-1	0	(-)	SW-2	1	(-)
SW-3	1	(-)	SW-4	0	(-)
SW-5	0	(-)	SW-6	1	(-)
SW-7	0	(-)	SW-8	0	(-)
SW-9	0	(-)	SW-10	0	(-)
Optimal decision variables					
Variable	Value	Unit	Variable	Value	Unit
$PR_{\text{LPC/MC}}$	2.9	(-)	p_{Merging}	87	(bar)
$SR_{\text{SP-1}}$	1	(-)	$SR_{\text{SP-2}}$	-	(-)
$SR_{\text{SP-3}}$	0	(-)			
Superstructure optimization results					
Objective	Unit	Initial value		Optimal value	
$c_{\text{P,total}}^{\text{av.}}$	($/GJex)	53.26		42.36	
Runtime	(min)	-		575	

In addition, the outlet stream of the C-R flows all to the merging point after the recuperation process. In other words, the split ratio within the SP-3, deciding where and how two sub-systems are merged, suggests a new merging point. In the initial structure design, the mixer's exergy destruction is noticeable due to the massive temperature difference between the outlet streams after the expansion process and the compression process in the power and refrigeration cycles, respectively. The new merging point after the LTR shrinks the temperature difference within the mixer since a lower stream temperature is obtained after the recuperation process.

Figure 6.16: Illustration of the optimized new system design based on superstructure optimization results for the Case_hot climate. Note that the red solid streams depict the selected optimal routes.

For the Case_cold climate, the electric power and the heating capacity are considered the system's final products. In Table 6.28, its optimal switch states, optimal decision variables,

and superstructure optimization results are presented. In Fig. 6.17, the optimized system structure is visualized. The optimal results reveal that the simplest base-case design is the best system configuration in the Case$_\text{cold climate}$. By altering the decision variables, the optimization objective ($c_\text{P,total}^\text{av.}$) is reduced by more than 9%. Also, the execution time of the structural optimization is significantly shorter (more than 45% runtime decrease) for the proposed polygeneration system operating in the cold climate (with the ambient temperature of 5 °C) compared to that in the hot climate (with the ambient temperature of 35 °C). Because the starting point in this optimization process is quite close to the optimal point, which results in a quick convergence.

Table 6.28: Superstructure optimization results for the Case$_\text{cold climate}$.

Optimal switch states					
Item	State	Unit	Item	State	Unit
SW-1	0	(-)	SW-2	0	(-)
SW-3	0	(-)	SW-4	0	(-)
SW-5	0	(-)	SW-6	0	(-)
SW-7	0	(-)	SW-8	0	(-)
SW-9	0	(-)	SW-10	0	(-)
Optimal decision variables					
Variable	Value	Unit	Variable	Value	Unit
$PR_\text{LPC/MC}$	2.7	(-)	p_Merging	82	(bar)
$SR_\text{SP-1}$	1	(-)	$SR_\text{SP-2}$	-	(-)
$SR_\text{SP-3}$	0.69	(-)			
Superstructure optimization results					
Objective	Unit	Initial value		Optimal value	
$c_\text{P,total}^\text{av.}$	($/GJex)	31.39		28.48	
Runtime	(min)	-		391	

The LTR and the PH, which are integrated into the base-case structure design to form the new system structure of the Case$_\text{hot climate}$, are not selected in the Case$_\text{cold climate}$. The design features of recuperation and preheating dramatically improve the power cycle's system performance if merely electric power is generated as the product. Once the heating capacity is also considered one of the system products, the influences of the recuperation and the preheating on the overall system may be ambiguous since increasing the electric power generation can lead to less heating capacity and a higher investment cost.

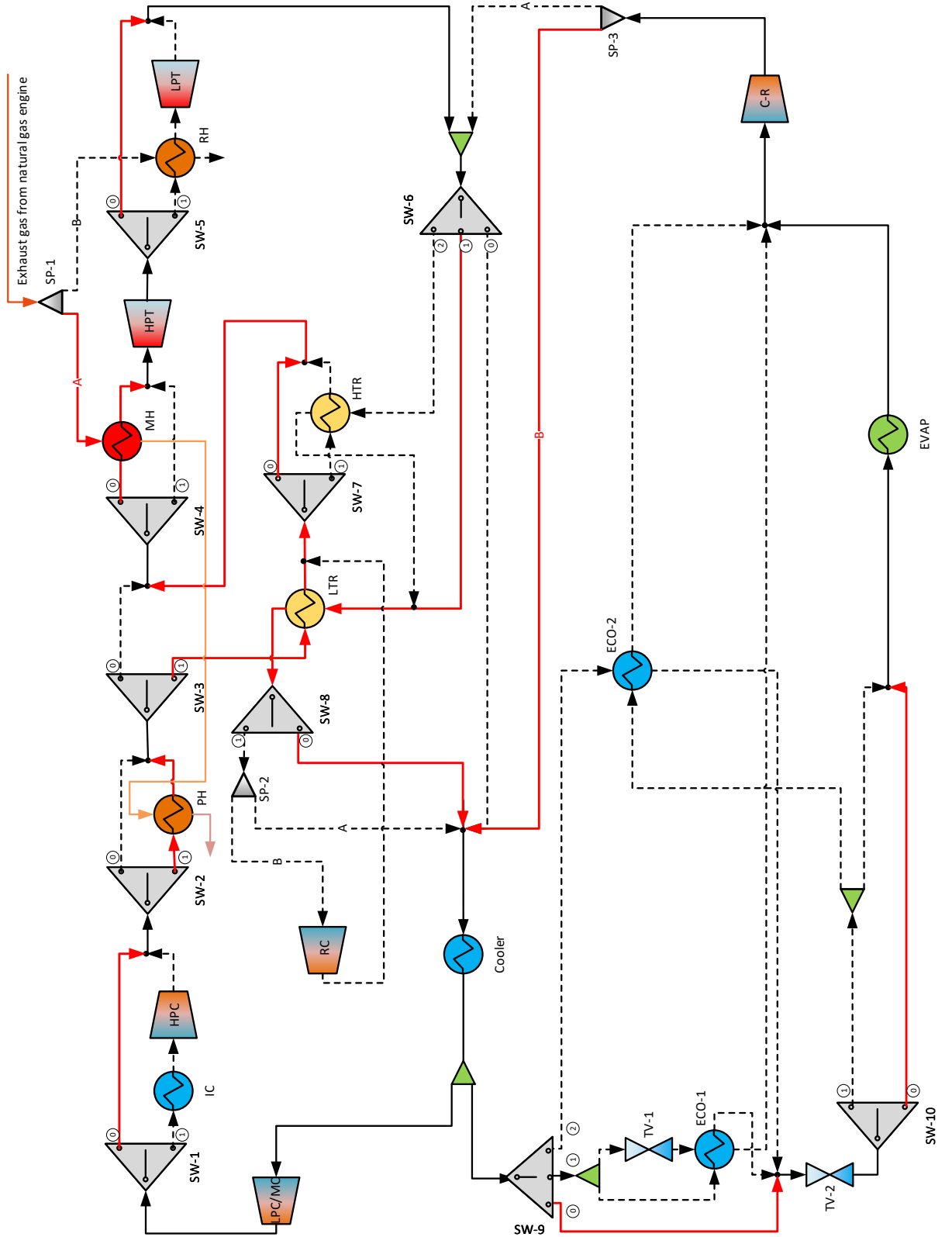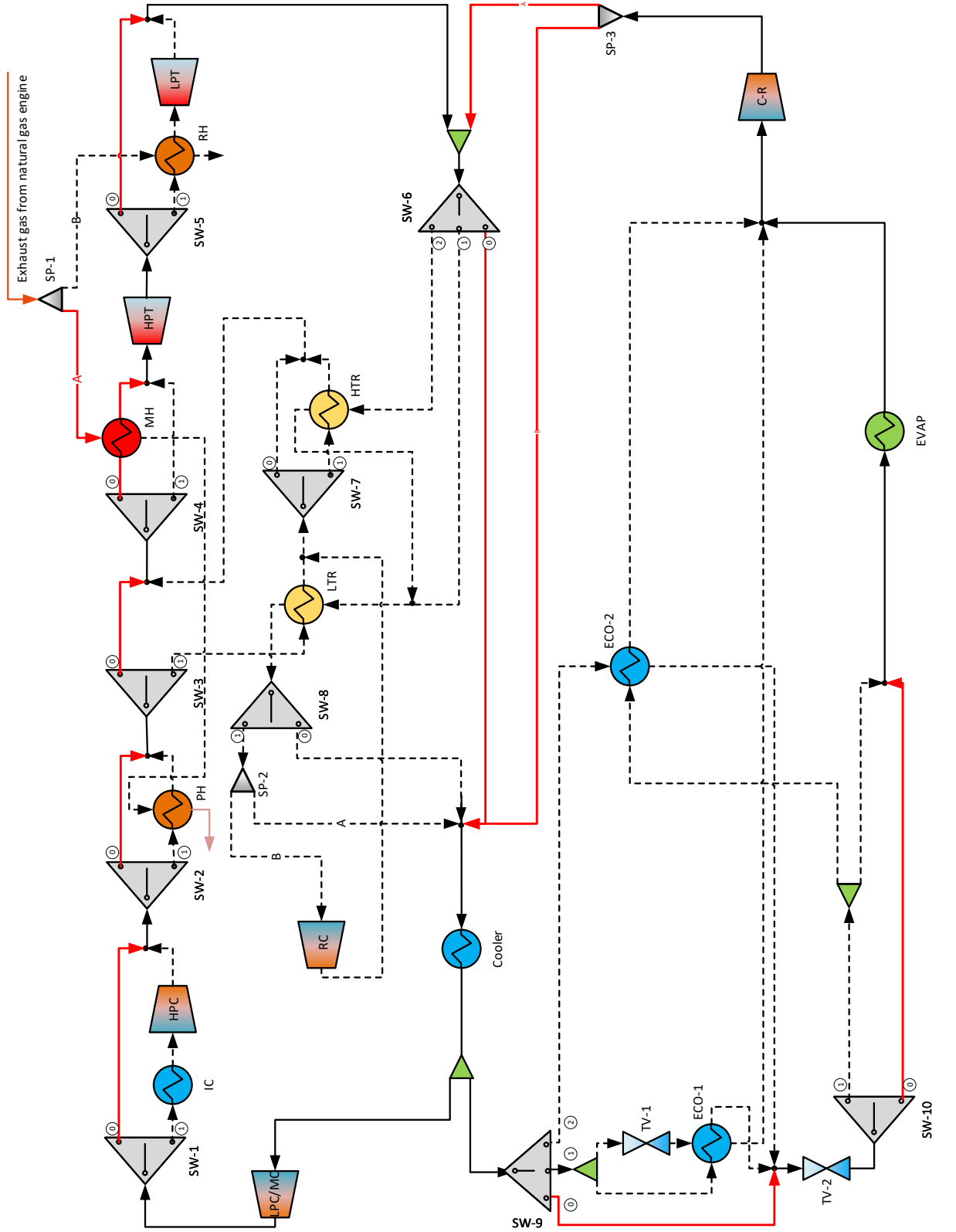**Figure 6.17:** Illustration of the optimized new system design based on superstructure optimization results for the Case$_{\text{cold climate}}$. Note that the red solid streams depict the selected optimal routes.

One can also notice that regardless of the ambient temperature, the optimal system structures of the proposed polygeneration system are simple due to its small capacity. It is

not necessary to design a small-capacity system with a complex structure, which causes a considerably high investment cost, but the increase in the system efficiency is trivial. However, due to the high uncertainty of the component PECs, better system designs can be nominated in the future when the vendor prices are available.

Based on the new configuration of the polygeneration system obtained from the superstructure-based optimization, the results of the energetic and exergetic analyses for the overall system, including the natural gas engine and the polygeneration system, are, respectively, presented in Table 6.29 and Table 6.30. More electric power is produced in the optimal cases, which contributes to a decrease in the overall system's average product cost since the electricity price per unit of exergy is the lowest amongst all the products. Moreover, the optimal results of the $\text{Case}_{\text{hot climate}}$ confirm that less heat capacity is available within the Cooler by adding the design features of recuperation and preheating. In contrast, the optimized $\text{Case}_{\text{cold climate}}$ generates more heat than that in the base-case design. It proves that the DE-based stochastic algorithm is "smart" to find sufficiently good and alternative solutions for different application cases.

Table 6.29: Energetic analysis results for the overall system (including the natural gas engine and the polygeneration system) after superstructure-based optimization.

Case	$\text{Case}_{\text{hot climate}}$		$\text{Case}_{\text{cold climate}}$	
Result	Initial	Optimal	Initial	Optimal
$\dot{Q}_{\text{in,total}}$* (kW)	5000.17	5000.17	5000.17	5000.17
$\dot{W}_{\text{net}}$ (kW)	2204.77	2298.76	2204.77	2225.97
$\dot{Q}_{\text{Cooling}}$ (kW)	100.00	100.00	-	-
$\dot{Q}_{\text{Heating}}$ (kW)	(1470.77)	(1451.62)	1470.77	1526.69
η_{total} (%)	46.09	47.97	73.51	75.05

*: Based on the lower heating value (LHV) of natural gas.

Table 6.30: Exergetic analysis results for the overall system (including the natural gas engine and the polygeneration system) after superstructure-based optimization.

Case	$\text{Case}_{\text{hot climate}}$		$\text{Case}_{\text{cold climate}}$	
Result	Initial	Optimal	Initial	Optimal
$\dot{E}_{\text{F,total}}$ (kW)	5144.97	5144.97	5147.67	5147.67
$\dot{W}_{\text{net}}$ (kW)	2204.77	2298.76	2204.77	2225.97
$\dot{E}_{\text{Cooling}}$ (kW)	6.25	6.26	-	-
$\dot{E}_{\text{Heating}}$ (kW)	(72.69)	(71.74)	183.29	190.25
$\varepsilon_{\text{total}}$ (%)	42.97	44.80	46.39	46.94

In Table 6.31, the product costs within components as well as the final products of the overall system, including the natural gas engine and the polygeneration system, are compared between the base-case design and the structure-optimized design. For the $\text{Case}_{\text{hot climate}}$, the heating price within the Cooler per exergy unit is reduced by more than 20% after the structural optimization. The dramatic decrease in the heating price within the Cooler lowers the cost rate of the exergy losses, which needs to be distributed to the final products of the overall system. Because the heating capacity, in the $\text{Case}_{\text{hot climate}}$, is released into the ambient environment as the waste heat, it is reasonable to design a new configuration aiming at reducing the amount of heat production and the heating price.

For the $\text{Case}_{\text{cold climate}}$, the differences between the initial results of the base-case design and the optimal results of the new system design are relatively inconspicuous. The most significant differences are the prices of the heating capacity per unit of exergy within the Cooler and of the overall system with their reductions of around 6%. Because the base-case system structure is identical to the optimized system structure in the $\text{Case}_{\text{cold climate}}$, only the continuous decision variables are optimized in the optimal case. Without a structure modification in the structural optimization process, the system performance improvement, as expected, is limited.

Table 6.31: Product costs of the overall system (including the natural gas engine and the polygeneration system) after superstructure-based optimization based on the natural gas price in Germany.

Case	$\text{Case}_{\text{hot climate}}$		$\text{Case}_{\text{cold climate}}$	
Result	Initial	Optimal	Initial	Optimal
Product costs within components				
$c_{\text{Electricity,NGE}}$ ($/GJex)	19.41	19.43	18.30	18.20
$c_{\text{Electricity,EX}}$ ($/GJex)	18.59	18.41	17.67	16.74
$c_{\text{Refrigeration,EVAP}}$ ($/GJex)	63.82	61.92	-	-
$c_{\text{Heating,Cooler}}$ ($/GJex)	55.34	43.87	28.54	26.83
Final product costs of the overall system				
$c_{\text{Electricity}}^{\text{av.}}$ ($/GJex)	22.42	21.85	20.08	19.85
$c_{\text{Refrigeration}}$ ($/GJex)	66.91	64.47	-	-
c_{Heating} ($/GJex)	-	-	30.42	28.63
$c_{\text{P,total}}^{\text{av.}}$ ($/GJex)	22.55	21.97	20.88	20.54

The structural optimization is conducted based on the natural gas price in Germany. For showing the influences of the natural gas price on the overall system performance, the product costs within the components and the final products of the overall system applying the natural

gas price in the U.S. are listed in Table 6.32. The same trends can be seen in Table 6.31 and in Table 6.32. By comparing the optimal results applying natural gas prices in the U.S. and Germany, the electricity price and the average product cost of the overall system per unit of exergy are 25% lower if the system is driven by the natural gas with its price in the U.S. regardless of the application scenarios. In the $\text{Case}_{\text{hot climate}}$, the reduction in the refrigeration price of the overall system per exergy unit is only less than 10% by applying the natural gas in the U.S., while the price of the heating capacity in the $\text{Case}_{\text{cold climate}}$ is noticeably decreased from 28.63 $/GJ with German natural gas price to 22.28 $/GJ with U.S. natural gas price.

Table 6.32: Product costs of the overall system (including the natural gas engine and the polygeneration system) after superstructure-based optimization based on the natural gas price in U.S..

Case	$\text{Case}_{\text{hot climate}}$		$\text{Case}_{\text{cold climate}}$	
Result	Initial	Optimal	Initial	Optimal
Product costs within components				
$c_{\text{Electricity,NGE}}$ ($/GJex)	14.19	14.21	13.44	13.33
$c_{\text{Electricity,EX}}$ ($/GJex)	15.12	14.90	14.05	13.56
$c_{\text{Refrigeration,EVAP}}$ ($/GJex)	57.89	56.52	-	-
$c_{\text{Heating,Cooler}}$ ($/GJex)	44.02	36.69	22.39	20.99
Final product costs of the overall system				
$c_{\text{Electricity}}^{\text{av.}}$ ($/GJex)	16.63	16.30	14.83	14.64
$c_{\text{Refrigeration}}$ ($/GJex)	60.24	58.52	-	-
c_{Heating} ($/GJex)	-	-	23.73	22.28
$c_{\text{P,total}}^{\text{av.}}$ ($/GJex)	16.76	16.41	15.52	15.24

6.4 Summary

In this chapter, the proposed polygeneration system, which recovers the waste heat of the exhaust gas from a 2 MW natural gas engine, was analyzed and optimized as a case study. Since the engine waste heat is one of the commonly applied medium-quality heat sources for bottoming cycle applications, the natural gas engine was integrated into the proposed polygeneration system. Ebsilon® Professional software was employed to simulate the 2 MW natural gas engine. The results regarding its exhaust gas were exported and then imported into Aspen HYSYS® for modeling the polygeneration system.

For analyzing and evaluating the system performance, two different system boundaries were considered: including the natural gas engine and excluding the natural gas engine. By considering the natural gas engine as a part of the entire system, the primary system product is the electric power (around 2.2 MW); the refrigeration capacity is 100 kW, while the heating

capacity is approximately 1.5 MW. Three cases with different environmental conditions and application scenarios were carried out in energetic, exergetic, and exergoeconomic analyses. Besides, the natural gas prices in the U.S. and in Germany were applied to compute the final product costs of the overall system.

By excluding the natural gas engine, the detailed component-wise and system-wise exergetic and exergoeconomic analyses were implemented, which aimed at focusing on the performance of the proposed polygeneration system since the results of these analyses are helpful for further optimizing the new system. In this step, only two representative cases among those three cases, including the natural gas engine, were selected and analyzed based on exergy-based methods. For the $\text{Case}_{\text{hot climate}}$, its ambient temperature was assumed as 35 °C, and the system final products comprise of the electric power and the refrigeration capacity. The available heating capacity, in this case, is redundant as the local heat requirement in a hot climate is relatively low. In contrast, the other case, namely, the $\text{Case}_{\text{cold climate}}$, was with an assumption of operating the system in a cold climate with the ambient temperature of 5 °C. The electricity and the heating capacity are the system's final products. Moreover, the advanced exergetic and exergoeconomic analyses were carried out for both cases ($\text{Case}_{\text{hot climate}}$ and $\text{Case}_{\text{cold climate}}$).

In the system optimization, the optimal design of the natural gas engine is out of the research scope in this work; therefore, the parameter optimization and structural optimization were implemented only for the proposed polygeneration system. The polygeneration system was optimized by conducting single-objective and multi-objective optimization by giving the ranges of the decision variables. The optimization results obtained from the DE and PSO algorithms were compared in the single-objective optimization. The implementations of these stochastic algorithms, applied in this energy-related problem, were given in detail. The multi-objective optimization technique, considering both the system exergetic efficiency and the average product cost per unit of exergy, was demonstrated in this work. It revealed that the DE algorithm is able to effectively find the Pareto frontiers of the overall system.

For finding the best configuration of the polygeneration system in this case study, structural optimization was performed. Both the system configuration and the decision variables were optimized simultaneously by applying the DE-based superstructure technique. The superstructure-based topology was designed by integrating several promising design features, including intercooling, preheating, recuperation, reheating, split-expansion, recompression, and introducing economizers. Ten controlling switches were applied to select the best routes, forming the best system configuration, in the superstructure optimization modeling and design. Theoretically, 2304 alternative configurations ($2^8 \times 3^2 = 2304$ since 8 switches are binary and 2 switches are ternary) were involved in the structural optimization; to accelerate the optimization process and maintain the robustness of the simulation, some of the implausible combinations were pre-screened in Python. The superstructure optimization exhibited the power of the automation process, connecting Aspen HYSYS® with the programming software to "communicate" and "exchange" information between them.

The main findings identified in this chapter are:

- The system exergetic efficiency is around 45% regardless of the case scenarios if the 2 MW natural gas engine is included in the overall system.

- By excluding the natural gas engine and focusing only on the polygeneration system, the system exergetic efficiencies in the Case$_\text{hot climate}$ and the Case$_\text{cold climate}$ are 31% and 47%, respectively.

- Regarding the final system product costs per unit of exergy in both cases (Case$_\text{hot climate}$ and Case$_\text{cold climate}$), the electric power has the lowest price. The refrigeration capacity is more expensive than the electricity by a factor of ranging from 3-4; for the heating price, the factor decreases to approximately between 1.5-2.

- Compared to the Case$_\text{hot climate}$, the average product cost of the overall system in the Case$_\text{cold climate}$ is lower, no matter which system boundary is defined. However, if the system includes the natural gas engine, the difference in the average system product cost between the Case$_\text{hot climate}$ and the Case$_\text{cold climate}$ is merely 7%. In contrast, the average system product cost in the Case$_\text{cold climate}$ is more than 40% lower than that in the Case$_\text{hot climate}$, if the research focus is solely the polygeneration system.

- According to results obtained from the conventional and advanced exergetic and exergoeconomic analyses, in both cases, the Cooler has the highest exergy destruction, followed by the HE, the MIX, and the EX. If only the avoidable part $(\dot{Z}_k^\text{AV} + \dot{C}_{\text{D},k}^\text{AV})$ associated with components is focused, the EX is the most prominent component due to its high investment cost. The HE and the Cooler also show their high improvement potentials, which need to be addressed in the optimization steps by reducing their avoidable costs.

- The DE and PSO algorithms generally obtained consistent optimization results. For better implementing these stochastic algorithms, many efforts for tuning the optimization parameters are needed.

- For the Case$_\text{hot climate}$, the structural optimization results revealed that the recuperation and preheating design features could improve the overall system performance, while the base-case structure design is the best system configuration for the Case$_\text{cold climate}$.

7

Summary, conclusion, and outlook

The goals for achieving sustainable development in the future are closely linked to the energy-related sectors' performance. The conventional energy system needs to be transformed into a sustainable energy system. Energy efficiency improvement is reported as the most cost-effective and near-term option, which can be achieved quickly and considered the "first fuel" of the global sustainable energy systems. Polygeneration systems show a significant boost in system efficiency since they can produce two or more than two energy products simultaneously in a single integrated process. If renewable energy sources can power the polygeneration systems, the renewable energy-based polygeneration systems are not only high-efficient but also environmental-friendly.

In this thesis, a new polygeneration system with CO_2 as working fluid was proposed. The system design was inspired by the initial idea of the heat-driven vapor-compression refrigeration machine. This work focused on the conceptual design and development of the proposed polygeneration system with the aid of exergy-based methods. The system was simulated in steady-state conditions in Aspen HYSYS®, and the system analyses, evaluation, and optimization were carried out in Python via the automation process, connecting Aspen HYSYS® with Python. The stochastic algorithms were implemented to optimize the system since the mathematical modeling in Aspen HYSYS® was unknown and considered a black box.

This chapter summarizes the work conducted in this thesis, the main identified findings, the research scope and limitations of this study, and the potential future work.

7.1   Summary of the conducted work

There are two major perspectives involved in the system analyses and evaluation: 1. the proposed polygeneration system was driven by a heat source, which was unspecified; 2. the polygeneration system was driven by the exhaust gas from a 2 MW natural gas engine. Regarding the system optimization, only the second perspective was considered.

The main conducted work is summarized as follows:

- To understand and investigate the proposed polygeneration system from a general perspective, the energetic, exergetic, and exergoeconomic analyses were implemented first for the polygeneration system without the heat source specification.

- To identify the main decision parameters for designing and optimizing the polygeneration system, the sensitivity analyses of the proposed system driven by unknown heat sources were carried out, including the influences of the power generation, the heat source temperature, the turbine inlet pressure, the merging pressure, and the ambient temperature on the overall system performance.

- By recovering the waste heat of the exhaust gas from a 2 MW natural gas engine, a case study of the proposed polygeneration system applied for natural gas engine waste-heat recovery was thoroughly performed. Two different natural gas prices in the U.S. and Germany were considered to evaluate the entire system, including the natural gas engine and the polygeneration system. Three cases under various ambient conditions and local requirements were assumed, and their exergoeconomic results were addressed for the comparison.

- Conventional and advanced exergetic and exergoeconomic analyses were performed on the component-level for two representative cases of the system excluding the natural gas engine since the detailed system evaluation and optimization focused only on the polygeneration system.

- The parameter optimization, including the single-objective and the multi-objective optimization, and the structural optimization were carried out for optimizing the proposed polygeneration system in terms of its decision parameters and system configuration. Moreover, the optimization results obtained from the differential evolution algorithm and the particle swarm optimization algorithm were compared in the parameter optimization process. For structural optimization, the differential evolution algorithm was applied for integrating several design features into the optimal system configuration to achieve the lowest average product cost of the overall system.

7.2 Conclusion of the main findings

The main findings identified in this thesis are:

- The automation process, which connects a programming language (in this work is Python) with simulation software (here is Aspen HYSYS®), allows the "communication" between different programs. This technique is beneficial in the application scenarios where the simulations need to be executed several times, and for each execution, the corresponding calculations need to be recomputed regarding the new simulation results. In other words, via automation, importing and exporting the values manually can be avoided; thus, the manual failures can be minimized.

- By taking advantage of applying supercritical CO_2 as the working fluid, the proposed polygeneration system is high-efficient, compact, and environmentally friendly. This system design can be integrated with the distributed heating and cooling systems as

well as renewable heat sources. Three potential energy products (electric power, heating and refrigeration capacities) can be generated simultaneously by this polygeneration system. Depending on the local ambient temperatures and specific requirements, the system performs differently, which in turn, the parameter and structural optimization results for different cases may vary.

- Increasing the system power production reduces each product's cost per unit of exergy of the polygeneration system; thus, the average product cost of the overall system shows a decrease, while the system exergetic efficiency boosts.

- The temperatures and costs of the heat sources, which are applied to drive the polygeneration system, influence each product's cost notably but in a rather complex way. The heating cost is, especially, very sensitive to the variations of the parameters of the heat sources; the average product cost of the overall system reveals a subtle but considerable correlation with the heat source temperature and cost.

- The turbine inlet pressure affects the exergetic efficiency of the polygeneration system dramatically: the higher the turbine inlet pressure, the higher the system efficiency; the average product cost is, however, hardly affected by varying the turbine inlet pressure.

- To further exploit the potentials of using supercritical CO_2 as the working fluid of the polygeneration system, the sensitivity analysis regarding the pressure, merging two sub-systems, was carried out. It reveals that merging the power cycle and the refrigeration cycle at a pressure nearing the CO_2 critical point provides a higher system efficiency and a lower average product cost in the application case where the heat sources were not specified.

- In terms of the system performance of the polygeneration system under different ambient temperature conditions, the case with a lower ambient temperature shows lower product costs, including each product's cost and the average product cost. Compared to the case with a higher ambient temperature, the large amount of heat produced from the system, in the case with a lower ambient temperature, is with a higher quality in terms of the exergy content, and all the heat can be utilized for the hot water and space heating purposes.

- If the 2 MW natural gas engine is included in the overall system, the system exergetic efficiency is then around 45% regardless of the case scenarios.

- By excluding the natural gas engine and focusing only on the polygeneration system, the system exergetic efficiencies are 31% and 47% in the $Case_{hot\ climate}$ and the $Case_{cold\ climate}$, respectively.

- By comparing the final system product costs per unit of exergy in both cases ($Case_{hot\ climate}$ and $Case_{cold\ climate}$), the cost of each final product in the $Case_{cold\ climate}$ is lower than that in the $Case_{hot\ climate}$. Besides, similarities can be observed in both cases: the electric power has the lowest price, while the refrigeration capacity is more expensive than the electricity by a factor of ranging from 3-4; for the heating price, the factor decreases to approximately between 1.5-2.

- In terms of the final average product cost of the overall system, the cost in the Case$_{\text{cold climate}}$ is always lower compared to the Case$_{\text{hot climate}}$, no matter which system boundary (including or excluding the natural gas engine) is defined. However, if the system includes the natural gas engine, the difference in the average system product cost between the Case$_{\text{hot climate}}$ and the Case$_{\text{cold climate}}$ is merely 7%. In contrast, the average system product cost in the Case$_{\text{cold climate}}$ is more than 40% lower than that in the Case$_{\text{hot climate}}$, if the research focuses solely on the polygeneration system.

- By implementing the conventional and advanced exergetic and exergoeconomic analyses for both cases, the results obtained from the conventional analyses show that the Cooler always has the highest exergy destruction, followed by the HE, the MIX, and the EX. According to the advanced exergy-based analyses, by considering only the avoidable part ($\dot{Z}_k^{\text{AV}} + \dot{C}_{\text{D},k}^{\text{AV}}$) associated with components, the EX is, however, the most prominent component due to its high investment cost. The HE and the Cooler also show their high improvement potentials, which need to be addressed in the optimization steps to reduce their avoidable costs.

- In general, the DE and PSO algorithms, which were selected as representatives of the stochastic algorithms applied in the parameter optimization, obtained consistent optimization results. Both of them were executed successfully in this study, and they were proved can achieve sufficiently good solutions. Nevertheless, to better implement these stochastic algorithms, a lot of efforts for tuning the settings of the optimization parameters are inevitable.

- For the Case$_{\text{hot climate}}$, the superstructure-based optimization showed that the overall system performance of the polygeneration system could be improved by adding the recuperation and preheating design features, while the initially proposed system structure is the best system configuration for the Case$_{\text{cold climate}}$.

7.3   Limitations of the present work

In this work, the study focused on the conceptual design and development of the proposed polygeneration system. However, only the system exergetic efficiency and the average final product cost of the overall system per unit of exergy were considered the design and evaluation criteria. Other important criteria, including market potential, risk management, and environmental friendliness, should also be considered to design a better energy system. This study proved the advantages of applying exergy-based methods over energy-based methods to analyze, evaluate, and optimize energy-conversion systems.

The proposed polygeneration system was designed, simulated, and optimized by fixing the cooling capacity within the EVAP as 100 kW. The net electric power and the heating capacity, which can produce by the polygeneration system, were computed based on the system design and decision parameters, as well as the quality and the amount of the potential heat sources, which are utilized for driving the system. By fixing the electricity production or the heat capacity based on the local requirement, the system design, analyses, and optimization may result in different conclusions. It is one of the unique characteristics of the polygeneration

system: the energy products are coupled in terms of their magnitudes. Since the proposed polygeneration system was inspired by the system design of a heat-driven vapor-compression refrigeration machine, the refrigeration capacity of the polygeneration system, in this thesis, was considered as one of the essential design parameters.

Moreover, the jacket water applied for cooling the natural gas engine was not harnessed for driving the polygeneration in this study since it was considered to directly produce heat capacity, which can be used for space heating and hot water supply. By integrating both the engine exhaust gas and the jacket water, the system designs, including the superstructure-based topology, need to be modified considering a (second) preheating feature to recover the waste heat from the jacket water.

For the economic evaluation, the purchased equipment costs of some components were estimated based on the information obtained from the vendors, while other components, which are not technically mature and not commercialized yet, can only be estimated based on the available sources from the literature. The cost estimations in the conceptual design phase are always exposed to large uncertainties, resulting in the uncertainties of the product cost estimation and the system optimization results. Shortly, when the technology is mature, the cost estimations can be carried out more accurately. The system evaluation and optimization of the newly proposed polygeneration system can be continuously updated, and the obtained results may differ significantly due to the system cost variations.

In the structural optimization, the optimal system configurations, by applying the superstructure-based technique, were selected from the pre-designed topology, which integrates several promising system structures. However, better configurations may exist beyond these considered structures. Superstructure-free techniques could overcome this problem and may result in better solutions. Nevertheless, the superstructure-based technique is, apparently, easier to be implemented than the superstructure-free techniques. It has been proven that simple configurations are preferred for this proposed polygeneration system due to its small size.

Only the stochastic optimization algorithms can be applied in this work since the mathematical models of the systems simulated in Aspen HYSYS® are not transparent. With unknown mathematical models, deterministic optimization algorithms are, unfortunately, not applicable. The stochastic optimization algorithms are able to find sufficiently good solutions, yet the optimality can not always be guaranteed. To ensure the accuracy of the optimization results, applying high-level modeling languages, such as GAMS, for mathematical programming and optimization, can be considered. With these high-level modeling languages, the energy systems can be modeled and optimized simultaneously. Furthermore, the optimization process can be carried out more efficiently and more accurately in less computation time. However, the modeling results obtained by coding in the mathematical programming languages need to be validated with values stated in literature or acquired from the industry.

7.4   Outlook of future work

Based on the main findings and the limitations of this work, future research is identified and can be conducted in the following directions:

- Implementation of the structure-free techniques for better solving the structural optimization problem.

- Application of a high-level modeling language (e.g., GAMS) to validate the optimization results obtained by the stochastic algorithms.

- Identification of the influences on the system performance by adopting CO_2-based mixtures. By blending other working fluids with CO_2 and forming CO_2-based mixtures, the system performance may increase significantly [25, 26]. The type and mixing ratio of the CO_2-based mixtures need to be tailored regarding the application scenarios.

- Experimental studies on the proposed polygeneration system to validate the simulation and optimization results and identify technological difficulties in detail, which can improve the system design by adding perspectives of empirical evidence.

- Implementation of an environmental assessment on the polygeneration system. The environmental assessment is used for evaluating the environmental performance of a targeted system and identifying the hot spots where the notable emissions of the entire system occur. Thus, other solutions for reducing the adverse environment-related effects may be suggested.

- Application of risk management on the proposed system to identify, evaluate, and prioritize the risks. It helps to minimize, monitor, and control the probability of unfortunate events [137], which are caused by identified hazards.

- Assessment of the market potential of the proposed polygeneration system. Since the polygeneration system is newly proposed, its potential customers, application scenarios, and preferable countries/locations need to be addressed by implementing more detailed market research and economic analyses.

References

[1] International Energy Agency. World Energy Outlook 2019. 2019. URL: https://www.iea.org/reports/world-energy-outlook-2019.

[2] International Energy Agency. Energy Efficiency 2019. 2019. URL: https://www.iea.org/reports/energy-efficiency-2019.

[3] Intergovernmental Panel on Climate Change. Global Warming of 1.5°C. An IPCC Special Report on the impacts of global warming of 1.5°C above pre-industrial levels and related global greenhouse gas emission pathways, in the context of strengthening the global response to the threat of climate change, sustainable development, and efforts to eradicate poverty. 2018. URL: https://www.ipcc.ch/sr15/.

[4] International Energy Agency. Global Energy Review 2019. 2020. URL: https://www.iea.org/reports/global-energy-review-2019.

[5] International Energy Agency. World Energy Outlook 2020. 2020. URL: https://www.iea.org/reports/world-energy-outlook-2020.

[6] Global Energy Assessment and International Institute for Applied Systems Analysis. Global Energy Assessment–Toward a Sustainable Future. 2012. URL: https://iiasa.ac.at/web/home/research/Flagship-Projects/Global-Energy-Assessment/GEA-Summary-web.pdf.

[7] Deepesh Sonar, Sandeep Soni, and Dilip Sharma. Micro-trigeneration for energy sustainability: Technologies, tools and trends. In: *Applied Thermal Engineering* 71.2 (2014), pp. 790–796.

[8] Aiying Rong and Risto Lahdelma. Role of polygeneration in sustainable energy system development challenges and opportunities from optimization viewpoints. In: *Renewable and Sustainable Energy Reviews* 53 (2016), pp. 363–372.

[9] Intergovernmental Panel on Climate Change. Climate Change 2014: Mitigation of Climate Change. Contribution of Working Group III to the Fifth Assessment Report of the Intergovernmental Panel on Climate Change. 2014. URL: https://www.ipcc.ch/report/ar5/wg3/.

[10] International Energy Agency. District Energy Systems in China. 2017. URL: https://www.iea.org/reports/district-energy-systems-in-china.

[11] International Energy Agency. World Energy Outlook 2013. 2013. URL: https://www.iea.org/reports/world-energy-outlook-2013.

REFERENCES

[12] Gustav Lorentzen. Revival of carbon dioxide as a refrigerant. In: *International journal of refrigeration* 17.5 (1994), pp. 292–301.

[13] Alberto Cavallini. Properties of CO_2 as a refrigerant. In: *European Seminar-CO_2 as a refrigerant: theoretical and design aspects.* 2004.

[14] Herbert W Stanford III and Adam F Spach. Analysis and Design of Heating, Ventilating, and Air-Conditioning Systems. CRC Press, 2019.

[15] Peng Liu, Gequn Shu, and Hua Tian. Carbon dioxide as working fluids in transcritical Rankine cycle for diesel engine multiple waste heat recovery in comparison to hydrocarbons. In: *Journal of Thermal Science* 28.3 (2019), pp. 494–504.

[16] Jahar Sarkar. Transcritical CO_2 refrigeration systems: comparison with conventional solutions and applications. In: *International Journal of Air-Conditioning and Refrigeration* 20.04 (2012), p. 1250017.

[17] 15th Informatory Note on Refrigerants-Carbon Dioxide as a Refrigerant. Tech. rep. International Institute of Refrigeration, Paris, (France), 2000.

[18] Gustav Lorentzen and Jostein Pettersen. A new, efficient and environmentally benign system for car air-conditioning. In: *International journal of refrigeration* 16.1 (1993), pp. 4–12.

[19] Gebrüder Sulzer. Verfahren zur erzeugung von arbeit aus warme. In: *Swiss Patent* 269599 (1950).

[20] Olumide Olumayegun, Meihong Wang, and Greg Kelsall. Closed-cycle gas turbine for power generation: A state-of-the-art review. In: *Fuel* 180 (2016), pp. 694–717.

[21] Yoonhan Ahn, Seong Jun Bae, Minseok Kim, Seong Kuk Cho, Seungjoon Baik, Jeong Ik Lee, and Jae Eun Cha. Review of supercritical CO_2 power cycle technology and current status of research and development. In: *Nuclear Engineering and Technology* 47.6 (2015), pp. 647–661.

[22] Marco Astolfi, Dario Alfani, Silvia Lasala, and Ennio Macchi. Comparison between ORC and CO_2 power systems for the exploitation of low-medium temperature heat sources. In: *Energy* 161 (2018), pp. 1250–1261.

[23] Silvia Lasala, Romain Privat, and Jean-Noël Jaubert. Inert and Reactive Working Fluids for Closed Power Cycles: Present Knowledge, Applications and Open Researches. In: *Organic Rankine Cycle Technology for Heat Recovery* (2018), p. 1.

[24] Silvia Lasala, Costante Invernizzi, Paolo Iora, Paolo Chiesa, and Ennio Macchi. Thermal stability analysis of perfluorohexane. In: *Energy Procedia* 75 (2015), pp. 1575–1582.

[25] Silvia Lasala, D Bonalumi, E Macchi, Romain Privat, and J-N Jaubert. The design of CO_2-based working fluids for high-temperature heat source power cycles. In: *Energy Procedia* 129 (2017), pp. 947–954.

[26] Giampaolo Manzolini, Marco Binotti, Davide Bonalumi, Costante Invernizzi, and Paolo Iora. CO_2 mixtures as innovative working fluid in power cycles applied to solar plants. Techno-economic assessment. In: *Solar Energy* 181 (2019), pp. 530–544.

[27]   Yuegeng Ma. Optimal design of supercritical carbon dioxide cycle based system for concentrated solar power application. PhD thesis. Technical University of Berlin, Institute for Energy Engineering, 2020. URL: http://dx.doi.org/10.14279/depositonce-9601.

[28]   Naeem Abas, Ali Raza Kalair, Nasrullah Khan, Aun Haider, Zahid Saleem, and Muhammad Shoaib Saleem. Natural and synthetic refrigerants, global warming: A review. In: *Renewable and Sustainable Energy Reviews* 90 (2018), pp. 557–569.

[29]   Guy F Hundy. Refrigeration, air conditioning and heat pumps. Butterworth-Heinemann, 2016.

[30]   Paul Maina and Zhongjie Huan. A review of carbon dioxide as a refrigerant in refrigeration technology. In: *South african journal of science* 111.9-10 (2015), pp. 01–10.

[31]   Petter Nekså, Harald Taxt Walnum, and Armin Hafner. CO_2-a refrigerant from the past with prospects of being one of the main refrigerants in the future. In: *9th IIR Gustav Lorentzen conference.* 2010, pp. 2–14.

[32]   James M Calm. The next generation of refrigerants–Historical review, considerations, and outlook. In: *international Journal of Refrigeration* 31.7 (2008), pp. 1123–1133.

[33]   Elvedin Halimic, Dixon Ross, Brian Agnew, Alexander Anderson, and Ian Potts. A comparison of the operating performance of alternative refrigerants. In: *Applied thermal engineering* 23.12 (2003), pp. 1441–1451.

[34]   Samira Benhadid-Dib and Ahmed Benzaoui. Refrigerants and their environmental impact Substitution of hydro chlorofluorocarbon HCFC and HFC hydro fluorocarbon. Search for an adequate refrigerant. In: *Energy Procedia* 18 (2012), pp. 807–816.

[35]   Mario J Molina and Frank Sherwood Rowland. Stratospheric sink for chlorofluoromethanes: chlorine atom-catalysed destruction of ozone. In: *Nature* 249.5460 (1974), pp. 810–812.

[36]   Robert Tom Sawyer. The closed cycle gas turbine, the most efficient turbine burning any fuel. In: *Turbo Expo: Power for Land, Sea, and Air.* Vol. 79481. American Society of Mechanical Engineers. 1984, V003T08A007.

[37]   Francesco Crespi, Giacomo Gavagnin, David Sánchez, and Gonzalo S Martıénez. Supercritical carbon dioxide cycles for power generation: A review. In: *Applied Energy* 195 (2017), pp. 152–183.

[38]   Colin F McDonald. The Nuclear Gas Turbine: Towards Realization After Half a Century of Evolution. In: *Turbo Expo: Power for Land, Sea, and Air.* Vol. 78804. American Society of Mechanical Engineers. 1995, V003T08A001.

[39]   Hans Ulrich Frutschi. Closed-cycle gas turbines: operating experience and future potential. Amer Society of Mechanical, 2005.

[40]   Curt Keller. Forty years of experience on closed-cycle gas turbines. In: *Annals of Nuclear Energy* 5.8-10 (1978), pp. 405–422.

[41]   Ernest G Feher. The supercritical thermodynamic power cycle. In: *Energy conversion and management* 8.2 (1968), pp. 85–90.

REFERENCES

[42] Gianfranco Angelino. Carbon dioxide condensation cycles for power production. In: *Journal of Engineering for Power* 90.3 (1968), pp. 287–295.

[43] R.A. Strub and A.J. Frieder. High pressure indirect CO_2 closed-cycle gas turbines. In: *Nuclear gas turbines* (1970), pp. 51–61.

[44] D.P. Gokhshtein, V.L. Dekhtyarev, and A.I. Kozorez. Future designs of thermal power-stations operating on carbon-dioxide. In: *Thermal Engineering* 18.4 (1971), pp. 36–38.

[45] Gianfranco Angelino. Real gas effects in carbon dioxide cycles. In: *International Gas Turbine Conference.* American Society of Mechanical Engineers. 1969.

[46] Ernest Feher. Investigation of supercritical (Feher) cycle. In: *Astropower Laboratory, Missile & Space Systems Division* (1968).

[47] Vaclav Dostal, Neil Todreas, Pavel Hejzlar, and Mujid Kazimi. Power conversion cycle selection for the LBE cooled reactor with forced circulation. Tech. rep. MIT-ANP-TR-085, 2002.

[48] Jim Pasch, Tom Conboy, Darryn Fleming, and Gary Rochau. Supercritical CO_2 recompression Brayton cycle: completed assembly. In: *Sandia Report, SAND* 9546 (2012), p. 2012.

[49] Ladislav Vesely, Vaclav Dostal, and Petr Hajek. Design of experimental loop with supercritical carbon dioxide. In: *International Conference on Nuclear Engineering.* Vol. 45936. American Society of Mechanical Engineers. 2014, V003T05A023.

[50] Kato Yasuyoshi, Nitawaki Takeshi, and Yoshizawa Yoshio. A carbon dioxide partial condensation direct cycle for advanced gas cooled fast and thermal reactors. In: *Proceedings of Global 2001 international conference on:"back-end of the fuel cycle: from research to solutions", INIS-FR-1118, Paris, France.* 2001, pp. 9–13.

[51] Echogen power systems' waste heat recovery system available as turnkey solution. 2014. URL: https://www.echogen.com/news-resources/news-events/echogen-power-systems-waste-heat-recovery-system-available-as-turnkey-solution.

[52] Klaus Brun, Peter Friedman, and Richard Dennis. Fundamentals and applications of supercritical carbon dioxide (sCO2) based power cycles. Woodhead publishing, 2017.

[53] International Renewable Energy Agency. Renewable energy in district heating and cooling: A sector roadmap for Remap. 2017. URL: https://www.irena.org/publications/2017/Mar/Renewable-energy-in-district-heating-and-cooling.

[54] Jon (The Guardian) Henley. World set to use more energy for cooling than heating. 2015. URL: https://www.theguardian.com/environment/2015/oct/26/cold-economy-cop21-global-warming-carbon-emissions.

[55] Léopold T Biardeau, Lucas W Davis, Paul Gertler, and Catherine Wolfram. Heat exposure and global air conditioning. In: *Nature Sustainability* 3.1 (2020), pp. 25–28.

[56] Lucas W Davis and Paul J Gertler. Contribution of air conditioning adoption to future energy use under global warming. In: *Proceedings of the National Academy of Sciences* 112.19 (2015), pp. 5962–5967.

[57]   Morna Isaac and Detlef P Van Vuuren. Modeling global residential sector energy demand for heating and air conditioning in the context of climate change. In: *Energy policy* 37.2 (2009), pp. 507–521.

[58]   International Energy Agency, Organisation for Economic Cooperation, and Development. The Future of Cooling - Opportunities for energy-efficient air conditioning. 2018. URL: https://www.iea.org/reports/the-future-of-cooling.

[59]   Sam Kubba. Handbook of green building design and construction: LEED, BREEAM, and Green Globes (Second edition). Butterworth-Heinemann, 2017.

[60]   Andy Pearson. What does the future hold for compressor manufacturers? In: *Proceedings of the Institution of Mechanical Engineers, Part E: Journal of Process Mechanical Engineering* 229.2 (2015), pp. 88–95.

[61]   Stephen A Rackley. Carbon capture and storage. Butterworth-Heinemann, 2017.

[62]   Robert T Balmer. Modern engineering thermodynamics. Academic Press, 2011.

[63]   Panaiyur Narasimah Ananthanarayanan. Basic refrigeration and air conditioning. Tata McGraw-Hill Education, 2013.

[64]   Roberto Best. Recent developments in thermal driven cooling and refrigeration systems. In: *1st European Conference on Polygeneration*. 2007.

[65]   Tomas Núñez. Thermally driven cooling: technologies, developments and applications. In: *Journal of sustainable energy* 1.4 (2010).

[66]   Satha Aphornratana and Thanarath Sriveerakul. Analysis of a combined Rankine–vapour–compression refrigeration cycle. In: *Energy Conversion and management* 51.12 (2010), pp. 2557–2564.

[67]   Hailei Wang, Richard Peterson, Kevin Harada, Erik Miller, Robbie Ingram-Goble, Luke Fisher, James Yih, and Chris Ward. Performance of a combined organic Rankine cycle and vapor compression cycle for heat activated cooling. In: *Energy* 36.1 (2011), pp. 447–458.

[68]   Hailei Wang, Richard Peterson, and Tom Herron. Design study of configurations on system COP for a combined ORC (organic Rankine cycle) and VCC (vapor compression cycle). In: *Energy* 36.8 (2011), pp. 4809–4820.

[69]   Xianbiao Bu, Huashan Li, and Lingbao Wang. Performance analysis and working fluids selection of solar powered organic Rankine-vapor compression ice maker. In: *Solar Energy* 95 (2013), pp. 271–278.

[70]   Huashan Li, Xianbiao Bu, Lingbao Wang, Zhen Long, and Yongwang Lian. Hydrocarbon working fluids for a Rankine cycle powered vapor compression refrigeration system using low-grade thermal energy. In: *Energy and buildings* 65 (2013), pp. 167–172.

[71]   Xianbiao Bu, Lingbao Wang, and Huashan Li. Performance analysis and working fluid selection for geothermal energy-powered organic Rankine-vapor compression air conditioning. In: *Geothermal Energy* 1.1 (2013), p. 2.

REFERENCES

[72] Kyoung Hoon Kim and Horacio Perez-Blanco. Performance analysis of a combined organic Rankine cycle and vapor compression cycle for power and refrigeration cogeneration. In: *Applied Thermal Engineering* 91 (2015), pp. 964–974.

[73] Francisco Molés, Joaquén Navarro-Esbrié, Bernardo Peris, Adrián Mota-Babiloni, and Konstantinos Kostas Kontomaris. Thermodynamic analysis of a combined organic Rankine cycle and vapor compression cycle system activated with low temperature heat sources using low GWP fluids. In: *Applied Thermal Engineering* 87 (2015), pp. 444–453.

[74] Sotirios Karellas and Konstantinos Braimakis. Energy–exergy analysis and economic investigation of a cogeneration and trigeneration ORC–VCC hybrid system utilizing biomass fuel and solar power. In: *Energy conversion and management* 107 (2016), pp. 103–113.

[75] Muhammad Tauseef Nasir and Kyung Chun Kim. Working fluids selection and parametric optimization of an Organic Rankine Cycle coupled Vapor Compression Cycle (ORC-VCC) for air conditioning using low grade heat. In: *Energy and Buildings* 129 (2016), pp. 378–395.

[76] Bahaa Saleh. Parametric and working fluid analysis of a combined organic Rankine-vapor compression refrigeration system activated by low-grade thermal energy. In: *Journal of advanced research* 7.5 (2016), pp. 651–660.

[77] Ata Delkhah Akbari and Seyed Mahmoudi. Thermoeconomic performance and optimization of a novel cogeneration system using carbon dioxide as working fluid. In: *Energy conversion and management* 145 (2017), pp. 265–277.

[78] Krishnappa Manjunath, Om Prakash Sharma, Sudhir Kumar Tyagi, and Shubhash Chandra Kaushik. Thermodynamic analysis of a supercritical/transcritical CO_2 based waste heat recovery cycle for shipboard power and cooling applications. In: *Energy Conversion and Management* 155 (2018), pp. 262–275.

[79] Shengya Hou, Fengyuan Zhang, Lijun Yu, Sheng Cao, Yaodong Zhou, Yuandan Wu, and Lingyi Hou. Optimization of a combined cooling, heating and power system using CO_2 as main working fluid driven by gas turbine waste heat. In: *Energy Conversion and Management* 178 (2018), pp. 235–249.

[80] Nasir El Bassam, Preben Maegaard, and Marcia Schlichting. Distributed renewable energies for off-grid communities: strategies and technologies toward achieving sustainability in energy generation and supply. Newnes, 2013.

[81] Michael Papapetrou, George Kosmadakis, Andrea Cipollina, Umberto La Commare, and Giorgio Micale. Industrial waste heat: Estimation of the technically available resource in the EU per industrial sector, temperature level and country. In: *Applied Thermal Engineering* 138 (2018), pp. 207–216.

[82] George Kosmadakis. Estimating the potential of industrial (high-temperature) heat pumps for exploiting waste heat in EU industries. In: *Applied Thermal Engineering* 156 (2019), pp. 287–298.

[83] Steven Lecompte, Erika Ntavou, Bertrand Tchanche, George Kosmadakis, Aditya Pillai, Dimitris Manolakos, and Michel De Paepe. Review of experimental research on supercritical and transcritical thermodynamic cycles designed for heat recovery application. In: *Applied Sciences* 9.12 (2019), p. 2571.

[84] Alberto Cavallini and Claudio Zilio. Carbon dioxide as a natural refrigerant. In: *International Journal of Low-Carbon Technologies* 2.3 (2007), pp. 225–249.

[85] Henrik Lund, Sven Werner, Robin Wiltshire, Svend Svendsen, Jan Eric Thorsen, Frede Hvelplund, and Brian Vad Mathiesen. 4th Generation District Heating (4GDH): Integrating smart thermal grids into future sustainable energy systems. In: *Energy* 68 (2014), pp. 1–11.

[86] Andrey Rozhentsev and Chi-Chuan Wang. Some design features of a CO_2 air conditioner. In: *Applied Thermal Engineering* 21.8 (2001), pp. 871–880.

[87] Chandra Prakash Arora. Refrigeration and air conditioning. Tata McGraw-Hill Education, 2000.

[88] Adrian Bejan, George Tsatsaronis, and Michael Moran. Thermal design and optimization. John Wiley & Sons, 1995.

[89] Alexandre C Dimian, Costin Sorin Bildea, and Anton A Kiss. Integrated design and simulation of chemical processes. Elsevier, 2014.

[90] Youqi Yang and Lei Shi. Integrating environmental impact minimization into conceptual chemical process design—a process systems engineering review. In: *Computers & Chemical Engineering* 24.2-7 (2000), pp. 1409–1419.

[91] Norbert Roozenburg and Johannes Eekels. Product design: fundamentals and methods. In: (1995).

[92] Qiao Zhao, Mounir Mecheri, Thibaut Neveux, Romain Privat, and Jean-Noël Jaubert. Thermodynamic model investigation for supercritical CO_2 Brayton cycle for coal-fired power plant application. In: *Proceedings of the 5th International Symposium–Supercritical CO_2 Power Cycles, San Antonio, TX, USA*. 28—31 March, 2016.

[93] Adrian Bejan. Fundamentals of exergy analysis, entropy generation minimization, and the generation of flow architecture. In: *International Journal of Energy Research* 26.7 (2002).

[94] Tatiana Morosuk and George Tsatsaronis. Splitting physical exergy: Theory and application. In: *Energy* 167 (2019), pp. 698–707.

[95] Tatiana Morosuk and George Tsatsaronis. Advanced exergy-based methods used to understand and improve energy-conversion systems. In: *Energy* 169 (2019), pp. 238–246.

[96] George Tsatsaronis and Moung-Ho Park. On avoidable and unavoidable exergy destructions and investment costs in thermal systems. In: *Energy conversion and management* 43.9-12 (2002), pp. 1259–1270.

[97] Andrea Lazzaretto and George Tsatsaronis. SPECO: a systematic and general methodology for calculating efficiencies and costs in thermal systems. In: *Energy* 31.8-9 (2006), pp. 1257–1289.

REFERENCES

[98]   Chimmiri Venkateswarlu and Satya Eswari Jujjavarapu. Stochastic Global Optimization Methods and Applications to Chemical, Biochemical, Pharmaceutical and Environmental Processes. Elsevier, 2019.

[99]   Rainer Storn and Kenneth Price. Differential evolution–a simple and efficient heuristic for global optimization over continuous spaces. In: *Journal of global optimization* 11.4 (1997), pp. 341–359.

[100] Budida Varahala Babu and Rakesh Angira. Optimization of non-linear chemical processes using evolutionary algorithm. In: *Proceedings of International Symposium & 55th Annual Session of IIChE (CHEMCON-2002)*. 2002, pp. 19–22.

[101] James Kennedy and Russell Eberhart. Particle swarm optimization. In: *Proceedings of ICNN'95-International Conference on Neural Networks*. Vol. 4. IEEE. 1995, pp. 1942–1948.

[102] Dan Simon. Evolutionary optimization algorithms. John Wiley & Sons, 2013.

[103] Dereje Shiferaw, Jorge Montero Carrero, and Renaud Le Pierres. Economic analysis of S-CO$_2$ cycles with PCHE recuperator design optimisation. In: *Proceedings of the 5th International Symposium–Supercritical CO$_2$ Power Cycles, San Antonio, TX, USA*. 28–31 March, 2016, pp. 29–31.

[104] Darryn Fleming, Thomas Holschuh, Tom Conboy, Gary Rochau, and Robert Fuller. Scaling considerations for a multi-megawatt class supercritical CO$_2$ Brayton cycle and path forward for commercialization. In: *ASME Turbo Expo 2012: Turbine Technical Conference and Exposition*. American Society of Mechanical Engineers Digital Collection. 2012, pp. 953–960.

[105] Heatric Printed Circuit Heat Exchanger (PCHE), accessed on 15th of December, 2018. URL: https://www.heatric.com/heat-exchangers/features/characteristics/.

[106] Knut Gezelius. Design of compact intermediate heat exchangers for gas cooled fast reactors. PhD thesis. Massachusetts Institute of Technology, 2004.

[107] Nitin N Sawant, Min Soo Kim, Vance Payne, Piotr A Domanski, and Yun Wook Hwang. A study of in-tube evaporation heat transfer of carbon dioxide. In: *International Conference of Refrigeration*. 2003, pp. 1–8.

[108] Mohamed Noaman, George Saade, Tatiana Morosuk, and George Tsatsaronis. Exergoeconomic analysis applied to supercritical CO$_2$ power systems. In: *Energy* 183 (2019), pp. 756–765.

[109] Vaclav Dostal, Michael J Driscoll, and Pavel Hejzlar. A supercritical carbon dioxide cycle for next generation nuclear reactors. PhD thesis. Massachusetts Institute of Technology, Department of Nuclear Engineering, 2004.

[110] Yuan Jiang, Eric Liese, Stephen E Zitney, and Debangsu Bhattacharyya. Design and dynamic modeling of printed circuit heat exchangers for supercritical carbon dioxide Brayton power cycles. In: *Applied Energy* 231 (2018), pp. 1019–1032.

[111] Richard Turton, Richard C Bailie, Wallace B Whiting, and Joseph A Shaeiwitz. Analysis, synthesis and design of chemical processes. Pearson Education, 2008.

[112] Robin Smith. Chemical process: design and integration. John Wiley & Sons, 2005.

[113] Farivar Fazelpour and Tatiana Morosuk. Exergoeconomic analysis of carbon dioxide transcritical refrigeration machines. In: *International Journal of Refrigeration* 38 (2014), pp. 128–139.

[114] Jian Song, Xuesong Li, Xiaodong Ren, and Chunwei Gu. Performance improvement of a preheating supercritical CO_2 (S-CO_2) cycle based system for engine waste heat recovery. In: *Energy Conversion and Management* 161 (2018), pp. 225–233.

[115] Alex Kacludis, Sean Lyons, Dan Nadav, and Edward Zdankiewicz. Waste heat to power (WH2P) applications using a supercritical CO_2-based power cycle. In: *Power-Gen International* 2012 (2012), pp. 11–13.

[116] Paul Breeze. Piston Engine-based Power Plants. Academic Press, 2018.

[117] Lingfeng Shi, Gequn Shu, Hua Tian, and Shuai Deng. A review of modified Organic Rankine cycles (ORCs) for internal combustion engine waste heat recovery (ICE-WHR). In: *Renewable and Sustainable Energy Reviews* 92 (2018), pp. 95–110.

[118] Paul Breeze. Power generation technologies. Newnes, 2019.

[119] Energy Information Administration. Natural Gas Prices. 2020. URL: `https://www.eia.gov/dnav/ng/ng_pri_sum_dcu_nus_a.htm`.

[120] Statista GmbH. Prices of natural gas for industry in Germany. 2020. URL: `https://www.statista.com/statistics/595604/natural-gas-price-germany/`.

[121] Gael D Ulrich and Palligarnai T Vasudevan. Chemical engineering: process design and economics; a practical guide. Process Publ., 2004.

[122] Marcin Jankowski and Aleksandra Borsukiewicz. A Novel Exergy Indicator for Maximizing Energy Utilization in Low-Temperature ORC. In: *Energies* 13.7 (2020), p. 1598.

[123] Senthil Arumugam Muthukumaraswamy and Chakradhara Rao. On the performance of the particle swarm optimization algorithm with various inertia weight variants for computing optimal control of a class of hybrid systems. In: *Discrete Dynamics in Nature and Society* 2006 (2006).

[124] Prabha Umapathy, Venkataseshaiah Chinthakunta, and Senthil Arumugam Muthukumaraswamy. Particle swarm optimization with various inertia weight variants for optimal power flow solution. In: *Discrete Dynamics in Nature and Society* 2010 (2010).

[125] Kalyanmoy Deb, Amrit Pratap, Sameer Agarwal, and Tamt Meyarivan. A fast and elitist multiobjective genetic algorithm: NSGA-II. In: *IEEE transactions on evolutionary computation* 6.2 (2002), pp. 182–197.

[126] Jian Songa, Xiaoya Lib, Xiaodong Renc, Hua Tianb, Gequn Shub, and Christos N Markidesa. Supercritical CO_2-cycle configurations for internal combustion engine waste-heat recovery: A comparative techno-economic investigation. In: ().

[127] Daqing Li and Eckhard A Groll. Transcritical CO_2 refrigeration cycle with ejector-expansion device. In: *International Journal of refrigeration* 28.5 (2005), pp. 766–773.

REFERENCES

[128] Silvia Minetto, Riccardo Brignoli, Krzysztof Banasiak, Armin Hafner, and Claudio Zilio. Performance assessment of an off-the-shelf R744 heat pump equipped with an ejector. In: *Applied thermal engineering* 59.1-2 (2013), pp. 568–575.

[129] Bourhan Tashtoush, Karima Megdouli, Mouna Elakhdar, Ezzedine Nehdi, and Lakdar Kairouani. A comprehensive energy and exergoeconomic analysis of a novel transcritical refrigeration cycle. In: *Processes* 8.7 (2020), p. 758.

[130] Van Nguyen, Saffa Riffat, and Prince Doherty. Development of a solar-powered passive ejector cooling system. In: *Applied Thermal Engineering* 21.2 (2001), pp. 157–168.

[131] Suhas Kshirsagar and Mandar Desgmukh. Combined vapour compression-ejector refrigeration system: a review. In: *International Journal of Engineering Research and Development* 6 (2013), pp. 41–52.

[132] Ricardo Chacartegui, David Sánchez, Francisco Jiménez-Espadafor, Antonio Blanco, and Tatiana Sánchez. Analysis of intermediate temperature combined cycles with a carbon dioxide topping cycle. In: *Turbo Expo: Power for Land, Sea, and Air.* 2008, pp. 673–680.

[133] Germán Pérez-Pichel, Jose Linares, Luis Herranz, and Beatriz Yolanda Moratilla. Thermal analysis of supercritical CO_2 power cycles: Assessment of their suitability to the forthcoming sodium fast reactors. In: *Nuclear Engineering and Design* 250 (2012), pp. 23–34.

[134] Saeb M Besarati and Dharendra Yogi Goswami. Analysis of advanced supercritical carbon dioxide power cycles with a bottoming cycle for concentrating solar power applications. In: *Journal of solar energy engineering* 136.1 (2014).

[135] Yoon Han Ahn, Seong Jun Bae, Min Seok Kim, Seong Kuk Cho, Seung Joon Baik, Jeong Lee, and Jae Eun Cha. Cycle layout studies of S-CO_2 cycle for the next generation nuclear system application. In: *The Korean Nuclear Society Autumn Meeting.* The Korean Nuclear Society. 2014.

[136] Jahar Sarkar. Review and future trends of supercritical CO_2 Rankine cycle for low-grade heat conversion. In: *Renewable and Sustainable Energy Reviews* 48 (2015), pp. 434–451.

[137] Douglas W Hubbard. The failure of risk management: Why it's broken and how to fix it. John Wiley & Sons, 2020.